Functional diversification of membrane microdomains in *Bacillus subtilis*

Funktionale Diversifizierung von Membran-Mikrodomänen in *Bacillus subtilis*

Doctoral thesis for a doctoral degree at the Graduate School of Life Sciences,
Julius-Maximilians-Universität Würzburg,
Section Infection and Immunity

submitted by

Johannes Schneider

from

Mannheim

Würzburg, 2015

Submitted on: ……..

Office stamp

Members of the Thesis Committee:

Chair:	**Prof. Dr. Thomas Dandekar**
Primary Supervisor:	**Dr. Daniel Lopez**
Supervisor (Second):	**Prof. Dr. Markus Sauer**
Supervisor (Third):	**Prof. Dr. Thorsten Mascher**

Date of Public Defence……

Date of Receipt of Certificates……..

Affidavit

I hereby confirm that my thesis entitled "**Functional diversification of membrane microdomains in *Bacillus subtilis***" is the result of my own work. I did not receive any help or support from commercial consultants. All sources and / or materials applied are listed and specified in the thesis.

Furthermore, I confirm that this thesis has not yet been submitted as part of another examination process neither in identical nor in similar form.

Würzburg, Johannes Schneider

Acknowledgements

First of all, I would like to thank Dr. Daniel Lopez for accepting me as a Ph.D student, for his support, patience and unparalleled enthusiasm for science. This motivation has infected me and I have been able to learn many things from Daniel and thus also to mature as a professional. To me, Daniel was a great leader, guiding me, advising me and keeping me motivated in every situation we encountered during the time in his lab. ¡Muchas gracias por todo!

Furthermore, I would like to thank all members of my thesis committee: Dr. Daniel Lopez, Prof. Dr. Markus Sauer and Prof. Dr. Thorsten Mascher, for their invaluable support and advice during my doctoral training. Likewise, I would like to thank the members of the Graduate School of Life Sciences for their commitment and support during the doctoral training.

It is a genuine pleasure to thank all the members of the Lopez lab: Ana and Gudrun, two very skilled Postdocs and also great friends! –May you find a well-equipped lab next to a beautiful beach in a close and warm country and continue your research! (And then hire me.) My fellow Ph.D. students Ben, JC and Charly (our almost grown-ups), and Rabea and Lara (the toddlers) and our technician Isa, thank you for your company and for keeping up the spirit in our lab. It was a wonderful time joking around with you guys and doing all sorts of fun things in our leisure time.

Finally, I would like to express my sincere gratitude to my wife Lena and my family for their unlimited support and patience, which enabled me to pursue my goals and dreams.

Table of Contents **Page**

1. Summary

Eukaryotic cells are considered as evolutionary complex organisms because they possess organelles that enable them to regulate the spatio-temporal organization of cellular processes. Spatio-temporal organization of signal transduction cascades occurs in eukaryotic cells via organization of membrane-associated microdomains or lipid rafts. Lipid rafts are nanoscale-sized domains in the plasma membrane that are constituted by a specific set of lipids and proteins and harbor a number of proteins related to signal transduction and trafficking. The integrity of lipid rafts is important for the assembly and functional coordination of a plethora of signaling networks and associated processes. This integrity is partially mediated by a chaperone protein called flotillin. Disruption of lipid raft integrity, for example via depletion or overproduction of flotillin, alters raft-associated signal transduction cascades and causes severe diseases like Alzheimer's, Parkinson's disease or cardiovascular disease.

It was traditionally assumed that a sophisticated compartmentalization of cellular processes like the one exhibited in lipid rafts was exclusive to eukaryotic cells and therefore, lipid rafts have been considered as a hallmark in the evolution of cellular complexity, suggesting that prokaryotic cells were too simple organisms to organize such sophisticated membrane platforms. However, it was recently discovered that bacteria are also able to organize Functional Membrane Microdomains (FMMs) in their cellular membrane that are able to organize and catalyze the functionality of many diverse cellular processes. These FMMs of bacterial membranes contain flotillin-like proteins which play important roles in the organization of FMM-associated cellular processes.

In this dissertation I describe the structural and biological significance of the existence of two distinct flotillin proteins, FloA and FloT, in the FMMs of the bacterial model *Bacillus subtilis*. Localization studies, proteomic data and transcriptomic analyses show that FloA and FloT are individual scaffold proteins that activate different regulatory programs during

bacterial growth. Using the tractable bacterial model system, I show that the functionality of important regulatory proteins, like the protease FtsH or the signaling kinases KinC, PhoR and ResE, is linked to the activity of FMMs and that this is a direct consequence of the scaffold activity of the bacterial flotillins. FloA and FloT distribute heterogeneously along the FMMs of *B. subtilis* thereby generating a heterogeneous population of FMMs that compartmentalize different signal transduction cascades. Interestingly, diversification of FMMs does not occur randomly, but rather in a controlled spatio-temporal program to ensure the activation of given signaling networks at the right place and time during cell growth.

2. Zusammenfassung

Eukaryotische Zellen werden als evolutionär komplexe Organismen betrachtet, weil sie Organellen besitzen, mit denen sie die raum-zeitliche Organisation von zellulären Prozessen steuern können. Die räumliche und zeitliche Organisation von Signalwegen in eukaryotischen Zellen erfolgt durch die Abgrenzung von membran-assoziierten Mikrodomänen oder Lipid Rafts. Lipid Rafts sind wenige Nanometer große Felder in der Plasmamembran, die aus einem spezifischen Set von Lipiden und Proteinen zusammengesetzt sind und eine Reihe von für die Signaltransduktion und den Proteintransfer erforderlichen Proteine enthalten. Die Integrität der Lipid Rafts ist wichtig um zahlreiche Signalwege und damit assoziierte Prozesse zu verbinden und funktional zu koordinieren. Diese Integrität wird zum Teil von einem Chaperon-Protein namens Flotillin vermittelt. Eine Beeinträchtigung der Integrität der Lipid Rafts, z.B. aufgrund eines Mangels an Flotillin oder einer Überproduktion von Flotillin, verändert Raft-assoziierte Signalwege und verursacht schwere Erkrankungen wie Alzheimer, Parkinson oder kardiovaskuläre Erkrankungen.

Bislang wurde angenommen, dass eine so anspruchsvolle Kompartimentierung zellulärer Prozesse wie im Falle der Lipid Rafts ausschließlich in eukaryotischen Zellen vorkommt. Lipid Rafts galten daher als Meilenstein in der Evolution der zellulären Komplexität und prokaryotische Zellen als zu einfache Organismen, um solch komplexe Plattformen in der Membran einzurichten. Vor kurzem wurde jedoch herausgefunden, dass Bakterien ebenfalls in der Lage sind, Funktionale Mikrodomänen in der Membran (FMMs) zu formen, die viele verschiedene zelluläre Prozesse organisieren und katalysieren können. Diese FMMs in bakteriellen Membranen enthalten Flotillin-ähnliche Proteine, die wichtige Aufgaben bei der Organisation von FMM-assoziierten Prozessen übernehmen.

In dieser Dissertation beschreibe ich die strukturelle und biologische Signifikanz des Vorkommens der beiden verschiedenen Flotillin-Proteine FloA und FloT in den FMMs des bakteriellen Modellorganismus *Bacillus subtilis*. Lokalisationsstudien, proteomische Daten und transkriptomische Analysen demonstrieren, dass FloA und FloT individuelle Gerüstproteine sind, die während des Bakterienwachstums verschiedene regulatorische Programme aktivieren. Mit Hilfe des zugänglichen bakteriellen Modellorganismus zeige ich, dass die Funktionsweise von wichtigen regulatorischen Proteinen, wie z.B. der Protease FtsH oder der Signalwegskinasen KinC, PhoR und ResE, an die Aktivität der FMMs gebunden ist, und dass dies eine direkte Folge der stützenden Tätigkeit der bakteriellen Flotilline ist. FloA und FloT sind unterschiedlich in den FMMs von *B. subtilis* verteilt, wodurch sie eine heterogene Population von FMMs erzeugen, die verschiedene Signalwege abgrenzen kann. Interessanterweise erfolgt die Diversifizierung der FMMs nicht zufällig, sondern durch ein räumlich und zeitlich kontrolliertes Programm, um die Aktivierung von bestimmten Signalwegen am richtigen Ort und zur richtigen Zeit während des Zellwachstums sicherzustellen.

3. Introduction

The cellular membrane is a common feature of all living cells that defines a dynamic boundary within their environment. It is composed of a specific set of lipids and proteins, which act together to shield the cell from the outside and to orchestrate a vast number of signaling processes along and across the membrane (*1*). Exploring the structural organization of biological membranes has therefore been an important subject of research during the last decades (*2, 3*). In 1972 Singer and Nicholson proposed the so-called fluid mosaic model of the cellular membrane, in which protein clusters can freely diffuse within the discontinuous lipid bilayer and thus are distributed randomly (*4*). This concept was further developed in the following years as new research suggested that membranes are constituted by various lipid species with distinct physicochemical properties (*5*). The intrinsic properties of these lipids allow them to laterally segregate into membrane microdomains which are also capable of merging together due to their chemical affinity (*6*). This dynamic organization of lipids leads to a heterogeneous compartmentalization of the cellular membrane and favors a specific distribution of membrane-associated proteins (*7*).

The concept of membrane domains has been developed predominantly in the field of eukaryotic cell research. Early experiments evidence the presence of microdomains in the plasma membrane of epithelial cells, in which segregation of membrane components occurs strictly dependent on polarization and sorting of apical and basolateral lipids (*8*). Furthermore, it was shown that neurons contain microdomain structures which significantly contribute to the functionality of synaptic signal transmission, neuronal cell adhesion and axon guidance by clustering of glycosylphosphatidylinositol (GPI)-anchored receptor proteins as well as other receptors within the membrane microdomains (*9*). Yet, possibly one of the most important concepts in membrane organization describes the existence of membrane rafts or lipid rafts in the membrane of eukaryotic cells. Membranes of eukaryotic cells are able to compartmentalize a large number of proteins related to signal transduction

and membrane trafficking into membrane microdomains that are enriched in specific lipids, such as cholesterol or sphingolipids (*10*). The integrity of lipid rafts is important for the functionality of the signaling processes that are associated in such that any alterations in the molecular structure of lipid rafts may lead to severe defects in signal transduction in the cells (*11-15*), which seems to be related to the occurrence of severe diseases, such as Alzheimer's and Parkinson's disease (*16*).

The fundamental basis for the organization of lipid rafts is the lateral segregation of specific lipid species, namely sphingolipids and cholesterol into dynamic microdomains. These microdomains attract a specific set of proteins related to signal transduction and organize a variety of signaling processes (*10*). One of the raft-associated proteins is commonly referred to as reggie or flotillin (*11-15*). Flotillin proteins are membrane-bound chaperones that localize to lipid rafts, where they may recruit the proteins that need to be localized in lipid rafts in order to be active and facilitate their interaction and oligomerization (*11-15*). Thus, flotillin proteins are important components of lipid rafts and play a central role in their organization (*12, 14, 15*). The activity of flotillin is important for the correct functionality of numerous raft-associated cellular processes, including membrane sorting, trafficking, cell polarization, and signal transduction (*11-15*).

3.1 Membrane organization and the discovery of lipid rafts

Lipid rafts have been proposed as a model for membrane organization via select lipid species such as sphingolipids and cholesterol and the generation of specific physicochemical properties determined by their interactions. Sphingolipids associate laterally with each other in the membrane most likely via their carbohydrate head groups (*10*). The head groups of adjacent sphingolipid molecules occupy a larger area than their saturated sphingosine hydrocarbon chains, thus generating gaps in their tail regions that are filled by cholesterol molecules (*10*). As a result, tightly packed sphingolipid-cholesterol clusters constitute stable

raft-like assemblies in the cellular membrane, surrounded by more fluid regions that contain unsaturated phospholipids (*10*). Lipid rafts harbor a variety of protein components that are associated with specific lipids or via typical protein aggregates and flotillin is generally among these proteins (*17*). Flotillin is a membrane-associated protein that exhibits chaperoning functions and contributes to the organization of the protein complexes that are located in lipid rafts. Therefore, flotillins are considered to be important components of the structural integrity and functionality of lipid rafts (*11, 18*).

So far membrane domains have been studied intensively in eukaryotic cells due to their importance in key cellular processes. The presence of these microdomains was generally attributed to eukaryotes, because one of their major components is cholesterol. This steroid lipid is an essential component of the cellular membrane that confers structural integrity to the plasma membrane. Importantly, with very few exceptions, cholesterol is absent in membranes of prokaryotic species and therefore lipid rafts have been considered to be a fundamental step in the evolution of cellular complexity. Prokaryotes however seemed to be very simple organisms that do not specifically control membrane protein complexes and signaling networks by organizing microdomains in their membrane.

3.2 Functional Membrane Microdomains (FMMs) in bacteria

It has recently been shown that bacteria are able to spatially compartmentalize many signal transduction cascades and protein transport into specific regions of the cellular membrane that are referred to as Functional Membrane Microdomains (FMMs). The FMMs are constituted by aggregation of specific lipids of polyisoprenoid nature (*19*) and their co-localization with flotillin-like proteins, which are also present in bacteria (*20*). Bacterial flotillins seem to play a similar role as eukaryotic flotillins, acting as protein scaffolds in recruiting proteins that need to be localized in lipid rafts to promote interactions and

oligomerization (*21, 22*). Similar to their eukaryotic counterparts, flotillins in bacteria play an essential role in organizing and maintaining the correct architecture of the FMMs.

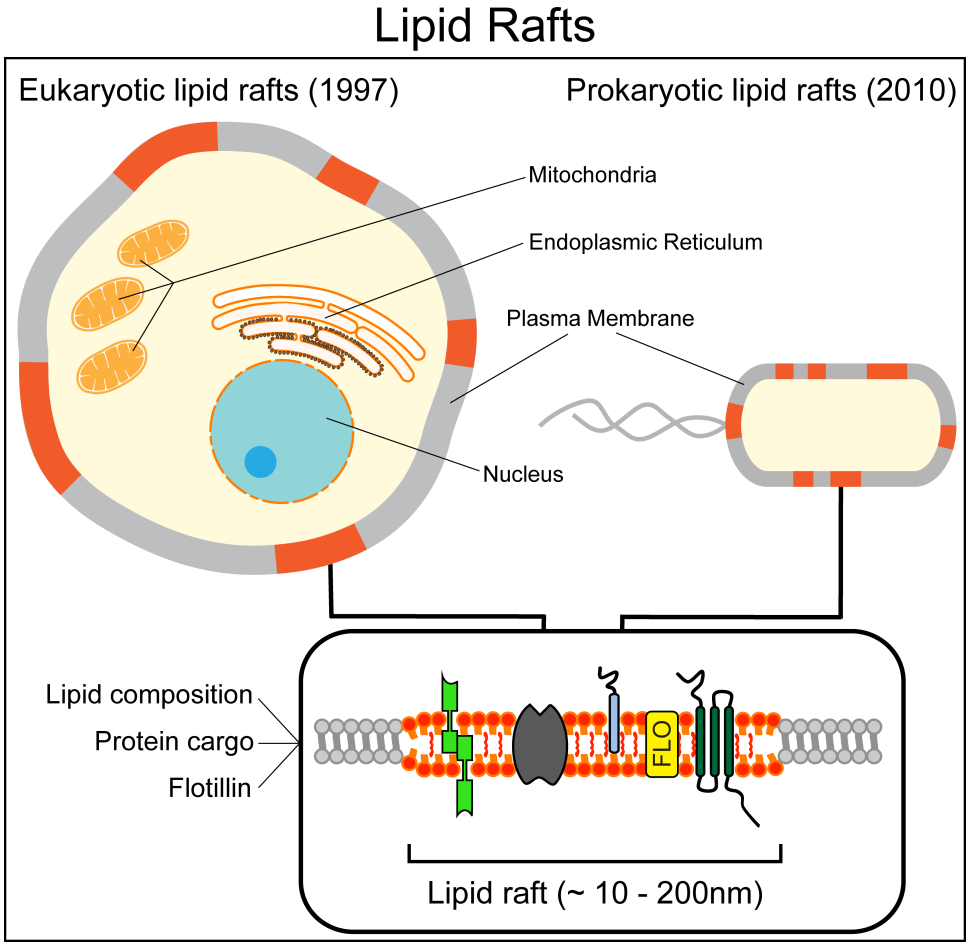

Figure 1. Eukaryotic and bacterial lipid rafts. Schematic representation of a eukaryotic (left) and a bacterial cell (right). Cellular compartments are indicated in the eukaryotic cell. Bacteria and eukaryotes both harbor lipid rafts in their plasma membrane. Lipid rafts are constituted by a specific set of lipids that include cholesterol and sphingolipids in eukaryotes and very similar lipid molecules in bacteria. The pool of lipid raft associated proteins is commonly referred to as the protein cargo. Flotillin proteins (FLO) localize exclusively in lipid rafts and contribute to the upkeep of the integrity of these membrane microdomains.

FMMs define a specialized area in the bacterial membrane, which is mainly constituted by polyisoprenoid lipids and probably other lipid species that due to their physicochemical properties preferentially localize to FMMs. The lipid composition of FMMs generates a nanoscale environment that is more hydrophobic than its surrounding area and

in these domains a specific pool of proteins tends to accumulate and become functional (*23*). This pool of proteins varies between physiological states of the cell during its life cycle. However, there are two structural components of the FMMs that define key properties and are present in any experimental condition. These are the constituent lipids that define the spatial segregation of FMMs in the membrane and the scaffold protein flotillin (*24*).

3.3 Lipid composition of FMMs

3.3.1 Sterol surrogates in bacterial membranes

Cellular membranes are composed of numerous lipid species that exhibit different molecular structure and physicochemical properties (*25*) and tend to aggregate into microdomains. This phenomenon, known as “lipid ordering”, is the organizing principle of membrane microdomains (*6, 26*) and is based on the ability of certain lipids like cholesterol and sphingolipids to laterally organize into microdomains in cellular membranes (*10*). Although the membranes of bacterial cells usually do not contain cholesterol and sphingolipids, they are equally composed of distinct lipid species that exhibit different molecular structures and physicochemical properties. Therefore, it is plausible that lateral segregation of these lipids into microdomains also occurs in bacterial membranes, in a similar fashion as it occurs in eukaryotic membranes (*6, 10, 27*). The lack of cholesterol in bacterial membranes made it seem unlikely that they could achieve a membrane organization similar to the one described for eukaryotic lipid rafts. There are however, a few notable exceptions of bacterial species that are able to incorporate eukaryotic cholesterol into their membranes (*Borrelia burgdorferi, Helicobacteri pylori*, *Mycoplasma spp., Ehrlichia chaffeensis* and *Anaplasma phagocytophilum*) (*28, 29*). In addition, there are four gram-negative bacteria known to produce membrane-associated sterols, namely *Nannocystis exedens*, *Polyangium spp.* and *Stigmatella aurantiaca* (Deltaproteobacteria) as well as *Methylococcus capsulatus* (Gammaproteobacteria) (*30, 31*).

3. Introduction

Despite the fact that bacteria generally lack cholesterol in their membranes, they harbor other lipid species with comparable physicochemical properties to cholesterol and therefore can provide the basis for a dynamic membrane organization and the formation of lipid raft equivalent membrane platforms. Genetic analyses have shown that a fraction of these lipids is of polyisoprenoid nature and structurally similar to eukaryotic cholesterol (*32*). These lipids are generally known as hopanoids and referred to as sporulenes in the case of *B. subtilis* (*33, 34*). Hopanoids are structurally diverse molecules (*35-41*). The simplest known hopanoid is diploptene (hop-22(29)-ene) and the most abundant class of hopanoids are hopanetetrols (e.g. tetrahydroxybacteriohopane) (*42*). Hopanoids are synthesized by the cyclization of the linear precursor molecule squalene, which is catalyzed by the squalene-hopene cyclase (SqhC) (*39, 40, 43, 44*). The biological role of hopanoids in bacterial membranes is still unclear but it is largely assumed that hopanoids modulate the membrane fluidity in order to increase the degree of lipid order or membrane rigidity (*45*) at higher temperatures. It is apparent that hopanoids are important for the correct functionality of numerous cellular processes and membrane-associated signal transduction cascades in bacteria (*33, 46-49*). Additionally, hopanoids can replace cholesterol in *Mycoplasma* cells without compromising cell growth (*46*). In fact, it has recently been demonstrated that hopanoid molecules are able to coalesce and induce phase separation when inserted into membranes (*45*). This suggested that hopanoids can act as bacterial cholesterol surrogates because they mediate lipid ordering, membrane rigidity and thus presumably play an important role in the organization of bacterial FMMs, similar to the function of sterols in eukaryotic lipid rafts.

In addition to hopanoids, bacteria harbor another class of terpenoid lipids called carotenoids (*50*). These non-cyclic polyisoprenoid lipids are produced either by condensation of two geranylgeranyl pyrophosphate (GGPP) subunits or two molecules of farnesyl pyrophosphate (FPP). They possess a variety of interesting properties that most likely have been evolved from a simple mechanical function in Archaea, where they were found to

reinforce cellular membranes (*51*). Notably, bacterial carotenoids effect membrane stabilization by bilayer condensation and increasing rigidity in an analogous manner to hopanoids and sterols of eukaryotic cells (*50*). Due to the structural diversity of carotenoid molecules, it is likely that they affect the structure and physiology of the bacterial membrane in many different fashions. A recent study in the gram-positive pathogen *Staphylococcus aureus* has shown for example that their golden pigment, a carotenoid termed staphyloxanthin, acts as a potent antioxidant via its ability to scavenge free oxygen radicals and therefore, the bacteria are able to evade oxidant-based killing by the host innate immune system (*52*). Furthermore, it was shown that several *Bacillus* species are able to produce carotenoids (*53, 54*), which contributes to the notion that a variety of lipids are important for the functional upkeep of bacterial FMMs (*32, 53, 54*).

In *Bacillus subtilis*, polyisoprenoid lipids are produced via the biosynthetic pathway that requires the action of the squalene synthase YisP (*32*). Similarly, the closely related gram-positive bacterium *Staphylococcus aureus* utilizes the enzyme CrtM to produce the carotenoid precursor molecule dehydrosqualene. Importantly, the integrity of bacterial FMMs is strongly affected in mutants lacking the *yisP* gene and thus carotenoids or hopanoids as a structural FMM component (*32*). As a consequence of the destabilized structure, protein components cannot be correctly localized in the Functional Membrane Microdomains and the functionality of these proteins is affected (*32*). These findings illustrate that polyisoprenoid lipids are very important components of bacterial FMMs and that the absence of those lipids in *B. subtilis* leads to a delocalization of kinase and flotillin proteins, which in turn affects a variety of cellular processes.

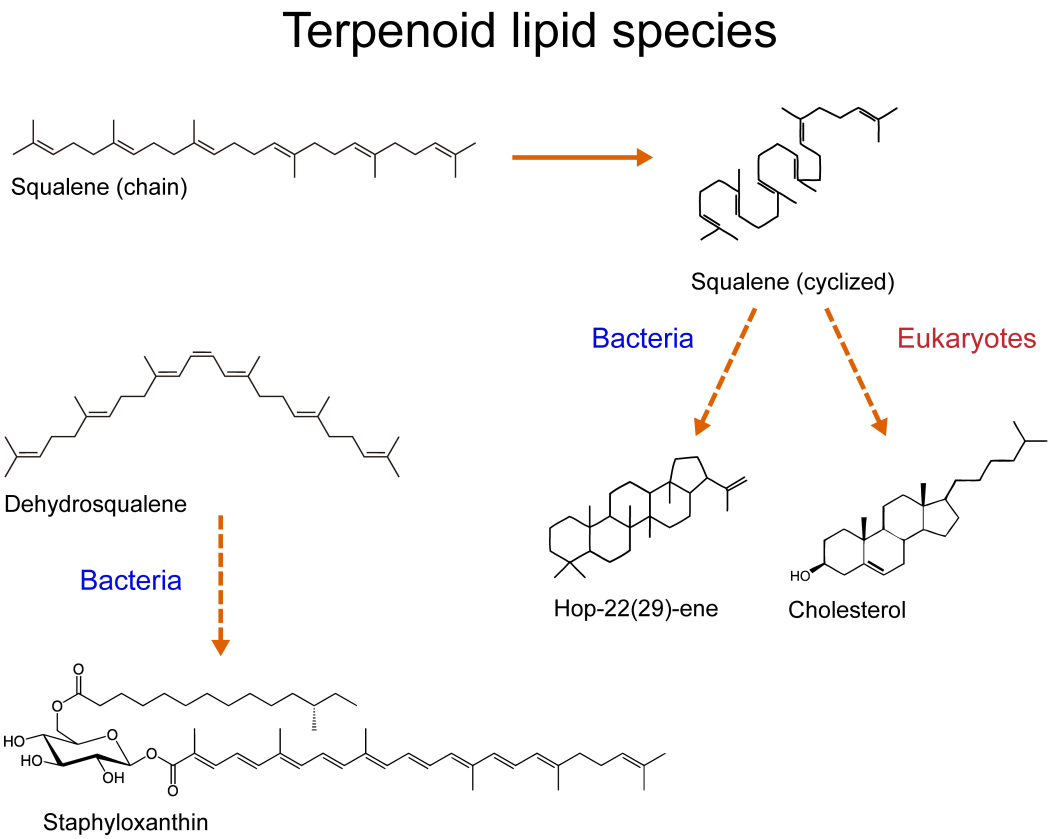

Figure 2. Terpenoid lipids. Squalene and Dehydrosqualene are both synthesized from the precursor molecule Presqualene diphosphate. Linear squalene molecules are synthesized and cyclized by both, eukaryotes and prokaryotes via similar enzymes. Bacteria synthesize hopanoids (Hop-22(29)-ene) or carotenoids (Staphyloxanthin), while eukaryotes possess specialized enzymes that allow them to generate the structurally more complex sterols (Cholesterol). Dashed lines indicate several intermediate synthesis steps.

3.3.2 Bacterial phospholipids

In membranes of the model organism *B. subtilis* cardiolipin was identified as a structural component that forms domains predominantly in septal and polar regions (*55*). Cardiolipin is a phospholipid with a glycerol backbone and a major component of membrane domains in mitochondria and in many bacteria (*56*). It is synthesized by cardiolipin synthases via the condensation of two phosphatidylglycerol molecules into a dimeric structure. These molecules were also described as flexible linkers that fill gaps at protein interfaces and thus stabilize interactions between subunits of oligomeric proteins and higher-order complexes (*57*). Another feature of cardiolipin is its ability to induce negative curvature to the lipid

bilayer, which explains the preferential localization to cell division sites and poles (*55, 58*). It has been shown that cardiolipin is an essential component for the functionality of membrane-bound protein complexes that are involved in energy metabolism in mitochondria (*59*). In bacteria, the correct localization and functionality of many proteins seems to be dependent on septal or polar cardiolipin domains, including for example the *E. coli* osmo-sensory transporter ProP, the *V. cholerae* Eps system to export the cholera toxin as well as *B. subtilis* cell division proteins MinD and FtsA/FtsZ (*60-62*). Furthermore, it has been shown that the gram-positive pathogen *Staphylococcus aureus* requires cardiolipin for survival in high-salt conditions and mutants of *E. coli* and *B. subtilis* lacking cardiolipin display severe growth defects in these conditions due to the high osmotic stress (*60, 63, 64*). These reports evidence that cardiolipin is a very important component to modulate membrane composition and fluidity, which has also been shown recently in an *in vitro* system (*65*). Interestingly, the *B. subtilis* flotillin FloT is upregulated specifically during stationary growth phase. At the same time, cardiolipin is very abundant in cells and it was shown that it could be co-purified with FloT from cellular membranes (*56, 66*). It is therefore likely that cardiolipin is an important component of bacterial FMMs, which assists in the recruitment of specific proteins to FMMs and thereby resembling the role of sphingomyelin in eukaryotic lipid rafts.

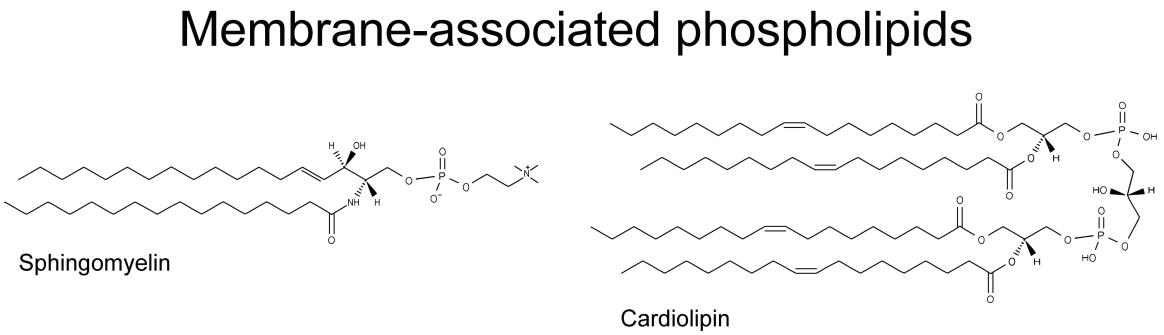

Figure 3. Membrane-associated phospholipids. Cardiolipin influences membrane fluidity and can be found in eukaryotic as well as prokaryotic cells. Sphingomyelin is a sphingosine-based phospholipid found in eukaryotic lipid rafts. The molecular structure of cardiolipin closely resembles the one of sphingomyelin.

3.4 The flotillin protein family

Flotillin proteins were initially described in 1997 with two different terminologies (*67, 68*). The description of flotillin was derived from proteins detected in detergent resistant membrane (DRM) fractions of mouse brain tissue that were buoyant in a sucrose gradient (from the floating membrane fraction, hereof its name of "flotillin") (*67*). This technique was used to isolate caveolae, which were already considered as detergent-insoluble membrane microdomains containing a specific set of proteins that are important for particular cellular functions and also flotillin as a marker protein (*67*). These studies were simultaneously published with another independent investigation showing an increased expression of the same protein during axonal regeneration in goldfish retinal ganglion cells. Because of this, the protein was called reggie (*68*). Both studies demonstrate the presence of two distinct proteins referred to as flotillin-1 and flotillin-2, or reggie-1 and reggie-2, respectively. Later it became evident that reggie-2 and flotillin-1, as well as reggie-1 and flotillin-2 were essentially the same proteins. For simplicity, I will not use the reggie terminology in this dissertation. Both flotillins are ubiquitously present in mammalian tissues, associated with each other in hetero-oligomeric complexes (*12, 13, 15, 69*) and seem to have a strong regulatory correlation (*70-72*).

Bioinformatic analyses revealed that eukaryotic flotillins are part of the SPFH (stomatin, prohibitin, flotillin and HFLK/C) domain containing protein family (*73*). Band 7 and PHB (prohibitin) domain are synonyms of the SPFH domain that are often used in the literature. Eukaryotic flotillins are associated with the plasma membrane presumably via their N-terminal PHB domain that shows characteristic acylation sites and hydrophobic hairpin structures (*11*). PHB domains also seem to be important for the general functionality of flotillin proteins but their exact role is unknown to date (*73*). The C-terminal part of flotillin-like proteins harbors an alpha helical coiled-coil region that is well conserved within their family and mediates oligomerization as well as other specific protein-protein interactions (*74*).

Studies in recent years using homology searches and advanced sequence analyses revealed that flotillin-like proteins are present in all domains of life, e.g. archaea, bacteria and eukarya (*32, 73, 75*). This implies that flotillin proteins and lipid rafts are very ancient components commonly found in cells and used by them to modulate cellular processes.

3.4.1 Eukaryotic flotillins

Eukaryotic flotillin-1 and flotillin-2 are highly homologous proteins that share 47% identity and 71% similarity (*76*). Flotillin-1 and flotillin-2 are anchored to the cytoplasmic membrane by their N-terminal regions via myristoyl and palmitoyl moieties respectively, like many other proteins that are known to localize in lipid rafts (*77, 78*). The N-terminal region is adjacent to the PHB domain that seems to play a role in the functionality of the protein. The C-terminal coiled-coil region, also referred to as “flotillin domain”, is characterized by several repeats of glutamic acid and alanine (EA repeats) (*67*). This C-terminal region is believed to participate in the formation of homo– and hetero-oligomeric complexes at the plasma membrane between flotillin-1 and flotillin-2 (*79*). The oligomerization of flotillins is thereby dependent on the C-terminal EA repeat motifs (*74*) but the precise mechanism whereby the two flotillins interact is rather unknown.

Since their discovery as proteins involved in neuronal regeneration, flotillins have been shown to participate in many other important cellular processes. For instance, flotillins participate in the endocytosis of GPI anchored receptor proteins that are known to co-cluster with them in lipid rafts (*80, 81*). Moreover, flotillins are involved in remodeling and regulation of the actin cytoskeleton as well as endosomal cargo protein sorting and recycling (*81-83*). However, one of the most relevant roles of flotillin proteins is to mediate receptor clustering and signal transduction in cellular membranes. This has been shown recently for several receptor tyrosine kinases like the insulin receptor, the Immunoglobulin E receptor and the epidermal growth factor receptor (EGFR) (*84-86*). Remarkably, foltillin-1 was shown to first

control EGFR clustering in the membrane and after that, act as scaffold protein for mitogen activated protein kinases (MAPK) during signaling (*86*). These are some of the most important examples that describe the scaffolding functions of flotillins in eukaryotic systems.

Understanding the precise role of flotillin is of particular importance, considering the role of this protein in the development of severe human neurodegenerative disorders like Alzheimer's or Parkinson's disease. Animal studies revealed increased levels of flotillin-1 gene expression in the substantia nigra of patients brains with Parkinson's disease and excess of flotillin-1 protein in catecholamine secreting cells (*87*). Likewise, Alzheimer's disease is mainly caused by senile plaque formation. The amyloid β precursor protein (APP) is processed to generate the amyloid β peptide (Aβ) that accumulates and forms extracellular neurotoxic plaques. Processing of APP very likely takes place in lipid rafts and flotillin-1 has been shown to directly bind to the secretase protein that is involved in the processing of APP, thereby positively influencing its trafficking via endosomes and its retrograde recycling (*83, 88*). Hence, flotillin-1 deficient cells accumulate secretases at lipid rafts that process APP and this leads to an increased production of the toxic Aβ peptide. Interestingly, flotillin-2 was shown to act as a scaffold protein that clusters APP in a cholesterol dependent manner and thus influences its endocytosis and processing (*89*).

Taking into account various reports of flotillin involvement in cellular growth and physiology via their role in signaling and actin cytoskeleton remodeling, it is not surprising that they are functionally associated with several types of cancer. In 2004 a study directly linked flotillin-2 overexpression with malignant melanoma progression and furthermore evidenced that flotillin-2 is highly expressed in different melanoma cell lines (*90*). The same study also found that flotillin-2 overexpression leads to the transformation of non-malignant melanoma cells into a highly metastatic state (*90*). Interestingly, it has been shown that flotillin-1 is highly expressed in breast cancer and its increased expression could be directly

correlated with poor survival of patients, while a different study evidenced that flotillin-2 was linked to the progression of this disease (*91, 92*). Moreover, flotillin-1 has recently been revealed as a marker protein for gastric cancer (*93*). Therefore, flotillins are nowadays more and more considered as prognostic cancer markers (*94*).

3.4.2 Bacterial flotillins

The presence of SPFH-containing proteins that are likely flotillins was demonstrated in diverse bacterial species, including gram-positive, gram-negative and archaeal organisms (*73*). Because bacterial flotillins show a highly similar domain organization as their eukaryotic homologues, it is reasonable to think that they could play a similar role as eukaryotic flotillins. The flotillin-homolog protein YqiK of the model organism *E. coli* for example has been suggested to play a role in maintaining membrane integrity (*95*). In addition to that, two other SPFH domain proteins are present in the *E. coli* membrane presumably acting as chaperones that assist in membrane protein quality control (*95*). YqiK is structurally similar to eukaryotic flotillins, showing a N-terminal transmembrane region adjacent to the SPFH domain and a C-terminal region that is enriched in EA repeat motifs.

However, there is a general lack of information regarding the structural and biological role of YqiK in *E. coli* because most of the experiments that explore the role of bacterial flotillins have been performed in gram-positive bacterial models. First experimental evidence of the association of bacterial flotillins to specific regions of the cellular membrane occurred when the protein content of the DRM fraction from the gram-positive bacterium *B. halodurans* was analyzed (*96*). Importantly, this study also showed that the flotillin-homolog protein BH3500 is an alkali inducible protein that shares common features of flotillin proteins, e.g. SPFH domain, flotillin domain and EA repeats (*96*). This study was preceded by several bioinformatic studies that pointed out genes coding for flotillin proteins in bacteria and therefore evidence the existence of bacterial flotillins. For instance, Tavernarakis *et al.*

detected HflK/C and flotillin proteins in bacteria and archaea homologous to their eukaryotic counterparts using genome sequence analyses (*73*). Specifically, these analyses revealed that the *B. subtilis* protein YuaG is located within the eukaryotic flotillin branch and thus evidenced high homology to eukaryotic flotillins (*73*). Similar to the BH3500 protein from *B. halodurans,* the expression of YuaG is highly induced in alkaline conditions (*97, 98*).

An important hallmark paper was reported in 2009 showing that YuaG organizes in discrete focal assemblies and distributes heterogeneously across the cellular membrane (*66*). This subcellular localization is similar to the pattern that was reported for eukaryotic flotillin in cellular membranes. The same report also showed that YuaG co-purified in DRMs with phosphatidlyglycerol or cardiolipin although the punctate distribution could not exclusively be attributed to interactions with these membrane lipids (*66*). In addition, the study also showed that a *yuaG* mutant in *Bacillus subtilis* was defective in endospore formation, which is one of the most intricate signal transduction pathways that are described in prokaryotic development (*66*). Hence, this report evidenced a connection between the presence of flotillin and the functionality of a signal transduction cascade in bacterial cells, in this case the sporulation pathway of *B. subtilis*.

A direct link between bacterial flotillins and FMMs was shown in 2010, when identified YqfA, a second flotillin of *B. subtilis* to colocalize with YuaG in discrete membrane puncta (*32*). It was also revealed that the two flotillins of *B. subtilis* influence signal transduction processes via their interaction with the histidine kinase C (KinC) in FMMs (*32*). Interestingly, depletion of polyisoprenoid lipids led to impaired functionality and localization of FMM associated proteins as well as disruption of cellular processes like biofilm formation, protein secretion and sporulation (*32*). This suggested a role of flotillins in conveying integrity to bacterial FMMs and consequently, mutants of *B. subtilis* lacking flotillins were defective in a number of cellular processes such as activation of natural competence, sporulation, motility,

cell division and cell shape, protein secretion and transport as well as regulating membrane heterogeneity (*99-101*). YuaG and YqfA were thereafter renamed FloT and FloA, respectively (*32, 99*). Very interesting mechanistic insights of bacterial flotillin functionality were elucidated when FloA and FloT were found to interact with the AAA membrane-bound protease FtsH and it was revealed that this interaction stabilizes the protease in FMMs (*101, 102*). Thereby it was demonstrated that flotillins could ultimately control processes like biofilm formation and sporulation.

Although flotillin proteins of *B. subtilis* differ in size, FloT (509aa) being larger than FloA (331aa), they have a similar molecular structure. Both flotillins are anchored in the membrane via one N-terminally located transmembrane region, followed by the characteristic PHB domain and a C-terminus containing typical EA repeat rich coiled coils. Simultaneous overexpression of *floA* and *floT* genes causes pleiotropic effects in differentiation and cell division, which do not occur in cells overexpressing only a single flotillin (*101*). Interestingly, cells lacking both flotillins show severe disruptions in FMM associated processes, which are not evident when either *floA* or *floT* are deleted from the genome (*102*). In relation to these observations it is important to mention that eukaryotic flotillin-1 and flotillin-2 show a functional and regulatory correlation accompanied by characteristic formation of homo- and hetero-oligomeric complexes (*103, 104*). Thus, based on their structural and functional resemblance, bacterial flotillin proteins seemed to behave alike and it was generally assumed that flotillins play redundant roles in the complex microdomain environment.

There is a growing interest in the scientific community in the existence of FMMs and flotillins in bacterial membranes and consequently, a number of reports are arising describing the physiological effects associated with flotillins in other bacterial systems. As an example, a flotillin protein seems to be essential in *Campylobacter jejuni* for bacterial adhesion and host cell invasion and it is likely involved in cell wall organization (*105*).

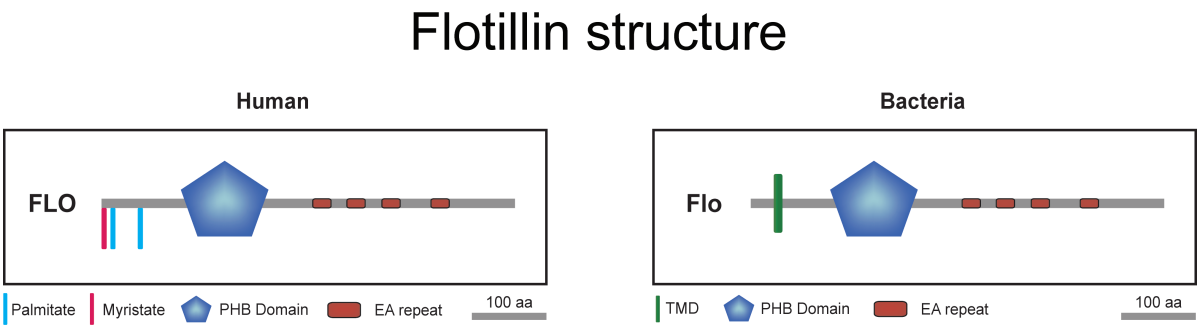

Figure 4. Flotillin structure. Human flotillins (left panel) attach to the cellular plasma membrane via palmitate or myristate residues. Bacterial flotillins (right panel) are anchored to the cellular membrane via transmembrane domains (TMD). Prokaryotic and eukaryotic flotillins both harbor the flotillin-characteristic PHB domain and amino acid repeats of glutamic acid and alanine (EA repeats). The scale bar indicates length of 100 amino acids (aa). Figure modified from Schneider *et al.*, *PLoS genetics* **11**, e1005140 (Apr, 2015).

3.5 Protein cargo of bacterial FMMs

Eukaryotic lipid rafts as well as FMMs of bacteria are of particular importance for proper regulation of various developmental and physiological processes. Due to their physicochemical properties these membrane regions are capable to attract and organize a specific set of proteins in space and time and facilitate the assembly of multiprotein complexes and signaling networks. To gain a better insight into the signaling networks and protein complexes that are regulated specifically by lipid rafts or bacterial FMMs, it is important to explore and characterize the pool of proteins that associates with FMMs and study how their functionality is affected when FMMs are perturbed. The separation of FMM associated proteins from the bulk of membrane proteins is usually achieved by detergent extraction followed by zonal centrifugation in a sucrose gradient and subsequent isolation of the DRM fraction. Proteins and lipids that are enriched in DRMs can then be detected but it is important to point out that DRMs are not considered as microdomain equivalents (*7*). Thus, further analyses of the identified components have to be conducted using various biochemical or biophysical approaches to ensure that the proteins detected belong to the cargo of FMMs (*106*). The experimental approach that is currently developed in our laboratory aims at validating whether one specific protein of interest belongs to the protein

cargo of the FMMs via verifying its direct interaction with the scaffold protein flotillin. In order to assay protein-protein interactions, pulldown experiments with flotillin or bacterial-two hybrid (BTH) screens can be used. Also, fluorescently labeled flotillin proteins can be colocalized with a specific protein of interest in FMMs by microscopy. Another approach to find proteins associated with FMMs relies on comparing isolated DRM fractions of the wildtype strain and a mutant lacking flotillins. Proteins missing in mutant strain DRMs but not in wildtype can then be examined in detail using the abovementioned methods.

Recent studies uncovered several proteins in DRM fractions of *B. subtilis* that are related to key regulatory processes like sporulation, protein secretion, cell division and biofilm formation (*32, 100, 102*). In order to form a biofilm, cells need to activate the genes of the *epsA-O* and *tapA-sipW-tasA* operons that control the production of exopolysaccharides (EPS) and amyloid protein components (TasA), which together form a rigid extracellular matrix (*107, 108*). The activation of the master regulator Spo0A in turn is required to control the expression of *eps* and *tasA* genes and thus biofilm formation (*109-112*). Spo0A itself is activated upon transfer of phosphoryl-groups by five different kinases (KinA-E) via the Spo0F/Spo0B phosphorelay (*113, 114*). Although most of the signals that activate these kinases and subsequently biofilm formation are unknown so far, it has recently been described that *B. subtilis* produces a signaling molecule called surfactin, which activates the histidine kinase C (KinC) (*115, 116*). KinC was thereafter detected in the DRM fraction and thus further investigated as possible candidate of FMM cargo (*32*). The localization of the signaling kinase in FMMs depended on the presence of flotillins FloA and FloT, and furthermore colocalization of KinC with FloT was shown (*32*). A mutant strain lacking both flotillins was not able to form biofilms in response to surfactin most likely due to KinC mislocalization and thus disrupted signaling, similar to a *kinC* defective strain (*32*). However, it is important to note that FloA and FloT are scaffolding proteins that assist in the localization of a variety of other proteins, but they are not absolutely required for the activity of these proteins. Therefore, it is possible that variations in the functionality of flotillin-associated

proteins can be detected using different experimental conditions (*117*). Interestingly, KinC was not present in the DRM fraction of a biofilm defective strain lacking YisP, a protein that produces lipid components of FMMs (*32*). Lastly, biofilm formation could be restored in the *ΔyisP* mutant by introducing a constitutively expressed version of *spo0A* that did not need to be activated by KinC (*32*). Theses results consolidated KinC as part of the protein cargo of *B. subtilis* FMMs. They furthermore evidenced that different components such as flotillin proteins and lipids are necessary for the integrity and proper functionality of FMMs and associated cellular processes.

After the initial discovery of FMMs in *B. subtilis,* more and more proteins belonging to the protein cargo were discovered. The protease FtsH for example was found to reside in DRM fractions and interacted with FloA and FloT (*102*). Interestingly, FtsH negatively affects the activation of Spo0A via phosphorylation by degrading the regulatory phosphatases RapA, RapB, RapE and Spo0E (*118*). In a *ΔftsH* mutant, decreased levels of active Spo0A~P lead to a severe defect in sporulation which was not observed in a strain lacking *kinC* (*102, 119*). Interestingly, *E. coli* harbors HflK/C proteins that are responsible for the correct oligomerization of FtsH (*120*). Thereby, they negatively regulate the activity of the metalloprotease FtsH in a similar fashion as it has been described for eukaryotic SPFH proteins, which negatively affect the activity of the m-AAA protease, a FtsH-homologous protein in *S. cervisiae* mitochondria (*121*). Nevertheless, HflK/C are not present in *B. subtilis* but since these proteins belong to the SPFH protein family, it was assumed that FloA and FloT might have an analogous function and thus effect FtsH oligomerization (*102*). Similar localization patterns were observed for fluorescently labeled FtsH and flotillin proteins in cellular membranes of *B. subtilis* and colocalization was observed predominantly in septal regions (*102*). This further indicated the interaction of FtsH with the flotillins FloA and FloT, which in addition were less dynamic when they localized in the septum (*102*). Moreover, the Δ*ftsH* mutant was shown to be defective in biofilm formation presumably because cells are not able to differentiate efficiently into matrix producers (*102*). Accordingly, recent analyses

have shown that overexpression of FtsH resulted in increased biofilm formation likely due to the high level of active Spo0A~P (*101*). Furthermore, overproduction of the two flotillins FloA and FloT resulted in high FtsH activity that led to cell length reduction caused by the formation of an increased amount of FtsZ rings and thus uncontrolled cell division (*101*). Regarding this effect on cell division, it was not surprising to find EzrA, a protein that negatively regulates FtsZ, in the DRM fraction of *B. subtilis* and subsequent analyses have shown that EzrA levels are down-regulated in a FloA/T or FtsH overexpressing system (*101*). These findings altogether show that *B. subtilis* flotillins function as chaperones yet in contrast to eukaryotic and *E. coil* SPFH proteins they positively influence FtsH activity and that EzrA is a substrate of the FtsH protease.

To identify direct interaction partners of FloT, pulldown experiments coupled with co-localization studies have been performed and revealed interactions between FloT and the protein SecY, which is part of the Sec protein secretion machinery (*100*). Furthermore, it was shown that the proper function of the Sec machinery depended on the presence of negatively charged phospholipids like cardiolipin in the membrane (*122, 123*), which provided another indication that Sec proteins localize in FMMs of bacteria, where flotillins presumably assist in their oligomerization. A similar experimental strategy was used to identify the ABC transporter type proteins OppA and FtsX as part of the protein cargo (*100*). In *B. subtilis*, Opp proteins actively transport small Phr peptides into the cell in a cell density dependent manner (i.e. quorum sensing) where they regulate processes like sporulation and genetic competence (*124*). Gram-negative bacteria also harbor Opp transporter proteins but in contrast, they are usually involved in recycling of cell wall components during growth (*125*). Besides FtsX, other proteins involved in cell wall metabolism identified via pulldown with FloT were Pbp5, TagU and GtaB (*100*). Together with FtsE, FtsX forms an ABC transporter module that controls the activity of essential peptidoglycan hydrolases during cell wall elongation while Pbp5 only affects peptidoglycan maturation in vegetative cells (*126, 127*). GtaB participates in teichoic acid synthesis and TagU is responsible for their attachment to

the cell wall (*128, 129*). Teichoic acids are major anionic cell wall polymers with various critical functions such as maintenance of cell shape, cation homeostasis and various aspects of pathogenesis (*128*). Importantly, *B. subtilis* mutants that are lacking either *floA* or *floT* did not present an abnormal cell shape (*99*). Mutants lacking both flotillins however displayed severe membrane distortions and irregularly shaped cells (*99*), pointing to the existence of a functional link between flotillins and cell wall metabolism in *B. subtilis*.

3.6 Experimental approaches that are suitable to study bacterial FMMs

The molecular architecture of FMMs has traditionally been studied in *B. subtilis* using molecular genetics and biochemical approaches. This methodology includes the purification and analysis of the DRM fraction via mass spectrometry, pulldown approaches coupled to fluorescence microscopy experiments and physiological studies comparing mutants that are defective in any of the structural components that constitute the bacterial FMMs. It is important to remark that the majority of approaches that have been developed so far address the study of flotillin proteins while only a limited number of techniques are available to explore the nature and organization of the constituent lipids of the FMMs.

An interesting new approach has recently been introduced in the study of bacterial FMMs. This is the blue native polyacrylamide gel electrophoresis (BN-PAGE), which is a very effective and sensitive electrophoretic approach suited for the separation of membrane-associated proteins in their native oligomeric state (*130*). BN-PAGE was developed by Schagger and van Jagow in 1991 and initially used to study membrane supercomplexes in yeast, mammalian and plant mitochondria (*131-133*). In general, membrane protein complexes with molecular weights between 10 and 10 000 kDa can be resolved and in combination with other techniques, the molecular structure, oligomeric state or enzymatic activity of proteins within the complexes can be determined (*134-136*). To ensure that complexes are preserved in their native state they are treated at low temperature and neutral

pH (*137*). In bacteria, mild non-ionic detergents such as n-dodecyl-β-d-maltoside (DDM), Triton X-100 or digitonin are commonly used to solubilize lipophilic membrane complexes and to prevent disruption of physiological protein-protein interactions (*138, 139*). The application of BN-PAGE enabled researchers to investigate diverse aspects of the oligomerization properties of protein complexes like the multidrug efflux transporter AcrAB (*140*), the SecYEG secretion system (*141*), the twin-arginine translocation system (Tat) (*142*), the ATP synthase (*140*), the cytochrome bd oxidase (*143*) and the proton-pumping NADH:ubiquinone oxidoreductase (*144*). Interestingly, a recent study found that purified PHB domains from the *B. subtilis* flotillin FloT form different oligomeric complexes using size exclusion chromatography (SEC) and BN-PAGE (*145*). By further analyzing their properties, the same study showed that extracted PHB domains are not capable of binding neither to isolated *B. subtilis* membranes nor to *E. coli* specific lipids (*145*). In contrast to the role of the PHB domains in eukaryotic flotillins where they mediate tethering to the membrane, these results indicated that PHB domains of prokaryotic flotillins are important for oligomerization and that they do not facilitate membrane association (*145, 146*). However, it is worth mentioning that posttranslational modifications are necessary in PHB domains for eukaryotic flotillins to become functional, which is dependent on their interaction via the C-terminal EA repeats (*74, 103, 147*).

Recent advances in fluorescence microscopy that occurred in the last decades provide a powerful tool for the visualization and analysis of bacterial membrane microdomains. A diverse array of fluorescent probes with specific physicochemical properties can be used to study organization and features of the cellular membrane. These include for example the earlier mentioned dye NAO, which accumulates in cardiolipin-rich domains in *B. subtilis* membranes. Laurdan is another example of polarity-sensitive dyes that is used to study membrane fluidity (*148-150*). This dye inserts into the lipid bilayer and displays a phase-dependent shift of the emission spectrum (*151*). Lipid rafts generally display tightly ordered lipids in membrane domains excluding water molecules and in these membrane

regions, Laurdan exhibits a blue shift of its emission spectrum. In the rest of the cellular membrane water molecules accumulate and the emission spectrum is red shifted. However, the low photostability of Laurdan only allows its visualization using 2-photon microscopy (*152*). Microscopy studies using Laurdan have provided several evidences for lipid domain co-existence in eukaryotes, bacteria and model membranes, demonstrating that this approach can be used to analyze cellular membrane organization (*100, 153-155*). Moreover, a recent study in *B. subtilis* shows that the actin homologue MreB generates membrane domains with increased fluidity and this was visualized using Luardan and the lipid dye Nile Red (*154*). This work also shows that the succinate dehydrogenase (SdhA) and F_0F_1 ATPase (AtpA), two proteins that have previously been associated with FMMs in bacterial membranes, do not localize in regions with increased fluidity (*32, 100, 154*).

Despite the fact that several raft-specific dyes exist to explore the existence of FMMs in bacteria, visualization of these nanometer-scale domains has been challenging because of the limitations inherent in the spatial resolution of the diffraction limit of visible light in conventional fluorescence microscopes. Nevertheless, there are several microscopy techniques that currently enable sub-diffraction imaging of cellular structures. Those include techniques that use information contained in evanescent waves like near field scanning optical microscopy (NSOM), 4Pi microscopy and other wide-field microscopic approaches such as I^5M microscopy and structured-illumination microscopy (SIM) (*156-159*). These microscopic techniques allow a resolution of cellular structures in the range of 50-100nm.

Furthermore, far-filed microscopy approaches, such as stochastic optical reconstruction microscopy (STORM), direct STORM (dSTORM), photoactivated localization microscopy (PALM) and stimulated emission depletion (STED) are capable of reaching 20 to 30 nm lateral and 50 to 60 nm axial resolution (*160-164*). Sub-diffraction resolution in STED microscopy is achieved by excitation of the target fluorophore and simultaneous de-excitation

of the surrounding fluorophores with a doughnut shaped spot of longer wavelength (*163*). This is a very fast process that allows acquiring of super-resolution images in living cells with 5 to 8 times higher precision than conventional confocal microscopy (*163*). PALM and STORM techniques both are based on the use of photoactivatable fluorescent probes, which can be reversibly switched into “on-state“ and “off-state” by exposure to different wavelengths of light. Using this technique, single fluorophore molecules can be localized in cells with highest precision (*161*). One such example is a study utilizing the photoswitchable protein Dronpa that was coupled to either θ-toxin or lysenin molecules, which show high affinity for cholesterol or sphingomyelin, respectively (*165*). PALM imaging of these probes consequently revealed cholesterol- and sphingomyelin-microdomains in the eukaryotic membrane with sizes of 118 to 124 nm (*165*). Another very interesting study focused on the localization of Lck, a protein tyrosine kinase involved in many signaling cascades that is targeted to lipid rafts via its acylated N-terminus (*166*). Lck fused to the photo-convertible protein tdEos and imaged using PALM and dSTORM revealed clusters of the kinase at the plasma membrane with a size of 20 to 190 nm (*166*). Two color PALM superresolution images also evidenced the difference between Lck, showing typical raft localization and the N-terminal part of the Src kinase that is also organized in similarly sized clusters but does not localize to raft domains because it harbors a different membrane targeting sequence (*166*). Remarkably, imaging the scaffolding protein LAT with dSTORM revealed that microclusters of these proteins are very diverse in size and molecular density (*166*). As an alternative to light microscopy, many researchers focus on the use of electron microscopy (EM) approaches. Techniques like transmission electron microscopy (TEM) or electron cryotomography (ECT) have been used to study membrane structures of eukaryotic and prokaryotic cells in great detail (*167, 168*). With the use of TEM, a recent study has shown that raft-like membrane platforms are present in the bacterium *Borrelia burgdorferi* (*169*). Modern electron microscopy techniques even enable atomic resolution (< 0.05 nm) and provide an unparalleled level of detail (*170*). However, a considerable disadvantage of EM techniques is that biological samples need to be prepared by chemical or cryo-fixation and

thus only allow for the analysis of structural properties. Therefore, cutting-edge light microscopy techniques like SIM, dSTORM or PALM are very well suited to study dynamic nano-scale structures such as membrane microdomains and associated protein complexes in living cells.

3.7 Microdomain heterogeneity

An increasing number of evidences suggest that different types of lipid rafts are simultaneously present in cellular membranes. It is likely that a spectrum of membrane microdomains exists with different compositions and physical characteristics suited to diverse purposes due to the different turnover rates, which could be generated by their main constituents. In 1995, a study by Schnitzer *et al.* first indicated that the total population of DRMs contained different types of microdomains (*171*). The basic components that organize lipid rafts are the constituent lipids, sphingomyelin/ cholesterol and residual proteins. A significant level of diversity has been shown for the levels of cholesterol in different rafts or the affinity of cholesterol for specific microdomains (*172*), which points to the existence of a first level of complexity among different rafts harboring a different lipid composition. Second, a number of studies have shown that alterations in sphingolipid content determined the recruitment of several proteins to or exclusion from lipid rafts (*173-175*). Furthermore, the factor that contributes most to lipid raft diversity are the residual proteins. As protein cargo of rafts can be affected by the lipid content and vice versa, both components are very important for structure determination of the membrane domains (*176*). Moreover, proteins can be targeted to lipid rafts via a multitude of mechanisms. These include the GPI anchor, fatty acylation and protein-based targeting motives such as specific transmembrane domains or for example the sorbin homology domain (SoHo), which facilitates interaction with the lipid raft marker protein flotillin (*177-182*). Altogether, these data strongly suggest that lipid-lipid, lipid-protein and protein-protein interactions generate lipid raft heterogeneity.

Consequently, this raises fundamental questions: Why do cells need a heterogeneous population of lipid rafts and how do they control this heterogeneity? It is very likely that different types of lipid rafts are needed to carry out a whole array of diverse functions, which have been attributed to them. However, so far we know very little about different types of lipid rafts and how cells control their heterogeneity in eukaryotes. Analyzing complex signaling networks, protein complex formation and membrane organization in eukaryotic systems is a very challenging task. Therefore, we chose the model organism *B. subtilis* to study FMMs, which are regarded as bacterial lipid raft equivalents (*183*). This model system can be easily manipulated and thus facilitates investigating complex cellular processes. Using the bacterial model allowed us to elucidate flotillin functionality, the generation of FMM heterogeneity and how it is controlled in time.

4. Results

This section is comprised of four manuscripts, where I describe molecular properties of the *B. subtilis* flotillins FloA and FloT and how they influence protein interaction partners that are associated with lipid rafts. Using different techniques I was able to show that flotillins are important regulators of different signal transduction cascades via their function as scaffold proteins. Elucidating flotillin functionality and their intrinsic properties is an important step towards understanding the role of lipid rafts in both prokaryotic and eukaryotic cells.

Manuscripts:

4.1 "The biofilm formation defect of a *Bacillus subtilis* flotillin defective mutant involves the protease FtsH." (*102*)

4.2 "Overproduction of flotillin influences cell differentiation and shape in Bacillus subtilis." (*101*)

4.3 "Spatio-temporal Remodeling of Functional Membrane Microdomains Organizes the Signaling Networks of a Bacterium." (*184*)

4.4 "*In vivo* characterization of the scaffold activity of flotillin on the membrane kinase KinC of *Bacillus subtilis.*" (*185*)

Molecular Microbiology (2012) 86(2), 457–471 ■
doi:10.1111/j.1365-2958.2012.08205.x
First published online 24 August 2012

The biofilm formation defect of a *Bacillus subtilis* flotillin-defective mutant involves the protease FtsH

Ana Yepes,[1] Johannes Schneider,[1] Benjamin Mielich,[1] Gudrun Koch,[1] Juan-Carlos García-Betancur,[1] Kumaran S. Ramamurthi,[2] Hera Vlamakis[3] and Daniel López[1]*

[1]*Research Center for Infectious Diseases ZINF, Würzburg University, 97080 Würzburg, Germany.*
[2]*Laboratory of Molecular Biology, National Cancer Institute, National Institutes of Health, Bethesda, MD 20892, USA.*
[3]*Department of Microbiology and Immunobiology, Harvard Medical School, Boston, MA 02115, USA.*

Summary

Biofilm formation in *Bacillus subtilis* requires the differentiation of a subpopulation of cells responsible for the production of the extracellular matrix that structures the biofilm. Differentiation of matrix-producing cells depends, among other factors, on the FloT and YqfA proteins. These proteins are present exclusively in functional membrane microdomains of *B. subtilis* and are homologous to the eukaryotic lipid raft-specific flotillin proteins. In the absence of FloT and YqfA, diverse proteins normally localized to the membrane microdomains of *B. subtilis* are not functional. Here we show that the absence of FloT and YqfA reduces the level of the septal-localized protease FtsH. The flotillin homologues FloT and YqfA are occasionally present at the midcell in exponentially growing cells and the absence of FloT and YqfA negatively affects FtsH concentration. Biochemical experiments indicate a direct interaction between FloT/YqfA and FtsH. Moreover, FtsH is essential for the differentiation of matrix producers and hence, biofilm formation. This molecular trigger of biofilm formation may therefore be used as a target for the design of new biofilm inhibitors. Accordingly, we show that the small protein SpoVM, known to bind to and inhibit FtsH activity, inhibits biofilm formation in *B. subtilis* and other distantly related bacteria.

Accepted 4 August, 2012. *For correspondence. E-mail daniel.lopez@uni-wuerzburg.de; Tel. (+49) 0931 3183831; Fax (+49) 0931 3182578.

Introduction

A widely conserved feature of bacteria is their ability to grow attached to almost any given surface, developing multicellular aggregates commonly referred to as biofilms (Davey and O'Toole, 2000; Stewart and Franklin, 2008; Lopez *et al.*, 2010). Although the strategies that bacteria use to form biofilms vary among species, production of an extracellular matrix is generally necessary to encase the microbial community (Costerton *et al.*, 1999; Donlan, 2002; Fux *et al.*, 2005; Karatan and Watnick, 2009). Matrix-encased microbial communities are often composed of heterogeneous populations of physiologically distinct yet genetically identical cell types that contribute to biofilm formation (Stewart and Franklin, 2008; Lopez *et al.*, 2009a). For instance, biofilm formation in the model organism *Bacillus subtilis* requires the differentiation of numerous cell types. Among these cell types, the matrix-producing cells that are responsible for the production and secretion of the extracellular matrix are absolutely necessary for proper biofilm formation (Branda *et al.*, 2004; Chai *et al.*, 2008; Vlamakis *et al.*, 2008).

In order to monitor the differentiation of distinct cell types, transcriptional reporters have been used in conjunction with fluorescence microscopy (Veening *et al.*, 2008; Lopez *et al.*, 2010). We have previously used this technique to observe that matrix-producing cells differentiate in response to the secretion of a self-produced signalling molecule called surfactin. Surfactin activates the membrane histidine kinase KinC (Lopez *et al.*, 2009b,c). KinC phosphorylates and activates the Spo0A master regulator (LeDeaux *et al.*, 1995; Jiang *et al.*, 2000), which, in turn, triggers the genetic cascade responsible for the differentiation of matrix producers.

Importantly, KinC localizes to membrane lipid microdomains that are functionally similar to the lipid rafts of eukaryotic cells (Lopez and Kolter, 2010a). The membrane microdomains of *B. subtilis* harbour two flotillin-like proteins: YqfA and FloT (formerly YuaG). In eukaryotes, flotillin proteins localize to lipid rafts and orchestrate diverse signal transduction processes that are harboured

within lipid rafts (Morrow and Parton, 2005; Brown, 2006; Browman *et al*., 2007). In bacteria, these membrane proteins can organize diverse proteins related to signal transduction and protein secretion (Lopez and Kolter, 2010a). *yqfA* was initially identified as a gene of unknown function when studying genes of *B. subtilis* whose expression is controlled by the extracytoplasmic function sigma factor SigW (Huang *et al*., 1999; Turner and Helmann, 2000; Wiegert *et al*., 2001; Cao *et al*., 2002; Butcher and Helmann, 2006). The second flotillin-like protein FloT was discovered in 1999 (Tavernarakis *et al*., 1999) and it has been referred to in subsequent studies as archetypical flotillin-like protein in bacteria (Huang *et al*., 1999; Tavernarakis *et al*., 1999; Cao *et al*., 2002; Malaga-Trillo *et al*., 2002; Moszer *et al*., 2002; Ding *et al*., 2005; Walker *et al*., 2008; Donovan and Bramkamp, 2009; Lopez and Kolter, 2010a; Lee *et al*., 2012). The absence of FloT and YqfA alters the localization of proteins that are normally found within the detergent-resistant membrane (DRM) microdomains of *B. subtilis* (Lopez and Kolter, 2010a). As a result, cells defective in FloT and YqfA do not produce extracellular matrix in response to surfactin, in part, due to mislocalization and misfunction of KinC (Lopez and Kolter, 2010a), among other physiological defects (Dempwolff *et al*., 2012; Lee *et al*., 2012).

Nevertheless, in the absence of a functional KinC, Spo0A can be phosphorylated by the action of four other histidine kinases (KinA, B, D and E) (Jiang *et al*., 2000). Different levels of phosphorylated Spo0A (Spo0A~P) can be achieved depending on the phosphorylation efficiency of these kinases. Lower levels of Spo0A~P induce matrix gene expression, whereas higher levels are necessary for sporulation gene expression (Fujita *et al*., 2005). The absence of KinC hinders the activation of matrix gene expression in response to the presence of surfactin (Lopez *et al*., 2009b), yet it does not affect the efficiency of sporulation (LeDeaux *et al*., 1995; Jiang *et al*., 2000).

The physiological defects associated with the absence of FloT and YqfA seem broader than simply a loss of KinC activity. A previous report showed that deletion of *floT* in *B. subtilis* reduced sporulation efficiency (Donovan and Bramkamp, 2009), suggesting that FloT and YqfA could influence other proteins involved in the activation of Spo0A. In this report we show that the deletion of *yqfA* and *floT* results in reduced levels of the FtsH protease, which has been shown to indirectly regulate the phosphorylation of Spo0A via phosphatase degradation (Lysenko *et al*., 1997; Zellmeier *et al*., 2003; Le and Schumann, 2009). We also show that FtsH is present at the midcell of exponentially growing cells (Wehrl *et al*., 2000) and that it occasionally coincides with FloT and YqfA. We found that FloT and YqfA directly interact with FtsH and their expression is important for FtsH functionality. Furthermore, we present evidence that the activity of FtsH is required for the differentiation of the subpopulation of matrix producers, and by extension, for biofilm formation. Indeed, inhibition of FtsH activity by exogenously added SpoVM peptide, a known *in vitro* inhibitor of FtsH, prevents biofilm formation (Cutting *et al*., 1997; Prajapati *et al*., 2000). We propose that inhibition of FtsH may represent a new strategy for the development of novel antimicrobials with additional activity against biofilm formation.

Results and discussion

The ΔyqfA ΔfloT *mutant exhibits diminished biofilm formation and sporulation*

KinC localization to the functional membrane microdomains of *B. subtilis* requires the two flotillin homologue proteins FloT and YqfA (Lopez and Kolter, 2010a). Deletion of *floT* and *yqfA* not only results in mislocalization of KinC but also abolishes KinC activity, which prevents this strain from expressing matrix genes and forming a biofilm in response to the signal surfactin, similar to a Δ*kinC* mutant (Lopez *et al*., 2009b,c). However, the Δ*floT* Δ*yqfA* mutant displayed a more severe defect in biofilm formation as well as an additional defect in sporulation as compared to the Δ*kinC* mutant. When both strains were grown in the biofilm-inducing medium (MSgg) for 24 h with no agitation, the Δ*floT* Δ*yqfA* mutant was not able to form a biofilm in the form of a floating pellicle on the surface of the liquid. Figure 1A shows the top view of a wild-type pellicle of *B. subtilis*, which appears white, thick and wrinkled, whereas the extracellular matrix mutant fails to form surface pellicles (Δ*eps* Δ*tasA*). The Δ*floT* Δ*yqfA* flotillin-deficient mutant grew dispersed in the MSgg cultures, similar to the cultures of the matrix-deficient mutant (Fig. 1A). In contrast, the Δ*kinC* mutant was still able to form a thin, weak pellicle on the surface of the culture, leading us to conclude that the Δ*floT* Δ*yqfA* mutant has a more severe defect in matrix production than the Δ*kinC* mutant.

We next asked if the Δ*floT* Δ*yqfA* mutant also differed from the Δ*kinC* mutant in its sporulation efficiency. To test this, both strains were grown shaking in MSgg medium for 48 h and vegetative cells were subsequently heat-killed. Serial dilutions of the surviving spores were plated on fresh rich medium to induce their germination. The number of colonies resulting from the surviving spores relative to the optical density of the initial MSgg cultures was calculated (Fig. 1B). The Δ*floT* Δ*yqfA* mutant was greatly defective in sporulation, while the Δ*kinC* mutant sporulated at a level similar to the wild-type strain. The sporulation defect observed in the Δ*floT* Δ*yqfA* double mutant likely resulted from the combination of both gene deletions, because the Δ*yqfA* single mutant showed reduced sporulation efficiency similar to the effect previ-

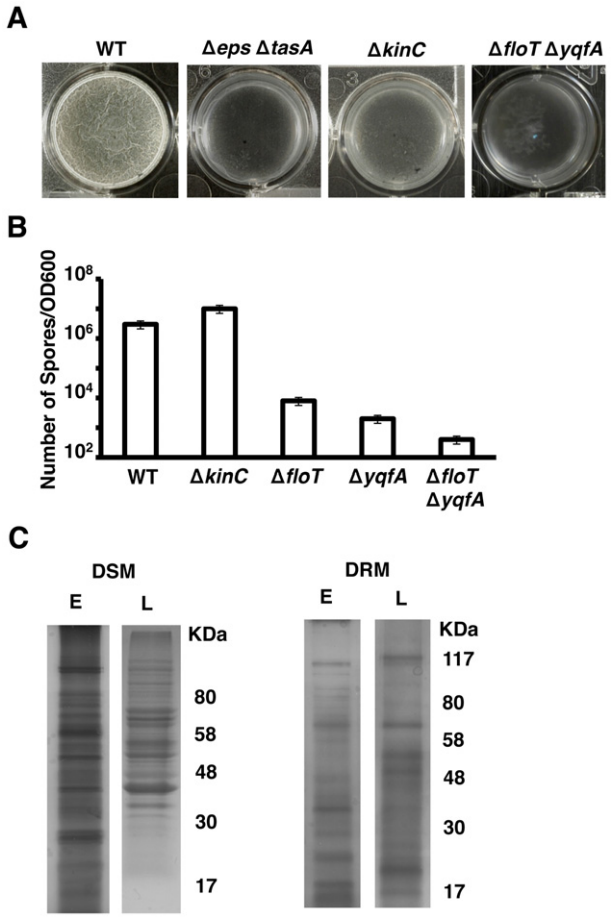

Fig. 1. Δ*floT* Δ*yqfA* mutant shows broader defect in biofilm formation and sporulation than the Δ*kinC* mutant.
A. Pellicle formation assay of different *B. subtilis* strains. Pictures show a top view of the pellicles formed on the surface of MSgg cultures incubated in 24-well plates at 30°C for 24 h. Positive and negative controls are represented by the wild-type strain (WT, DL1) and the matrix-deficient mutant (Δ*eps* Δ*tasA*, DL7) respectively.
B. Viable spore counts comparing Δ*floT* (DL1442) and Δ*yqfA* (DL1401) single mutants and Δ*floT* Δ*yqfA* (AY93) double mutant in relation to Δ*kinC* (DL227) mutant and WT strain. Cultures were grown in shaking MSgg at 30°C for 48 h. The number of spores was correlated to the optical density of the MSgg cultures. Error bars indicate standard error of the means.
C. Membrane fractionation of WT cells according to differential sensitivity to detergent solubilization. SDS-PAGE analyses of the membrane fractions that are sensitive and resistant to detergent solubilization (DSM and DRM respectively). Samples were taken at early (E) and late (L) stages of growth in biofilm-inducing conditions. The protein pattern was analysed by Coomassie staining. The molecular weights are represented at the right of the gels.

ously described for the Δ*floT* mutant (Fig. 1B) (Donovan and Bramkamp, 2009). Given that sporulation and matrix production are both processes regulated by Spo0A, we posited that the Δ*floT* Δ*yqfA* mutant had other defects in addition to a non-functional KinC, which further inhibited the activation of the Spo0A genetic cascade.

To identify additional proteins that might influence the activation of Spo0A, we analysed the proteins that localize in the membrane microdomains along with FloT and YqfA. To this end, we purified the protein fraction associated with the DRM microdomains and analysed these samples as described previously (Zhang *et al.*, 2005; Donovan and Bramkamp, 2009; Lopez and Kolter, 2010a). Briefly, cell extracts were treated with a mixture of non-ionic detergents and then separated by zonal centrifugation in sucrose gradients. This treatment resulted in two fractions: one that is sensitive to detergents (detergent-sensitive membrane fraction, DSM) and another fraction composed of larger membrane fragments that were more resistant to detergent disruption (detergent-resistant membrane fraction, DRM). Whereas it is important not to equate the pool of proteins present in the DRM fraction with raft-associated proteins, it is known that the DRM fraction is highly enriched in proteins associated with lipid rafts (Brown, 2002; 2006). Consequently, we analysed the DRM and DSM fractions from cultures in our biofilm-inducing medium at an early stage (2 h of incubation) or at a late stage of growth (24 h of incubation). Proteins associated with the DRM and the DSM fractions were analysed by SDS-PAGE. As was previously reported (Zhang *et al.*, 2005; Donovan and Bramkamp, 2009; Lopez and Kolter, 2010a), there was a heterogeneous distribution of proteins in *B. subtilis* membranes (Fig. 1C). Moreover, substantial changes in the protein content of the DRM fraction were observed when we compared the cultures at early (E) or late (L) stage of growth in our experimental conditions (Fig. 1C). The DRM fraction at late stage of growth showed a similar banding pattern to what was previously reported (Lopez and Kolter, 2010a). To identify previously undetected proteins associated with the DRM, individual bands from the DRM fraction of 2 h cultures were excised from the gel and proteins were identified using mass spectrometry.

Mass spectrometry analysis of the prominent protein bands from the DRM fraction early stage of growth revealed a number of proteins involved in cell signalling and protein secretion, as previously described for more mature cultures (Lopez and Kolter, 2010a). For a complete list of proteins identified by mass spectrometry, see Table S1. Interestingly, the membrane-bound protease FtsH was found associated with the DRM fraction (Fig. S1). FtsH has been reported to indirectly affect the levels of phosphorylated Spo0A by degrading four regulatory phosphatase proteins, RapA, RapB, RapE and Spo0E, which feed into the Spo0A phosphorelay to ultimately decrease the levels of Spo0A~P (Le and Schumann, 2009). Accordingly, previous publications have shown that the Δ*ftsH* mutant has a severe defect in sporulation, consistent with a decrease in the levels of Spo0A~P (Lysenko *et al.*, 1997; Zellmeier *et al.*, 2003). Because FtsH affects the activation of Spo0A, we hypothesized that the Δ*floT* Δ*yqfA* mutant

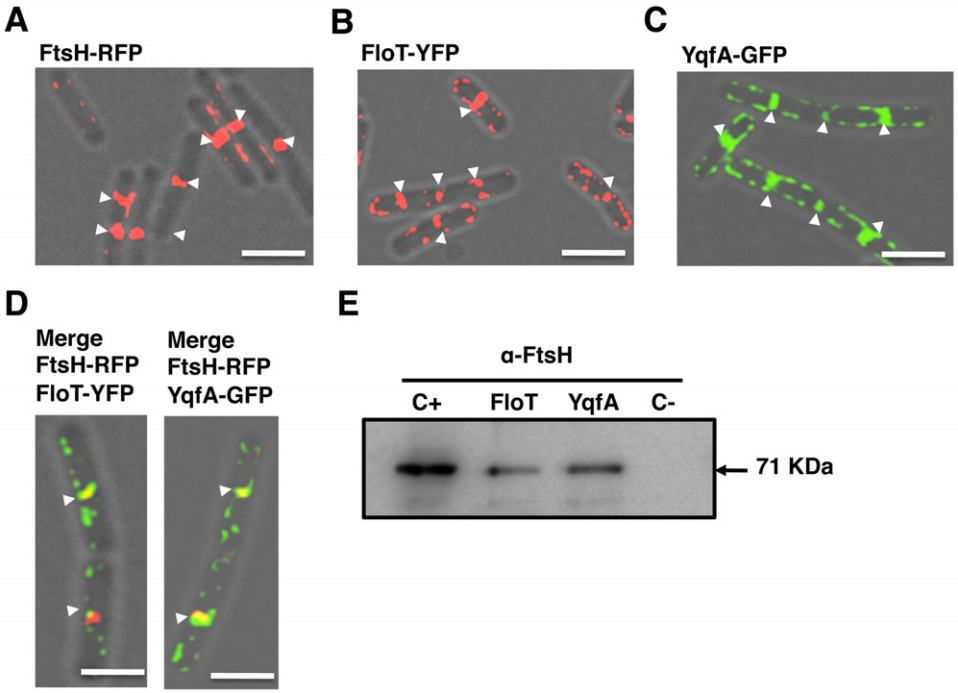

Fig. 2. FloT and YqfA interact with FtsH. Overlays of fluorescence micrographs and transmitted light images of cells grown in liquid shaking MSgg at 30°C harvested in mid-exponential phase (approximately 8 h of incubation). Midcell fluorescence is labelled with white arrows. Scale bars are 2 μm.
A. FtsH–RFP translational fusion (AY224, false coloured in red). IPTG concentration required for protein induction was 1 mM.
B. FloT–YFP translational fusion (DL1295, false coloured in red).
C. YqfA–GFP translational fusion (DL1367, false coloured in green).
D. Colocalization of both signals in the double-labelled strains FloT–YFP FtsH–RFP and YqfA–GFP FtsH–RFP (AY240 and AY238) appears as yellow in the merge panels (YFP signal is false coloured in green and RFP signal false coloured in red).
E. Immunoblot assay using polyclonal antibodies against FtsH to detect FtsH in the protein samples pulled down with YqfA-His^6 and FloT-His^6 proteins. The arrow indicates the presence of a band with the size predicted for FtsH. Positive control (C+) is the wild-type membrane fraction. Negative control (C–) is what eluted from the nickel-charged columns when loaded with a sample of wild-type membrane fraction. Protein samples that were pulled down with FloT-His^6 (JS202) and YqfA-His^6 (JS201) are presented in lanes FloT and YqfA respectively.

might have abrogated the functionality of FtsH and that this could be one of the reasons why the Δ*floT* Δ*yqfA* mutant was defective in sporulation and matrix production. We therefore examined FtsH protein levels by Western blot analysis of cell extracts using polyclonal antibodies against the FtsH protease. In wild-type *B. subtilis*, FtsH was detectable in the DRM fraction and the signal was absent in the DRM fraction of the Δ*floT* Δ*yqfA* mutant (Figs S1B and S2A). This result was important, but perhaps not surprising, as the protein profile from the DRM fraction of Δ*floT* Δ*yqfA* mutant showed a general decrease in the overall protein content (Fig. S2B).

FloT *and* YqfA *interact with* FtsH *in* B. subtilis *cells*

In order to determine if FtsH interacts with FloT and YqfA in the functional microdomains of *B. subtilis*, we first examined the subcellular distribution pattern of FtsH in relation to the flotillin homologue proteins FloT and YqfA using fluorescence microscopy. A previous report showed that FtsH preferentially localized to the septum of dividing cells (Wehrl *et al.*, 2000), yet the distribution pattern of FloT and YqfA had not been investigated in exponentially growing cells. Accordingly, we constructed functional translational fusions of FloT or YqfA to fluorescent proteins under the control of their natural promoters (Lopez and Kolter, 2010a). In addition, we generated an FtsH–RFP translational fusion under the control of an IPTG inducible promoter. Using these strains, we analysed the distribution pattern of the three proteins in cells harvested at early stages of growth in MSgg medium. The translational fusion FtsH–RFP rendered a fully functional protein as shown in Figs S3, S4 and S11. As described previously, FtsH–RFP largely localized as a band at division septa (Fig. 2A). Fluorescence was also occasionally detected in discrete foci across the membrane (Fig. 2A; see also a larger field of view in Fig. S4). The fluorescence signal emitted by the FloT–YFP (Fig. 2B) and YqfA–GFP (Fig. 2C) was distributed as foci across the plasma membrane, and occasionally detected at the midcell with elevated fluorescence (white arrows in Fig. 2B and C; larger fields of view in Figs S5 and S6). Examination of

cells harbouring both FtsH–RFP and FloT–YFP or FtsH–RFP and YqfA–GFP indicated that the proteins coincided at division septa in a significant number of cells (Fig. 2D; merge of the green and red signals is shown as yellow). Interference between green and red fluorescence signals was not detectable in our working conditions (Fig. S7).

To investigate if FloT and YqfA interact with FtsH at division septa, we attempted to co-purify FloT and YqfA with FtsH from cell extracts. We therefore constructed two *B. subtilis* strains producing C-terminal His^6-tagged variants of FloT and YqfA flotillin proteins (FloT-His^6 and YqfA-His^6 respectively). These strains were grown to exponential phase (OD600 = 0.8) in MSgg medium. Cells were harvested and the membrane fraction purified and solubilized with 0.2% of DDM. Samples were loaded onto a column of nickel-charged resin (Qiagen) that selectivity binds His^6-tagged proteins and the proteins that are directly or indirectly bound to them. The pool of proteins bound to the resin was eluted from the column using an imidazole-containing buffer and resolved by SDS-PAGE. Western blot analysis was carried out using polyclonal antibodies against FtsH. A protein band corresponding to FtsH was detected in the protein sample that co-eluted with FloT-His^6 (Fig. 2E, lane 'FloT'). FtsH was also detected in the protein sample that co-eluted with YqfA-His^6 protein (Fig. 2E, lane named YqfA). As a positive control, we detected FtsH in the total membrane fraction purified from wild-type cells (Fig. 2E, lane C+). In contrast, as a negative control, FtsH was not detected in the elution fraction of purified membranes from otherwise wild-type cells that did not harbour a His^6-tagged protein, suggesting that retention of FtsH on the column was dependent on FloT-His^6 or YqfA-His^6 (Fig. 2E, lane C–). Altogether, these results are consistent with the idea that a direct interaction occurs between FloT and YqfA with FtsH. Studies in *Escherichia coli* showed that FtsH must oligomerize to properly function (Bieniossek *et al.*, 2006; 2009) and that its oligomerization requires the chaperone activity of two proteins, HflC and HflK (Schumann, 1999; Ito and Akiyama, 2005; Hinderhofer *et al.*, 2009). Interestingly, these two proteins are structurally similar to FloT and YqfA as well as other flotillin-like proteins (Winter *et al.*, 2007; Hinderhofer *et al.*, 2009). As *B. subtilis* lacks HflC and HflK proteins in their genome, it is tempting to speculate that FloT and YqfA might be the functional replacement of HflC and HflK.

Because FtsH principally localizes to the septum of dividing cells (Wehrl *et al.*, 2000), we reasoned that the interactions between FloT and YqfA with FtsH should be mainly localized at midcell. In this regard, we observed that, in the cases that flotillin-like proteins were detected in the septum, they behaved differently from the flotillins distributed throughout the membrane. Figure 3 shows time-lapse fluorescence microscopy of strains labelled with FloT–YFP or YqfA–GFP, to visualize FloT and YqfA

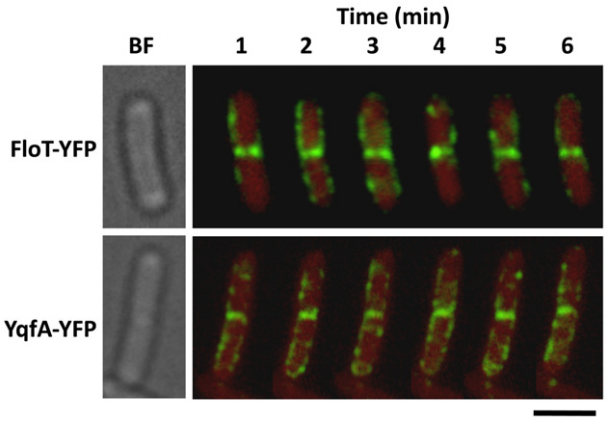

Fig. 3. Flotillins appear static at the midcell. Time-lapse fluorescence analysis of the distribution pattern of FloT–YFP and YqfA–GFP foci. Cells were grown in liquid shaking MSgg at 30°C for 8 h. Exponentially growing cells were mounted on agarose-coated slides. The upper row shows the distribution of the FloT–YFP foci (DL1295, false-coloured green) within the same cell for 6 min. The bottom row shows the distribution of the YqfA–GFP foci (DL1367, false-coloured green) within the same cell for 6 min. Background is represented in red for better contrast of the fluorescent signal. Scale bar is 2 μm.

foci every 60 s over a period of 6 min. The fluorescence signal that was distributed in foci across the membrane displayed a highly dynamic reorganization process, as the distribution pattern along the cell periphery continuously changed as previously reported for FloT (Donovan and Bramkamp, 2009). However, the fluorescence signal present at the septum for both FloT and YqfA flotillin proteins remained largely constant (Fig. 3). Quantitative measurements of the fluorescence signal detected in the time-lapse fluorescence microscopy experiments are shown in Figs S8–S10. As fluorescence signal was constantly detected at the septum of dividing cells during the time-lapse experiment, we reasoned that the continued presence of FloT and YqfA at the septum might be due to interactions between FloT and YqfA with FtsH (and probably with other proteins). It is currently unclear why FloT and YqfA behaved differently when located at the septum, but it is worth noting that the septal membrane has different lipid composition, and thus different physicochemical properties, to the cellular membrane (Kawai *et al.*, 2004; Matsumoto *et al.*, 2006; Donovan and Bramkamp, 2009) that might affect the behaviour of FloT and YqfA.

Thus far, our data indicated that FtsH and the flotillin homologues directly interact and that FtsH does not localize to the DRM microdomains in a strain lacking *floT* and *yqfA* (Fig. S2). In order to determine the dependence of FtsH localization on FloT and YqfA, we examined the localization of FtsH–RFP in a Δ*floT* Δ*yqfA* double mutant. The absence of FloT and YqfA resulted in a decrease in the intensity of FtsH–RFP fluorescence signal. What faint signal we were able to detect appeared largely as foci

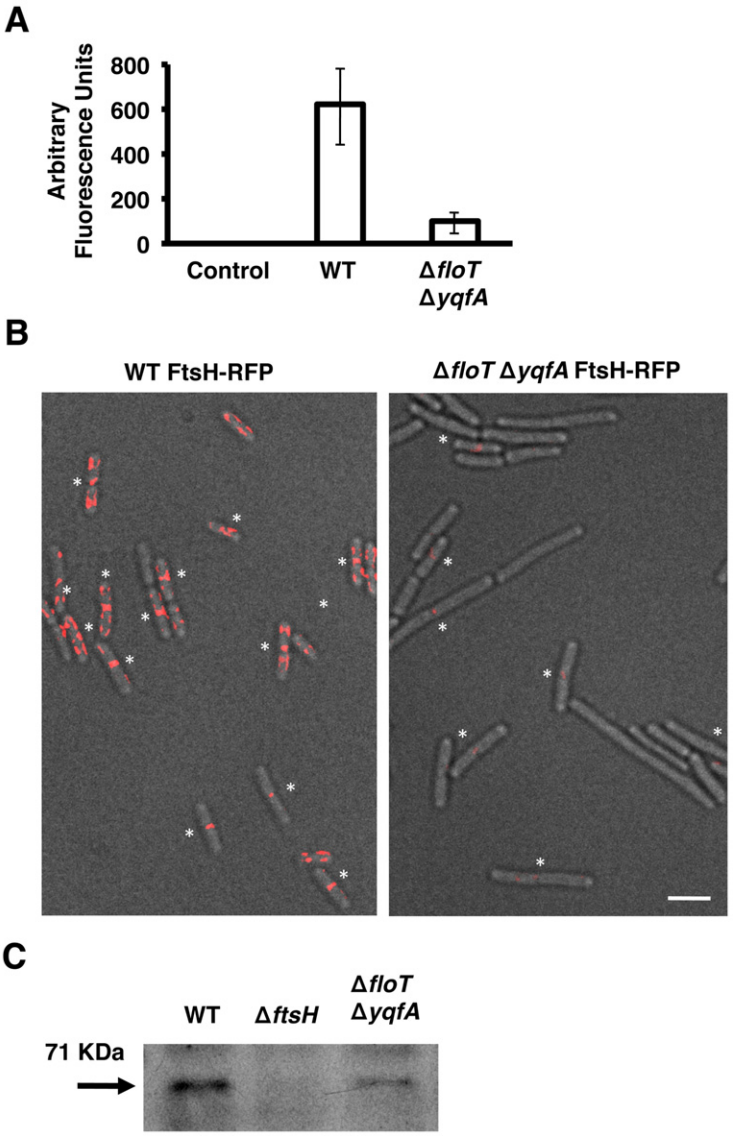

Fig. 4. The Δ*floT* Δ*yqfA* mutant displays lower levels of FtsH.
A. Relative fluorescence of wild-type (WT) strain and Δ*floT* Δ*yqfA* mutant labelled with the translational fusion FtsH–RFP (AY224 and DL1565 respectively). Cells were grown in liquid shaking MSgg at 30°C and harvested at mid-exponential phase (approximately 8 h of incubation; OD600 = 0.8). Quantification of relative fluorescence signal was assigned as fluorescence arbitrary units and presented in a graph. Error bars indicate standard error of the means.
B. Fluorescence micrographs overlayed on transmitted light images of WT and Δ*floT* Δ*yqfA* mutant, both harbouring the translational fusion FtsH–RFP (false coloured in red). Asterisks indicate the fluorescence signal positioned in the septum of dividing cells for better visualization. Scale bar is 2 μm.
C. Immunoblot of FtsH protein in the indicated *B. subtilis* strains using polyclonal antibodies against FtsH. The arrow indicates the presence of a band with the size predicted for FtsH. Each lane contained 25 μg of total protein.

near division septa (Fig. 4A and B). Immunoblot analysis using antibodies against FtsH confirmed that there were indeed lower levels of FtsH protein in the whole cell extracts of the Δ*floT* Δ*yqfA* double mutant as compared to wild-type cells (Fig. 4C), confirming a functional link between FloT and YqfA and FtsH and possibly other septal-localized proteins (Dempwolff *et al.*, 2012; Lee *et al.*, 2012).

FtsH *is required for the differentiation of the subpopulation of matrix producers and biofilm development*

We wondered if the above results, suggesting that FloT and YqfA influence FtsH activity, could explain the defect in biofilm formation observed the Δ*floT* Δ*yqfA* mutant. Previous research suggested that FtsH exerts a positive effect on the activation of Spo0A (Le and Schumann, 2009), yet its effect on the differentiation of matrix producers and thus, biofilm formation was not examined because the *B. subtilis* strains used in these studies were laboratory strains unable to produce the extracellular matrix necessary to form biofilms (Branda *et al.*, 2001; McLoon *et al.*, 2011).

To test whether FtsH is required for the differentiation of the matrix producers, we monitored expression of matrix genes in the presence and absence of FtsH. Upon activation of Spo0A~P, *B. subtilis* cells transition from expressing motility genes to expressing genes involved in matrix production (Lopez and Kolter, 2010b). Thus, we measured the relative proportion of the subpopulations of motile cells and matrix producers using cultures of a double-labelled strain harbouring transcriptional fusions for structural components of the flagellum and matrix pro-

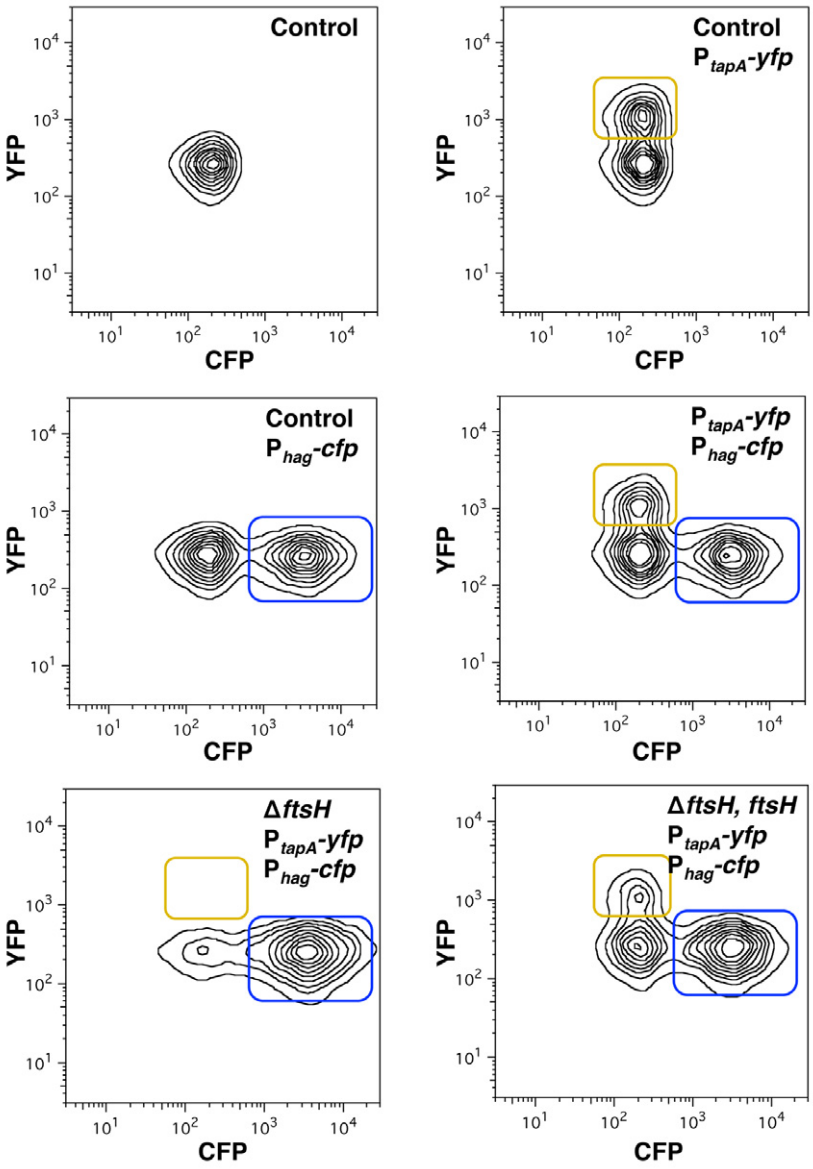

Fig. 5. FtsH is necessary for the differentiation of matrix producers. Flow cytometry monitoring the expression of the reporter P_{tapA}-*yfp* (YFP fluorescence on the *y*-axis) and P_{hag}-*cfp* (CFP fluorescence on the *x*-axis) from cells grown on MSgg medium. The number of cells is represented by isolines. The top left panel shows the control of background fluorescence for both CFP and YFP in a strain harbouring no fluorescent protein genes (DL1). Top right panel: the strain harbouring P_{tapA}-*yfp* (DL382). The subpopulation expressing fluorescence above background is framed in yellow. Centre left panel: the strain harbouring P_{hag}-*cfp* (DL1056) showed a subpopulation of cells highly expressing the reporter framed in blue. Centre right panel: the strain harbouring both reporters, P_{tapA}-*yfp* and P_{hag}-*cfp* (DL1079). Bottom left panel: the *ΔftsH* mutant strain harbouring both reporters, P_{tapA}-*yfp* and P_{hag}-*cfp* (DL1521). Bottom right panel: the *ΔftsH* mutant strain harbouring both reporters, P_{tapA}-*yfp* and P_{hag}-*cfp*, complemented with the gene *ftsH* controlled by an IPTG-inducible promoter (DL1523, induction with 1 mM IPTG).

teins. The P_{hag}-*cfp* reporter is only expressed in the subpopulation of motile cells, whereas the P_{tapA}-*yfp* fusion (formerly P_{yqxM}-*yfp*) is exclusively expressed in matrix-producing cells (Chai *et al*., 2008; Vlamakis *et al*., 2008) A double-labelled strain harbouring the P_{hag}-*cfp* and P_{tapA}-*yfp* reporters was grown in standing biofilm-inducing medium MSgg cultures for 24 h. The subpopulations of motile cells and matrix producers were monitored by flow cytometry analysis of 50 000 cells (Fig. 5). The number of cells expressing each reporter was represented as contour isolines. The top left panel shows the background fluorescence in a strain harbouring no fluorescent reporters. Two additional controls were performed to distinguish the individual subpopulations in each channel using single-labelled strains and we observed about 38% of cells expressed the matrix reporter and 52% expressed motility reporter. When the double-labelled strain was monitored, both subpopulations appeared in each channel with approximately 30% and 50% of the population expressing either matrix or motility genes respectively (Fig. 5, right panel, middle row). In the absence of *ftsH*, about 67% of cells expressed the motility reporter, but there was no detectable expression of the P_{tapA}-*yfp* matrix reporter (Fig. 5, bottom left panel), indicating that matrix producers did not differentiate in the absence of FtsH. The *ΔftsH* mutant complemented with an IPTG-inducible copy of the *ftsH* gene recovered the matrix fluorescence signal with about 21% of cells expressing matrix and 54% of cells expressing the motility reporter (Fig. 5, bottom right panel). The results suggested that FtsH has a role in

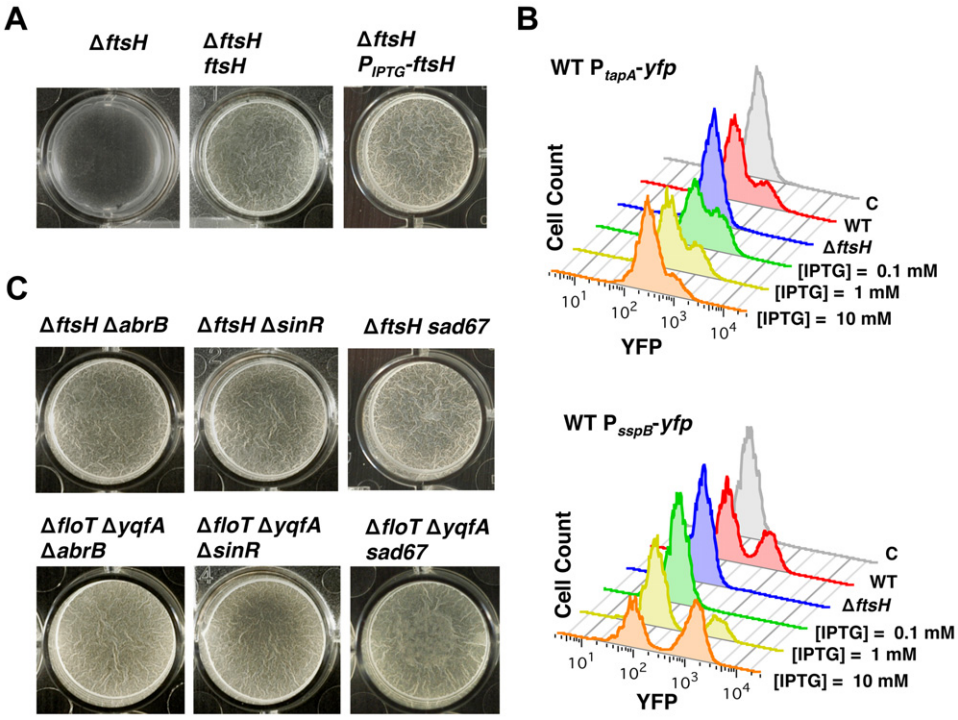

Fig. 6. Influence of FtsH on biofilm formation.
A. Pellicle formation of the Δ*ftsH* mutant (DL1308, left panel), the Δ*ftsH* mutant complemented with *ftsH* controlled by its native promoter (DL1433, middle panel) and Δ*ftsH* mutant complemented with an IPTG-inducible promoter (DL1361, right panel). IPTG was added to a final concentration of 1 mM. Pictures show a top view of the pellicles formed on the surface of MSgg cultures incubated in 24-well plates at 30°C for 24 h.
B. Flow cytometry analysis of the same strains as in A harbouring P_{tapA}-*yfp* reporter to monitor the differentiation of the subpopulation of matrix producers. Control strain harbouring no reporter fusion (grey profile). Wild-type (WT) profile shows a subpopulation of cells with high relative fluorescence, seen as the shoulder to the right of the main peaks (red profile) (DL382). The FtsH-defective mutant does not show the differentiation of this subpopulation (blue profile) (DL1404). Expression of *ftsH* under the control of an IPTG-inducible promoter led to a gradual expression of FtsH in the FtsH-defective mutant, which in turn caused a differentiation of matrix producers (different concentrations of IPTG are shown) (DL1461). Flow cytometry profiles of the reporter P_{sspB}-*yfp* to detect sporulating cells. WT profile shows a subpopulation of cells with high relative fluorescence (red profile) (DL1089). The FtsH-defective mutant does not show the differentiation of this subpopulation (blue profile) (1349). Expression of *ftsH* under the control of an IPTG-inducible promoter led to a gradual expression of FtsH in the FtsH-defective mutant, which in turn caused a differentiation of sporulating cells (different concentrations of IPTG are shown) (DL1364).
C. Pellicle formation assay of the indicated strains of *B. subtilis* when incubated in MSgg at 30°C for 24 h. The *sad67* variant was expressed under the control of an IPTG-inducible promoter with 1 μM IPTG.

assuring the fate of matrix-producing cells, perhaps by stabilizing the levels of active Spo0A (Spo0A~P).

We predicted that the inability of the Δ*ftsH* mutant to express matrix genes should abrogate biofilm formation. We tested this by allowing cultures to form floating pellicles on the surface of liquid MSgg (Figs 6A and S11). After 24 h of incubation, the Δ*ftsH* mutant grew dispersed in the cultures and no pellicle formed. The ability to form pellicles could be restored in the Δ*ftsH* mutant when complemented *in trans* with *ftsH* under the control of an IPTG-inducible promoter and partially restored when *ftsH* expression was under the control of its natural promoter (Figs 6A and S11). Flow cytometry was used to monitor expression of the P_{tapA}-*yfp* reporter in the Δ*ftsH*, P_{IPTG}-*ftsH* strain. The ability of this strain to form pellicles was associated with the differentiation of the subpopulation of matrix producers (Fig. 6B). In addition, consistent with the sporulation defect that was previously described (Lysenko *et al.*, 1997; Zellmeier *et al.*, 2003), the Δ*ftsH* mutant was unable to express the sporulation specific promoter P_{sspB}-*yfp* unless the Δ*ftsH*, P_{IPTG}-*ftsH* strain was grown in the presence of IPTG (Fig. 6B).

The biofilm defect observed in the Δ*ftsH* mutant appeared to be due to its inability to express matrix genes (see Figs 5 and 6B). If this was due to a signalling defect, we reasoned that we should be able to restore biofilm formation by uncoupling signalling and matrix gene expression. There are two repressor proteins, SinR and AbrB, which negatively regulate expression of the genes responsible for matrix production (Hamon *et al.*, 2004; Chu *et al.*, 2006; Chai *et al.*, 2008; Murray *et al.*, 2009) (Fig. S12). Thus, the absence of either SinR or AbrB repressors leads to constitutive expression of extracellular matrix. Deletion of either *sinR* or *abrB* in the Δ*ftsH*

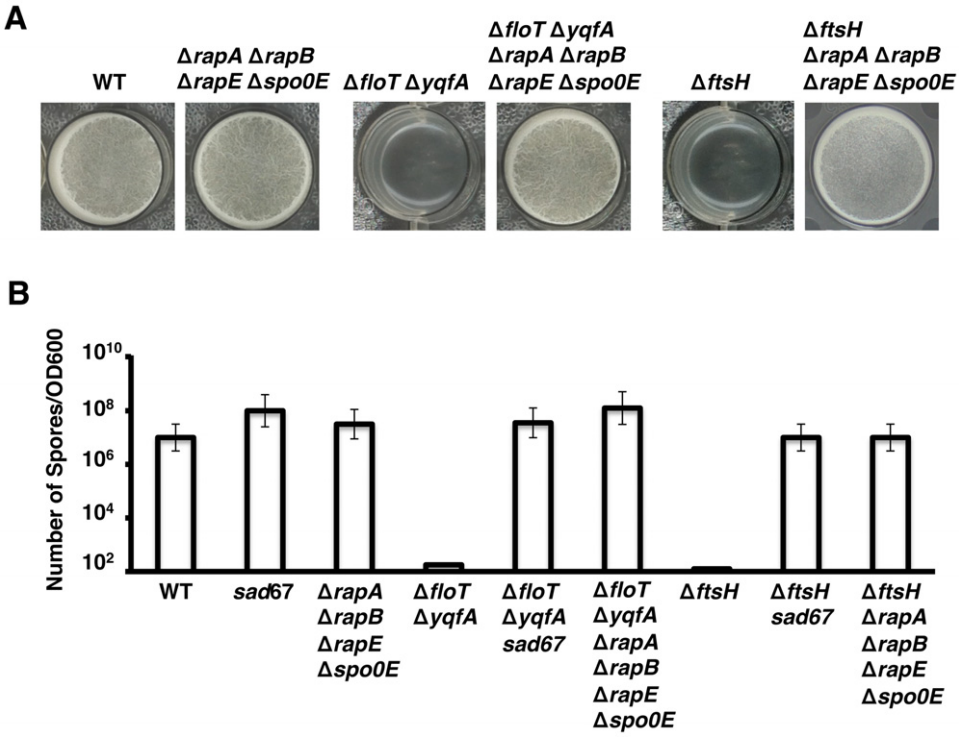

Fig. 7. Epistasis analysis of the Δ*ftsH* mutant and Δ*floT* Δ*yqfA* double mutant to restore biofilm formation.
A. Pellicle formation of the indicated strains of *B. subtilis*. Pictures show a top view of the pellicles formed on the surface of MSgg incubated in 24-well plates at 30°C for 24 h. Positive control is represented by the wild-type strain (WT) and negative controls are represented by the Δ*floT* Δ*yqfA* double mutant (strain JS163) and the Δ*ftsH* mutant (DL1308).
B. Viable spore counts comparing WT, Δ*floT* Δ*yqfA* and Δ*ftsH* strains when complemented with the *sad67* variant (strains DL1148, DL1375 and DL1363 respectively) or with a deletion of the FtsH-regulated phosphatases (*rapA*, *rapB*, *rapE* and *spo0E*) (strains DL1430, DL1554 and DL1375 respectively). *sad67* was expressed under the control of an IPTG-inducible promoter with 1 μM IPTG. Cultures were grown in shaking MSgg at 30°C for 48 h. Number of spores was correlated to the optical density of the cultures. Error bars indicate standard error of the means.

mutant strain restored pellicle formation. Similarly, deletion of *sinR* or *abrB* suppressed the biofilm formation defect of strains that did not produce the flotillin proteins YqfA and FloT (Fig. 6C). These results indicated that both the Δ*ftsH* and Δ*floT* Δ*yqfA* mutants were physiologically capable of forming biofilms and their impairment in biofilm formation is likely due to an inhibition of the genetic cascade to matrix production.

The expression of the SinR and AbrB repressors is controlled by Spo0A~P and levels of Spo0A~P are indirectly regulated by the protease FtsH (Le and Schumann, 2009). Epistasis analyses were carried out in Δ*ftsH* and Δ*floT* Δ*yqfA* mutants by expressing a constitutively active variant of *spo0A* (*sad67*) produced under the control of an IPTG-inducible promoter. Sad67 does not require any upstream regulation to maintain high active levels of the Spo0A protein (Ireton *et al*., 1993). Pellicle formation was assayed in cells expressing *sad67* and harbouring a deletion in either *ftsH* or *floT* and *yqfA*. Standing MSgg cultures incubated for 24 h showed pellicle formation in both strains, indicating that the artificial activation of Spo0A~P restored pellicle formation in the absence of FtsH or the flotillin homologue proteins (Fig. 6C).

The absence of the FtsH protease increases the level of the phosphatase proteins, RapA, RapB, RapE and Spo0E, which ultimately decrease the levels of Spo0A~P (Le and Schumann, 2009). To bypass the reduction in the functionality of the FtsH in the Δ*floT* Δ*yqfA* double mutant, we generated a strain lacking the pool of phosphatases degraded by FtsH using the Δ*floT* Δ*yqfA* strain as genetic background. The resultant strain Δ*floT* Δ*yqfA* Δ*rapA* Δ*rapB* Δ*rapE* Δ*spo0E* was tested for its ability to form biofilm in biofilm-inducing conditions. This strain recovered the ability to form pellicles in standing MSgg cultures (Fig. 7A). Thus, the biofilm formation defect of the Δ*floT* Δ*yqfA* double mutant can be bypassed by deleting the FtsH-regulated phosphatases that ultimately dephosphorylate Spo0A~P. Indeed, the ability to form pellicles in standing MSgg cultures was also recovered in the strain Δ*ftsH* Δ*rapA* Δ*rapB* Δ*rapE* Δ*spo0E* (Fig. 7A).

Several studies have described that the Δ*ftsH* mutant is unable to sporulate (Lysenko *et al*., 1997; Zellmeier *et al*.,

2003; Le and Schumann, 2009), and similar results are presented in this work for the Δ*floT* Δ*yqfA* double mutant (see Fig. 1). As wild-type levels of sporulation could be restored in the Δ*ftsH* mutant when complemented with *sad67* (Le and Schumann, 2009), we wondered if expression of *sad67* could restore sporulation to the Δ*floT* Δ*yqfA* double mutant. Indeed, we found that expression of *sad67* in Δ*floT* Δ*yqfA* mutant cells restored sporulation efficiency to near wild-type levels (Fig. 7B). Importantly, wild-type levels of sporulation were also observed in the Δ*floT* Δ*yqfA* Δ*rapA* Δ*rapB* Δ*rapE* Δ*spo0E* and Δ*ftsH* Δ*rapA* Δ*rapB* Δ*rapE* Δ*spo0E* strains. Wild-type levels of sporulation were also observed in the Δ*ftsH sad67* strain and Δ*ftsH* Δ*rapA* Δ*rapB* Δ*rapE* Δ*spo0E* strains (Fig. 7B). Altogether, the various phenotypes arising from the absence of the FtsH protease, including biofilm formation and sporulation, were restored in the Δ*ftsH* or Δ*floT* Δ*yqfA* double mutants either by inhibiting the pool of FtsH-regulated phosphatases that decrease the levels of Spo0A~P or alternatively, by expressing a *spo0A* variant (*sad67*), whose activation is not influenced by the phosphorelay in which the FtsH-regulated phosphatases are involved.

Synthetic SpoVM *protein inhibited* FtsH *protease and biofilm formation*

The interconnection between FtsH protease activity and matrix production presented in this study led us to explore new possibilities to develop anti-biofilm compounds by targeting FtsH protease activity. Previous studies have reported that the small protein SpoVM, a 26-amino-acid-long protein that is normally present in the forespore membrane of *B. subtilis* (Cutting *et al*., 1997; van Ooij and Losick, 2003; Ramamurthi *et al*., 2006; 2009; Wang *et al*., 2009), binds to and inhibits FtsH protease *in vitro* (Cutting *et al*., 1997; Prajapati *et al*., 2000). Thus, we tested the ability of SpoVM to inhibit biofilm formation in cultures of *B. subtilis*. To this end, we synthetically engineered SpoVM peptide, and sub-growth-inhibitory concentrations (50 nM) of a stock buffered solution of SpoVM were added to the pellicle formation assay in MSgg medium. We observed that nanomolar concentrations of the peptide were sufficient to inhibit pellicle formation after 24 h (Fig. 8A). Interestingly, the presence of nanomolar concentrations of SpoVM did not affect the ability of the Δ*rapA* Δ*rapB* Δ*rapE* Δ*spo0E* mutant to form biofilm (Fig. 8A). Biofilm inhibition was also observed in solid MSgg when SpoVM was added to the MSgg agar as evidenced by flatter colony morphology (Fig. S13). Single-cell analysis for gene expression in the double-labelled strain P_{hag}-*cfp*, P_{tapA}-*yfp* treated with nanomolar concentrations of the SpoVM peptide showed that *B. subtilis* was unable to express matrix-specific genes in the presence of SpoVM. Unlike untreated samples, the majority of the SpoVM-treated cells remained as motile cells (Fig. 8B). Furthermore, sub-growth-inhibitory concentrations of SpoVM inhibited biofilm formation in other bacterial species such as *Staphylococcus aureus* and *Pseudomonas aeruginosa* (Fig. S14). Whether this inhibition occurs in an FtsH-dependent manner remains to be determined. Nevertheless, the small protein SpoVM, an amphipathic alpha helical FtsH inhibitor (Cutting *et al*., 1997), is an appealing molecule that shows great potency and versatility against biofilms of diverse organisms could be further exploited to develop novel anti-biofilm agents.

Experimental procedures

Strains, media and culture conditions

Strains used in this study were *B. subtilis* strain NCIB3610 (Branda *et al*., 2001), *S. aureus* strains SC-01 (Beenken *et al*., 2003) and *P. aeruginosa* PA14 (O'Toole and Kolter, 1998a). Additional laboratory strains of *E. coli DH5*α and *B. subtilis* 168 were used for cloning purposes. A complete strain list is shown in Table S2.

To monitor cell differentiation during cell division, *B. subtilis* was incubated in liquid MSgg without shaking at 30°C. Incubation times varied depending on the requirements of the experiment. Specific conditions are presented in the figure legends. Generally, pellicle formation assays required incubation times of 24 h at 30°C. Cells harvested at early stages of growth in biofilm-inducing conditions required 2 h of incubation time at 30°C, while cells harvested at late stages of growth in biofilm-inducing conditions required 24 h of incubation at 30°C. To monitor cell division in shaking cultures, *B. subtilis* was incubated in liquid MSgg at 200 r.p.m. at 30°C. Incubation times are specified for each experiment in the figure legends. Biofilm formation assay for the strain *B. subtilis* 3610 was carried out as follows. Overnight cultures grown in LB were diluted 1:100 in biofilm-inducing medium MSgg (Branda *et al*., 2001). For pellicle formation assays, 1 ml of culture was dispensed in polystyrene well plates and incubated overnight at 30°C.

To grow biofilms of the strain *S. aureus* SC-01, a preculture grown overnight in TSB liquid medium was diluted 1:00 in TSB + glucose 0.5% + NaCl 3% (Beenken *et al*., 2003). One millilitre of the culture was dispensed in polystyrene well plates and incubated overnight at 37°C. To grow biofilms of *P. aeruginosa*, a preculture grown overnight in TB medium (O'Toole and Kolter, 1998b) was diluted 1:100. Two hundred microlitres of the culture was dispensed in polystyrene well plates and incubated overnight at 37°C. Biofilms formed by *S. aureus* and *P. aeruginosa* were stained with crystal violet for better visualization, according to the protocol described by O'Toole and Kolter (1998b).

Selective media were prepared in LB agar using antibiotics at the following final concentrations: ampicillin 100 μg ml^{-1}, kanamycin 50 μg ml^{-1}, chloramphenicol 5 μg ml^{-1}, tetracycline 5 μg ml^{-1}, spectinomycin 100 μg ml^{-1} and erythomycin 2 μg ml^{-1} + lincomycin 25 μg ml^{-1} for MLS. When required, MSgg culture medium was supplemented with threonine 1%. When needed, IPTG was added at concentrations 1 mM for the overexpression of *ftsH*, *floT* and *yqfA* and 1 μM for the

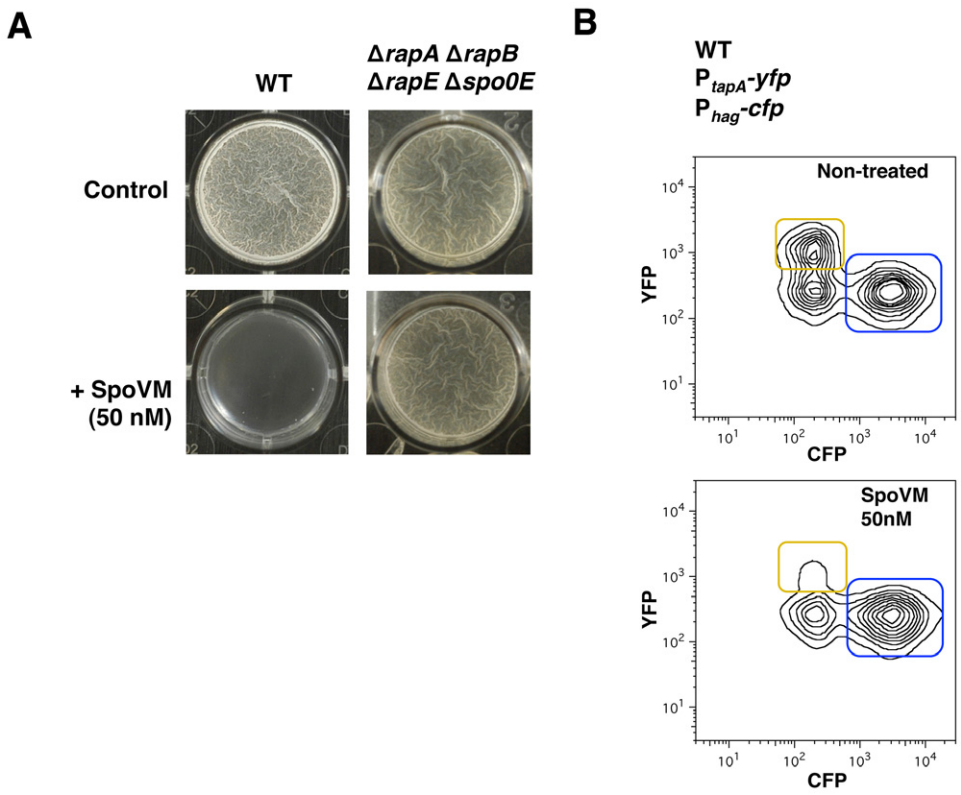

Fig. 8. SpoVM protein inhibits differentiation of matrix producers and biofilm formation.
A. Pellicle formation of *B. subtilis* wild-type (WT) or *rapA*, *rapB*, *rapE* and *spo0E* mutant in the presence or absence (control) of the protein SpoVM (50 nM).
B. Flow cytometry monitoring the expression of the reporter P_{tapA}-*yfp* (YFP fluorescence on the *y*-axis) and P_{hag}-*cfp* (CFP fluorescence on the *x*-axis) from *B. subtilis* cells grown on the pellicle formation assay. Fluorescence for both CFP and YFP in a strain harbouring both reporters, P_{tapA}-*yfp* and P_{hag}-*cfp* which correspond to the matrix producers and motile cells, framed in yellow and blue respectively. Non-treated (top panel) or treated with the SpoVM protein 50 nM (bottom panel).

overexpression of *sad67*. When required, SpoVM was added to the medium at a concentration of 50 nM.

Strain construction and reporters

Deletion mutants were generated using long flanking homology PCR (Wach, 1996) (using the primers listed in Table S3). Markerless gene deletions were used to generate the Δ*floT* Δ*yqfA* double mutant. Upstream and downstream regions of the *floT* and *yqfA* genes were joined by long flanking homology PCR (Wach, 1996) and cloned into the temperature-sensitive vector pMAD. Gene deletion occurs by a sequential process of double recombination. Isolation of the mutants was achieved by counterselection, as described in Arnaud *et al*. (2004). Transcriptional reporters used in this study were previously constructed and published (Vlamakis *et al*., 2008; Lopez *et al*., 2009c,d; Aguilar *et al*., 2010; Lopez and Kolter, 2010a). Translational fusions used in this study were generated using long flanking homology PCR. Unless specified differently in the figure legends, transcriptional fusions are expressed under the control of their natural promoters. Translational fusions were cloned in pKM008 or pKM003 vectors, and integration into the bacterial genome occurs at the *amyE* locus. pKM008 or pKM003 vectors were kindly provided by Prof. Dr David Rudner (Harvard Medical School, Boston, MA, USA) as was the pDR183 vector which allows the integration of the translational fusions into the *lacA* locus. pDG1663 was used for integration into the *thrC* locus (Guerout-Fleury *et al*., 1996). In all cases, plasmids were linearized to favour a double recombination process and added to a culture of *B. subtilis* strain 168 grown in conditions that promotes the activation of natural competence (Hardwood and Cutting, 1990). After 2 h of incubation, cells were plated in the corresponding selection media.

Overexpression of *ftsH* occurred under the control of the IPTG-inducible promoter $P_{hyperspank}$ using the plasmid pDR111 (Britton *et al*., 2002; Nakano *et al*., 2003; Erwin *et al*., 2005). Additional subcloning into pDR183 allowed the integration of the construct $P_{hyperspank}$-*ftsH* into the *lacA* locus. The concentration of IPTG used to induce the expression of *ftsH* was 1 mM. Constructions were transferred to the strain NCIB3610 by SPP1 phage transduction (Yasbin and Young, 1974; Novick, 1991). Briefly, donor strain was grown in TY medium (LB + 10 mM $MgSO_4$ + 10 μM $MnSO_4$). A diluted sample of a SPP1 phage stock was added to the culture and, after 30 min of incubation, 3 ml of soft TY agar was added to the culture. Phage halos arised after incubation overnight at 37°C. Soft agar was resuspended in TY liquid medium and supernatant

was passed through a 0.22 μm syringe filter. This supernatant was used to infect a culture of the NCIB3610 or mutant derivative recipient strain grown in TY medium. A full protocol of this process is available in the literature (Garcia-Betancur *et al.*, 2012).

Image capture and analysis

Unless different conditions were specified in figure legends, samples were fixed with paraformaldehyde treatment before single-cell analysis. Cells were resuspended in 1 ml of 4% paraformaldehyde solution and incubated at room temperature for 7 min. After washing, samples were resuspended in PBS buffer. Samples were repeatedly washed prior to single-cell analysis. Images were processed using Leica Application Suite V3.7 software. Microscopy images were taken on a Leica DMI6000B microscope equipped with a Leica CRT6000 illumination system. The microscope was equipped with a HCX PL APO oil immersion objective with 100 × 1.47 magnification that was used in this study. The microscope was also equipped with a colour camera Leica DFC630FX and temperature-control system. Image processing was performed using Leica Application Suite Advance Fluorescence Software and Photoshop. Deconvolution of fluorescence signal was performed using AutoQuant™ Deconvolution algorithms software, from Media Cibernetics. Signals were detected using the following filters: GFP signal was detected using an excitation filter BP480/40 and an emission filter BP527/30; YFP signal was detected using an excitation filter BP500/20 and an emission filter BP535/30; RFP signal was detected using an excitation filter BP546/40 and a emission filter BP600/40. Excitation times for GFP, YFP and RFP signals were between 100 and 200 ms. Transmitted light images were taken with 36 ms of excitation time. Pellicles formed in microtitre plates were photographed using a Nikon D100 camera coupled to a Kaiser RB5000 illumination system. Pictures were processed using Photoshop software. Fluorescence intensity analyses were performed in cells growing in MSgg agar for 24 h at 30°C using a Luminiscent Image Analyzer ImageQuant® LAS4000 (General Electric) coupled with ImageQuant-TL software for quantification of fluorescence.

Flow cytometry

For flow cytometric analysis, cells were dispersed from biofilms with 12 sonication pulses (power output 0.7 and cycle 50%). After dispersion, cells were fixed with a treatment of 4% paraformaldehyde, washed and resuspended in PBS buffer. Dilution of samples 1:100 was necessary prior to flow cytometry analyses. Further sonication treatment was required to separate single cells in the sample. In this case, samples were subjected to three consecutive series of 12 pulses (power output 50% and cycle 0.7 s). Flow cytometry analysis was carried out in a BD Fortessa flow cytometer (BD Biosciences). For YFP fluorescence, we used a laser excitation of 488 nm coupled with 530/30 and 505LP sequential filters. For CFP fluorescence, we used laser excitation at 405 nm coupled with 408/40 and 460LP sequential filters. The photomultiplier voltage was set between 400 and 500 V. No gates were required during the analysis of the samples. Every sample was analysed measuring 50 000 events using FACS Diva (BD Biosciences) software to capture the data. Further data analysis was performed in FlowJo 9.2 (http://www.flowjo.com).

Spore counting

Strains were grown in shaking MSgg at 30°C for 48 h. The optical density of each culture was recorded to represent the total cell density in Figs 1B and 8B. For the quantification of spores in the cultures, a sample from each culture was normalized to 1 ml of a final optical density (OD600 nm) of 1. Vegetative cells were killed by incubating samples at 80°C for 30 min. Serial dilutions were plated from the normalized preparation and colony forming units were counted. Colony forming units grown from viable spores were represented in relation to the optical density of the culture, which the sample was extracted. This protocol was adapted from previous publications (Aguilar *et al.*, 2010).

Cell membrane fractionation and Western blot analysis

To purify the membrane fraction at late time points during cell growth, 30 ml of MSgg was inoculated and cells incubated for 24 h at 30°C to a final OD600 of about 3.0. Cultures were centrifuged and cells resuspended in PBS buffer. To purify the membrane fraction at early time points during cell growth, 500 ml of MSgg culture was inoculated to an OD600 of 0.1. After 2 h of incubation time at 30°C and a final OD600 of about 0.2, cells were harvested and processed. Cell suspensions were treated with lysozyme 1 mg ml^{-1} at 37°C for 30 min. Cell debris was eliminated by normal centrifugation (13 000 r.p.m. for 2 min). Supernatant was subjected to ultracentrifugation (75 000 r.p.m. for 40 min) to separate the membrane fraction. Next, the membrane fraction was resuspended in PBS buffer and treated with the CellLytic MEM protein extraction kit (Sigma-Aldrich) to purify proteins associated with detergent-resistant fractions. CellLytic MEM protein extraction kit separates two samples containing the DRM and the DSM fractions. Both samples were run on SDS-PAGE and proteins were detected by Coomassie blue staining. Coomassie-stained bands were excised from the gel and analysed by mass spectrometry (Thermo Scientific LTQ Orbitrap XL). Immunoblot was carried out as previously described (Lopez *et al.*, 2009b) using polyclonal antibody against FtsH, kindly provided by Prof. Dr Thomas Wiegert (Institute of Genetics, University of Bayreuth, Germany). When specified, the protein content was adjusted to 25 μg of total protein per lane by using Nanodrop® Spectrophotometer ND-1000 to quantify the protein concentration of the samples.

Pull down assays

The two strains overexpressing the His-tagged variants of the flotillin FloT-His^6 and YqfA-His^6 proteins were grown in 100 ml of MSgg cultures to exponential phase (OD600 of 0.8). The cell pellet was harvested and the membrane fraction was purified according to the protocol described in the above section. The membrane fraction was solubilized in 5 ml of Buffer S (HEPES 20 mM, glycerol 20%, DTT 1 mM, DDM

0.02%) and loaded into a column of Ni-NTA superflow (Qiagen). The column was washed with 20 ml of PBS buffer DDM 0.02%. Proteins bound to the column were eluted using 2 ml of PBS buffer DDM 0.02% + imidazol 250 mM. Elution fraction was collected and the proteins precipitated by adding three volumes of acetone and further incubation overnight at –20°C. Samples were centrifuged and intensely washed with acetone. Protein samples were resuspended in 0.1 ml of PBS buffer and tested for the presence of FtsH by Western blot analysis, using polyclonal antibodies against FtsH. Immunoblot was carried out as previously described (Lopez *et al*., 2009b).

Acknowledgements

We thank all members of the Institute of Molecular Infection Biology (IMIB), especially Isa Westedt for technical assistance. We thank Prof. Dr Thomas Wiegert (University of Bayreuth, Germany) for kindly providing FtsH antibody and the strain harbouring the deletion *ftsH*::*tet*. This work was funded by the Young Investigator Program of the Research Center of Infectious Diseases (ZINF) of the University of Würzburg, Germany and the grant LO 1804/2-1 from The German Research Foundation DFG. G.K. is recipient of Schrödinger fellowship (FWF). J.C.G.B. is recipient of PhD fellowship from the Graduate School of Life Sciences (GSLS) of the University of Wuerzburg. K.S.R. acknowledges funding from the Intramural Research Program of the NIH National Cancer Institute Center for Cancer Research.

Authors contribution

D.L. designed research; A.Y., J.S., B.M., G.K., J.C.G.B., H.V. and D.L. performed research; A.Y., J.S., B.M., G.K., J.C.G.B., H.V., K.S.R. and D.L. analysed data and H.V. and D.L. wrote the paper.

Conflict of interest

The authors declared no conflict of interest.

References

Aguilar, C., Vlamakis, H., Guzman, A., Losick, R., and Kolter, R. (2010) KinD is a checkpoint protein linking spore formation to extracellular-matrix production in *Bacillus subtilis* biofilms. *MBio* **1:** 00035-10.

Arnaud, M., Chastanet, A., and Debarbouille, M. (2004) New vector for efficient allelic replacement in naturally nontransformable, low-GC-content, gram-positive bacteria. *Appl Environ Microbiol* **70:** 6887–6891.

Beenken, K.E., Blevins, J.S., and Smeltzer, M.S. (2003) Mutation of sarA in *Staphylococcus aureus* limits biofilm formation. *Infect Immun* **71:** 4206–4211.

Bieniossek, C., Schalch, T., Bumann, M., Meister, M., Meier, R., and Baumann, U. (2006) The molecular architecture of the metalloprotease FtsH. *Proc Natl Acad Sci USA* **103:** 3066–3071.

Bieniossek, C., Niederhauser, B., and Baumann, U.M. (2009) The crystal structure of apo-FtsH reveals domain movements necessary for substrate unfolding and translocation. *Proc Natl Acad Sci USA* **106:** 21579–21584.

Branda, S.S., Gonzalez-Pastor, J.E., Ben-Yehuda, S., Losick, R., and Kolter, R. (2001) Fruiting body formation by *Bacillus subtilis*. *Proc Natl Acad Sci USA* **98:** 11621–11626.

Branda, S.S., Gonzalez-Pastor, J.E., Dervyn, E., Ehrlich, S.D., Losick, R., and Kolter, R. (2004) Genes involved in formation of structured multicellular communities by *Bacillus subtilis*. *J Bacteriol* **186:** 3970–3979.

Britton, R.A., Eichenberger, P., Gonzalez-Pastor, J.E., Fawcett, P., Monson, R., Losick, R., and Grossman, A.D. (2002) Genome-wide analysis of the stationary-phase sigma factor (sigma-H) regulon of *Bacillus subtilis*. *J Bacteriol* **184:** 4881–4890.

Browman, D.T., Hoegg, M.B., and Robbins, S.M. (2007) The SPFH domain-containing proteins: more than lipid raft markers. *Trends Cell Biol* **17:** 394–402.

Brown, D.A. (2002) Isolation and use of rafts. *Curr Protoc Immunol* **Chapter 11:** Unit 11 10.

Brown, D.A. (2006) Lipid rafts, detergent-resistant membranes, and raft targeting signals. *Physiology (Bethesda)* **21:** 430–439.

Butcher, B.G., and Helmann, J.D. (2006) Identification of *Bacillus subtilis* sigma-dependent genes that provide intrinsic resistance to antimicrobial compounds produced by Bacilli. *Mol Microbiol* **60:** 765–782.

Cao, M., Kobel, P.A., Morshedi, M.M., Wu, M.F., Paddon, C., and Helmann, J.D. (2002) Defining the *Bacillus subtilis* sigma(W) regulon: a comparative analysis of promoter consensus search, run-off transcription/macroarray analysis (ROMA), and transcriptional profiling approaches. *J Mol Biol* **316:** 443–457.

Chai, Y., Chu, F., Kolter, R., and Losick, R. (2008) Bistability and biofilm formation in *Bacillus subtilis*. *Mol Microbiol* **67:** 254–263.

Chu, F., Kearns, D.B., Branda, S.S., Kolter, R., and Losick, R. (2006) Targets of the master regulator of biofilm formation in *Bacillus subtilis*. *Mol Microbiol* **59:** 1216–1228.

Costerton, J.W., Stewart, P.S., and Greenberg, E. (1999) Bacterial biofilms: a common cause of persistent infections. *Science* **284:** 1318–1322.

Cutting, S., Anderson, M., Lysenko, E., Page, A., Tomoyasu, T., Tatematsu, K., *et al*. (1997) SpoVM, a small protein essential to development in *Bacillus subtilis*, interacts with the ATP-dependent protease FtsH. *J Bacteriol* **179:** 5534–5542.

Davey, M.E., and O'Toole, A.G. (2000) Microbial biofilms: from ecology to molecular genetics. *Microbiol Mol Biol Rev* **64:** 847–867.

Dempwolff, F., Moeller, M.H., and Graumann, P.L. (2012) Synthetic motility and cell shape defects for deletions of flotillin/reggie paralogs in *Bacillus subtilis* and interplay with NfeD proteins. *J Bacteriol* **194:** 4652–4661.

Ding, Y., Jiang, M., Jiang, W., Su, Y., Zhou, H., Hu, X., and Zhang, Z. (2005) Expression, purification, and characterization of recombinant human flotillin-1 in *Escherichia coli*. *Protein Expr Purif* **42:** 137–145.

Donlan, R.M. (2002) Biofilms: microbial life on surfaces. *Emerg Infect Dis* **8:** 881–890.

Donovan, C., and Bramkamp, M. (2009) Characterization

and subcellular localization of a bacterial flotillin homologue. *Microbiology* **155:** 1786–1799.

Erwin, K.N., Nakano, S., and Zuber, P. (2005) Sulfate-dependent repression of genes that function in organosulfur metabolism in *Bacillus subtilis* requires Spx. *J Bacteriol* **187:** 4042–4049.

Fujita, M., Gonzalez-Pastor, J.E., and Losick, R. (2005) High- and low-threshold genes in the Spo0A regulon of *Bacillus subtilis*. *J Bacteriol* **187:** 1357–1368.

Fux, C.A., Costerton, J.W., Stewart, P.S., and Stoodley, P. (2005) Survival strategies of infectious biofilms. *Trends Microbiol* **13:** 34–40.

Garcia-Betancur, J.C., Yepes, A., Schneider, J., and Lopez, D. (2012) Single-cell analysis of *Bacillus subtilis* biofilms using fluorescence microscopy and flow cytometry. *J Vis Exp* **60:** e3796.

Guerout-Fleury, A.M., Frandsen, N., and Stragier, N.P. (1996) Plasmids for ectopic integration in *Bacillus subtilis*. *Gene* **180:** 57–61.

Hamon, M.A., Stanley, N.R., Britton, R.A., Grossman, A.D., and Lazazzera, B.A. (2004) Identification of AbrB-regulated genes involved in biofilm formation by *Bacillus subtilis*. *Mol Microbiol* **52:** 847–860.

Hardwood, C.R., and Cutting, S.M. (1990) *Molecular Biological Methods for Bacillus*. New York: Wiley.

Hinderhofer, M., Walker, C.A., Friemel, A., Stuermer, C.A., Moller, H.M., and Reuter, A. (2009) Evolution of prokaryotic SPFH proteins. *BMC Evol Biol* **9:** 10.

Huang, X., Gaballa, A., Cao, M., and Helmann, J.D. (1999) Identification of target promoters for the *Bacillus subtilis* extracytoplasmic function sigma factor, sigma W. *Mol Microbiol* **31:** 361–371.

Ireton, K., Rudner, D.Z., Siranosian, K.J., and Grossman, A.D. (1993) Integration of multiple developmental signals in *Bacillus subtilis* through the Spo0A transcription factor. *Genes Dev* **7:** 283–294.

Ito, K., and Akiyama, Y. (2005) Cellular functions, mechanism of action, and regulation of FtsH protease. *Annu Rev Microbiol* **59:** 211–231.

Jiang, M., Shao, W., Perego, M., and Hoch, J.A. (2000) Multiple histidine kinases regulate entry into stationary phase and sporulation in *Bacillus subtilis*. *Mol Microbiol* **38:** 535–542.

Karatan, E., and Watnick, P. (2009) Signals, regulatory networks, and materials that build and break bacterial biofilms. *Microbiol Mol Biol Rev* **73:** 310–347.

Kawai, F., Shoda, M., Harashima, R., Sadaie, Y., Hara, H., and Matsumoto, K. (2004) Cardiolipin domains in *Bacillus subtilis* marburg membranes. *J Bacteriol* **186:** 1475–1483.

Le, A.T., and Schumann, W. (2009) The Spo0E phosphatase of *Bacillus subtilis* is a substrate of the FtsH metalloprotease. *Microbiology* **155:** 1122–1132.

LeDeaux, J.R., Yu, N., and Grossman, A.D. (1995) Different roles for KinA, KinB, and KinC in the initiation of sporulation in *Bacillus subtilis*. *J Bacteriol* **177:** 861–863.

Lee, Y.H., Kingston, A.W., and Helmann, J.D. (2012) Glutamate dehydrogenase affects resistance to cell wall antibiotics in *Bacillus subtilis*. *J Bacteriol* **194:** 993–1001.

Lopez, D., and Kolter, R. (2010a) Functional microdomains in bacterial membranes. *Genes Dev* **24:** 1893–1902.

Lopez, D., and Kolter, R. (2010b) Extracellular signals that define distinct and coexisting cell fates in *Bacillus subtilis*. *FEMS Microbiol Rev* **34:** 134–149.

Lopez, D., Vlamakis, H., and Kolter, R. (2009a) Generation of multiple cell types in *Bacillus subtilis*. *FEMS Microbiol Rev* **33:** 152–163.

Lopez, D., Fischbach, M.A., Chu, F., Losick, R., and Kolter, R. (2009b) Structurally diverse natural products that cause potassium leakage trigger multicellularity in *Bacillus subtilis*. *Proc Natl Acad Sci USA* **106:** 280–285.

Lopez, D., Vlamakis, H., Losick, R., and Kolter, R. (2009c) Paracrine signaling in a bacterium. *Genes Dev* **23:** 1631–1638.

Lopez, D., Vlamakis, H., Losick, R., and Kolter, R. (2009d) Cannibalism enhances biofilm development in *Bacillus subtilis*. *Mol Microbiol* **74:** 609–618.

Lopez, D., Vlamakis, H., and Kolter, R. (2010) Biofilms. *Cold Spring Harb Perspect Biol* **2:** a000398.

Lysenko, E., Ogura, T., and Cutting, S.M. (1997) Characterization of the ftsH gene of *Bacillus subtilis*. *Microbiology* **143** (Pt 3): 971–978.

McLoon, A.L., Guttenplan, S.B., Kearns, D.B., Kolter, R., and Losick, R. (2011) Tracing the domestication of a biofilm-forming bacterium. *J Bacteriol* **193:** 2027–2034.

Malaga-Trillo, E., Laessing, U., Lang, D.M., Meyer, A., and Stuermer, C.A. (2002) Evolution of duplicated reggie genes in zebrafish and goldfish. *J Mol Evol* **54:** 235–245.

Matsumoto, K., Kusaka, J., Nishibori, A., and Hara, H. (2006) Lipid domains in bacterial membranes. *Mol Microbiol* **61:** 1110–1117.

Morrow, I.C., and Parton, R.G. (2005) Flotillins and the PHB domain protein family: rafts, worms and anaesthetics. *Traffic* **6:** 725–740.

Moszer, I., Jones, L.M., Moreira, S., Fabry, C., and Danchin, A. (2002) SubtiList: the reference database for the *Bacillus subtilis* genome. *Nucleic Acids Res* **30:** 62–65.

Murray, E.J., Strauch, M.A., and Stanley-Wall, N.R. (2009) SigmaX is involved in controlling *Bacillus subtilis* biofilm architecture through the AbrB homologue Abh. *J Bacteriol* **191:** 6822–6832.

Nakano, S., Kuster-Schock, E., Grossman, A.D., and Zuber, P. (2003) Spx-dependent global transcriptional control is induced by thiol-specific oxidative stress in *Bacillus subtilis*. *Proc Natl Acad Sci USA* **100:** 13603–13608.

Novick, R.P. (1991) Genetic systems in staphylococci. *Methods Enzymol* **204:** 587–636.

van Ooij, C., and Losick, R. (2003) Subcellular localization of a small sporulation protein in *Bacillus subtilis*. *J Bacteriol* **185:** 1391–1398.

O'Toole, G.A., and Kolter, R. (1998a) Flagellar and twitching motility are necessary for *Pseudomonas aeruginosa* biofilm development. *Mol Microbiol* **30:** 295–304.

O'Toole, G.A., and Kolter, R. (1998b) Initiation of biofilm formation in Pseudomonas fluorescens WCS365 proceeds via multiple, convergent signalling pathways: a genetic analysis. *Mol Microbiol* **28:** 449–461.

Prajapati, R.S., Ogura, T., and Cutting, S.M. (2000) Structural and functional studies on an FtsH inhibitor from *Bacillus subtilis*. *Biochim Biophys Acta* **1475:** 353–359.

Ramamurthi, K.S., Clapham, K.R., and Losick, R. (2006) Peptide anchoring spore coat assembly to the outer fore-

spore membrane in *Bacillus subtilis*. *Mol Microbiol* **62:** 1547–1557.

Ramamurthi, K.S., Lecuyer, S., Stone, H.A., and Losick, R. (2009) Geometric cue for protein localization in a bacterium. *Science* **323:** 1354–1357.

Schumann, W. (1999) FtsH – a single-chain charonin? *FEMS Microbiol Rev* **23:** 1–11.

Stewart, P.S., and Franklin, M.J. (2008) Physiological heterogeneity in biofilms. *Nat Rev Microbiol* **6:** 199–210.

Tavernarakis, N., Driscoll, M., and Kyrpides, N.C. (1999) The SPFH domain: implicated in regulating targeted protein turnover in stomatins and other membrane-associated proteins. *Trends Biochem Sci* **24:** 425–427.

Turner, M.S., and Helmann, J.D. (2000) Mutations in multidrug efflux homologs, sugar isomerases, and antimicrobial biosynthesis genes differentially elevate activity of the sigma(X) and sigma(W) factors in *Bacillus subtilis*. *J Bacteriol* **182:** 5202–5210.

Veening, J.W., Smits, W.K., and Kuipers, O.P. (2008) Bistability, epigenetics, and bet-hedging in bacteria. *Annu Rev Microbiol* **62:** 193–210.

Vlamakis, H., Aguilar, C., Losick, R., and Kolter, R. (2008) Control of cell fate by the formation of an architecturally complex bacterial community. *Genes Dev* **22:** 945–953.

Wach, A. (1996) PCR-synthesis of marker cassettes with long flanking homology regions for gene disruptions in *S. cerevisiae*. *Yeast* **12:** 259–265.

Walker, C.A., Hinderhofer, M., Witte, D.J., Boos, W., and Moller, H.M. (2008) Solution structure of the soluble domain of the NfeD protein YuaF from *Bacillus subtilis*. *J Biomol NMR* **42:** 69–76.

Wang, K.H., Isidro, A.L., Domingues, L., Eskandarian, H.A., McKenney, P.T., Drew, K., *et al*. (2009) The coat morphogenetic protein SpoVID is necessary for spore encasement in *Bacillus subtilis*. *Mol Microbiol* **74:** 634–649.

Wehrl, W., Niederweis, M., and Schumann, W. (2000) The FtsH protein accumulates at the septum of *Bacillus subtilis* during cell division and sporulation. *J Bacteriol* **182:** 3870–3873.

Wiegert, T., Homuth, G., Versteeg, S., and Schumann, W. (2001) Alkaline shock induces the *Bacillus subtilis* sigma(W) regulon. *Mol Microbiol* **41:** 59–71.

Winter, A., Kamarainen, O., and Hofmann, A. (2007) Molecular modeling of prohibitin domains. *Proteins* **68:** 353–362.

Yasbin, R.E., and Young, F.E. (1974) Transduction in *Bacillus subtilis* by bacteriophage SPP1. *J Virol* **14:** 1343–1348.

Zellmeier, S., Zuber, U., Schumann, W., and Wiegert, T. (2003) The absence of FtsH metalloprotease activity causes overexpression of the sigmaW-controlled pbpE gene, resulting in filamentous growth of *Bacillus subtilis*. *J Bacteriol* **185:** 973–982.

Zhang, H.M., Li, Z., Tsudome, M., Ito, S., Takami, H., and Horikoshi, K. (2005) An alkali-inducible flotillin-like protein from *Bacillus halodurans* C-125. *Protein J* **24:** 125–131.

Supporting information

Additional supporting information may be found in the online version of this article.

Please note: Wiley-Blackwell are not responsible for the content or functionality of any supporting materials supplied by the authors. Any queries (other than missing material) should be directed to the corresponding author for the article.

A

FtsH

MNRVFRNTIFYLLILLVVIGVVSYFQTSNPKTENMSYSTFIKNLDDGKVDSVSVQP
VRGVYEVKGQLKNYDKDQYFLTHVPEGKGADQIFNALKKTDVKVEPAQETSGWVTF
LTTIIPFVIIFILFFFLLNQAQGGGSRVMNFGKSKAKLYTEEKKRVKFKDVAGADE
EKQELVEVVEFLKDPRKFAELGARIPKGVLLVGPPGTGKTLLAKACAGEAGVPFFS
ISGSDFVEMFVGVGASRVRDLFENAKKNAPCLIFIDEIDAVGRQRGAGLGGGHDER
EQTLNQLLVEMDGFSANEGIIIIAATNRADILDPALLRPGRFDRQITVDRPDVIGR
EAVLKVHARNKPLDETVNLKSIAMRTPGFSGADLENLLNEAALVAARQNKKKIDAR
DIDEATDRVIAGPAKKSRVISKKERNIVAYHEGGHTVIGLVLDEADMVHKVTIVPR
GQAGGYAVMLPREDRYFQTKPELLDKIVGLLGGRVAEEIIFGEVSTGAHNDFQRAT
NIARRMVTEFGMSEKLGPLQFGQSQGGQVFLGRDFNNEQNYSDQIAYEIDQEIQRI
IKECYERAKQILTENRDKLELIAQTLLKVETLDAEQIKHLIDHGTLPERNFSDDEK
NDDVKVNILTKTEEKKDDTKE

B

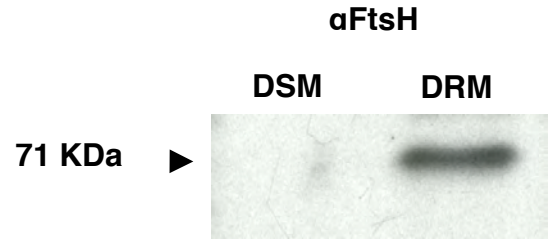

Figure S1: Detection of FtsH in the DRM fraction by mass spectrometry and western blot analysis. (A) Amino acid sequence of FtsH from *B. subtilis*. The oligopeptides from FtsH that were identified in the sample by mass spectrometry analysis are underlined. **(B)** Detection of FtsH by western blot analysis in of the DRM and DSM fraction using polyclonal antibodies against FtsH. The signal was only detected in the DRM fraction. Arrow indicates the molecular weight marker of 71 KDa.

Figure S1

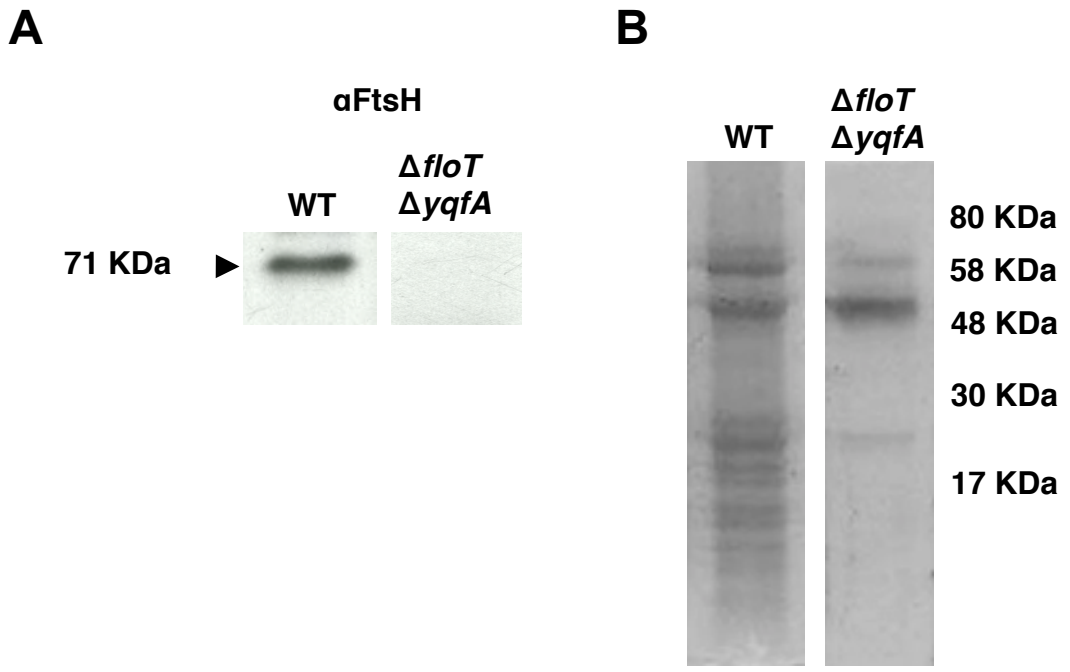

Figure S2: Proteins associated to the DRM fraction decreased in the absence of the flotillin homologs. (A) Western blot analysis using polyclonal antibodies against FtsH to detect the presence of FtsH in the DRM fraction of the wild type strain and the Δ*floT* Δ*yqfA* mutant. Signal was only detected in the DRM fraction of the wild type strain. The arrow indicates the molecular weight expected for FtsH protein. **(B)** SDS-PAGE showing the pool of proteins associated with the membrane fraction that is resistant to detergent solubilization (DRM). The panel shows samples from the wild type strain and in the double Δ*floT* Δ*yqfA* mutant. The protein pattern was analyzed by coomassie staining. Molecular weights are labeled on the right. The protein content of the DRM fractions decreases in the absence of the flotillin-like proteins FloT and YqfA.

Figure S2

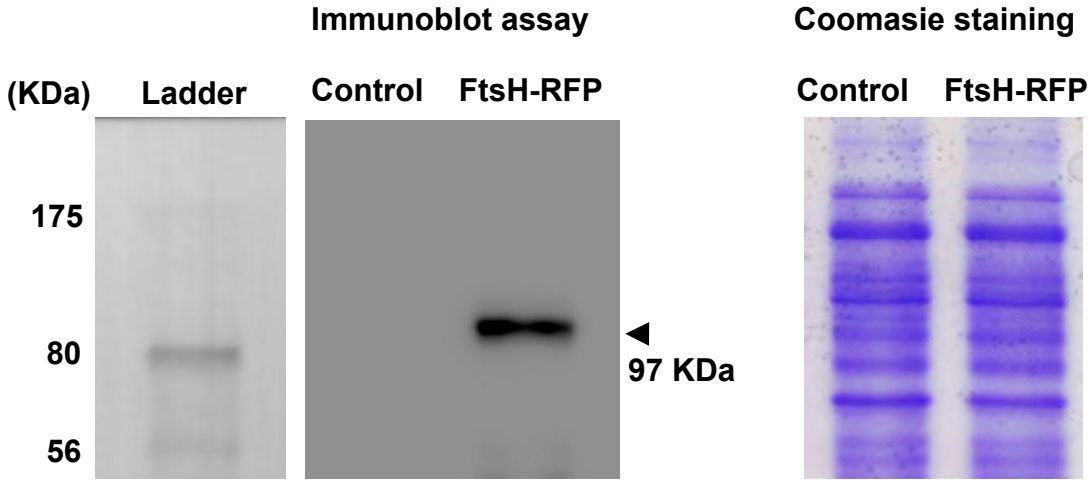

Figure S3: FtsH-RFP is not subject to proteolytic cleavage. Western blot analysis using polyclonal antibodies against RFP to detect the expression and the molecular weight of the translational fusion FtsH-RFP (MW_{FtsH} = 71 KDa + MW_{RFP} = 26 KDa; Total 97 KDa). Negative control in the immunoblot assay is represented by wild-type cell extracts expressing no translational fusion (left lane). The right lane shows the immunoblot analysis extracts from the Δ*ftsH lacA*::P_{hp}-FtsH-RFP strain. The arrow indicates the molecular weight expected for FtsH protein. Coomassie staining of the SDS-PAGE is shown on the right for analysis of the protein content of the cell extracts.

Figure S3

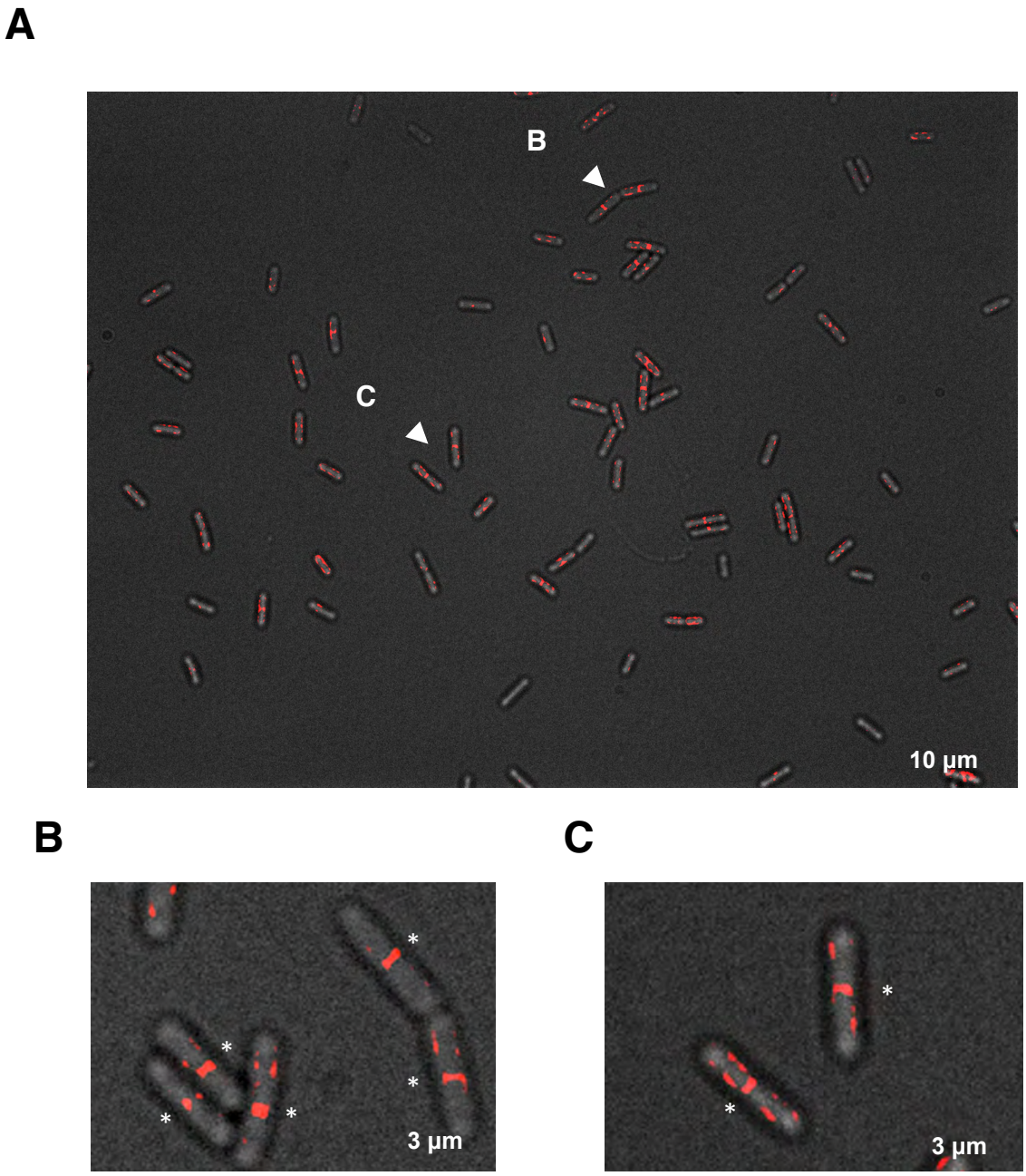

Figure S4: Subcellular localization of the protease FtsH using the translational fusion FtsH-RFP. Fluorescence micrographs of a field of exponentially growing cells labeled with the translational fusion FtsH-RFP (false colored in red). The fluorescence signal shows high concentration in the midcell and lower concentration in certain foci across the cellular membrane. Cells were grown in liquid shaking MSgg at 30°C and cells were harvested in the middle of the exponential phase (approx. 8h of incubation). Arrows indicate detailed fields that are magnified in panels B and C. Asterisks in panels B and C show the midcell position of the signal FtsH-RFP in some cells. The expression of FtsH-RFP was controlled by an IPTG-inducible promoter (induction with 1mM IPTG).

Figure S4

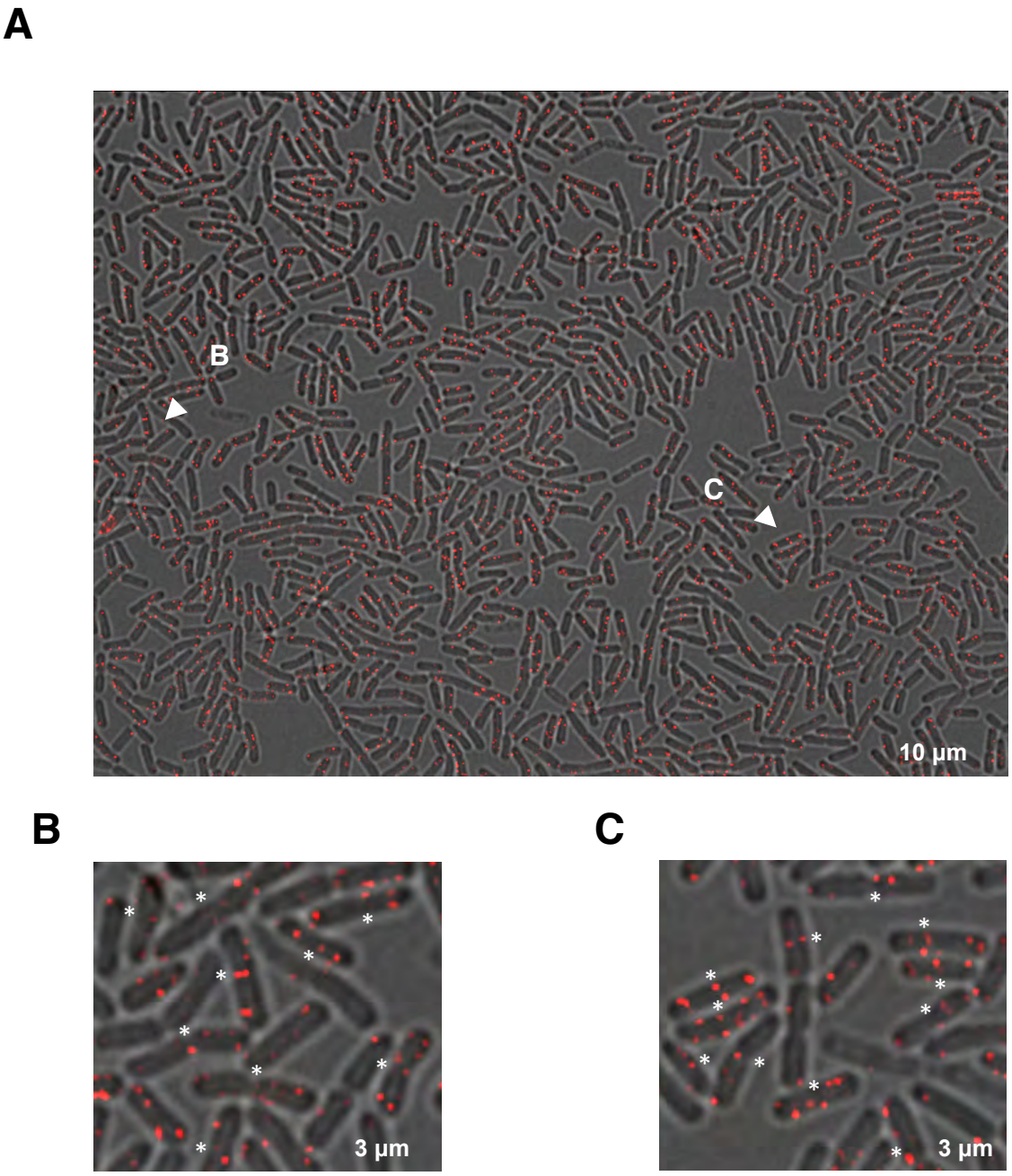

Figure S5: Subcellular localization of the flotillin-like protein FloT using the translational fusion FloT-YFP. Fluorescence micrographs of a field of exponentially growing cells labeled with the translational fusion FloT-YFP (false colored in red). The fluorescence signal shows the typical distribution in foci across the cellular membrane with a high concentration in the midcell. Cells were grown in liquid shaking MSgg at 30°C and cells were harvested in the middle of the exponential phase (approx. 8h of incubation). Arrows indicate detailed fields that are magnified in panels B and C. Asterisks in panels B and C show the midcell position of the signal FloT-YFP in cells.

Figure S5

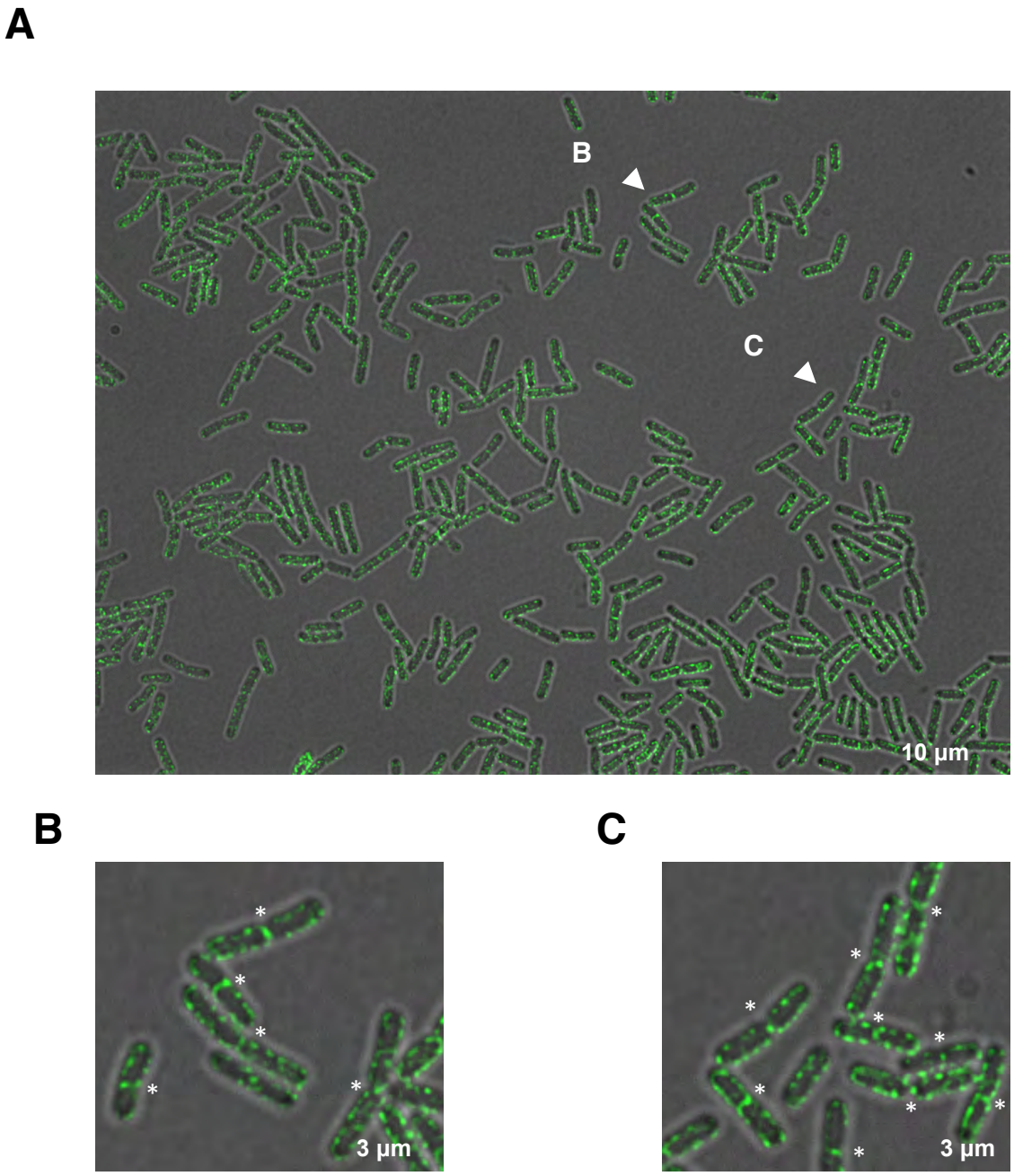

Figure S6: Subcellular localization of the flotillin-like protein YqfA using the translational fusion YqfA-GFP. Fluorescence micrographs of a field of exponentially growing cells labeled with the translational fusion YqfA-GFP (false colored in green). The fluorescence signal shows the typical distribution in foci across the cellular membrane with a high concentration in the midcell. Cells were grown in liquid shaking MSgg at 30°C and cells were harvested in the middle of the exponential phase (approx. 8h of incubation). Arrows indicate detailed fields that are magnified in panels B and C. Asterisks in panels B and C show the midcell position of the signal YqfA-GFP in cells.

Figure S6

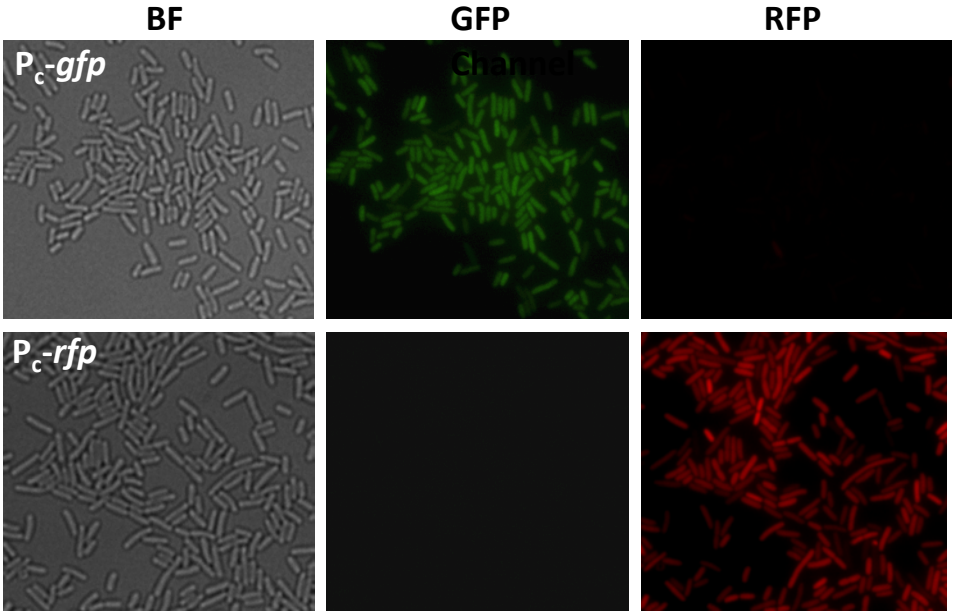

Figure S7: There is no interference between the green and red fluorescence signal. Fluorescence micrographs and transmitted light images of *E. coli* strains grown in liquid shaking LB at 37°C for 24h. The strains expressed GFP (upper row) or RFP (bottom row) under the control of a constitutive promoter (P_c). scale bar is 5 µm. Fluorescence signal detected in the green and red channel are presented in GFP and RFP labeled columns, respectively. Transmitted light images are presented in the column labeled as BF.

Figure S7

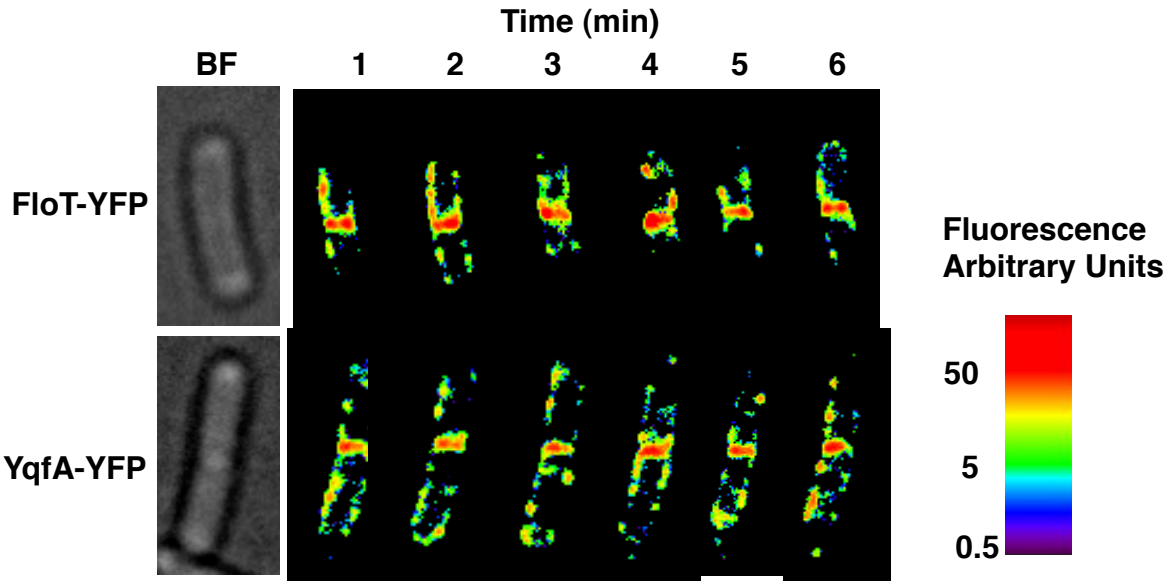

Figure S8: Flotillins are permanently present at the midcell. Time-lapse fluorescence analysis of the distribution pattern of FloT-YFP and YqfA-GFP foci. Cells were grown in liquid shaking MSgg at 30°C for 8h. Exponentially growing cells were mounted on agarose-coated slides. The upper row shows the distribution of the FloT–YFP foci within the same cell for 6 min. The bottom row shows the distribution of the YqfA–GFP foci within the same cell for 6 min. This figure corresponds to figure 7 of the body of the paper. Fluorescence signal is quantified in relation to the background fluorescence using a color spectrum logarithmic scale, in which higher intensity of the fluorescence signal is represented in red tones (scale is presented on the right). Scale bar is 2 μm.

Figure S8

FloT-YFP

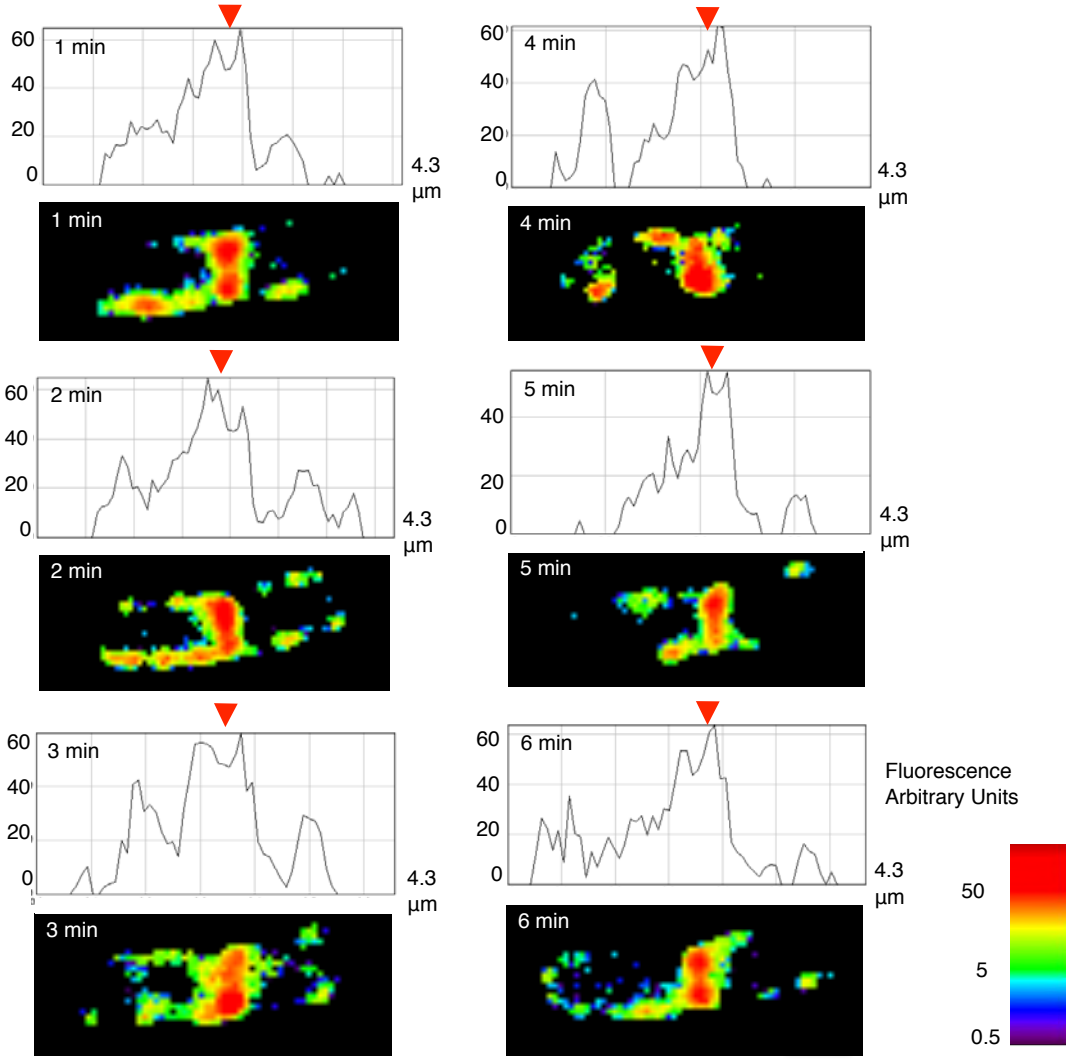

Figure S9: Quantification of relative fluorescence intensity detected in the time-lapse fluorescence analysis of FloT-YFP. Time-lapse fluorescence analysis of the distribution pattern of FloT-YFP foci for a time period of 6 min. Each panel shows a detailed micrograph of the distribution of the FloT–YFP foci within the same cell at every point (in min). Fluorescence signal is quantified in relation to the background fluorescence, using a color spectrum logarithmic scale (spectrum scale is presented on the right). The relative fluorescence intensity values of each micrograph is represented in a graph (above each micrograph). X-axis represents the cell length and y-axis represents the value of relative fluorescence intensity detected. The midcell is marked with a red arrow. Scale bar is 1 µm.

Figure S9

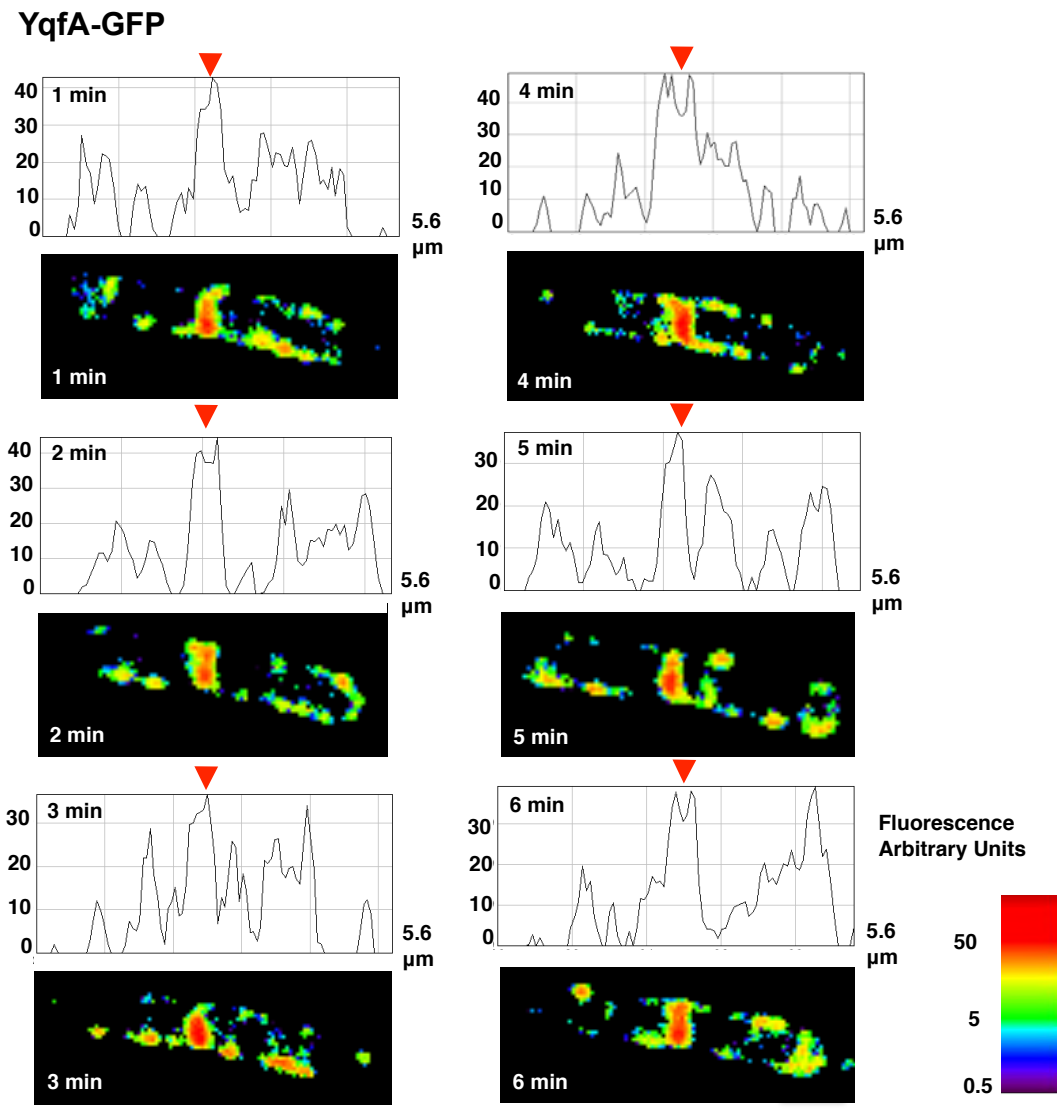

Figure S10: Quantification of relative fluorescence intensity detected in the time-lapse fluorescence analysis of YqfA-GFP. Time-lapse fluorescence analysis of the distribution pattern of YqfA-GFP foci for a time period of 6 min. Each panel shows a detailed micrograph of the distribution of the YqfA–GFP foci within the same cell at every point (in min). Fluorescence signal is quantified in relation to the background fluorescence, using a color spectrum logarithmic scale (spectrum scale is presented on the right). The relative fluorescence intensity values of each micrograph is represented in a graph (above each micrograph). X-axis represents the cell length and y-axis represents the value of relative fluorescence intensity detected. The midcell is marked with a red arrow. Scale bar is 1 μm.

Figure S10

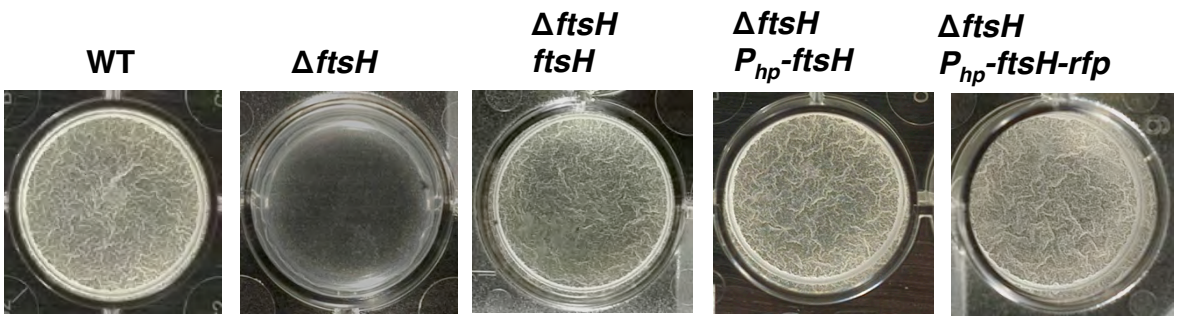

Figure S11: Complementation of the Δ*ftsH* mutant with a wild-type copy of *ftsH* restored biofilm formation. Pellicle formation assay of different strains of *B. subtilis*. Pictures show a top view of the pellicles formed on the surface of MSgg liquid cultures incubated in 24-well plates at 30°C for 24h. Positive control is represented by the wild-type strain (WT) (left panel). Δ*ftsH* mutant shows no pellicle formation (second panel). Complementation of Δ*ftsH* mutant with a copy of *ftsH* induced by its own promoter partially restored biofilm formation (third panel). Complementation of Δ*ftsH* mutant with an IPTG-inducible copy of *ftsH* restored wild-type levels of biofilm formation. Similar results were obtained when the Δ*ftsH* mutant was complemented with the translational fusion FtsH-RFP (right panel). IPTG was added to a final concentration of 1mM.

Figure S11

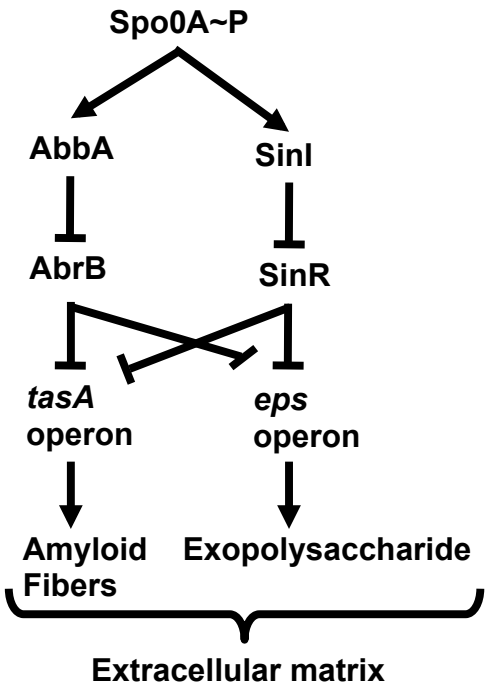

Figure S12: Flow scheme of the regulatory circuit involved in extracellular matrix production. Arrows indicate activation of transcription and T bars indicate repression. AbrB and SinR are two regulatory repressors that independently repress the genes required for the production of amyloid fibers and exopolysaccharide production. Both exopolysacchride and amyloid fibers are important constituent of the extracellular matrix of the biofilm. Repression of AbrB and SinR expression is driven by the activation of the master regulator Spo0A~P.

Figure S12

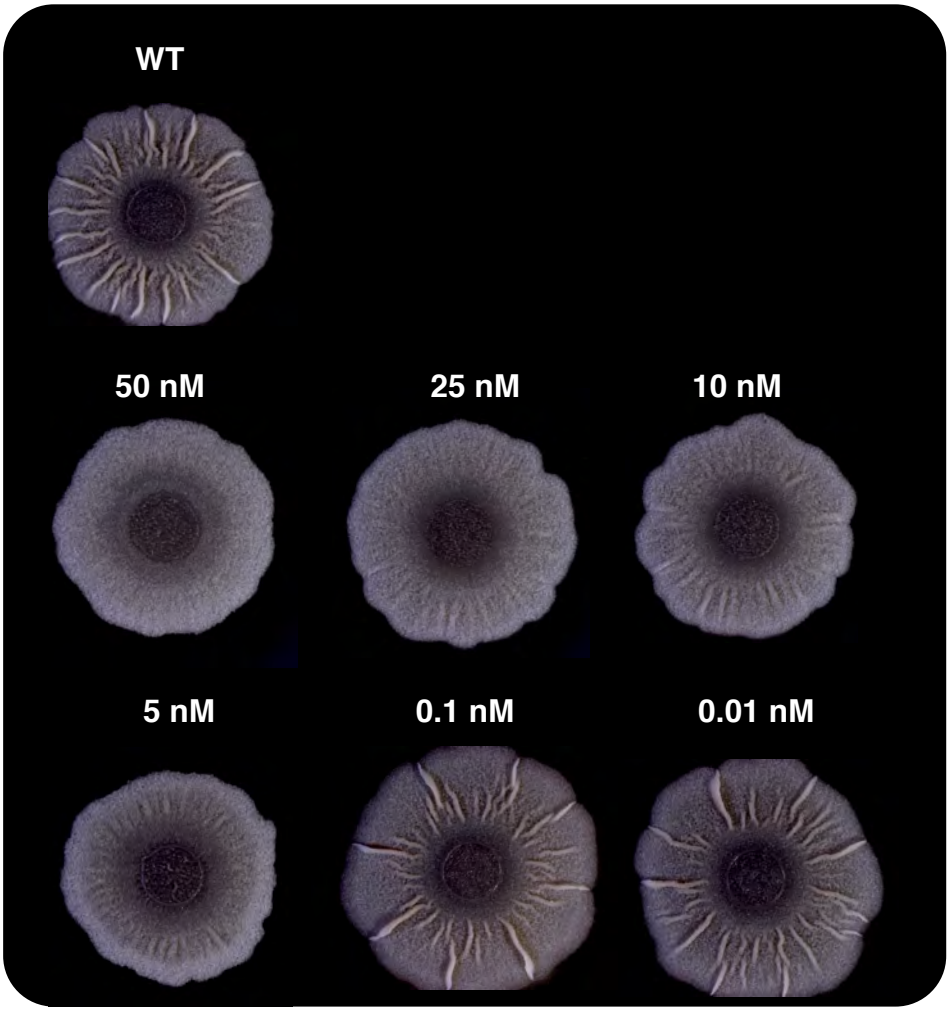

Figure S13: Colony morphology assay of *B. subtilis* NCIB3610 in the presence of a range of concentrations of the SpoVM protein. The ability of *B. subtilis* 3610 to make biofilm in solid MSgg agar can be correlated to the amount of wrinkles that are present in the surface of the colony. Addition of small concentrations of SpoVM inhibited the formation of wrinkles, which is indicative of an inhibition of biofilm formation. Gradual decrease of the concentration of SpoVM restored the formation of wrinkles in the colonies of *B. subtilis*. Colonies were incubated in MSgg agar at at 30°C for 72h.

Figure S13

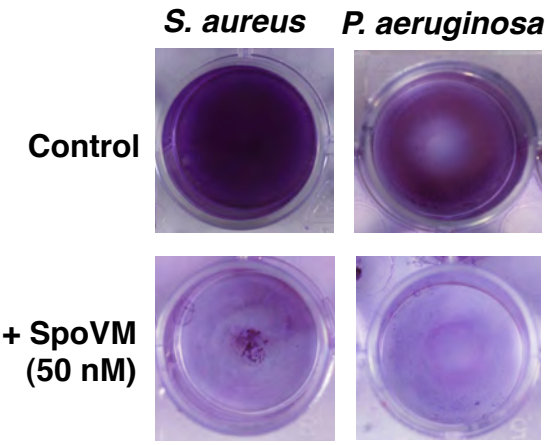

Figure S14: SpoVM inhibits biofilm formation. Biofilm formation assay of *S. aureus* SC-01 and *P. aeruginosa* PA14. 1ml of the culture was dispensed in polystyrene well plates and incubated overnight at 37° C. Biofilms were stained with crystal violet for better visualization. Addition of 50 nM of the peptide SpoVM inhibited the ability of both strains to form biofilm attached to the bottom of the well, evidenced by the absence of crystal violet dye after staining.

Figure S14

Table S1: Proteins associated with the DRM fraction in *B. subtilis*

Protein	Function	Functional Category
FtsH	Metalloprotease	Cell shape
MreBH	Actin-like protein	
MreC	Actin-associated protein	
EzrA	Tubulin-associated protein	
OppA	Oligopeptide ABC transporter	Quorum sensing
PrsA	Protease secretion chaperone.	Protease secretion
FeuA	Iron-uptake system (binding protein)	Iron uptake
FeuB	Iron-uptake system (membrane protein)	
PbpC	Penicillin-binding protein 3	Penicillin-binding proteins
DacA	Penicillin-binding protein 5	
DacC	Penicillin-binding protein	
YxeB	Unknown. Similar to ABC transporter	Unknown
YwjA	Unknown. Similar to ABC transporter	
YknZ	Unknown. Similar to ABC transporter	
YwbM	Unknown	
YcdA	Unknown	
YerH	Unknown	
YufN	Unknown	
AdcA	Lipoprotein	Transporter
BdbD	Thiol-disulfide oxidorreductase	Protein folding
Qox2	Quinol oxidase	Redox enzyme
YxeM	ABC transporter	Transporter
RbsB	ABC transporter	Transporter
YkwC	Unknown	Unknown
YeeF	Unknown	
YpuA	Unknown	

Table S1 (continuation): Proteins associated with the DRM fraction in *B. subtilis*

Amino acid sequence of the proteins listed in table S1. The oligopeptides that were identified in the samples by mass spectrometry analysis are underlined. The percentage coverage value obtained for each protein is shown in parenthesis.

FtsH (38.93 %)

MNRVFRNTIFYLLILLVVIGVVSYFQTSNPKTENMSYSTFIKNLDDGKVDSVSVQPVRGVYEVKGQLKNYD
KDQYFLTHVPEGKGADQIFNALKKTDVKVEPAQETSGWVTFLTTIIPFVIIFILFFFLLNQAQGGGSRVMN
FGKSKAKLYTEEKKRVKFKDVAGADEEKQELVEVVEFLKDPRKFAELGARIPKGVLLVGPPGTGKTLLAKA
CAGEAGVPFFSISGSDFVEMFVGVGASRVRDLFENAKKNAPCLIFIDEIDAVGRQRGAGLGGGHDEREQTL
NQLLVEMDGFSANEGIIIIAATNRADILDPALLRPGRFDRQITVDRPDVIGREAVLKVHARNKPLDETVNL
KSIAMRTPGFSGADLENLLNEAALVAARQNKKKIDARDIDEATDRVIAGPAKKSRVISKKERNIVAYHEGG
HTVIGLVLDEADMVHKVTIVPRGQAGGYAVMLPREDRYFQTKPELLDKIVGLLGGRVAEEIIFGEVSTGAH
NDFQRATNIARRMVTEFGMSEKLGPLQFGQSQGGQVFLGRDFNNEQNYSDQIAYEIDQEIQRIIKECYERA
KQILTENRDKLELIAQTLLKVETLDAEQIKHLIDHGTLPERNFSDDEKNDDVKVNILTKTEEKKDDTKE

MreBH (48.06 %)

MFQSTEIGIDLGTANILVYSKNKGIILNEPSVVAVDTTTKAVLAIGADAKNMIGKTPGKIVAVRPMKDGVI
ADYDMTTDLLKHIMKKAAKSIGMSFRKPNVVVCTPSGSTAVERRAISDAVKNCGAKNVHLIEEPVAAAIGA
DLPVDEPVANVVVDIGGGTTEVAIISFGGVVSCHSIRIGGDQLDEDIVSFVRKKYNLLIGERTAEQVKMEI
GHALIEHIPEAMEIRGRDLVTGLPKTIMLQSNEIQDAMRESLLHILEAIRATLEDCPPELSGDIVDRGVIL
TGGGALLNGIKEWLTEEIVVPVHVAQNPLESVAIGTGRSLEVIDKLQKAIK

MreC (52.41 %)

MPNKRLMLLLLCIIILVAMIGFSLKGGRNTTWPEKVIGDTTGVFQNIFHTPAEFFAGIFENINDLKNTYKE
NERLREKLDGQTQYEAKLQELEEENKSLRDELGHVKSIKDYKPILATVIARSPDNWAKQVTINKGTQQNVA
FDMAVTNEKGALIGKIKSSGLNNFTSAVQLLSDPDRNNRVATKISGKKGSKGYGLIEGYDKEKKRLKMTII
ERKDKQDVKKGDLIETSGTGGVFPEGLTIGEVTDIESDSYGLTKVAYVKPAADLTDLNNVIVVNRDVPTVD
TEEEGS

EzrA (52.85 %)

MEFVIGLLIVLLALFAAGYFFRKKIYAEIDRLESWKIEILNRSIVEEMSKIKHLKMTGQTEEFFEKWREEW
DEIVTAHMPKVEELLYDAEENADKYRFKKANQVLVHIDDLLTAAESSIEKILREISDLVTSEEKSREEIEQ
VRERYSKSRKNLLAYSHLYGELYDSLEKDLDEIWSGIKQFEEETEGGNYITARKVLLEQDRNLERLQSYID
DVPKLLADCKQTVPGQIAKLKDGYGEMKEKGYKLEHIQLDKELENLSNQLKRAEHVLMTELDIDEASAILQ
LIDENIQSVYQQLEGEVEAGQSVLSKMPELIIAYDKLKEEKEHTKAETELVKESYRLTAGELGKQQAFEKR
LDEIGKLLSSVKDKLDAEHVAYSLLVEEVASIEKQIEEVKKEHAEYRENLQALRKEELQARETLSNLKKTI
SETARLLKTSNIPGIPSHIQEMLENAHHHIQETVNQLNELPLNMEEAGAHLKQAEDIVNRASRESEELVEQ
VILIEKIIQFGNRFRSQNHILSEQLKEAERRFYAFDYDDSYEIAAAAVEKAAPGAVEKIKADISA

OppA (59.63 %)

MKKRWSIVTLMLIFTLVLSACGFGGSGSNGEGKKDSKGKTTLNININKTEPFSLHPGLANDSVSGGVIRQTF
EGLTRINADGEPEEGMASKIETSKDGKTYTFTIRDGVKWSNGDPVTAQDFEYAWKWALDPNNESQYAYQLY
YIKGAEAANTGKGSLDDVAVKAVNDKTLKVELNNPTPYFTELTAFYTYMPINKKIAEKNKKWNTNAGDDYV
SNGPFKMTAWKHSGSITLEKNDQYWDKDKVKLKKIDMVMINNNNTELKKFQAGELDWAGMPLGQLPTESLP
TLKKDGSLHVEPIAGVYWYKFNTEAKPLDNVNIRKALTYSLDRQSIVKNVTQGEQIPAMAAVPPTMKGFED
NKEGYFKDNDVKTAKEYLEKGLKEMGLSKASDLPKIKLSYNTDDAHAKIAQAVQEMWKKNLGVDVELDNSE
WNVYIDKLHSQDYQIGRMGWLGDFNDPINFLELFRDKNGGNNDTGWENPEFKKLLNQSQTETDKTKRAELL
KKAEGIFIDEMPVAPIYFYTDTWVQDENLKGVIMPGTGEVYFRNAYFK

PrsA (72.60 %)
MKKIAIAAITATSILALSACSSGDKEVIAKTDAGDVTKGELYTNMKKTAGASVLTQLVQEKVLDKKYKVSD
KEIDNKLKEYKTQLGDQYTALEKQYGKDYLKEQVKYELLTQKAAKDNIKVTDADIKEYWEGLKGKIRASHI
LVADKKTAEEVEKKLKKGEKFEDLAKEYSTDSSASKGGDLGWFAKEGQMDETFSKAAFKLKTGEVSDPVKT
QYGYHIIKKTEERGKYDDMKKELKSEVLEQKLNDNAAVQEAVQKVMKKADIEVKDKDLKDTFNTSSTSNST
SSSSSNSK

FeuA (61.51 %)
MKKISLTLLILLLALTAAACGSKNESTASKASGTASEKKKIEYLDKTYEVTVPTDKIAITGSVESMEDAKL
LDVHPQGAISFSGKFPDMFKDITDKAEPTGEKMEPNIEKILEMKPDVILASTKFPEKTLQKISTAGTTIPV
SHISSNWKENMMLLAQLTGKEKKAKKIIADYEQDLKEIKTKINDKAKDSKALVIRIRQGNIYIYPEQVYFN
STLYGDLGLKAPNEVKAAKAQELSSLEKLSEMNPDHIFVQFSDDENADKPDALKDLEKNPIWKSLKAVKED
HVYVNSVDPLAQGGTAWSKVRFLKAAAEKLTQN

FeuB (38.32 %)
MYSKQWTRIILITSPFAIALSLLLSILYGAKHLSTDIVFTSLIHFDPGNTDHQIIWHSRIPRAAGALLIGA
ALAVSGALMQGITRNYLASPSIMGVSDGSAFIITLCMVLLPQSSSIEMMIYSFIGSALGAVLVFGLAAMMP
NGFTPVQLAIIGTVTSMLLSSLSAAMSIYFQISQDLSFWYSARLHQMSPDFLKLAAPFFLIGIIMAISLSK
KVTAVSLGDDISKSLGQKKKTIKIMAMLSVIILTGSAVALAGKIAFVGLVVPHITRFLVGSDYSRLIPCSC
ILGGIFLTLCDLASRFINYPFETPIEVVTSIIGVPFFLYLIKRKGGEQNG

PbpC (56.14 %)
MLKKCILLVFLCVGLIGLIGCSKTDSPEDRMEAFVKQWNDQQFDDMYQSLTKDVKKEISKKDFVNRYKAIY
EQAGVKNLKVTAGEVDKDDQDNKTMKHIPYKVSMNTNAGKVSFKNTAVLKLEKTDDEESWNIDWDPSFIFK
QLADDKTVQIMSIEPKRGQIYDKNGKGLAVNTDVPEIGIVPGELGDKKEKVIKELAKKLDLTEDDIKKKLD
QGWVKDDSFVPLKKVKPDQEKLVSEATSLQGVTRTNVSSRYYPYGEKTAHLTGYVRAITAEELKKKKEGTY
SDTSNIGIAGLENVYEDKLRGTTGWKIYVPQTGEVIAEKKAKDGEDLHLTIDIKTQMKLYDELKDDSGAAV
ALQPKTGETLALVSAPSYDPNGFIFGWSDKEWKKLNKDKNNPFSAKFNKTYAPGSTIKPIAAAIGIKNGTL
KADEKKTIKGKEWQKDSSWGGYSVTRVSERLQQVDLENALITSDNIYFAQNALDMGADTFTKGLKTFGFSE
DVPYEFPIQKSSIANDKLDSDILLADTGYGQGQMQMSPLHLATAYTPFVDNGDLVKPTLIKKDSQTADVWH
KQVVTKEGAADITKGLKGVVEDERGSAYQPVVKGITVAGKTGTAELKTSKDDKDGTENGWFVGYDYENKDL
LVAMMIQNVQDRGGSHYVVEKAKKQFQSN

DacA (63.66 %)
MNIKKCKQLLMSLVVLTLAVTCLAPMSKAKAASDPIDINASAAIMIEASSGKILYSKNADKRLPIASMTKM
MTEYLLLEAIDQGKVKWDQTYTPDDYVYEISQDNSLSNVPLRKDGKYTVKELYQATAIYSANAAAIAIAEI
VAGSETKFVEKMNAKAKELGLTDYKFVNATGLENKDLHGHQPEGTSVNEESEVSAKDMAVLADHLITDYPE
ILETSSIAKTKFREGTDDEMDMPNWNFMLKGLVSEYKKATVDGLKTGSTDSAGSCFTGTAERNGMRVITVV
LNAKGNLHTGRFDETKKMFDYAFDNFSMKEIYAEGDQVKGHKTISVDKGKEKEVGIVTNKAFSLPVKNGEE
KNYKAKVTLNKDNLTAPVKKGTKVGKLTAEYTGDEKDYGFLNSDLAGVDLVTKENVEKANWFVLTMRSIGG
FFAGIWGSIVDTVTGWF

DacC (26.27 %)
MKKSIKLYVAVLLLFVVASVPYMHQAALAAEKQDALSGQIDKILADHPALEGAMAGITVRSAETGAVLYEH
SGDTRMRPASSLKLLTAAAALSVLGENYSFTTEVRTDGTLKGKKLNGNLYLKGKGDPTLLPSDFDKMAEIL
KHSGVKVIKGNLIGDDTWHDDMRLSPDMPWSDEYTYYGAPISALTASPNEDYDAGTVIVEVTPNQKEGEEP
AVSVSPKTDYITIKNDAKTTAAGSEKDLTIEREHGTNTITIEGSVPVDANKTKEWISVWEPAGYALDLFKQ
SLKKQGITVKGDIKTGEAPSSSDVLLSHRSMPLSKLFVPFMKLSNNGHAEVLVKEMGKVKKGEGSWEKGLE
VLNSTLPEFGVDSKSLVLRDGSGISHIDAVSSDQLSQLLYDIQDQSWFSAYLNSLPVAGNPDRMVGGTLRN
RMKGTPAQGKVRAKTGSLSTVSSLSGYAETKSGKKLVFSILLNGLIDEEDGKDIEDQIAVILANQ

YxeB (60.19 %)
MKKNILLVGMLVLLLMFVSACSGTASKGSSSDSASEKTEMRTYKSPKGNVNIPAHPKRIVTDFYAGELLSV
GANVVGSGSWSFDNPFLKSKLKNVKDVGDPISVEKVMELQPDLIVVMNEENVDKLKKIAPTVVIPYNTAKN
VEDTVSMFGDIAGAKDQAKSFMADFNKKAEAAKKKIAGVIDKDATFGIYENTDKGEFWVFNDNGGRGGQAV
YNALGLKAPEKIEQDVIKKGEMKQLSQEVIPEYAADYMFITDYNPKGESKTLDKLENSSIWKNLDAVKHNR
VFINDFDSFYPYDPISVSKQVDIITDMLIKRAEEN

YwjA (36.17 %)
MLRQFFSYYKPYKTLFFLDFFSAIAGGLMELSFPLIVNYFIDTLLPGRDWGLIIATSIGLFAVYALSSALQ
YIVTYWGHMLGINIETDMRKSLFDHLQKLSFKFYDNNKTGTLMSKLTNDLMYIGEVAHHGPEDLFIAVMTI
LGAFGVMLFINWQLALLTFIIMPIVIWLALYFNKKMTKAFTTLNKDIGDFSARVENNIGGIRLVQAFGNEA
FEKERFAVNNQRFRVTKLSSYKIMAKNGSISYMLTRFVTLFVLLCGTWFVIRGSLSYGEFVAFVLLTNVLF
RPIDKINAIIEMYPRGIAGFKSYMELMETEPDIQDSPDSKDVSGLKGNIRYKHVSFGYDDHHNVLNDINLS
IQAGETVAFVGPSGAGKSTLCSLLPRFYEASEGDITIDGISIKDMTLSSLRGQIGVVQQDVFLFSGTLRENI
AYGRLGASEEDIWQAVKQAHLEELVHNMPDGLDTMIGERGVKLSGGQKQRLSIARMFLKNPSILILDEAT
SALDTETEAAIQKALQELSEGRTTLVIAHRLATIKDADRIVVVTNNGIEEQGRHQDLIEAGGLYSRLHQAQ
FGQMVHR

YknZ (8.8 %)
MSLLENIRMALSSVLAHKMRSILTMLGIIIGVGSVIVVVAVGQGGEQMLKQSISGPGNTVELYYMPSDEEL
ASNPNAAAESTFTENDIKGLKGIEGIKQVVASTSESMKARYHEEETDATVNGINDGYMNVNSLKIESGRTF
TDNDFLAGNRVGIISQKMAKELFDKTSPLGEVVWINGQPVEIIGVLKKVTGLLSFDLSEMYVPFNMMKSSF
GTSDFSNVSLQVESADDIKSAGKEAAQLVNDNHGTEDSYQVMNMEEIAAGIGKVTAIMTTIIGSIAGISLL
VGGIGVMNIMLVSVTERTREIGIRKSLGATRGQILTQFLIESVVLTLIGGLVGIGIGYGGAALVSAIAGWP
SLISWQVVCGGVLFSMLIGVIFGMLPANKAAKLDPIEALRYE

YwbM (78.7 %)
MNFTKIAVSAGCILALCAGCGANDTSSTKEKASSEKSGVTKEITASVNKMETIISKLNDSVEKGDQKEIEK
KGKELNSYWLSFENDIRSDYPFEYTEIEKHLQPIYTEAQKDKPDAGKIKTESESLKASLEDLTEAKKSGKK
ASDQLAKAADEYKGYVKEQSDQLVKATEAFTGAVKSGDIEKSKTLYAKARVYYERIEPIAESLGDLDPKID
ARENDVEEGDKWTGFHKLEKAIWKDQDISGEKATADQLLKDVKELDGSIQSLKLTPEQIVAGAMELLNEAG
ISKITGEEERYSRIDLVDLMANVEGSEAVYQTVKSALVKDHSDLTEKLDTEFSEFEVLMAKYKTNDQSYTS
YDKLSEKQIRELSTKLTTLSETMSKIANVL

YcdA (75.99 %)
MFQKKTYAVFLILLLMMFTAACSGSKTSAEKKESETEKSSDIAQVKIKDVSYTLPSKYDKSTSDDQLVLKV
NVAVKNTGKDPLNVDSMDFTLYQGDTKMSDTDPEDYSEKLQGSTINADKSVEGNLFFVVDKGKQYELNYTP
ESYGDKKPKSVTFKIDGKDKKILATADKLQDSAKALSAYVDVLLFGKDNADFEKITGANKNEIVNDFNESA
KDGYLSASGLSSTYADSKALDNIVNGIKEGLSKNSSIQAKTTSISKDEAIVEATVKPVDASSLSDRIEDKV
KDYYSKNSSASYEEAVKYALQVYPEEFKKLGPASSEKTVEVKMKKNDIDQWQLDMDDYRAAELVEAFIKE

YerH (55.05 %)
MKKTLALAATAAVLMLSACSSGFGGEKEEEITQKTAKSSEKAIVPKYNISDSYYKMVLPFKAGKARGLTTE
QLNTRLDIDEFETGLMRLAQDSFSTDDYLFQEGQYLDEDTVLSWLARKKTGSDLKKAEKEDKNFKNEGLNP
ALPSSGSTEEKNESSPIYLASMLEHDYLVRKDKNSIQLGGVMIGLALNSVYYYREKTGDPQKEVEIKDSTL
RQQGEKIAQEVINRLRKKDNLKNVPITVALYKQASKTSIVPGNFIAKTEVKAGSTDISNWDDINEKYVFYP
ADTTTAEKYPDDTEVFKRFKNSIEEYFPNYTGVVGTALYENDEMKKMKIDIPMQFYGKSEVVAFTQFLTGE
VMDYYSKSSVDVEVNITSSDGQEAVIIRNAGDKEPTVHIYD

YufN (77.14 %)
MSLVIAAGTILGACGNSEKSSGSGEGKNKFSVAMVTDVGGVDDKSFNQSAWEGIQAFGKENGLKKGKNGYD
YLQSKSDADYTTNLNKLARENFDLIYGVGYLMEDSISEIADQRKNTNFAIIDAVVDKDNVASITFKEQEGS
FLVGVAAALSSKSGKIGFVGGMESELIKKFEVGFRAGVQAVNPKAVVEVKYAGGFDKADVGKATAESMYKS
GVDVIYHSAGATGTGVFTEAKNLKKEDPKRDVWVIGVDKDQYAEGQVEGTDDNVTLTSMVKKVDTVVEDVT
KKASDGKFPGGETLTYGLDQDGVGISPSKQNLSDDVIKAVDKWKKKIIDGLEIPATEKELKTFKAE

AdcA (45.14 %)
MFKKWSGLFVIAACFLLVAACGNSSTKGSADSKGDKLHVVTTFYPMYEFTKQIVKDKGDVDLLIPSSVEPH
DWEPTPKDIANIQDADLFVYNSEYMETWVPSAEKSMGQGHAVFVNASKGIDLMEGSEEEHEEHDHGEHEHS
HAMDPHVWLSPVLAQKEVKNITAQIVKQDPDNKEYYEKNSKEYIAKLQDLDKLYRTTAKKAEKKEFITQHT
AFGYLAKEYGLKQVPIAGLSPDQEPSAASLAKLKTYAKEHNVKVIYFEEIASSKVADTLASEIGAKTEVLN
TLEGLSKEEQDKGLGYIDIMKQNLDALKDSLLVKS

BdbD (74.32 %)
MKKKQQSSAKFAVILTVVVVVLLAAIVIINNKTEQGNDAVSGQPSIKGQPVLGKDDAPVTVVEFGDYKCPS
CKVFNSDIFPKIQKDFIDKGDVKFSFVNVMFHGKGSRLAALASEEVWKEDPDSFWDFHEKLFEKQPDTEQE
WVTPGLLGDLAKSTTKIKPETLKENLDKETFASQVEKDSDLNQKMNIQATPTIYVNDKVIKNFADYDEIKE
TIEKELKGK

Qox2 (53.27 %)
MIFLFRALKPLLVLALLTVVFVLGGCSNASVLDPKGPVAEQQSDLILLSIGFMLFIVGVVFVLFTIILVKY
RDRKGKDNGSYNPEIHGNTFLEVVWTVIPILIVIALSVPTVQTIYSLEKAPEATKDKEPLVVYATSVDWKW
VFSYPEQDIETVNYLNIPVDRPILCKISSADSMASLWIPQLGGQKYAMAGMLMDQYLQADKVGTYEGRNAN
FTGEHFADQEFDVNAVTEKDFNSWVKKTQNEAPKLTKEKYDELMLPENVDELTFSSTHLKYVDHGQDAEYA
MEARKRLGYQAVSPHCKTDPFENVKKNEFKKSDDTEE

YxeM (50.38 %)
MKMKKWTVLVVAALLAVLSACGNGNSSSKEDDNVLHVGATGQSYPFAYKENGKLTGFDVEVMEAVAKKIDM
KLDWKLLEFSGLMGELQTGKLDTISNQVAVTDERKETYNFTKPYAYAGTQIVVKKDNTDIKSVDDLKGKTV
AAVLGSNHAKNLESKDPDKKINIKTYETQEGTLKDVAYGRVDAYVNSRTVLIAQIKKTGLPLKLAGDPIVY
EQVAFPFAKDDAHDKLRKKVNKALDELRKDGTLKKLSEKYFNEDITVEQKH

RbsB (29.51 %)
MKKAVSVILTLSLFLLTACSLEPPQWAKPSNSGNKKEFTIGLSVSTLNNPFFVSLKKGIEKEAKKRGMKVI
IVDAQNDSSKQTSDVEDLIQQGVDALLINPTDSSAISTAVESANAVGVPVVTIDRSAEQGKVETLVASDNV
KGGEMAAAFIADKLGKGAKVAELEGVPGASATRERGSGFHNIADQKLQVVTKQSADFDRTKGLTVMENLLQ
GHPDIQAVFAHNDEMALGALEAINSSGKDILVIGFDGNKDALASIKDRKLSATVAQQPELIGKLATEAADD
ILHGKKVQKTISAPLKLETQK

YkwC (89.24 %)
MKKTIGFIGLGVMGKSMASHILNDGHPVLVYTRTKEKAESILQKGAIWKDTVKDLSKEADVIITMVGYPSD
VEEVYFGSNGIIENAKEGAYLIDMTTSKPSLAKKIAEAAKEKALFALDAPVSGGDIGAQNGTLAIMVGGEK
EAFEACMPIFSLMGENIQYQGPAGSGQHTKMCNQIAIAAGMIGVAEAMAYAQKSGLEPENVLKSITTGAAG
SWSLSNLAPRMLQGNFEPGFYVKHFIKDMGIALEEAELMGEEMPGLSLAKSLYDKLAAQGEENSGTQSIYK
LWVK

YeeF (21.04 %)
MKVFEAKTLLSEATDRAKEYKELRTQMVNLRKALKGVADLSDSEFSGKGASNIKAFYTTNVGVADRWIDYI
DMKIAFFNSIAGAAEDKGLSDAYIEESFLEHELANANKKSKSIMSEQKKAMKDILNDIDDILPLDLFSTET
FKDELADANDKRKKTLEKLDALDEDLKTEYALSEPNEQFIKSDFQKLQEATGKGKNATPIHYNAKAYRESD
IHKKRRHLKRRTEAYLKIKKEEAKEREIEKLKERLKNYDYADADEFYEMAKTIGYENLTAEQQRYFTQIEN
TRELEAGFKGVAVGLYDSGKDAVVGLWDMVTDPGGTVEAITGAMAHPIKTYEAISAAIEESYQKDMVNGDT
YSRARWVSYAVGTVVTSIVGTKGVGAVSKTGTAAKVTTKVKTAASKSATAQKAITVSKQTVDHIKQKVNTG
IEVSKKHVKTKLNQIGDLTLADILPYHPRHDLVPAGVPYNAVNGVTLKEGLQKFAKVILPKPYGTSSSGRR
TPAPHVPPVTVKYGEHFARWSRKKVLKPNIIYKTKEGYTYTTDNYGRITSVKADLQLGEAKRNQYAQTNAG
KPQDRKPDDDGGHLIATQFKGSGQFDNIVPMNSQINRSGGKWYEMEQEWAKALSKKPPKKVAVQIEPVYSG
DSLRPSYFDVTYKIGSRKEISVSIKISLGVRRMETRKMQDLYQLIGEKLNDIIPGEWTKIYLYAEVLDDST
MVLFHFRTPENNQIIYSQDIPSHYNVSKDIFKTLLRELRELFEELRTEHRNNNDDVWTNLTLTLDRSGEFQ
LDYNYDDILASELDGYERIAIWEYKNLGILPEDEDDKEFVISYLGL

YpuA (36.21 %)
MKKIWIGMLAAAVLLLMVPKVSLADAAVGDVIVTLGADLSESDKQKVLDEMNVPDNATTVTVTNKEEHEYL
GKYISNAQIGSRAISSSSITIAKKGSGLNVETHNISGITDEMYLNALMTAGVKDAKVYVTAPFEVSGTAAL
TGLIKAYEVSSDEAISEDVKQVANQELVTTSELGDKIGNENAAALIAKIKEEFAKNGVPDNKADIEKQVDD
AASDLNVTLTDSQKNQLVSLFNKMKNADIDWGQVSDQLDKAKDKITKFIESDEGKNFIQKVIDFFVSIWNA
IVSIFK

Table S2: Strain list.

Strain	Genotype	Reference
Bacillus subtilis		
DL1	Wild type (NCIB3610)	(Branda *et al.*, 2001)
DL2	Wild type 168	(Moszer *et al.*, 2002)
DL7	Δ*eps::tet* Δ*tasA::km*	(Lopez *et al.*, 2009c)
DL1308	Δ*ftsH::km*	This study
DL1315	Δ*ftsH::tet*	(Zellmeier *et al.*, 2003)
DL1211	Δ*floT::km*	(Lopez & Kolter, 2010)
DL1442	Δ*floT::spc*	This study
DL1401	Δ*yqfA::mls*	(Lopez & Kolter, 2010)
JS119	Δ*floT* (markerless)	This study
JS152	Δ*yqfA* (markerless)	This study
AY93	Δ*floT::spc*, Δ*yqfA::mls*	This study
DL1419	Δ*floT::km* Δ*yqfA::mls*	This study
JS163	Δ*floT* Δ*yqfA* (markerless)	This study
BM59	*amyE::* P_{hp}-*floT* (*spc*) *lacA*::P_{hp}-*yqfA* (*mls*)	This study
BM28	*amyE::* P_{hp}-*floT* (*spc*)	This study
BM26	*lacA*::P_{hp}-*yqfA* (*mls*)	This study
DL147	Δ*kinC::km*	(Lopez *et al.*, 2009a)
DL227	Δ*kinC::mls*	(Lopez et al., 2009a)
DL1295	*amyE*:: FloT-YFP (*spc*)	(Lopez & Kolter, 2010)
DL1367	*amyE*::YqfA-GFP (*spc*)	This study
AY224	*lacA*::P_{hp}-FtsH-RFP (*mls*)	This study
AY225	*lacA*::P_{ftsH}-FtsH-RFP (*mls*)	
DL1565	Δ*floT* Δ*yqfA* (markerless) *lacA*::FtsH-RFP (*mls*)	This study
AY238	*amyE*::YqfA-GFP (*spc*) *lacA*:: FtsH-RFP (*mls*)	This study
AY240	*amyE*::FloT-YFP (*spc*) *lacA*:: FtsH-RFP (*mls*)	(Lopez & Kolter, 2010)
DL1056	*lacA*::P_{hag}-*cfp* (*mls*)	(Vlamakis et al., 2008)
DL382	*amyE*::P_{tapA}-*yfp* (*spc*)	(Vlamakis et al., 2008)
DL1089	*amyE*::P_{sspB}-*yfp* (*spc*)	(Vlamakis et al., 2008)
DL1079	*amyE*::P_{tapA}-*yfp* (*spc*) *lacA*::P_{hag}-*cfp* (*mls*)	(Vlamakis *et al.*, 2008)
DL1521	Δ*ftsH::km amyE*::P_{tapA}-*yfp* (*spc*) *lacA*::P_{hag}-*cfp* (*mls*)	This study
DL1523	Δ*ftsH::km amyE::*P_{hp}*ftsH(spc) thrC*::P_{tapA}-*yfp (cm)* *lacA*::P_{hag}-*cfp (mls)*	This study
DL1433	Δ*ftsH::km amyE::*P_{ftsH}-*ftsH* (*spc*)	This study
DL1361	Δ*ftsH::km amyE::*P_{hp}-*ftsH* (*spc*)	This study
DL1568	Δ*ftsH::km amyE::*P_{hp}-FtsH-RFP (*spc*)	This study
DL1349	Δ*ftsH::km amyE::*P_{hp}-*ftsH* (*spc*)	This study
DL1404	Δ*ftsH::km amyE::*P_{hp}-FtsH-RFP (*spc*)	This study
DL1461	Δ*ftsH::km amyE::*P_{hp}-*ftsH* (*spc*) *lacA*::P_{tapA}-*yfp* (*mls*)	This study
DL1364	Δ*ftsH::km amyE::*P_{hp}-*ftsH* (*spc*) *lacA*::P_{sspB}-*yfp* (*mls*)	This study
DL383	Δ*abrB::km*	(Chu et al., 2008)
DL5	Δ*sinR::spc*	(Branda *et al.*, 2006)
DL1148	*amyE::sad67* (*cm*)	(Ireton *et al.*, 1993)
DL1362	Δ*ftsH::tet* Δ*abrB::km*	This study
DL1360	Δ*ftsH::km* Δ*sinR::spc*	This study
DL1363	Δ*ftsH::km amyE::sad67* (*cm*)	This study
DL1372	Δ*floT::spc* Δ*yqfA::mls* Δ*abrB::km*	This study
DL1374	Δ*floT::km* Δ*yqfA::mls* Δ*sinR::spc*	This study

DL1375	Δ*floT::spc* Δ*yqfA::mls amyE*::*sad67* (*cm*)	This study
DL1365	Δ*floT::km* Δ*yqfA::mls,* amyE::*sad67* (*cm*)	This study
DL1430	Δ*rapA::cm* Δ*rapB::spc* Δ*rapE::mls* Δ*spo0E::km*	This study
DL1554	Δ*floT* Δ*yqfA* (markerless) Δ*rapA::cm* Δ*rapB::spc,* Δ*rapE::mls* Δ*spo0E::km*	This study
JS201	Δ*yuaG* (markerless) *amyE*::P_{hp}-FloT-His^6 (*spc*)	This study
JS202	Δ*yqfA* (markerless) *amyE*::P_{hp}-YqfA-His^6 (*spc*)	This study
Other species used in this work		
DL1128	*Staphylococcus aureus* wild type SC-01	(Beenken *et al.*, 2003)
DL95	*Escherichia coli* DH5α	(Reusch *et al.*, 1986)
DL127	*Escherichia coli* DH5α pBR322 P_c-*gfp*	This study
JC163	*Escherichia coli* DH5α pBR322 P_c-*rfp*	This study
DL1205	*Pseudomonas aeruginosa* PA14	(O'Toole & Kolter, 1998)

Abbreviations

Antibiotics

mls	Encodes erythromycin + lincomycin resistance protein
km	Encodes kanamycin resistance protein
cm	Encodes chloramphenicol resistance protein
tet	Encodes tetracycline resistance protein
spc	Encodes spectinomycin resistance protein

Protein tags

GFP	Green fluorescent protein
YFP	Yellow fluorescent protein
RFP	Red fluorescent protein
His^6	Six histidines

Promoters

P_{hp}	Hyperspank IPTG-inducible promoter
P_c	Constitutive promoter
P*ftsH*	Natural promoter that controls the expression of *ftsH*
P*tasA*	Natural promoter that controls the expression of *tasA*
P*sspB*	Natural promoter that controls the expression of *sspB*
P*hag*	Natural promoter that controls the expression of *hag*

Table S3: Primer list.

Name	Sequence (5'-3')	Purpose
AY84B	ATGGTGAGCAAGGGCGAGGAGG	Forward RFP
AY85B	TTTTTTGCTAGCTTACTTGTACAGCTCG	Reverse RFP
AY82	TTTTTTGTCGACATGGTACTATTGAACATAGTTGTG	Forward FtsH
AY83B	ATCCTCCTCGCCCTTGCTCACCATCTCTTTCGTATCGTCTTTC	RFP tail
AY132	TGCTAAGCTTACATAAGGAGGAACTACTATGACAATGCCGATTAT	Forward FloT
AY133	ATCCTCCTCGCCCTTGCTCACCATCTCTGATTTTTGGATCGTTT	Reverse FloT (LFH) RFP
AY134	TTTTTGGATCCTTACTTGTACAGCTCGTCCAT	Reverse RFP (BamH1)
Ftshfwsal	AAAAGTCGACATGGTACTATTGAACATAGTTGT	Forward IPTG-controlled FtsH
Ftshrvsph	AAAAGCATGCTGATTGTAAAAGCCGCAGC	Reverse IPTG-controlled FtsH
Pftshfw	TTTTGAATTCAACGAGCGAGTATCAAGATACA	Forward Promoter *ftsH*
Pftshrv	TTTTAAGCTTTCCTTACCTCCTCCCACAGT	Reverse Promoter *ftsH*
Ftsh1	CAGCGACCGCATTGTATT	Δ*ftsH* cassette
Ftshkm2	CCTATCACCTCAAATGGTTCGCTGCCGATCAGCTTTCATAA	Δ*ftsH* cassette
Ftshtet2	GAGAACAACCTGCACCATTGCAAGATGCCGATCAGCTTTCATAA	Δ*ftsH* cassette
Ftshkm3	CGAGCGCCTACGAGGAATTTGTATGCTGCCAAGAGAAGACCGTT	Δ*ftsH* cassette
Ftshtet3	GGGATCAACTTTGGGAGAGAGTTCTATGCTGCCAAGAGAAGACCGTT	Δ*ftsH* cassette
Ftsh4	AGCTTTGCTGCACGCGA	Δ*ftsH* cassette
AY86	ATTTGCAGCATATCATGGCGTG	Δ*pbpE* cassette
AY87	CTTGATAATAAGGGTAACTATTGCCCCTCCACCTCCCATATCTCTG	Δ*pbpE* cassette
AY88	GGGTAACTAGCCCTCGCCGGTCCACGAAAGGAATGAATGAATTTGATGATCGG	Δ*pbpE* cassette
AY89	AGCTTTGATAAGCAAGATATGTG	Δ*pbpE* cassette
JS15	TTTTGGATCCCCATTTSTAAAGCACTTCAAATGG	Flotfw1
JS16	AGTTACCATACGGTTCTGCCCCAAATTCCTCCTCCTTTTTATGTAAAATG	Flotrv2
JS17	GGGCAGAACCGTATGGTAACTG	Flotfw3
JS18	TTTTGTCGACCTTTAACTTATAATGCGACTTAC	Flotrv4
JS19	TTTTGGATCCCCAGATCAGCTATGCAAAGGAG	Yqfafw1
JS21	GCGTTCTCCCTTCTTAGAGAGGTTGACGGACCCATATAACTTC	Yqfarv2
JS22	CTCTCTAAGAAGGGAGAACGC	Yqfafw3
JS39	TTTTGTCGACCAGATATGATGCAGTGGCCCTG	Yqfarv4
BM5	AAAAGTCGACTAAGGAGGAACTACTATGACAATGCCGATTATAAT	Forward IPTG-controlled FloT
BM6	AAAAGCATGCTTACTCTGATTTTTGGATCG	Reverse IPTG-controlled FloT
BM7	AAAAGTCGACTAAGGAGGAACTACTATGGATCCGTCAACACTTA	Forward IPTG-controlled YqfA
BM8	AAAAGCATGCTTATGATTTGCGGTCTTCAT	Reverse IPTG-controlled YqfA
JS44	AAAAGCATGCTTAGTGATGATGATGATGATGGCTGCTCTCTGATTTTTGGATCG	FloT Reverse (His6)
JS45	AAAAGCATGCTTAGTGATGATGATGATGATGGCTGCTTGATTTGCGGTCTTCAT	YqfA Reverse (His6)

Reference list

Beenken, K. E., J. S. Blevins & M. S. Smeltzer, (2003) Mutation of sarA in Staphylococcus aureus limits biofilm formation. *Infect Immun* **71**: 4206-4211.

Branda, S. S., F. Chu, D. B. Kearns, R. Losick & R. Kolter, (2006) A major protein component of the Bacillus subtilis biofilm matrix. *Mol Microbiol* **59**: 1229-1238.

Branda, S. S., J. E. Gonzalez-Pastor, S. Ben-Yehuda, R. Losick & R. Kolter, (2001) Fruiting body formation by Bacillus subtilis. *Proc Natl Acad Sci U S A* **98**: 11621-11626.

Chu, F., D. B. Kearns, A. McLoon, Y. Chai, R. Kolter & R. Losick, (2008) A novel regulatory protein governing biofilm formation in Bacillus subtilis. *Mol Microbiol* **68**: 1117-1127.

Ireton, K., D. Z. Rudner, K. J. Siranosian & A. D. Grossman, (1993) Integration of multiple developmental signals in Bacillus subtilis through the Spo0A transcription factor. *Genes Dev* **7**: 283-294.

Lopez, D., M. A. Fischbach, F. Chu, R. Losick & R. Kolter, (2009a) Structurally diverse natural products that cause potassium leakage trigger multicellularity in Bacillus subtilis. *Proc Natl Acad Sci U S A* **106**: 280-285.

Lopez, D. & R. Kolter, (2010) Functional microdomains in bacterial membranes. *Genes Dev* **24**: 1893-1902.

Lopez, D., H. Vlamakis, R. Losick & R. Kolter, (2009b) Cannibalism enhances biofilm development in Bacillus subtilis. *Mol Microbiol* **74**: 609-618.

Lopez, D., H. Vlamakis, R. Losick & R. Kolter, (2009c) Paracrine signaling in a bacterium. *Genes Dev* **23**: 1631-1638.

Moszer, I., L. M. Jones, S. Moreira, C. Fabry & A. Danchin, (2002) SubtiList: the reference database for the Bacillus subtilis genome. *Nucleic Acids Res* **30**: 62-65.

O'Toole, G. A. & R. Kolter, (1998) Flagellar and twitching motility are necessary for Pseudomonas aeruginosa biofilm development. *Mol Microbiol* **30**: 295-304.

Reusch, R. N., T. W. Hiske & H. L. Sadoff, (1986) Poly-beta-hydroxybutyrate membrane structure and its relationship to genetic transformability in Escherichia coli. *J Bacteriol* **168**: 553-562.

Vlamakis, H., C. Aguilar, R. Losick & R. Kolter, (2008) Control of cell fate by the formation of an architecturally complex bacterial community. *Genes Dev* **22**: 945-953.

Zellmeier, S., U. Zuber, W. Schumann & T. Wiegert, (2003) The absence of FtsH metalloprotease activity causes overexpression of the sigmaW-controlled pbpE gene, resulting in filamentous growth of Bacillus subtilis. *J Bacteriol* **185**: 973-982.

RESEARCH ARTICLE

Overproduction of Flotillin Influences Cell Differentiation and Shape in *Bacillus subtilis*

Benjamin Mielich-Süss, Johannes Schneider, Daniel Lopez

Research Center for Infectious Diseases ZINF, Würzburg University, Würzburg, Germany

ABSTRACT **Bacteria organize many membrane-related signaling processes in functional microdomains that are structurally and functionally similar to the lipid rafts of eukaryotic cells. An important structural component of these microdomains is the protein flotillin, which seems to act as a chaperone in recruiting other proteins to lipid rafts to facilitate their interaction. In eukaryotic cells, the occurrence of severe diseases is often observed in combination with an overproduction of flotillin, but a functional link between these two phenomena is yet to be demonstrated. In this work, we used the bacterial model *Bacillus subtilis* as a tractable system to study the physiological alterations that occur in cells that overproduce flotillin. We discovered that an excess of flotillin altered specific signal transduction pathways that are associated with the membrane microdomains of bacteria. As a consequence of this, we detected significant defects in cell division and cell differentiation. These physiological alterations were in part caused by an unusual stabilization of the raft-associated protease FtsH. This report opens the possibility of using bacteria as a working model to better understand fundamental questions related to the functionality of lipid rafts.**

IMPORTANCE **The identification of signaling platforms in the membrane of bacteria that are functionally and structurally equivalent to eukaryotic lipid rafts reveals a level of sophistication in signal transduction and membrane organization unexpected in bacteria. It opens new and promising venues to address intricate questions related to the functionality of lipid rafts by using bacteria as a more tractable system. This is the first report that uses bacteria as a working model to investigate a fundamental question that was previously raised while studying the role of eukaryotic lipid rafts. It also provides evidence of the critical role of these signaling platforms in orchestrating diverse physiological processes in prokaryotic cells.**

Received 29 August 2013 **Accepted** 17 October 2013 **Published** 12 November 2013

Citation Mielich-Süss B, Schneider J, Lopez D. 2013. Overproduction of flotillin influences cell differentiation and shape in *Bacillus subtilis*. mBio 4(6):e00719-13. doi:10.1128/mBio.00719-13.

Editor Michael Gilmore, Harvard Medical School

Address correspondence to Daniel Lopez, Daniel.Lopez@uni-wuerzburg.de.

Bacterial membranes are composed of different types of lipids, which tend to aggregate according to their physicochemical properties and accumulate into lipid domains that are immiscible with the surrounding lipids (1). The heterogeneous organization of membrane lipids leads to a lateral segregation of the embedded membrane proteins, which seems important for their functionality (2). One of the most interesting examples of the heterogeneous segregation of lipids and proteins is the formation of functional microdomains in the membrane of bacteria that are structurally and functionally equivalent to the lipid rafts of eukaryotic cells (3–5). Bacterial microdomains are membrane platforms that organize a group of proteins related to signal transduction and protein secretion (6). The integrity of these signaling platforms is essential for the correct functionality of the harbored proteins. Consequently, any alteration in their architecture severely inhibits the physiological processes related to the harbored proteins, such as biofilm formation, motility, competence, or protease secretion (6, 7).

The integrity of bacterial lipid rafts relies on the biosynthesis and aggregation of polyisoprenoid lipids and the presence of flotillin proteins (6, 8). Flotillins are membrane-bound proteins that localize exclusively in the lipid rafts and are usually considered a bona fide marker for the localization of lipid rafts. The function of flotillins in lipid rafts is not entirely understood, yet it is believed that they may act as chaperone proteins to recruit protein cargo to lipid rafts and facilitate interactions and oligomerization (9–12). Hence, the presence of flotillin in lipid rafts is necessary for the correct functionality of the associated signaling processes. In eukaryotic cells, alterations in the functionality of flotillins often occur in association with severe physiological dysfunctions in cells (13). For instance, the development of Alzheimer's disease or Parkinson's disease is usually observed in cells that concomitantly overproduce flotillin proteins (14, 15), as well as in neuronal cells with severe lesions (16, 17). Despite this interesting correlation, it is still unclear whether the overproduction of flotillin contributes to the physiological alterations or is actually a consequence of the disease. The number of technical challenges associated with the manipulation of eukaryotic cells has complicated the study of the role of flotillins (18). This motivated us to use the bacterium *Bacillus subtilis* as a working model to evaluate whether the overproduction of flotillins causes any alteration in the cellular physiology of the bacterium and whether this effect could possibly result in cellular dysfunction.

The functional membrane microdomains of the bacterial model organism *Bacillus subtilis* contain two structurally similar flotillin-like proteins, which are referred to as FloA (formerly

YqfA) (6, 19) and FloT (formerly YuaG) (6, 8). Cells lacking FloA and FloT are defective in a number of signal transduction pathways that are associated with the protein cargo of the functional membrane microdomains (e.g., biofilm formation, sporulation, motility, or competence) (6, 8, 20, 21). Thus, it is believed that FloA and FloT facilitate the interaction and oligomerization of the protein cargo in the functional microdomains of *B. subtilis* in a fashion similar to that described for eukaryotic lipid rafts. Supporting this hypothesis, a direct interaction of FloA and FloT with the protein cargo protease FtsH (22) has been reported that is important for the protease activity of FtsH. Furthermore, an additional number of FloT-interacting proteins have been identified recently, including a number of proteins related to signal transduction and protein secretion (20). Accordingly, protein secretion was reduced in cells lacking flotillin, which suggests that the associated protein secretion machinery loses its functionality in the absence of flotillin (20).

The first signal transduction pathway described in association with the flotillins of *B. subtilis* leads cells to specialize in the production of extracellular matrix to ultimately form biofilms (6). The induction of this signaling pathway is driven by the activation of the master regulator Spo0A via phosphorylation (Spo0A~P) (23, 24). The membrane-bound sensor kinase KinC, responsible for phosphorylating Spo0A~P, is part of the protein cargo, and its activity depends on the functionality of FloA and FloT (6) in a similar manner to the protease FtsH (22). FtsH is responsible for degrading the phosphatase enzymes that ultimately inactivate Spo0A~P by dephosphorylation (25) and actively contributes to the differentiation of matrix-producing cells (22). Therefore, published data suggest that the signal transduction pathway that is involved in biofilm formation is controlled by regulatory proteins, which localize in the functional membrane microdomains.

Further evidence was presented that exponentially growing *B. subtilis* cells accumulate FloA and FloT in the septum of dividing cells (22), suggesting that flotillins interact with septum-localized proteins, with FtsH as one example of this kind. This suggests a possible involvement of flotillins in processes related to cell division or cell shape. Related to this observation, other laboratories have determined that *B. subtilis* cells lacking flotillins underwent an aberrant cell division process (7). Thus, these two physiological features involving cell division and biofilm formation seemed affected by FloA and FloT in *B. subtilis* cells and could be studied to monitor the functionality of flotillins in *B. subtilis* cells.

In this report, we show that a 5-fold induction in the production of FloA and FloT significantly increased the amount of flotillin harbored in the microdomains, and this severely affected biofilm formation and cell division in *B. subtilis*. The subpopulation of cells specialized to produce extracellular matrix increased due to an implementation of FtsH activity. Cells overproducing FloA and FloT showed a more efficient septation process, which resulted in shortened cells, minicells, and cells with aberrant septa. As a consequence of the FloA and FloT overproduction, an implementation of the FtsH protease activity occurs, which negatively affects the stability of the protein EzrA (Extra Z-rings assembly), an inhibitor of septum formation (26–28). Altogether, overproduction of flotillins severely affected important cellular processes that directly impacted the physiology of the cells and could potentially contribute to the development of severe diseases in other living organisms.

RESULTS AND DISCUSSION

The overproduction of FloT and FloA reached saturation in *B. subtilis*. The bacterial model *B. subtilis* was used to overexpress the *floA* and *floT* genes under the control of an isopropyl-β-D-thiogalactopyranoside (IPTG)-inducible promoter, P_{hp} (the Hyperspank promoter). To first compare the overexpression levels to the natural expression levels, we generated translational fusions of *floA* and *floT* to a green fluorescent protein (GFP) gene (*gfp*) anchored to the cytosolic C-terminal part of the protein. PY79 P_{floA}FloA-GFP-, P_{floT}FloT-GFP-, P_{hp}FloA-GFP-, and P_{hp}FloT-GFP-labeled strains were grown in liquid cultures of the chemically defined medium MSgg at 30°C until they reached the stationary phase (29). Cells were harvested, fixed with paraformaldehyde, and examined with a fluorescence microscope. Expression from the native promoter showed that the fluorescence signal attributable to FloA and FloT was organized as discrete foci across the cellular membrane and was occasionally positioned in the septum of dividing cells, as previously reported (Fig. 1A and B) (22). The strains expressing P_{hp}FloA-GFP and P_{hp}FloT-GFP constructs showed expression levels below the natural level of expression in the absence of IPTG (see Fig. S1 in the supplemental material). Indeed, the addition of IPTG to the cultures induced the expression of FloA and FloT. Fluorescence microscopy analysis showed that 0.1 mM IPTG resulted in expression levels comparable to those of the native promoters (see Fig. S1). Saturation of flotillin levels was achieved by adding 15 mM IPTG to the cell cultures. No significant changes in the expression of FloA or FloT were detected in cells that grew with IPTG concentrations above 15 mM. The presence of IPTG did not cause any significant growth alteration in cultures of the PY79 strain (see Fig. S2 in the supplemental material).

Next, we compared the increment in the relative fluorescence signal between native expression and IPTG-inducible full expression. On average, our results showed that full induction by IPTG caused an approximately 5-fold increase in the production of FloA and FloT fluorescence signals in comparison to the native expression level. Further examination at the single-cell level showed that the induction of FloA and FloT expression resulted in an increase of the fluorescence intensity of the membrane foci and, to a lesser extent, in the number of foci. Figure 1C and D show the analysis of the subcellular organization of the fluorescence signal in representative single cells expressing FloA-GFP and FloT-GFP at native and full induction levels, respectively.

Saturation of FloT and FloA affects biofilm formation and cell differentiation. Biofilm formation in *B. subtilis* requires the differentiation of numerous cell types. Among those, the matrix-producing cell type is responsible for the production and secretion of the extracellular matrix of the biofilm (24, 30, 31). The subpopulation of matrix producers simultaneously expresses the *epsA-O* operon (henceforth called the *eps* operon) and the *tapA-sipW-tasA* operon (henceforth called the *tasA* operon). The *eps* operon encodes the enzymes responsible for the production of the extracellular exopolysaccharide (32–34). The *tasA* operon is required for the production of extracellular amyloid fibers that structurally give consistency to the biofilm (35–39).

To investigate whether the overexpression of FloA and FloT affects biofilm formation, strains overproducing FloA and FloT were constructed and used to assay biofilm formation. The morphology of *B. subtilis* colonies grown on solid biofilm-inducing

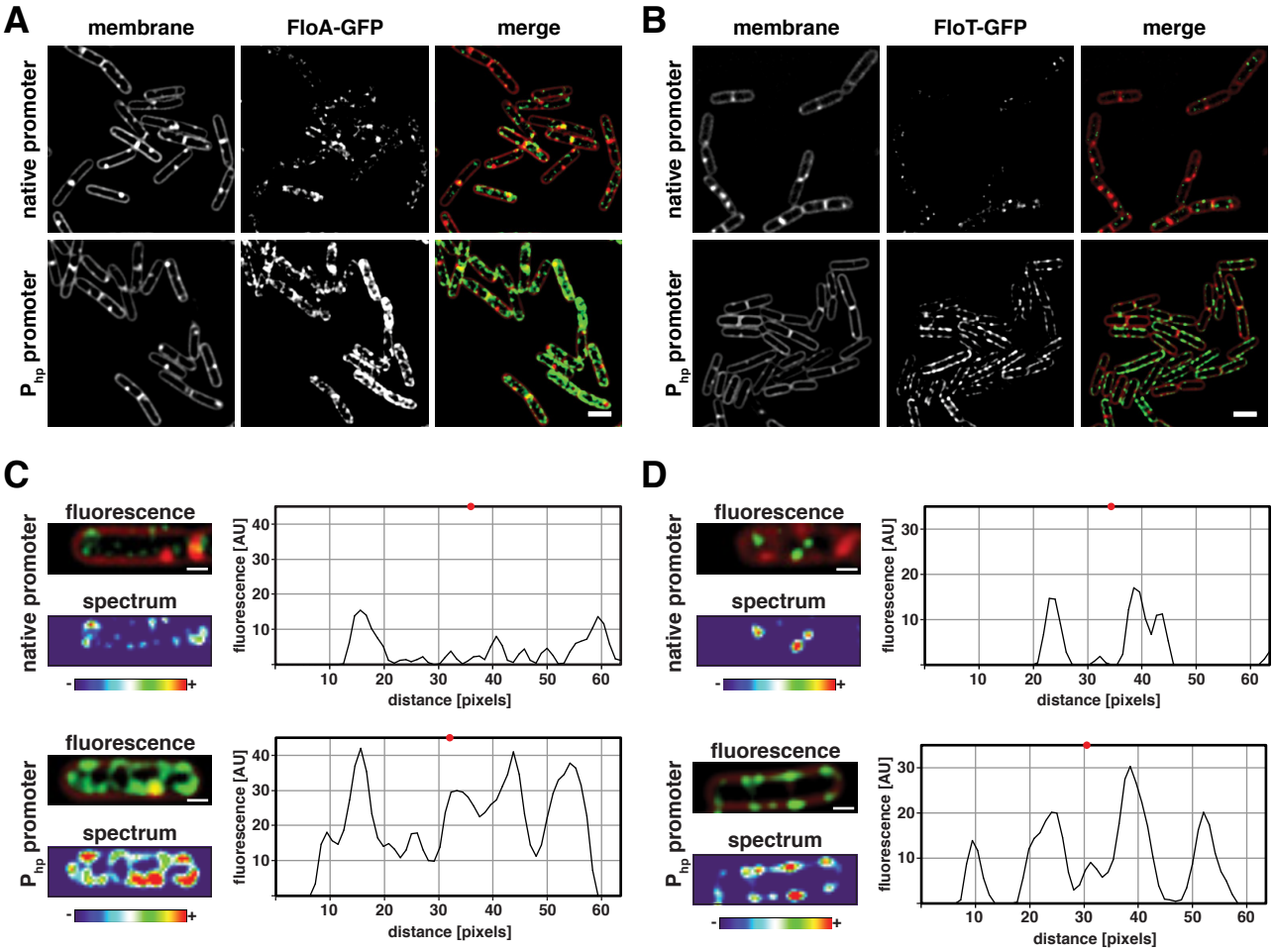

FIG 1 Saturation of FloA and FloT in functional membrane microdomains of *B. subtilis*. Shown are levels of expression in cells expressing FloA-GFP (A) or FloT-GFP (B) under the control of an IPTG-inducible promoter (P_{hp}) (bottom row) compared to natural expression levels obtained with their native promoters (upper row). Cells were grown in MSgg medium until they reached the stationary phase. IPTG was added to a final concentration of 15 mM. Membrane staining (left column) was performed with FM4-64 membrane dye. The center column shows the fluorescence signal emitted by the GFP. The right column shows the merged signals. The FM4-64 signal is false colored in red, and GFP is false colored in green. Scale bars are 2 μm. (C and D) Quantification of the fluorescence signal in single cells expressing FloA-GFP and FloT-GFP. The upper row shows the fluorescence signal obtained when expressed under the control of their native promoters. The bottom row shows the fluorescence signal obtained when expressed under the control of an IPTG-inducible promoter. The fluorescent micrographs show membrane staining false colored in red and the GFP fluorescence signal false colored in green. Additionally, the relative GFP fluorescence signal is quantified in relation to the background fluorescence, using a color spectrum logarithmic scale. (The spectrum scale is presented on the bottom.) The relative fluorescence intensity values of each micrograph are represented in a graph (on the left of each micrograph). The *x* axis represents the cell length (in pixels), and the *y* axis represents the value of relative fluorescence intensity detected (in arbitrary units [AU]). The midcell is marked with a red dot. The scale bar is 1 μm.

MSgg agar medium was examined. To generate biofilms on agar, 3 μl of an LB preculture was spotted on MSgg medium supplemented with 15 mM IPTG and allowed to grow at 30°C for 72 h. After incubation, the biofilms develop into integrated microbial communities with great complexity, manifested by the number of wrinkles present on the surface of the biofilm, which is representative of the robustness and the consistency of the extracellular matrix of the biofilm. Two different genetic backgrounds were used to perform this assay—the PY79 and NCIB3610 strains. Strain PY79 is a laboratory strain that is partially deficient in biofilm formation due the acquisition of a point mutation in the *eps* operon (Fig. 2A) (40). While this strain still possesses an intact *tasA* operon, the lack of extracellular polysaccharide makes the PY79 microbial communities flat, and they lack any distinctive complex architecture (40). A deletion of the transcriptional repressor SinR, which uncouples the regulation of the biofilm (33, 41), resulted in a slightly wrinkled colony even in the absence of a functional *eps* operon, suggesting that overexpression of the TasA strain partially restored biofilm formation when overproduced in the PY79 strain. Accordingly, the double mutant Δ*sinR* Δ*tasA* strain showed a biofilm-null phenotype, suggesting that biofilms generated by PY79 are mainly caused by expression of TasA (Fig. 2B). In contrast, the NCIB3610 strain (henceforth 3610) is the undomesticated *B. subtilis* strain and is considered the ancestor strain of PY79 (32). This strain possesses intact and functional *eps* and *tasA* operons and shows a great ability to form biofilms. Mutations in the *eps* or the *tasA* operons significantly reduce the ability of this strain to form biofilm, and a depletion of SinR results in a hyperwrinkled colony that overproduces extracellular matrix (see Fig. S3 in the supplemental material).

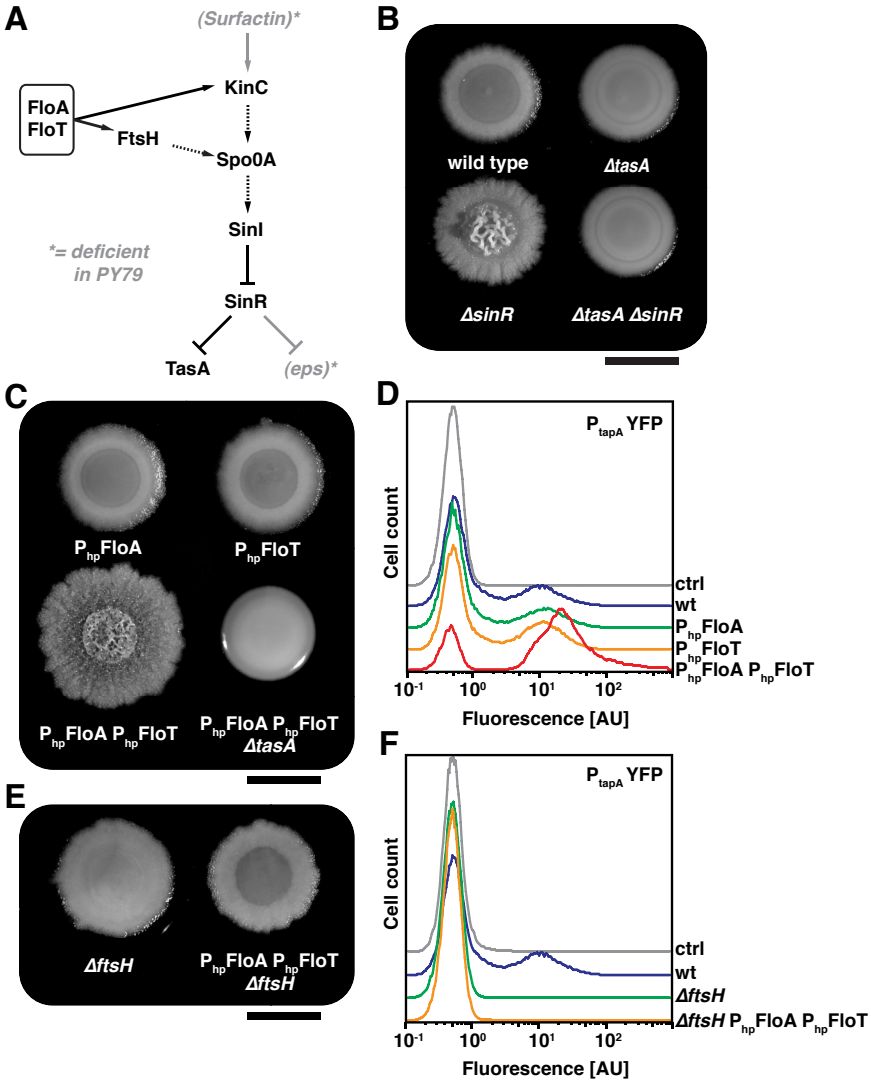

FIG 2 Overexpression of the flotillin-like proteins FloA and FloT promotes biofilm formation via FtsH. (A) Schematic representation of how FloA and FloT influence the signaling pathway leading to matrix production. Spo0A is activated by phosphorylation (Spo0A~P) and indirectly derepresses the expression of the *eps* and *tapA* operons. Phosphorylation of Spo0A~P is driven by the action of the membrane-bound kinase KinC, which is stabilized by FloA and FloT. Spo0A~P is subjected to dephosphorylation by a pool of phosphates that are degraded by the protease FtsH. The activity of FtsH is dependent on FloA and FloT. Solid arrows denote direct regulation, and dashed arrows denote indirect regulation. The asterisk denotes mutations in PY79. (B) Colonies of diverse mutants in the PY79 strain grown in MSgg agar medium for 72 h at 30°C. (C) Effects of flotillin overexpression in colony morphology of PY79 grown on solid MSgg agar medium for 72 h at 30°C with 15 mM IPTG. The scale bar represents 0.5 cm. (D) Flow cytometry analysis to monitor the subpopulation of matrix-producing cells in different genetic backgrounds using the P_{tapA}-*yfp* reporter system. Cells were grown for 72 h on solid MSgg medium in the presence of 15 mM IPTG. Approximately 50,000 ungated cells were analyzed. Fluorescence is represented in arbitrary units (AU). ctrl, control; wt, wild type. (E) Diverse mutants in the PY79 genetic background grown on MSgg medium and incubated for 72 h at 30°C supplemented with 15 mM IPTG. The scale bar represents 0.5 cm. (F) Flow cytometry analysis to monitor the subpopulation of matrix-producing cells in different genetic backgrounds that lack FtsH using the P_{tapA}-*yfp* reporter system. Cells were grown for 72 h on solid MSgg medium in the presence of 15 mM IPTG. Approximately 50,000 ungated cells were analyzed.

Strains expressing P_{hp}FloA, P_{hp}FloT, and P_{hp}FloA P_{hp}FloT were constructed in different genetic backgrounds. The resultant strains were assayed for variations in their ability to form biofilm by allowing them to grow in agar MSgg medium supplemented with 15 mM IPTG at 30°C for 72 h. After incubation, the biofilms of the strains overexpressing FloA or FloT were morphologically indistinguishable from the wild-type strain, indicating that the overexpression of a single flotillin protein did not influence biofilm formation (Fig. 2C). However, the P_{hp}FloA P_{hp}FloT strain that simultaneously overexpressed FloA and FloT resulted in a more robust, biofilm-like colony morphology that was especially evident in the experiments that used the PY79 strain (Fig. 2C; see Fig. S3 in the supplemental material to compare it to other genetic backgrounds). Because PY79 harbors a nonfunctional *eps* operon, we reasoned that the biofilm formation phenotype observed in the PY79 P_{hp}FloA P_{hp}FloT strain was attributable to the overexpression of TasA protein and the high production of amyloid fibers. A similar effect was observed in the experiments that used the 3610 strain, although this genetic background showed milder effects for reasons that are unknown to us. Hence, based on the robustness and the consistency of the biofilm formation phenotype observed in the PY79 strain, we used this genetic background to further explore the molecular effects in cell differentiation associated with the overproduction of FloA and FloT in *B. subtilis*.

Subsequently, we tested whether the overexpression of *tasA* was responsible for the acquisition of biofilm formation in the PY79 P_{hp}FloA P_{hp}FloT strain. To do this, we first compared the subpopulation of *tasA*-expressing cells in the wild-type strain and the flotillin-overexpressing strains. All strains were labeled with the yellow fluorescent protein (YFP) transcriptional fusion P_{tapA}-*yfp* and grown in MSgg medium plus IPTG (15 mM) at 30°C for 72 h. After incubation, cells were harvested and fixed with 4% paraformaldehyde. The fluorescence signal of 50,000 cells was monitored by flow cytometry and plotted on the graph presented in Fig. 2D. An unlabeled strain served as negative control with the absence of fluorescence signal. The wild-type strain harboring the P_{tapA}-*yfp* reporter served as a positive control, where the subpopulation of matrix producers represented approximately 30% of the total cell count. Overproduction of FloA or FloT did not alter the size of this subpopulation. However, when we assayed the size of the subpopulation of matrix producers in the P_{hp}FloA P_{hp}FloT strain, we detected a 3-fold increase in the number of cells that highly expressed the P_{tapA}-*yfp* reporter, suggesting that the overproduction of FloA and FloT led the cells to excessively produce

TasA, which ultimately induced biofilm formation in the PY79 strain.

Overproduction of flotillin stimulates FtsH activity. The genetic cascade responsible for the differentiation of matrix producers is triggered by phosphorylation of Spo0A~P. The membrane kinase KinC induces Spo0A~P phosphorylation in response to the secretion of the signal surfactin (Fig. 2A) (42). Moreover, the activity of the membrane-bound protease FtsH is equally important for matrix production, because FtsH degrades the phosphatases that are responsible for the deactivation of Spo0A~P by dephosphorylation (25). Importantly, both KinC and FtsH proteins localize to the functional membrane microdomains in *B. subtilis*, and their functionality is dependent on the activity of FloA and FloT (6, 22). Figure 2A shows an overview of the regulatory cascade leading to biofilm formation.

We hypothesized that the molecular mechanism underlying the evident increase in the subpopulation of matrix producers could be related to the positive effects of FloA and FloT on the activity of KinC or FtsH. Importantly, the PY79 strain is not able to produce surfactin due to the acquisition of a point mutation in the *sfp* gene during laboratory domestication (Fig. 2A) (40). The Sfp protein is a phosphopantetheinyl transferase that posttranslationally modifies the surfactin biosynthesis machinery. This is an essential process for the correct functionality of the surfactin biosynthesis machinery (43, 44). Thus, the activation of KinC via surfactin is not possible in the PY79 strain. This fact led us to focus on the activity of the membrane-bound protease FtsH.

FtsH indirectly affects the levels of Spo0A~P by degrading four regulatory phosphatase proteins, RapA, RapB, RapE, and Spo0E, which feed into the Spo0A phosphorelay to ultimately decrease the levels of Spo0A~P. The absence of FloA and FloT negatively affects the FtsH protein (22), which prevents the degradation of the RapA, RapB, RapE, and Spo0E phosphatases (25). To explore whether the overproduction of FloA and FloT decreased the levels of Spo0A~P via FtsH, we deleted the *ftsH* gene in the wild-type and P_{hp}FloA P_{hp}FloT strains, and we monitored biofilm formation. The Δ*ftsH* and Δ*ftsH* P_{hp}FloA P_{hp}FloT strains were grown in MSgg agar medium supplemented with 15 mM IPTG and were incubated at 30°C for 72 h. After incubation, the microbial communities of the Δ*ftsH* P_{hp}FloA P_{hp}FloT strain showed no particular biofilm architecture but a flat morphology comparable to that of the wild-type and Δ*ftsH* strains (Fig. 2E). Next, these strains were labeled with the P_{tapA}-*yfp* transcriptional fusion to monitor possible variations in the subpopulation of matrix producers by using flow cytometry. Flow cytometry analysis showed that the overproduction of FloA and FloT did not differentiate the subpopulation of matrix producers in cells lacking FtsH (Fig. 2F). This suggests that FtsH mediated the differentiation of matrix producers when FloA and FloT were artificially overproduced.

These results are in agreement with published literature showing that the oligomerization of FtsH in *E. coli* requires the chaperone activity of HflC and HflK, two proteins that are structurally similar to FloA and FloT (45–48). *B. subtilis* lacks the HflC and HflK proteins, and thus, it is possible that FloA and FloT might play the role of HflC and HflK in stabilizing FtsH in *B. subtilis*. To test this hypothesis, whole-cell extracts of the P_{hp}FloA P_{hp}FloT strain were used to semiquantitatively detect FtsH by immunoblot analysis using polyclonal antibodies against FtsH. An increase in FtsH protein was detected in normalized cell extracts from the P_{hp}FloA P_{hp}FloT strain compared to the wild-type strain (Fig. 3A). Next, we observed that these higher levels of FtsH coincided with higher levels of TasA. We performed an immunoblot analysis using polyclonal antibodies against TasA. The extracts of cells that overproduced FloA and FloT, which showed higher levels of FtsH, also showed higher levels of TasA. Importantly, when the *ftsH* gene was deleted, the detection of TasA was not possible in the strain that overproduced FloA and FloT (Fig. 3B).

Altogether, the data are consistent with the hypothesis that the functional link between FloA/FloT and FtsH mediated the increase of the subpopulation of matrix-producing cells in the PY79 strain that overproduced FloA and FloT. This, in turn, caused an increase in the production of TasA, which resulted in an overproduction of biofilm formation. In those lines, the interaction of FtsH-like proteins with flotillin-like proteins has been described in many systems and organelles (e.g., mitochondria, yeast, or plants), and it has been shown that the stability of FtsH-like proteins depends on the presence of flotillin-like proteins (49, 50). It is hypothesized that the chaperone activity of the flotillin-like proteins acts as a regulator to fine-tune the proteolytic activity of FtsH (49, 50). It also is suggested that flotillins serve as scaffolding proteins to limit the mobility of the FtsH protease across the membrane (49). Based on these current hypotheses, it is probably not surprising that the overproduction of FloA and FloT affected the activity of FtsH of *B. subtilis*.

Flotillin overexpression results in decreased cell length. FtsH principally localizes to the septum of dividing cells (51), where the interaction with FloA and FloT presumably occurs (22). Possibly, flotillins provide stability to protein septum-associated proteins. Accordingly, there is evidence of a significant number of septum-localized proteins among the interactome of FloT (20, 22). Furthermore, the absence of flotillins in *B. subtilis* has been associated with pleiotropic effects on cell shape (7), which led us to reason that septum-localized membrane microdomains could influence septum-associated processes, like septum formation or shape determination.

Septum formation and cell shape determination were analyzed at the single-cell level in cells that overproduced flotillins. To do this, the P_{hp}FloA, P_{hp}FloT, and P_{hp}FloA P_{hp}FloT strains were grown in liquid MSgg medium plus IPTG (15 mM) at 37°C with vigorous agitation until the late exponential growth phase (optical density at 600 nm [OD_{600}] of 0.8 to 1.0). After incubation, cells were stained with the membrane dye FM4-64 before examination under the fluorescence microscope. We observed that under these growth conditions, the simultaneous overexpression of FloA and FloT resulted in a dramatic reduction of cell length (Fig. 4A, column 4; see Fig. S4 in the supplemental material). We randomly selected 500 cells from each microscopic field and measured the cell length (Fig. 4B). On average, wild-type cells showed a cell length of 2.41 ± 0.52 μm. This result was comparable to the length of cells expressing FloA (2.47 ± 0.60 μm) or FloT (2.34 ± 0.65 μm). However, overproduction of FloA and FloT resulted in a cell length of 1.11 ± 0.52 μm. Probably as a consequence of the reduction of cell length, P_{hp}FloA P_{hp}FloT cells also showed a partial loss of the typical *B. subtilis* rod shape, and a subfraction of cells (approximately 19% of the total) became spherical. Among those, we detected a significant number of small, circular, anucleate minicells (approximately 28% of the total) (52–54), as well as small, spherical cells that contained DNA (72% of the total).

The effect on cell length associated by the overexpression of FloA and FloT pointed to an influence of flotillins on the efficiency

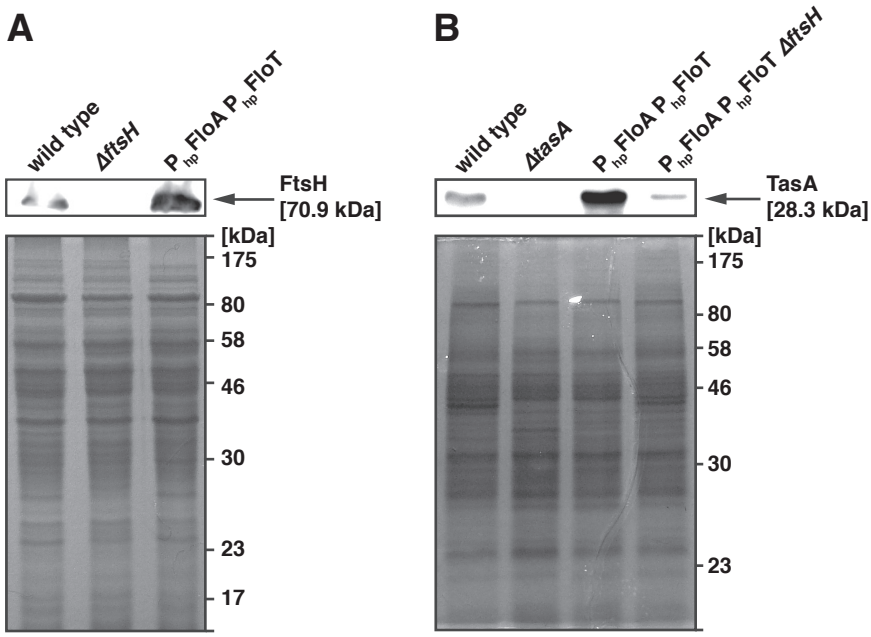

FIG 3 Overproduction of FloA and FloT increase the levels of FtsH and TasA proteins. (A) Immunoblot analysis to detect FtsH in different mutants using polyclonal antibodies against FtsH. The wild-type strain is used as a positive control, while the Δ*ftsH* mutant is used as a negative control. The immunoblot signal is presented in the upper panel, and the respective SDS-PAGE result is presented in the lower panel as a loading control. (B) Detection of TasA production in different mutants by immunoblot analysis using polyclonal antibodies against TasA. The wild-type strain (PY79) is used as a positive control, while the Δ*tasA* mutant is used as a negative control. The immunoblot signal is presented in the upper panel, and the respective SDS-PAGE result is presented in the lower panel. Samples were obtained from the extracellular protein fraction of pellicles that were grown in liquid cultures for 24 h at 30°C. Protein levels were normalized relative to cell number.

of septum formation. To investigate the influence of FloA and FloT in the assembly of proteins with a relevant role in septum formation, we chose the FtsZ protein as a septum-related protein to monitor septum formation in *B. subtilis* cells. FtsZ forms a ring structure (Z-ring) to ultimately drive cell septation (55, 56), and mutants showing an increase in FtsZ assembly also showed additional division events per cell cycle, with the formation of extra septa that led to the occurrence of a minicell-like phenotype (55, 57). Thus, the phenotypic similarities between cells overexpressing FloA and FloT and cells with increases in FtsZ assembly led us to hypothesize a functional connection between these two genotypes. We first tested whether the overproduction of FloA and FloT affects the septation efficiency. To do this, cultures of the P_{hp}FloA P_{hp}FloT mutant were grown in liquid MSgg medium with vigorous agitation, and the cell length was measured at early stages of exponential growth (OD_{600} of 0.1). Our measurements of cell length showed that actively dividing cells were substantially shorter when overproducing FloA and FloT than wild-type cells (Fig. 5A). To elucidate if the reduction of cell length involved FtsZ, we constructed the P_{xyl}FtsZ-GFP and P_{hp}FloA P_{hp}FloT P_{xyl}FtsZ-GFP strains that expressed a labeled FtsZ under the control of a xylose-inducible promoter. In these strains, transcription of FtsZ-GFP is strictly dependent on the amount of xylose that was added to the cultures. This allowed us to correlate the variations in the FtsZ-GFP protein levels to the differences in protein processing or stability. We used these strains to determine that cell length per FtsZ ring (L/R ratio) (58) was significantly reduced in cells overexpressing FloA and FloT in comparison to that in the wild-type strain (Fig. 5B and C). Furthermore, cultures of cells that overproduced FloA and FloT showed a significant increase in the number of Z-rings compared to that in the wild-type strain (Fig. 4D), suggesting an increase in the number of Z-rings in the shorter cells that overproduced FloA and FloT.

We revisited the pool of proteins associated with the functional membrane microdomains in *B. subtilis* to find those proteins whose activity affects the assembly of the Z-ring. To purify the protein fraction associated with the functional membrane microdomains, the membrane fraction was treated with nonionic detergents and separated by centrifugation in a sucrose gradient. This resulted in one fraction that was sensitive to detergents and another fraction that is composed of larger membrane fragments that were more resistant to detergent disruption (detergent-resistant membrane [DRM] fraction). It is known that the DRM fraction is enriched in proteins associated with lipid rafts (4, 59, 60) and is the fraction that contains the proteins of the functional membrane microdomains when assayed with *B. subtilis* membranes. We detected the protein EzrA in the DRM fraction of *B. subtilis*, with identification coverage of 53% (see Fig. S5 in the supplemental material) (22). EzrA is a negative regulator of the assembly of the Z-ring that localizes in the midcell in an FtsZ-dependent manner. Cells depleted of EzrA (Extra Z-rings assembly) show multiple Z-rings located at the polar and medial sites (27, 61). We hypothesized that overproduction of FloA and FloT could negatively affect the activity of EzrA to promote an accelerated assembly of FtsZ.

To address this question, we generated P_{xyl}EzrA-GFP and P_{hp}-FloA P_{hp}FloT P_{xyl}EzrA-GFP strains to compare the levels of expression of EzrA in cells overexpressing FloA and FloT. Examination of cells under the fluorescence microscope did not render conclusive results. Instead, we performed a semiquantitative im-

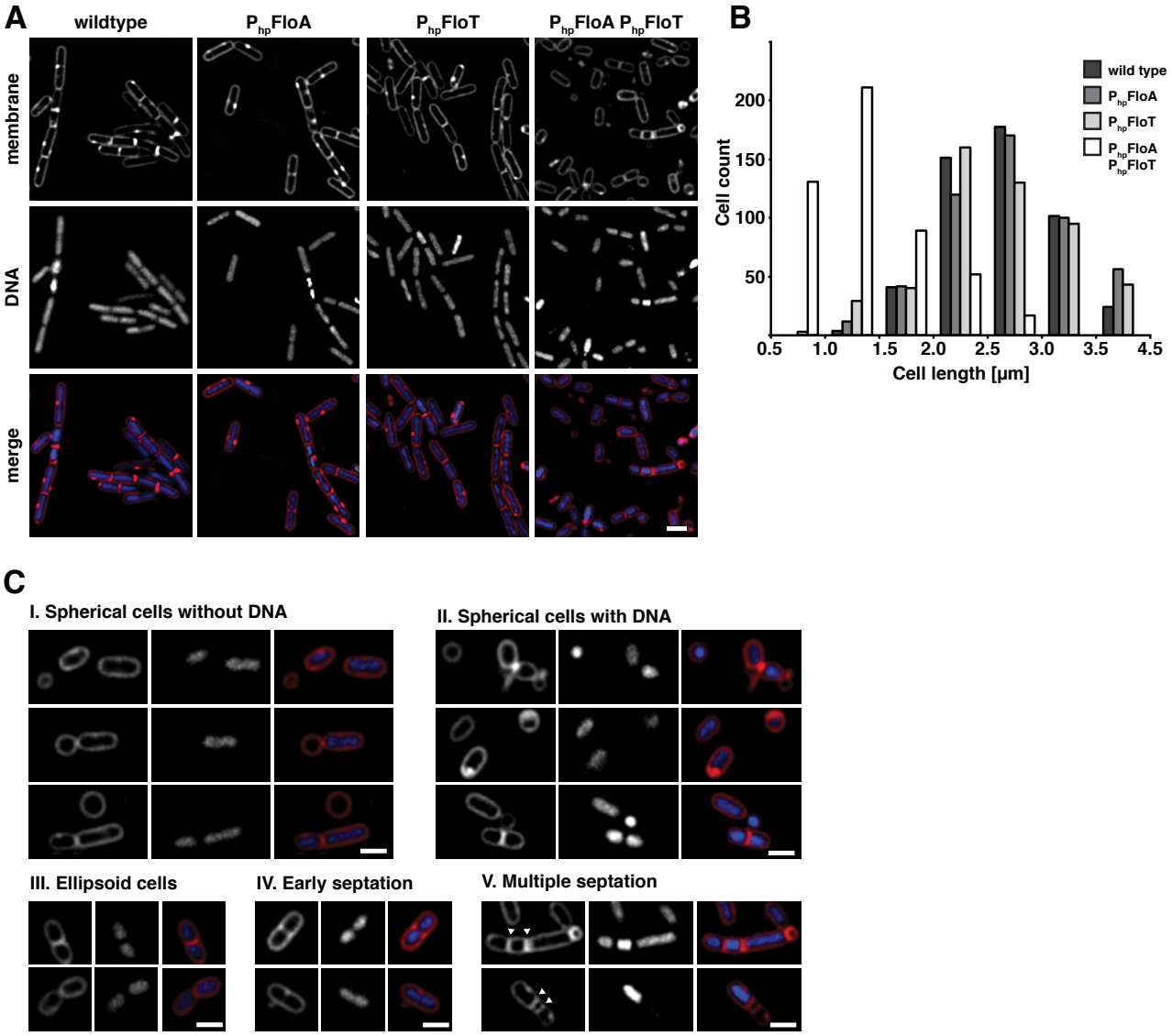

FIG 4 Overexpression of FloA and FloT affects cell shape. (A) Fluorescence micrographs of strains overexpressing FloA, FloT, or both FloA and FloT compared to wild-type cells. The upper row presents membrane staining using FM4-64. The center row shows DNA staining using Hoechst 33342. The bottom row shows the merge of the previous images, with the membrane staining false colored in red and the DNA staining false colored in blue. Cells were grown in liquid MSgg medium at 37°C until they reached the late exponential growth phase. IPTG was added to a final concentration of 15 mM. The scale bar represents 2 μm. (B) Histogram representing the variation in cell length in the different mutants. The number of the cells considered for this analysis was 500. The cell count is represented in the *y* axis. Calculation of cell length was performed using Leica Application Suite Advance Fluorescence software. (C) Detailed view of cell shape aberrations in cells that simultaneously overexpressed FloA and FloT. Spherical cells are shown in panel I. Spherical anucleate cells are shown in panel II. Elipsoid cells are shown in panel III, and cells with a failure in septation are shown in panels IV and V. The scale bars represent 2 μm.

munoblot assay using polyclonal antibodies against GFP. Using this assay, we observed a significant reduction of EzrA levels in the extracts of the P_{hp}FloA P_{hp}FloT P_{xyl}EzrA-GFP strains in comparison to the P_{xyl}EzrA-GFP strain (Fig. 6A). Although this result explained the higher efficiency to form Z-rings and septates in cells overproducing FloA and FloT, it was somewhat unexpected, as one might anticipate that an enhanced chaperone activity of flotillins should always affect the stability of the associated proteins in a positive fashion. One plausible hypothesis that could explain this result is that additional proteins that are stabilized by FloA and FloT negatively influence EzrA. Supporting this hypothesis, we found evidence in the literature that EzrA of *B. subtilis* is degraded by an ATP-dependent protease that is structurally similar to FtsH (62), suggesting that FtsH could target EzrA in the strain that overexpressed FloA and FloT. This is consistent with the filamentous growth that is described in the mutant lacking FtsH, which is also observed in strains with defective cell septation (63). Consequently, we tested whether FtsH influenced the reduced levels of EzrA observed in cells overexpressing FloA and FloT. To do this, the levels of EzrA-GFP were tested in the presence or absence of FtsH by semiquantitative immunoblot assays, using whole-cell extracts of the P_{hp}FloA P_{hp}FloT P_{xyl}EzrA-GFP and Δ*ftsH* P_{hp}FloA P_{hp}FloT P_{xyl}EzrA-GFP strains. Using this approach, we observed that cells lacking FtsH showed increased lev-

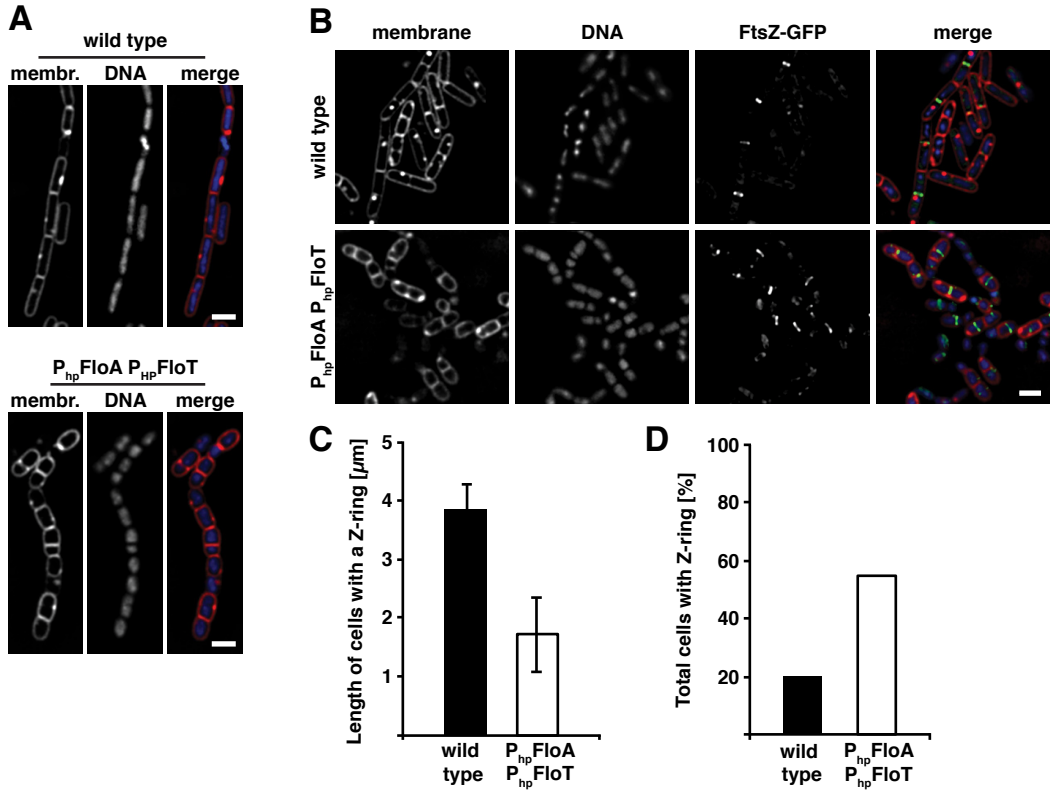

FIG 5 Simultaneous overproduction of FloA and FloT affects formation of the division septum and formation of the Z-ring. (A) Comparison between wild-type cells and the P_{hp}FloA P_{hp}FloT strain during the early exponential growth phase. Cells were grown in liquid MSgg medium at 37°C until they reached an OD_{600} of 0.1. For overexpression, the medium was supplemented with 15 mM IPTG. The membrane (membr.) was stained with FM4-64 (left panel), and the DNA was visualized with Hoechst 33342 (middle panel). The right panel shows merges of the two signals, with the membrane false colored in red and DNA false colored in blue. The scale bar represents 2 μm. (B) Visualization of Z-ring formation in a wild-type strain and the P_{hp}FloA P_{hp}FloT strain bearing an FtsZ-GFP fusion. The first column shows the membrane stained with FM4-64, the second column shows the DNA stained with Hoechst 33342, and the third column shows the FtsZ-GFP signal. In the fourth column, all signals were merged, with the membrane false colored in red, the DNA false colored in blue, and the GFP false colored with green. The cells were grown in liquid MSgg medium at 37°C and harvested in the exponential growth phase. IPTG was added to the growth medium at a final concentration of 15 mM, and basal induction of FtsZ-GFP was achieved with 1% (wt/vol) xylose. The scale bar is 2 μm. (C) Graphical illustration of the length of cells with a visible Z-ring. Approximately 500 cells were used for counting. (D) Graphical illustration of the percentage of cells with a Z-ring; approximately 500 cells were used for counting.

els of EzrA (Fig. 6B). Moreover, we generated the P_{hp}FtsH P_{xyl}EzrA-GFP strain, which overexpressed P_{hp}FtsH, and whole-cell extracts of this strain were used to compare the abundance of EzrA before and after FtsH overproduction. Figure 6B shows that the overproduction of FtsH was associated with reduced EzrA levels. We detected an intriguing protein band in this strain that could be attributed to an alternative processed form of EzrA protein. More experiments should be performed in this direction to fully address whether a direct interaction exists between FtsH and EzrA. Experiments presented in this report are consistent with the idea that the overexpression of flotillins causes severe physiological changes in bacterial cells.

Overall, our study showed that overexpression of FloA and FloT in the functional membrane microdomains of *B. subtilis* resulted in severe defects in cell differentiation and cell shape. We provide evidence that physiological alterations were mediated by an unusual activity of the FtsH protease (22). We expect that other yet unknown molecular mechanisms may participate in this phenotype, since numerous signal transduction pathways are harbored in the functional membrane microdomains of *B. subtilis*. Among those, we consider particularly interesting the dual role of the FtsH protease in regulating bacterial cell differentiation and cell shape, as illustrated in Fig. 7. It is probably not surprising that this important regulatory node localizes in the functional membrane microdomains, under the direct control of the two flotillin-like proteins FloA and FloT, in a manner similar to that found in other biological systems (49, 50). Yet, when focusing on *B. subtilis*, it is still unknown whether both FloA and FloT play redundant functions in the functional microdomains. Further experiments are necessary to clarify why the overexpression of two structurally different flotillin proteins is required to achieve the described effects. We tend to think that FloA and FloT are partially redundant and some physiological processes are functionally linked to both FloA and FloT, while other physiological processes are specifically linked to FloA or FloT.

MATERIALS AND METHODS

Strains, media, and culture conditions. For general purposes, the *B. subtilis* strains PY79 and NCIB3610 were used in this study. *Escherichia coli* DH5α was used for cloning purposes. A detailed list of the genetically

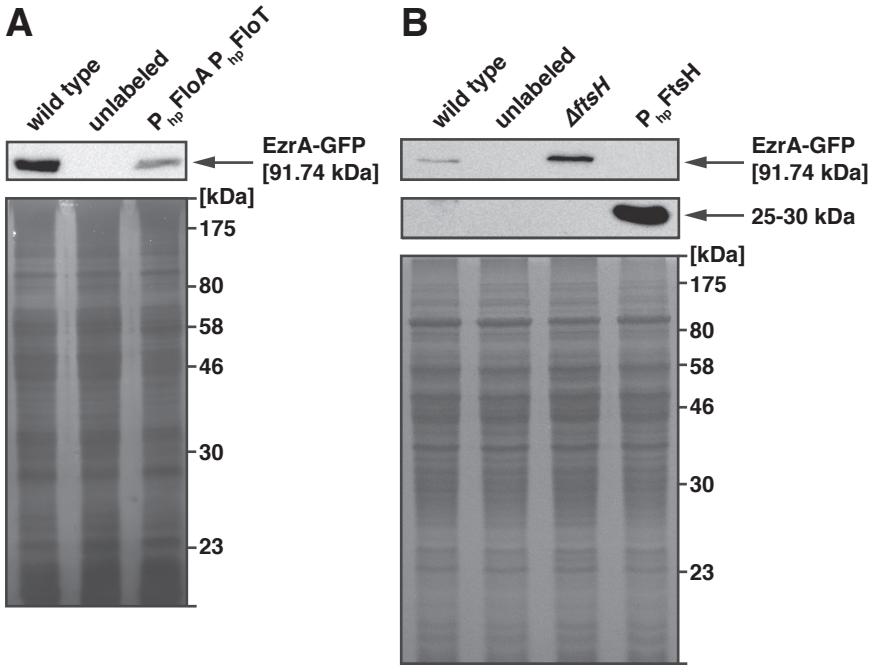

FIG 6 Levels of EzrA are influenced by FtsH. (A and B) Western blot analysis of whole-cell extracts of different mutants to detect the level of EzrA-GFP using polyclonal antibodies against GFP. The extra protein band is shown at 25 to 30 kDa in panel B, which was only detected in the extract of cells that overproduced FtsH. SDS-PAGE results are shown as loading controls. The protein amount was normalized relative to cell number.

modified strains is shown in Table S1 in the supplemental material. For routine growth, cells were propagated on LB medium. Selective media were prepared in LB agar using the antibiotics (final concentrations in parentheses) ampicillin (100 μg/ml), kanamycin (50 μg/ml), chloramphenicol (5 μg/ml), tetracycline (5 μg/ml), spectinomycin (100 μg/ml), and erythromycin (2 μg/ml) plus lincomycin (25 μg/ml) for macrolide-lincosamide-streptogramin B (MLS) determination. Biofilm assays and growth of cells for microscopy or biochemical analysis were performed with MSgg medium (29). When required, MSgg culture medium was supplemented with 1% threonine. Unless otherwise stated, induced expression was achieved with 1 mM IPTG or 1% (wt/vol) xylose. To generate biofilms, 3 μl of an LB overnight culture was spotted onto 1.5% agar MSgg plates and incubated for 72 h at 30°C. For liquid cultures, an overnight culture was diluted 1:20 in MSgg medium and grown at 30°C with agitation at 200 rpm until reaching the desired growth stage. If necessary, inducers were added to the culture as stated in the figure legends.

Strain construction. Genomic modifications in *B. subtilis* were performed according to standard protocols (64). Linearized plasmid DNA or PCR products were brought into cells by inducing natural competence, leading to incorporation of the foreign DNA into the genome by heterologous recombination (65). SPP1-mediated phage transduction was used to shuttle constructs among strains, in order to combine mutant alleles (66). For plasmid construction, genes were amplified from genomic DNA with primers carrying a 5′ extension with desired restriction sites to clone the PCR product into the target plasmids. A list of all of the primers used in this study is presented in Table S2 in the supplemental material. For overexpression with the IPTG-inducible Hyperspank promoter, the genes were cloned into pDR111 (67, 68) or into the pBM001 plasmid, a chimera of pDR111 and pDR183 (kindly provided by David Rudner at the Harvard Medical School, Boston, MA). pBM001 has a pDR183 backbone to integrate the plasmid into the *lacA* locus combined with a fragment from pDR111 that carries the Hyperspank promoter, the multiple-cloning site, and the Lac repressor. The FtsZ-GFP strain was created with the plasmid pX (69), which integrates genes into the *amyE* locus and expresses them from a xylose-inducible promoter. FtsZ was joined with GFPmut1 by long-flanking homology (LFH) PCR and inserted into pX. For the construction of EzrA-GFP, we made use of the pSG1154 plasmid (70), which allows in-frame fusions to GFPmut1 and further expression under the control of a xylose-inducible promoter. For the independent overexpression of both flotillins and a third xylose-inducible gene, we decided to construct a bicistronic mRNA of *floA* and *floT* via LFH-PCR, which was integrated into the *lacA* locus with pBM001. The strain showed similar overexpression of *floA* and *floT* in the presence of IPTG compared to expression of a single gene, as determined by reverse transcription (RT)-PCR (data not shown).

Image analysis. Biofilms were documented using a Nikon SMZ 1500 stereoscope equipped with a Leica DFC295 color camera and Zeiss Axio Vision software. Final processing of the images was done with Photoshop. For microscopy, an overnight culture was diluted 1:20 in MSgg medium and grown at 30°C with agitation at 200 rpm until reaching the desired growth stage. If necessary, inducers were added to the culture as stated in the figure legends. Prior to analysis, 1 μM FM4-64 (Invitrogen, Carlsbad, CA) was added to stain the membrane, and Hoechst 33342 was added to a final concentration of 1 μg/ml to stain the DNA. For static images, cells were fixed with 4% paraformaldehyde for 7 min and washed with phosphate-buffered saline (PBS) several times. Finally, cells were spotted on a microscopic slide covered with a 1% agarose pad made with PBS. Images were captured with a Leica DMI6000B microscope equipped with a Leica CRT6000 illumination system coupled with a Leica DFC630FX color camera. Deconvolution was performed with a software algorithm of the LAS AF software. Fluorescence quantification and generation of color spectra were performed with Fiji. Images were processed with Leica LAS AF software and Photoshop.

Flow cytometry. For flow cytometry analysis, 3-day-old biofilms were detached from the agar surface, resuspended in PBS, and mildly sonicated (power output of 0.7 and cycle of 50%) in order to separate cells from extracellular matrix material. Subsequently, cells were fixed with 4% paraformaldehyde for 7 min and washed several times. For analysis, cells were diluted 1:1,000 in PBS. Analysis was carried out with the benchtop MACSquant analyzer (Miltenyi Biotech, Germany). YFP signals were detected

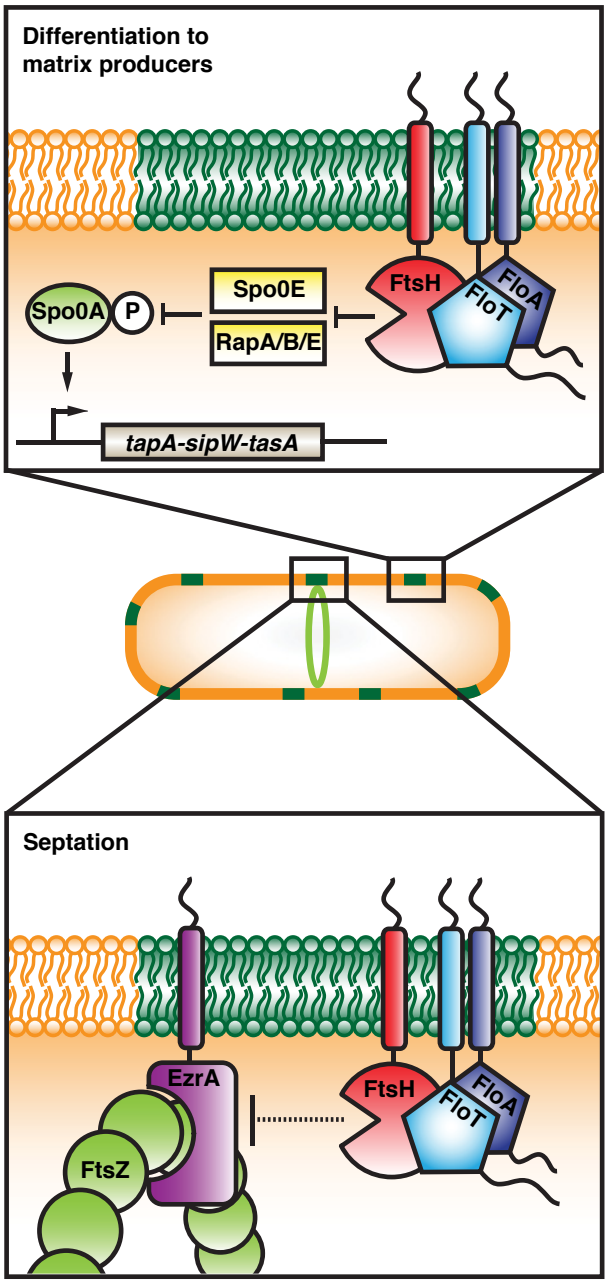

FIG 7 Hypothetical model for the dual role of FtsH activity in *B. subtilis* membrane microdomains. In the membrane microdomains (green), the flotillins FloA and FloT regulate the protease activity of FtsH. The upper panel represents a situation with FtsH degrading regulatory phosphatases, which ultimately leads to biofilm formation via activation of the TasA operon. During cell division (lower panel), FtsH might also degrade the negative regulator for Z-ring formation, EzrA, by a yet unknown mechanism (referred to as dashed lines) and thus contribute indirectly to formation of the division septum.

using a 488-nm laser with the corresponding 525/50-nm filter. The photomultiplier voltage was set at 462 V. For each sample, 50,000 nongated cells were measured. Data analysis was performed using the FlowJo v 9.5.1 software (Tree Star, Inc., Ashland, OR).

Western blot analysis. For extraction of whole-cell fractions, cells were grown in liquid MSgg medium at 30°C; the length of cultivation varied according to the corresponding experiment. Cells were collected by centrifugation and subsequently lysed with 1 mg/ml lysozyme at 37°C for 30 min. After lysozyme treatment, samples were subjected to SDS-PAGE, and proteins were detected by Coomassie staining. The extracellular fraction was extracted as previously described (37, 71) with minor modifications. Briefly, cells were grown in liquid MSgg medium without agitation at 30°C. The floating biofilm, including the liquid medium, was recovered and mild sonication was applied to separate the extracellular fraction from the cells. After that, cells were pelleted and the supernatant was filter sterilized (0.2-μm pore size). The extracellular proteins in the supernatant were precipitated with trichloroacetic acid with a final concentration of 10% (vol/vol). Precipitated proteins were harvested by centrifugation and taken up in 1× SDS sample buffer. Immunoblot analysis was performed according to standard protocols. Antibodies were purchased from Invitrogen (anti-GFP) and Bio-Rad (anti-rabbit IgG, horseradish peroxidase [HRP] conjugate). The TasA antibody was kindly provided by Kürsad Turgay (Freie University of Berlin, Germany). The FtsH antibody was a kind gift from Thomas Wiegert (Hochschule Zittau/Görlitz, Germany).

SUPPLEMENTAL MATERIAL

Supplemental material for this article may be found at http://mbio.asm.org/lookup/suppl/doi:10.1128/mBio.00719-13/-/DCSupplemental.

Figure S1, EPS file, 1.9 MB.
Figure S2, EPS file, 1.2 MB.
Figure S3, EPS file, 20 MB.
Figure S4, EPS file, 8.9 MB.
Figure S5, EPS file, 1.2 MB.
Table S1, DOCX file, 0.1 MB.
Table S2, DOCX file, 0.1 MB.

ACKNOWLEDGMENTS

We thank all members of the Institute of Molecular Infection Biology (IMIB), especially Isa Westedt for technical assistance. We thank Thomas Wiegert (University of Bayreuth, Germany) and Kürsad Turgay (Freie University of Berlin, Germany) for kindly providing antibodies and the *ftsH*::*tet* mutant.

This work was funded by the Young Investigator Program of the Research Center of infectious diseases (ZINF) of the University of Würzburg (Germany) and grant LO 1804/2-1 from the German Research Foundation DFG. B.M.-S. was supported by the German Excellence Initiative to the Graduate School of Life Sciences of the University of Würzburg.

REFERENCES

1. **Matsumoto K, Kusaka J, Nishibori A, Hara H.** 2006. Lipid domains in bacterial membranes. Mol. Microbiol. **61:**1110–1117.
2. **Rudner DZ, Losick R.** 2010. Protein subcellular localization in bacteria. Cold Spring Harb. Perspect. Biol. **2:**a000307. doi:10.1101/cshperspect.a000307.
3. **Simons K, Gerl MJ.** 2010. Revitalizing membrane rafts: new tools and insights. Nat. Rev. Mol. Cell Biol. **11:**688–699.
4. **Simons K, Ikonen E.** 1997. Functional rafts in cell membranes. Nature **387:**569–572.
5. **Simons K, Sampaio JL.** 2011. Membrane organization and lipid rafts. Cold Spring Harb. Perspect. Biol **3:**a004697. doi:10.1101/cshperspect.a004697.
6. **López D, Kolter R.** 2010. Functional microdomains in bacterial membranes. Genes Dev. **24:**1893–1902.
7. **Dempwolff F, Moller HM, Graumann PL.** 2012. Synthetic motility and cell shape defects for deletions of flotillin/reggie paralogs in *Bacillus subtilis* and interplay with NfeD proteins. J. Bacteriol. **194:**4652–4661.
8. **Donovan C, Bramkamp M.** 2009. Characterization and subcellular localization of a bacterial flotillin homologue. Microbiology **155:**1786–1799.
9. **Zhao F, Zhang J, Liu YS, Li L, He YL.** 2011. Research advances on flotillins. Virol. J. **8:**479–484.
10. **Stuermer CA.** 2010. The reggie/flotillin connection to growth. Trends Cell Biol. **20:**6–13.
11. **Morrow IC, Parton RG.** 2005. Flotillins and the PHB domain protein family: rafts, worms and anaesthetics. Traffic **6:**725–740.

12. **Stuermer CA.** 2011. Reggie/flotillin and the targeted delivery of cargo. J. Neurochem. **116:**708–713.
13. **Allen JA, Halverson-Tamboli RA, Rasenick MM.** 2007. Lipid raft microdomains and neurotransmitter signalling. Nat. Rev. Neurosci. **8:**128–140.
14. **Kokubo H, Lemere CA, Yamaguchi H.** 2000. Localization of flotillins in human brain and their accumulation with the progression of Alzheimer's disease pathology. Neurosci. Lett. **290:**93–96.
15. **Girardot N, Allinquant B, Langui D, Laquerrière A, Dubois B, Hauw JJ, Duyckaerts C.** 2003. Accumulation of flotillin-1 in tangle-bearing neurones of Alzheimer's disease. Neuropathol. Appl. Neurobiol. **29:**451–461.
16. **Koch JC, Solis GP, Bodrikov V, Michel U, Haralampieva D, Shypitsyna A, Tönges L, Bähr M, Lingor P, Stuermer CA.** 2013. Upregulation of reggie-1/flotillin-2 promotes axon regeneration in the rat optic nerve in vivo and neurite growth in vitro. Neurobiol. Dis. **51:**168–176.
17. **Schulte T, Paschke KA, Laessing U, Lottspeich F, Stuermer CA.** 1997. Reggie-1 and reggie-2, two cell surface proteins expressed by retinal ganglion cells during axon regeneration. Development **124:**577–587.
18. **Munro S.** 2003. Lipid rafts: elusive or illusive? Cell **115:**377–388.
19. **Butcher BG, Helmann JD.** 2006. Identification of *Bacillus subtilis* sigma-dependent genes that provide intrinsic resistance to antimicrobial compounds produced by bacilli. Mol. Microbiol. **60:**765–782.
20. **Bach JN, Bramkamp M.** 2013. Flotillins functionally organize the bacterial membrane. Mol. Microbiol. **88:**1205–1217.
21. **Dempwolff F, Möller HM, Graumann PL.** 2012. Synthetic motility and cell shape defects associated with deletions of flotillin/reggie paralogs in *Bacillus subtilis* and interplay of these proteins with NfeD proteins. J. Bacteriol. **194:**4652–4661.
22. **Yepes A, Schneider J, Mielich B, Koch G, García-Betancur JC, Ramamurthi KS, Vlamakis H, López D.** 2012. The biofilm formation defect of a *Bacillus subtilis* flotillin-defective mutant involves the protease FtsH. Mol. Microbiol. **86:**457–471.
23. **Hamon MA, Lazazzera BA.** 2001. The sporulation transcription factor Spo0A is required for biofilm development in *Bacillus subtilis*. Mol. Microbiol. **42:**1199–1209.
24. **Lopez D, Vlamakis H, Kolter R.** 2009. Generation of multiple cell types in *Bacillus subtilis*. FEMS Microbiol. Rev. **33:**152–163.
25. **Le AT, Schumann W.** 2009. The Spo0E phosphatase of *Bacillus subtilis* is a substrate of the FtsH metalloprotease. Microbiology **155:**1122–1132.
26. **Haeusser DP, Garza AC, Buscher AZ, Levin PA.** 2007. The division inhibitor EzrA contains a seven-residue patch required for maintaining the dynamic nature of the medial FtsZ ring. J. Bacteriol. **189:**9001–9010.
27. **Haeusser DP, Schwartz RL, Smith AM, Oates ME, Levin PA.** 2004. EzrA prevents aberrant cell division by modulating assembly of the cytoskeletal protein FtsZ. Mol. Microbiol. **52:**801–814.
28. **Singh JK, Makde RD, Kumar V, Panda D.** 2007. A membrane protein, EzrA, regulates assembly dynamics of FtsZ by interacting with the C-terminal tail of FtsZ. Biochemistry **46:**11013–11022.
29. **Branda SS, González-Pastor JE, Ben-Yehuda S, Losick R, Kolter R.** 2001. Fruiting body formation by *Bacillus subtilis*. Proc. Natl. Acad. Sci. U. S. A. **98:**11621–11626.
30. **López D, Kolter R.** 2010. Extracellular signals that define distinct and coexisting cell fates in *Bacillus subtilis*. FEMS Microbiol. Rev. **34:**134–149.
31. **Vlamakis H, Chai Y, Beauregard P, Losick R, Kolter R.** 2013. Sticking together: building a biofilm the *Bacillus subtilis* way. Nat. Rev. Microbiol. **11:**157–168.
32. **Branda SS, González-Pastor JE, Dervyn E, Ehrlich SD, Losick R, Kolter R.** 2004. Genes involved in formation of structured multicellular communities by *Bacillus subtilis*. J. Bacteriol. **186:**3970–3979.
33. **Kearns DB, Chu F, Branda SS, Kolter R, Losick R.** 2005. A master regulator for biofilm formation by *Bacillus subtilis*. Mol. Microbiol. **55:**739–749.
34. **Chai L, Romero D, Kayatekin C, Akabayov B, Vlamakis H, Losick R, Kolter R.** 2013. Isolation, characterization, and aggregation of a structured bacterial matrix precursor. J. Biol. Chem. **288:**17559–17568.
35. **Stöver AG, Driks A.** 1999. Control of synthesis and secretion of the *Bacillus subtilis* protein YqxM. J. Bacteriol. **181:**7065–7069.
36. **Stöver AG, Driks A.** 1999. Regulation of synthesis of the *Bacillus subtilis* transition-phase, spore-associated antibacterial protein TasA. J. Bacteriol. **181:**5476–5481.
37. **Branda SS, Chu F, Kearns DB, Losick R, Kolter R.** 2006. A major protein component of the *Bacillus subtilis* biofilm matrix. Mol. Microbiol. **59:**1229–1238.
38. **Romero D, Aguilar C, Losick R, Kolter R.** 2010. Amyloid fibers provide structural integrity to *Bacillus subtilis* biofilms. Proc. Natl. Acad. Sci. U. S. A. **107:**2230–2234.
39. **Romero D, Vlamakis H, Losick R, Kolter R.** 2011. An accessory protein required for anchoring and assembly of amyloid fibres in *B. subtilis* biofilms. Mol. Microbiol. **80:**1155–1168.
40. **McLoon AL, Guttenplan SB, Kearns DB, Kolter R, Losick R.** 2011. Tracing the domestication of a biofilm-forming bacterium. J. Bacteriol. **193:**2027–2034.
41. **Chu F, Kearns DB, Branda SS, Kolter R, Losick R.** 2006. Targets of the master regulator of biofilm formation in *Bacillus subtilis*. Mol. Microbiol. **59:**1216–1228.
42. **López D, Fischbach MA, Chu F, Losick R, Kolter R.** 2009. Structurally diverse natural products that cause potassium leakage trigger multicellularity in *Bacillus subtilis*. Proc. Natl. Acad. Sci. U. S. A. **106:**280–285.
43. **Quadri LE, Weinreb PH, Lei M, Nakano MM, Zuber P, Walsh CT.** 1998. Characterization of Sfp, a *Bacillus subtilis* phosphopantetheinyl transferase for peptidyl carrier protein domains in peptide synthetases. Biochemistry **37:**1585–1595.
44. **Reuter K, Mofid MR, Marahiel MA, Ficner R.** 1999. Crystal structure of the surfactin synthetase-activating enzyme sfp: a prototype of the 4′-phosphopantetheinyl transferase superfamily. EMBO J. **18:**6823–6831.
45. **Schumann W.** 1999. FtsH—a single-chain charonin? FEMS Microbiol. Rev. **23:**1–11.
46. **Ito K, Akiyama Y.** 2005. Cellular functions, mechanism of action, and regulation of FtsH protease. Annu. Rev. Microbiol. **59:**211–231.
47. **Bieniossek C, Schalch T, Bumann M, Meister M, Meier R, Baumann U.** 2006. The molecular architecture of the metalloprotease FtsH. Proc. Natl. Acad. Sci. U. S. A. **103:**3066–3071.
48. **Bieniossek C, Niederhauser B, Baumann UM.** 2009. The crystal structure of apo-FtsH reveals domain movements necessary for substrate unfolding and translocation. Proc. Natl. Acad. Sci. U. S. A. **106:**21579–21584.
49. **Janska H, Kwasniak M, Szczepanowska J.** 2013. Protein quality control in organelles—AAA/FtsH story. Biochim. Biophys. Acta **1833:**381–387.
50. **Tatsuta T, Langer T.** 2009. AAA proteases in mitochondria: diverse functions of membrane-bound proteolytic machines. Res. Microbiol. **160:**711–717.
51. **Wehrl W, Niederweis M, Schumann W.** 2000. The FtsH protein accumulates at the septum of *Bacillus subtilis* during cell division and sporulation. J. Bacteriol. **182:**3870–3873.
52. **Barák I, Prepiak P, Schmeisser F.** 1998. MinCD proteins control the septation process during sporulation of *Bacillus subtilis*. J. Bacteriol. **180:**5327–5333.
53. **Feucht A, Errington J.** 2005. ftsZ mutations affecting cell division frequency, placement and morphology in *Bacillus subtilis*. Microbiology **151:**2053–2064.
54. **Reeve JN, Mendelson NH, Coyne SI, Hallock LL, Cole RM.** 1973. Minicells of Bacillus subtilis. J. Bacteriol. **114:**860–873.
55. **Bi EF, Lutkenhaus J.** 1991. FtsZ ring structure associated with division in *Escherichia coli*. Nature **354:**161–164.
56. **Errington J, Daniel RA, Scheffers DJ.** 2003. Cytokinesis in bacteria. Microbiol. Mol. Biol. Rev. **67:**52–65.
57. **Bi E, Lutkenhaus J.** 1993. Cell division inhibitors SulA and MinCD prevent formation of the FtsZ ring. J. Bacteriol. **175:**1118–1125.
58. **Weart RB, Lee AH, Chien AC, Haeusser DP, Hill NS, Levin PA.** 2007. A metabolic sensor governing cell size in bacteria. Cell **130:**335–347.
59. **Brown DA.** 2002. Isolation and use of rafts. Curr. Protoc. Immunol. Chapter 11:Unit 11.10. doi:10.1016/j.cell.2007.05.043.
60. **Lingwood D, Simons K.** 2007. Detergent resistance as a tool in membrane research. Nat. Protoc. **2:**2159–2165.
61. **Levin PA, Kurtser IG, Grossman AD.** 1999. Identification and characterization of a negative regulator of FtsZ ring formation in *Bacillus subtilis*. Proc. Natl. Acad. Sci. U. S. A. **96:**9642–9647.
62. **Kang MS, Kim SR, Kwack P, Lim BK, Ahn SW, Rho YM, Seong IS, Park SC, Eom SH, Cheong GW, Chung CH.** 2003. Molecular architecture of the ATP-dependent CodWX protease having an N-terminal serine active site. EMBO J. **22:**2893–2902.
63. **Zellmeier S, Zuber U, Schumann W, Wiegert T.** 2003. The absence of FtsH metalloprotease activity causes overexpression of the sigmaW-controlled pbpE gene, resulting in filamentous growth of *Bacillus subtilis*. J. Bacteriol. **185:**973–982.

64. **Hardwood CR, Cutting SM.** 1990. Molecular biological methods for *Bacillus*. Wiley, New York, NY.
65. **Dubnau D.** 1991. Genetic competence in *Bacillus subtilis*. Microbiol. Rev. **55:**395–424.
66. **Yasbin RE, Young FE.** 1974. Transduction in *Bacillus subtilis* by bacteriophage SPP1. J. Virol. **14:**1343–1348.
67. **Britton RA, Eichenberger P, Gonzalez-Pastor JE, Fawcett P, Monson R, Losick R, Grossman AD.** 2002. Genome-wide analysis of the stationary-phase sigma factor (sigma-H) regulon of *Bacillus subtilis*. J. Bacteriol. **184:** 4881–4890.
68. **Nakano S, Küster-Schöck E, Grossman AD, Zuber P.** 2003. Spx-dependent global transcriptional control is induced by thiol-specific oxidative stress in *Bacillus subtilis*. Proc. Natl. Acad. Sci. U. S. A. **100:** 13603–13608.
69. **Kim L, Mogk A, Schumann W.** 1996. A xylose-inducible *Bacillus subtilis* integration vector and its application. Gene **181:**71–76.
70. **Lewis PJ, Marston AL.** 1999. GFP vectors for controlled expression and dual labelling of protein fusions in *Bacillus subtilis*. Gene **227:**101–110.
71. **Kobayashi K, Iwano M.** 2012. BslA(YuaB) forms a hydrophobic layer on the surface of *Bacillus subtilis* biofilms. Mol. Microbiol. **85:**51–66.

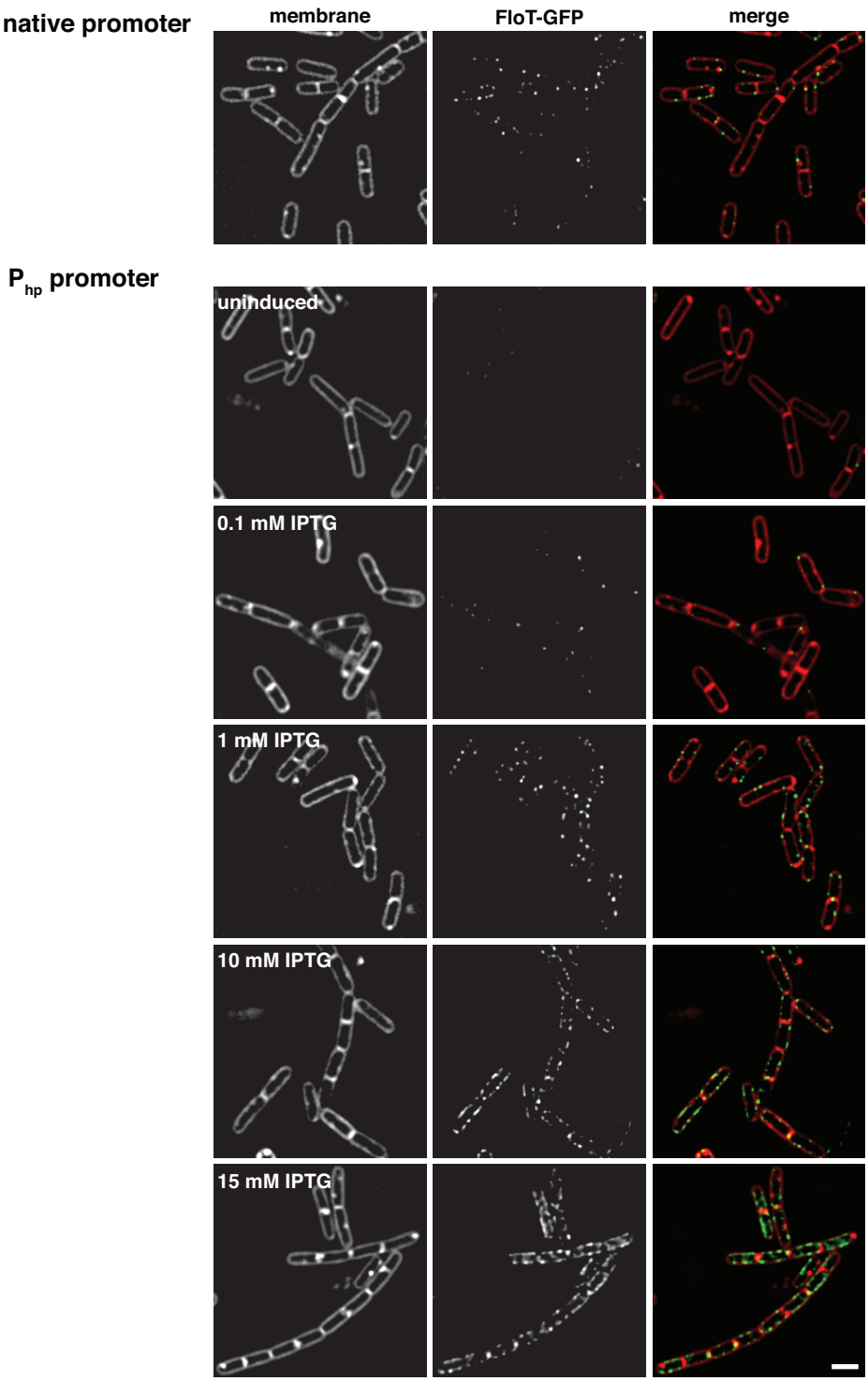
native promoter
membrane
FloT-GFP
merge
P hp promoter
uninduced
0.1 mM IPTG
1 mM IPTG
10 mM IPTG
15 mM IPTG

Figure S1

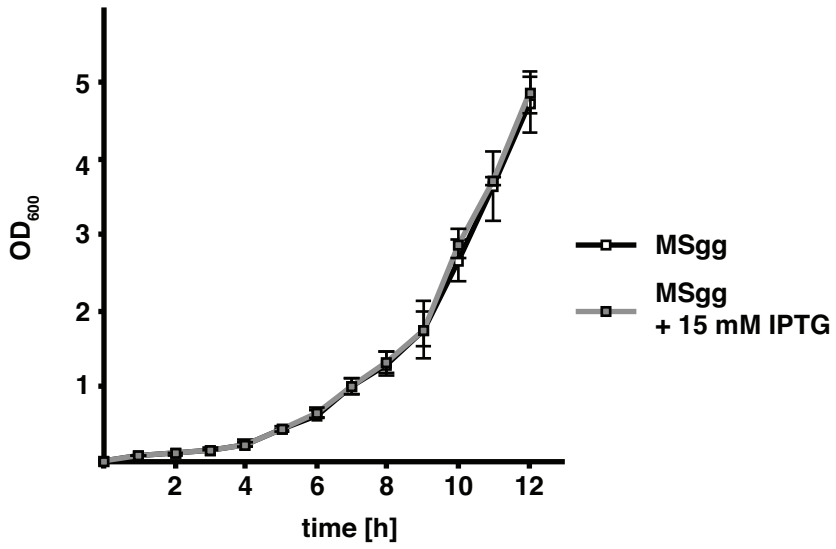

Figure S2

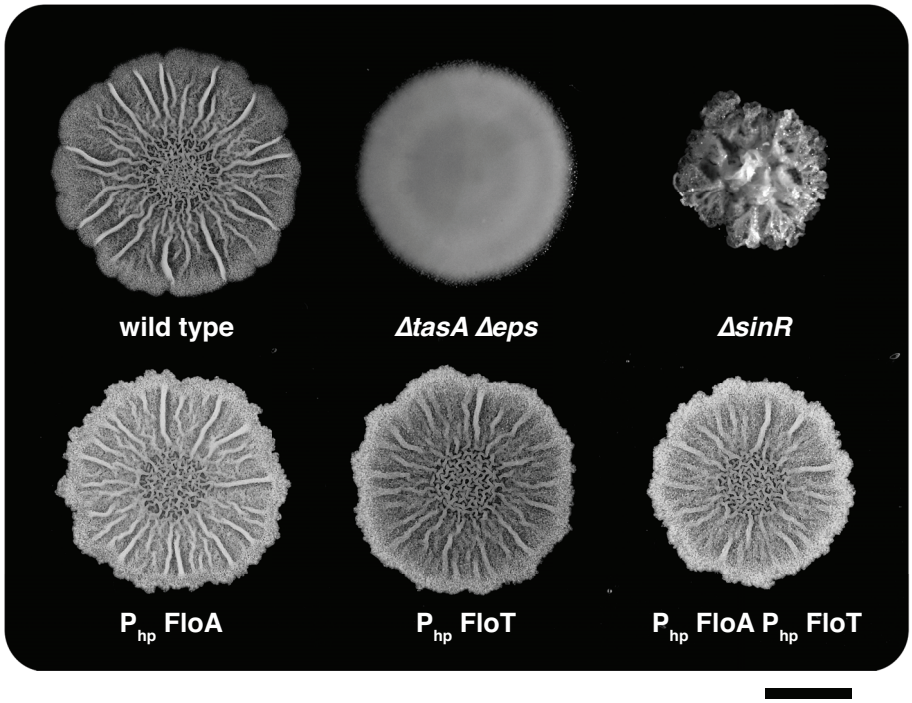
wild type
ΔtasA Δeps
ΔsinR
P hp FloA
P hp FloT
P hp FloA P hp FloT

Figure S3

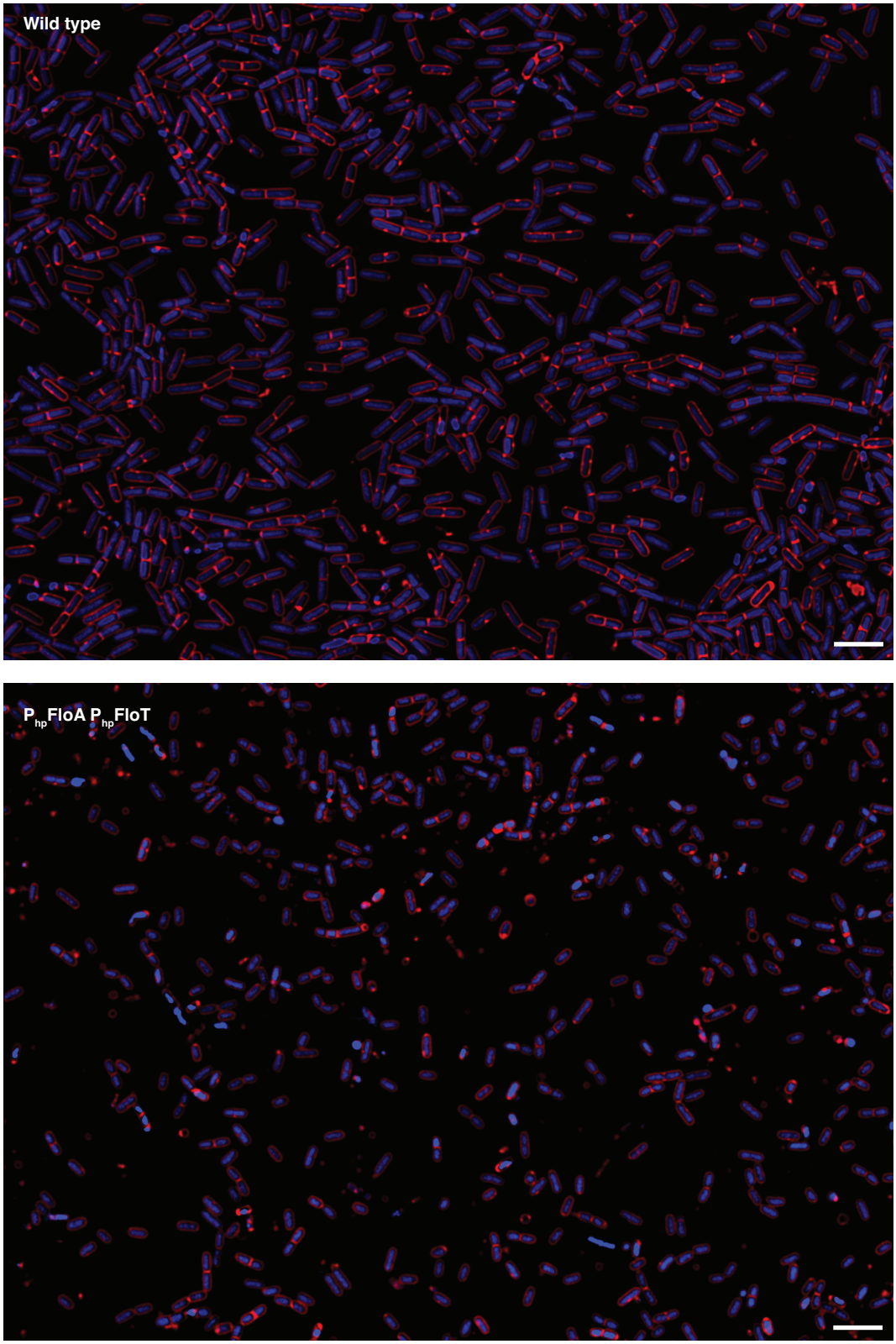

Figure S4

EzrA (Coverage: 52.85%)

MEFVIGLLIVLLALFAAGYFFRKKIYAEIDRLESWKIEILNRSIVEEMSKIKHLKMTG
QTEEFFEKWREEWDEIVTAHMPKVEELLYDAEENADKYRFKKANQVLVHIDDLLTAAE
SSIEKILREISDLVTSEEKSREEIEQVRERYSKSRKNLLAYSHLYGELYDSLEKDLDE
IWSGIKQFEEETEGGNYITARKVLLEQDRNLERLQSYIDDVPKLLADCKQTVPGQIAK
LKDGYGEMKEKGYKLEHIQLDKELENLSNQLKRAEHVLMTELDIDEASAILQLIDENI
QSVYQQLEGEVEAGQSVLSKMPELIIAYDKLKEEKEHTKAETELVKESYRLTAGELGK
QQAFEKRLDEIGKLLSSVKDKLDAEHVAYSLLVEEVASIEKQIEEVKKEHAEYRENLQ
ALRKEELQARETLSNLKKTISETARLLKTSNIPGIPSHIQEMLENAHHHIQETVNQLN
ELPLNMEEAGAHLKQAEDIVNRASRESEELVEQVILIEKIIQFGNRFRSQNHILSEQL
KEAERRFYAFDYDDSYEIAAAAVEKAAPGAVEKIKADISA

Figure S5

Table S1

Strain	Genotype	Reference
***Bacillus subtilis* PY79**		
BM-18	Wild type PY79	Youngman et al. 1984
BM-224	*amyE::*P_{yqeZ} *floA-gfp* (spc)	Yepes et al. 2012
BM-20	*amyE::*P_{hp} *floA-gfp* (spc)	This study
BM-223	*amyE::*P_{yuaF} *floT-gfp* (spc)	Yepes et al. 2012
BM-21	*amyE::*P_{hp} *floT-gfp* (spc)	This study
BM-246	Δ*tasA::spc*	This study
BM-225	Δ*sinR::spc*	This study
BM-248	Δ*tasA::km* Δ*sinR::spc*	This study
BM-19	*amyE::*P_{hp} *floA* (spc)	This study
BM-28	*amyE::*P_{hp} *floT* (spc)	This study
BM-29	*amyE::*P_{hp} *floT* (spc) *lacA*::P_{hp} *floA* (mls)	This study
BM-247	*amyE::*P_{hp} *floT* (spc) *lacA*::P_{hp} *floA* (mls) Δ*tasA::km*	This study
BM-126	*thrC::*P_{tapA} *yfp* (km)	This study
BM-243	*amyE::*P_{hp} *floA* (spc) *thrC*::P_{tapA} *yfp* (km)	This study
BM-244	*amyE::*P_{hp} *floT* (spc) *thrC::*P_{tapA} *yfp* (km)	This study
BM-242	*amyE::*P_{hp} *floT* (spc) *lacA*::P_{hp} *floA* (mls) *thrC::*P_{tapA} *yfp* (km)	This study
BM-168	*amyE::*P_{hp} *floT* (spc) *lacA*::P_{hp} *floA* (mls) Δ*ftsH::km*	This study
BM-249	Δ*ftsH::tet*	This study
BM-250	Δ*ftsH::tet* *thrC::*P_{tapA} *yfp (km)*	This study
BM-245	*amyE::*P_{hp} *floT* (spc) *lacA*::P_{hp} *floA* (mls) *thrC::*P_{tapA} *yfp* (km) Δ*ftsH::tet*	This study
BM-222	*amyE::*P_{xyl} *ftsZ-gfp* (cm)	This study
BM-226	*amyE::*P_{xyl} *ftsZ-gfp* (cm) *lacA::*P_{hp} *floT/floA* (mls)	This study
BM-144	*amyE::*P_{xyl} *ezrA-gfp* (spc)	This study
BM-151	*amyE*:P_{xyl} *ezrA-gfp* (spc) *lacA*::P_{hp} *floT/floA* (mls)	This study
BM-198	*amyE::*P_{xyl} *ezrA-gfp* (spc) *lacA::*P_{hp} *floT*/*floA* (mls) Δ*ftsH::km*	This study
BM-197	*amyE::*P_{xyl} *ezrA-gfp* (spc) Δ*ftsH::km*	This study

BM-207	*amyE*::P_{xyl} *ezrA-gfp* (spc) *lacA*::P_{hp} *ftsH* (mls)	This study
***Bacillus subtilis* NCIB3610**		
DL-1	Wild type NCIB3610	Branda et al. 2001
DL-7	Δ*tasA::spc* Δ*eps::tet*	Lopez et al. 2009
DL-5	Δ*sinR::spc*	Kearns et al. 2005
BM-40	*amyE*::P_{hp} *floA* (spc)	This study
BM-37	*amyE*::P_{hp} *floT* (spc)	This study
BM-59	*amyE*::P_{hp} *floT* (spc) *lacA*::P_{hp} *floA* (mls)	This study

References

1. Youngman P, Perkins JB, Losick R. 1984. Construction of a cloning site near one end of Tn917 into which foreign DNA may be inserted without affecting transposition in *Bacillus subtilis* or expression of the transposon-borne erm gene. Plasmid 12:1–9.

2. Yepes A, Schneider J, Mielich B, Koch G, García-Betancur J-C, Ramamurthi KS, Vlamakis H, López D. 2012. The biofilm formation defect of a *Bacillus subtilis* flotillin-defective mutant involves the protease FtsH. Mol Microbiol 86(2):457-471.

3. Branda SS, González-Pastor JE, Ben-Yehuda S, Losick R, Kolter R. 2001. Fruiting body formation by *Bacillus subtilis*. Proc. Natl. Acad. Sci. U.S.A. 98:11621–11626.

4. Kearns DB, Chu F, Branda SS, Kolter R, Losick R. 2005. A master regulator for biofilm formation by *Bacillus subtilis*. Mol Microbiol 55:739–749.

5. López D, Vlamakis H, Losick R, Kolter R. 2009. Paracrine signaling in a bacterium. Genes & Development 23:1631–1638.

Abbreviations

Antibiotics

cm Encodes chloramphenicol resistance protein
km Encodes kanamycin resistance protein
mls Encodes erythromycin + lincomycin resistance protein
spc Encodes spectinomycin resistance protein
tet Encodes tetracycline resistance protein

Protein tags

GFP Green fluorescent protein

Promoters

P_{hp} IPTG-inducible Hyperspank promoter
P_{xyl} Xylose-inducible promoter
P_{yuaF} Natural promoter that controls the expression of *yuaG*
P_{tapA} Natural promoter that controls the expression of *tasA*

Table S2

Purpose	Name	Sequence (5'-3')
Overexpression of FloT	YuaGSalIfw	AAAAGTCGACTAAGGAGGAACTACTATGACAATGCCGATTATAAT
	YuaGSphIrv	AAAAGCATGCTTACTCTGATTTTTGGATCG
Overexpression of FloA	YqfASalIfw	AAAAGTCGACTAAGGAGGAACTACTATGGATCCGTCAACACTTA
	YqfASphIrv	AAAAGCATGCTTATGATTTGCGGTCTTCAT
Overexpression of FloA-GFP or FloT-YFP	GFPSphIrv	AAAAGCATGCTTATTTGTATAGTTCATCCATGC
Overexpression of bicistronic FloA+FloT	YuaGYqfAOp2	CAGTTACCATACGGTTCTG
	YuaGYqfAOp3	CAGAACCGTATGGTAACTGATGGATCCGTCAACACTTA
Overexpression of FtsH	FtsHSalIfw	AAAAGTCGACTAAGGAGGAACTACTATGAATCGGGTCTTCCGT
	FtsHSphI	AAAAGCATGCAGAAAGCGAATTACTCTTTC
Translation fusion FtsZ-GFP	FtsZSpeIfw	AAAAACTAGTTAAGGAGGAACTACTGCATGTTGGAGTTCGAAAC
	FtsZ-GFP 2	AGTTCTTCTCCTTTACTCATGCCGCGTTTATTACGGTT
	FtsZ-GFP 3	AACCGTAATAAACGCGGATGAGTAAAGGAGAAGAACT
	GFPBamHIrv	AAAAGGATCCATCTGAAGTCTGGACATTTA
Translational fusion EzrA-GFP	EzrAKpnIfw	AAAAGGTACCATGGAGTTTGTCATTGGATT
	EzrAXhoIrv	AAAACTCGAGAGCGGATATGTCAGCTTTG

PLOS | GENETICS

RESEARCH ARTICLE

Spatio-temporal Remodeling of Functional Membrane Microdomains Organizes the Signaling Networks of a Bacterium

Johannes Schneider[1], Teresa Klein[2], Benjamin Mielich-Süss[1], Gudrun Koch[1], Christian Franke[2], Oscar P. Kuipers[3], Ákos T. Kovács[4], Markus Sauer[2], Daniel Lopez[1]*

1 Research Center for Infectious Diseases ZINF, University of Würzburg, Würzburg, Germany, **2** Department of Biotechnology and Biophysics, University of Würzburg, Würzburg, Germany, **3** Molecular Genetics Group, Groningen Biomolecular Sciences and Biotechnology Institute, University of Groningen, Groningen, The Netherlands, **4** Terrestrial Biofilms Group, Institute of Microbiology, Friedrich Schiller University of Jena, Jena, Germany

* Daniel.Lopez@uni-wuerzburg.de

OPEN ACCESS

Citation: Schneider J, Klein T, Mielich-Süss B, Koch G, Franke C, Kuipers OP, et al. (2015) Spatio-temporal Remodeling of Functional Membrane Microdomains Organizes the Signaling Networks of a Bacterium. PLoS Genet 11(4): e1005140. doi:10.1371/journal.pgen.1005140

Editor: Josep Casadesús, Universidad de Sevilla, Spain

Received: September 22, 2014

Accepted: March 11, 2015

Published: April 24, 2015

Data Availability Statement: Our transcriptomic data is deposited at Gene Expression Omnibus (GEO): Accession database number GSE47918.

Funding: This work was funded by the European Research Council ERC-Starting Grant ERC335568 (DL) and German Federal Ministry of Education and Research (BMBF) grant number 13N11019 (MS). This publication was funded by the German Research Foundation (DFG) and the University of Wuerzburg in the funding programme Open Access Publishing. The funders had no role in study design,

Abstract

Lipid rafts are membrane microdomains specialized in the regulation of numerous cellular processes related to membrane organization, as diverse as signal transduction, protein sorting, membrane trafficking or pathogen invasion. It has been proposed that this functional diversity would require a heterogeneous population of raft domains with varying compositions. However, a mechanism for such diversification is not known. We recently discovered that bacterial membranes organize their signal transduction pathways in functional membrane microdomains (FMMs) that are structurally and functionally similar to the eukaryotic lipid rafts. In this report, we took advantage of the tractability of the prokaryotic model *Bacillus subtilis* to provide evidence for the coexistence of two distinct families of FMMs in bacterial membranes, displaying a distinctive distribution of proteins specialized in different biological processes. One family of microdomains harbors the scaffolding flotillin protein FloA that selectively tethers proteins specialized in regulating cell envelope turnover and primary metabolism. A second population of microdomains containing the two scaffolding flotillins, FloA and FloT, arises exclusively at later stages of cell growth and specializes in adaptation of cells to stationary phase. Importantly, the diversification of membrane microdomains does not occur arbitrarily. We discovered that bacterial cells control the spatio-temporal remodeling of microdomains by restricting the activation of FloT expression to stationary phase. This regulation ensures a sequential assembly of functionally specialized membrane microdomains to strategically organize signaling networks at the right time during the lifespan of a bacterium.

Author Summary

Cellular membranes organize proteins related to signal transduction, protein sorting and membrane trafficking into the so-called lipid rafts. It has been proposed that the functional

data collection and analysis, decision to publish, or preparation of the manuscript.

Competing Interests: The authors have declared that no competing interests exist.

diversity of lipid rafts would require a heterogeneous population of raft domains with varying compositions. However, a mechanism for such diversification is not known due in part to the complexity that entails the manipulation of eukaryotic cells. The recent discovery that bacteria organize many cellular processes in membrane microdomains (FMMs), functionally similar to the eukaryotic lipid rafts, prompted us to explore FMMs diversity in the bacterial model *Bacillus subtilis*. We show that diversification of FMMs occurs in cells and gives rise to functionally distinct microdomains, which compartmentalize distinct signal transduction pathways and regulate the expression of different genetic programs. We discovered that FMMs diversification does not occur randomly. Cells sequentially regulate the specialization of the FMMs during cell growth to ensure an effective and diverse activation of signaling processes.

Introduction

Cells typically compartmentalize their cellular processes into subcellular structures (e.g. organelles) to optimize their efficiency and improve their activity. One of the most interesting concepts in cellular compartmentalization is the proposed existence of *lipid rafts* in the membranes of eukaryotic cells [1]. Eukaryotic membranes organize a large number of proteins related to signal transduction, protein sorting and membrane trafficking into discrete nanoscale domains termed lipid rafts [1,2]. The functional diversity of lipid rafts is currently attributed to a different lipid and protein composition, as compelling evidence suggests that a heterogeneous population of lipid rafts could exist on a given cell [3–5]. Yet, the molecular mechanisms by which cells generate and regulate raft heterogeneity are still unclear. In eukaryotic systems, it is known that the integrity of lipid rafts requires the activity of two different raft-associated proteins termed flotillins (FLO-1 and FLO-2) [6,7]. Flotillins are scaffolding proteins, which may redundantly act as chaperones in recruiting the protein cargo to lipid rafts and interact with the recruited proteins that activate the signal transduction processes [8–10]. Consequently, the perturbation of the activity of flotillins causes serious defects in several signal transduction and membrane trafficking processes, which seems to be intimately related to the occurrence of severe human diseases, such as Alzheimer's disease, Parkinson's disease or muscular dystrophy (reviewed in [11]).

The spatial organization of signaling networks in lipid rafts has been considered a hallmark in cellular complexity because their existence is exclusively associated with eukaryotic cells. However, we recently discovered that bacteria organize many proteins related to signal transduction in functional membrane microdomains (FMMs) that are structurally and functionally similar to the lipid rafts of eukaryotic cells [12]. Bacterial flotillins are important components for the organization and the maintenance of the architecture of FMMs. Similar to the eukaryotic flotillins, bacterial flotillins probably act as scaffolding proteins in tethering protein components to the FMMs, thereby facilitating their efficient interaction and oligomerization and to mediate the efficient activation of signal transduction pathways harbored in FMMs. Consequently, mutants lacking flotillins show a severe defect in FMM-localized signaling pathways concomitantly with a severe dysfunction of diverse physiological processes, such as biofilm formation, natural competence or sporulation [12–17].

The FMMs of the bacterial model *Bacillus subtilis* contain two different flotillin-like proteins, FloA and FloT [12]. FloA and FloT flotillins physically interact [13] and presumably play a redundant role because the dysfunction of specific FMM-associated physiological processes, like biofilm formation, only occurs in the Δ*floA* Δ*floT* defective mutant and is not observed in

either of the Δ*floA* or Δ*floT* single mutants [17]. Likewise, the overexpression of both *floA* and *floT* causes pleiotropic effects in cell division and cell differentiation but this effect is not observed in cells that overexpress one single flotillin gene [16]. In this respect, bacterial flotillins seem to behave similarly to human flotillins FLO-1 and FLO-2, given that both FLO-1 and FLO-2 are associated with each other in hetero-oligomeric complexes and have a strong regulatory correlation [18–20]. These experimental evidences led to the general assumption that both flotillins play a redundant function in both eukaryotic lipid rafts and bacterial FMMs.

In this report, we provide evidence that a heterogeneous population of membrane microdomains coexists on bacterial cells. We show that FloA and FloT are two functionally different flotillins that physically interact but unevenly distribute within the FMMs of bacterial cells. FloA and FloT act as specific scaffold proteins that tether a defined group of FMMs-associated proteins. This generates functionally distinct microdomains, which compartmentalize distinct signal transduction pathways and regulate different genetic programs. Importantly, we show that cells sequentially regulate the functional specialization of the FMMs during cell growth. Cells restrict the expression of the *floT* gene to stationary phase to ensure an effective activation of signaling processes at specific times during the lifespan of the bacterium.

Results

FloA and FloT are differentially regulated in *B. subtilis*

While exploring flotillin redundancy in the FMMs of *B. subtilis*, we discovered that the expression of FloA and FloT is controlled by different genetic programs, which could indicate that these are two functionally different flotillins. We came across this finding by examining the expression profiles of *floA* and *floT* genes in the 249 different growing conditions that are published in [21,22], and are available in SubtiExpress (http://subtiwiki.uni-goettingen.de/apps/expression). By doing this, we consistently found high expression of *floA* in all the growing conditions tested, including LB and MSgg growth media, the two growth media that we normally used in the laboratory to grow *B. subtilis* (S1A Fig) [23]. However, the expression of *floT* showed more variability among the growth conditions tested and exhibited an important difference in gene expression between LB (lower expression of *floT*) and MSgg (higher expression of *floT*). To test this in the laboratory, we constructed *B. subtilis* strains harboring the P_{floA}-*yfp* and P_{floT}-*yfp* transcriptional fusions (YFP is yellow fluorescence protein) and grew them in LB and MSgg media [23]. Our laboratory uses the chemically-defined medium MSgg to induce sporulation and the formation of robust biofilms in *B. subtilis* cultures and differs to LB medium in which *B. subtilis* did not show any of the developmental characteristics of MSgg [24]. By growing *B. subtilis* cells in these two growth conditions, we detected an activation of *floT* expression in MSgg (S1A Fig), while LB medium showed poor activation of *floT* expression (S1B Fig). In contrast, *floA* was equally expressed in both MSgg and LB media. Furthermore, we generated strains labeled with the FloA-GFP and FloT-GFP translational fusions (GFP is green fluorescence protein) to visualize and quantify flotillin protein production using flow cytometry. The FloT-GFP labeled strain showed a reduction of the fluorescence signal when grown in LB medium while FloA-GFP was equally expressed in both MSgg and LB media (S1C Fig).

To investigate whether the differential production of FloA and FloT is a cell-regulated process, the strains labeled with P_{floA}-*yfp* and P_{floT}-*yfp* transcriptional fusions were used to systematically inactivate regulatory genes of *B. subtilis* and search for mutants capable of altering the expression of *floT* in MSgg medium (S1D Fig). We detected a uniform expression of *floA* in all mutants tested. However, we discovered that cells lacking the *abrB* gene showed increased expression of *floT*. Additionally, we found inhibition of *floT* expression in cells when the *spo0A* gene was deleted. Importantly, *spo0A* and *abrB* belong to the same signaling pathway. AbrB is

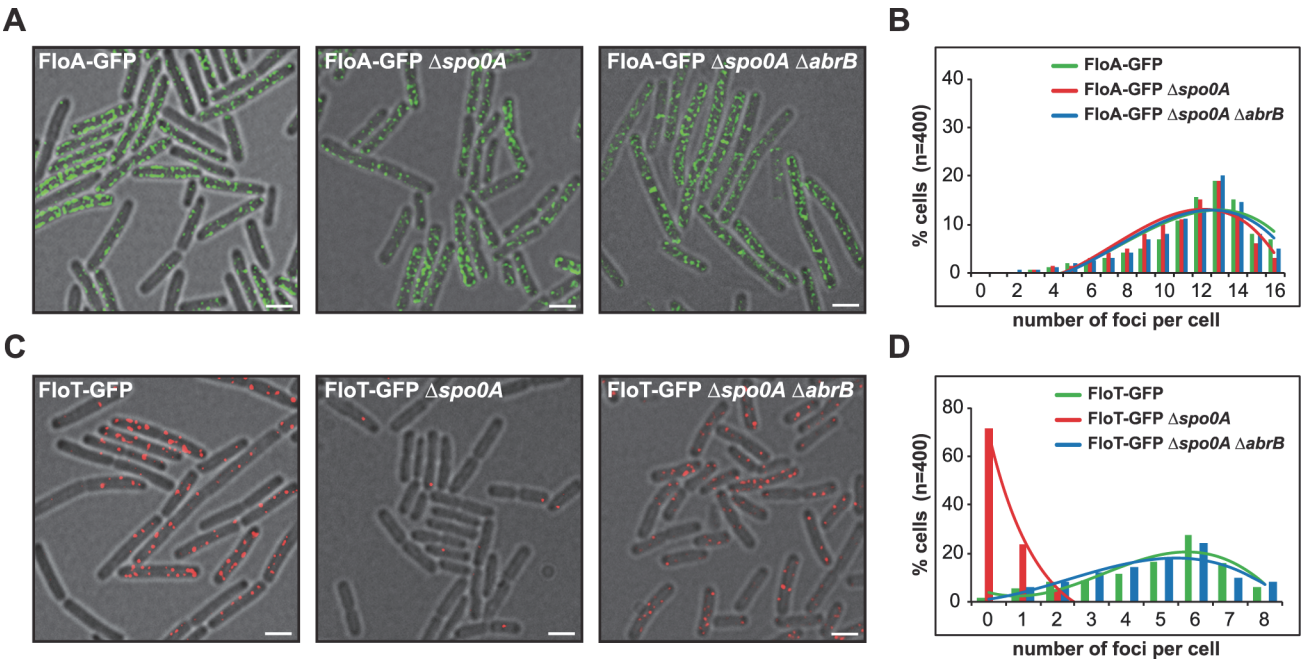

Fig 1. Spo0A regulates *floT* and not *floA* expression via inhibition of AbrB. (A) Fluorescence microscopy pictures of different strains expressing FloA-GFP translational fusion (Fluorescence signal in green). Scale bars are 2 μm. **(B)** Quantification of fluorescence foci of different strains expressing FloA-GFP translational fusion. **(C)** Fluorescence microscopy pictures of different strains expressing FloT-GFP translational fusion (Fluorescence signal in red). Scale bars are 2 μm. **(D)** Quantification of fluorescence foci of different strains expressing FloT-GFP translational fusion. Cells were grown in MSgg medium at 37°C until stationary phase.

doi:10.1371/journal.pgen.1005140.g001

a repressor of biofilm formation among other processes [25] and its expression is negatively regulated by Spo0A [26]. Spo0A is a master regulatory protein necessary for the activation of many physiological processes related to stationary phase [27]. Therefore, this provides epistatic evidence that Spo0A positively regulates *floT* expression at stationary phase via inhibition of *abrB* and that this genetic cascade does not affect the expression of *floA*. To test this hypothesis, we deleted *spo0A* and/or *abrB* genes in FloA-GFP and FloT-GFP labeled strains and monitored the subcellular distribution pattern of flotillins using fluorescence microscopy and applying a deconvolution algorithm to eliminate out-of-focus signal and to improve their correct visualization (see material and methods section) (Fig 1). Indeed, Δ*spo0A* or Δ*spo0A* Δ*abrB* mutants showed no variation in the distribution pattern of fluorescence foci that were generated by FloA (Fig 1A and 1B). In contrast, Δ*spo0A* mutant showed a severe reduction of fluorescence foci that were generated by FloT, which could be reconstituted in the Δ*spo0A* Δ*abrB* double mutant (Fig 1C and 1D).

Activation of Spo0A (Spo0A~P) occurs at stationary phase due in part to the activation of the histidine kinase C (KinC) [28,29], which is driven by the action of the self-produced signaling molecule surfactin. Thus, FloA-GFP and FloT-GFP labeled strains were grown in LB medium and complemented with exogenously added surfactin (5 μM) (S2A and S2C Fig). FloA-GFP labeled cells showed no alteration of the fluorescence signal but FloT-GFP labeled cells showed an increase in the number of foci (S2A–S2D Fig). This is a Spo0A-depedent effect because the *spo0A* deficient strain showed no recovery of FloT expression upon addition of surfactin (S2E and S2F Fig). Altogether, these results show an upregulation of FloT production at stationary phase in a Spo0A-dependent manner likely via AbrB. In contrast, the production of FloA is not influenced by this regulatory cascade.

Flotillins distribute unevenly within the FMMs of *B. subtilis*

The distinct regulatory programs for FloA and FloT production led us to hypothesize that FloA and FloT may play different roles in *B. subtilis* cells. To investigate this hypothesis, we first explored whether FloA and FloT show any structural difference. FloT is a larger protein (509 aa) that has an extended C-terminal region compared to FloA (331 aa) (Figs 2A and S3A). To determine if these structural differences are associated with a different subcellular distribution pattern, we used strains labeled with the FloA-GFP and FloT-GFP translational fusions to visualize and quantify the number of fluorescent foci (n = 400) using fluorescence microscopy. On average, FloA distributed in 13 foci per cell while FloT distributed approximately in 6 foci (Figs 2B, 2C and S3B). These results are consistent with the number of foci that we detected in the genetic analysis that are shown in Fig 1. However, to validate that these results were not a consequence of clustering artifacts [30], we compared their distribution pattern using non-dimerizing monomeric red fluorescence protein mCherry (mCh) in a total of 400 cells. Likewise, FloA distributed in 13 foci per cell while FloT distributed in 6 foci, as previously observed (Figs 2B, 2C and S3B). Importantly, the subcellular localization of flotillins consistently showed that FloA distributed in more foci per cell than FloT. To gain more insight about the differential distribution pattern of flotillins, we performed co-localization experiments using FloA-GFP, FloT-mCh and FloA-mCh, FloT-GFP double-labeled strains. Co-localization of both signals was detected by fluorescence microscopy, showing colocalization of FloT with FloA in all cells examined (Fig 2D), which adds to the previous notion that FloA and FloT physically interact [12,13,17]. However, the obvious differences in the number of foci between FloA and FloT resulted in the colocalization of both FloA and FloT signals only in a subset of foci (Pearson's correlation coefficient $R^2 = 0.81$). This diversified the pool of FMMs of a given cell into two different types of microdomains: one family of microdomains that contains solely FloA signal and a second type of microdomains in which both FloA and FloT signals converge. We performed time-lapse fluorescence microscopy experiments using a FloA-GFP FloT-mCherry double-labeled strain to investigate the dynamics of the subcellular co-localization. A series of images were taken at one-second time interval (Fig 2E). The fluorescence signal attributable to FloA and FloT reorganized dynamically within the membrane and consistently showed co-localization of signals from FloA and FloT.

The asymmetrical distribution pattern of FloA and FloT was further examined at higher resolution using super-resolution imaging by PALM [31,32]. To this end, FloA and FloT were labeled with the photoactivatable monomeric protein mEOS2 and expressed in *B. subtilis* cells. FloA-mEOS2 and FloT-mEOS2 proteins were activated by low intensity irradiation at 405 nm. Photoactivated proteins were excited at 568 nm, imaged and bleached before the next cycle of photoactivation. Individual protein positions were determined (localized) in each image frame and used to reconstruct a high-resolution PALM image (Fig 3A and 3B). Clusters candidates were defined by either one connected pixel area in image-based analysis or by a cloud of scattered localizations with spatial coherence in localization based analysis. Spatial coherence implies that the increase local density of localizations follows a Gaussian distribution within the cluster, which is indicative of the nonrandom distribution of localizations. Using the raw localization data and the corresponding super-resolved image, we generated a mask to define possible cluster candidates and separate them from the localization pseudo background. By using this technique, we confirmed that FloA assembled in 13 small clusters per cell (Diameter = 46.73 ± 1.35 nm). FloT however, assembled in approximately 6 larger clusters per cell (Diameter = 63.39 ± 2.28 nm) with a higher content of proteins (Fig 3C–3F). To validate these results, we also monitored the distribution pattern of FloA and FloT when fused to photoactivatable monomeric PAmCherry using PALM (S4A and S4B Fig). The statistical analysis of the

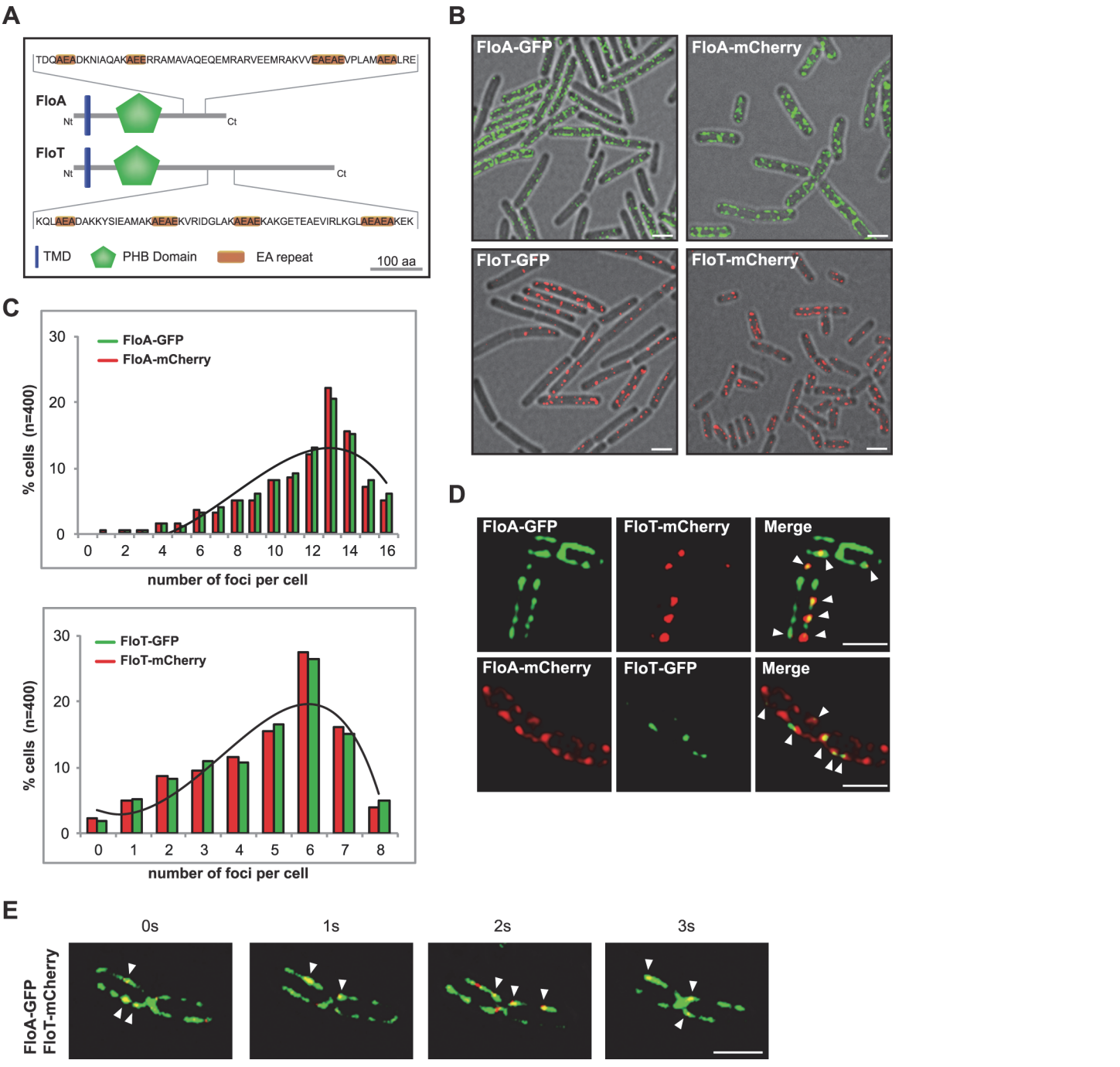

Fig 2. FloA and FloT are two distinct flotillins. (A) Comparative diagram of FloA and FloT protein structures. The membrane-anchored region is represented in blue. The PHB domain is represented in green and the coil-coiled region is magnified and EA repeats are labeled in orange. Scale bar is 100 amino acids. **(B)** Fluorescence microscopy pictures of cells labeled with FloA-GFP, FloA-mCherry (upper panel), FloT-GFP and FloT-mCherry (lower panel) translational fusions. Fluorescence signal associated with FloA is represented in green and fluorescence signal associated with FloT is represented in red. Cultures were grown in MSgg medium at 37°C until stationary phase. Scale bars are 2 μm. **(C)** Quantification of the number of foci per cell (n = 400). **(D)** Fluorescence microscopy pictures of double-labeled strains. Cultures were grown in MSgg medium at 37°C until stationary phase. GFP signal is represented in green and mCherry signal is represented in red. Right panel shows the merge of the two fluorescence signals, which is visualized as yellow fluorescence signal. Scale bars are 2 μm. **(E)** Time lapse fluorescence microscopy analysis of cells expressing FloA-GFP (green signal) and FloT-mCherry (red signal) translational fusions. Signal was monitored within the same cells at 1 sec intervals. Cultures were grown in MSgg medium at 37°C until stationary phase. Scale bar is 2 μm.

doi:10.1371/journal.pgen.1005140.g002

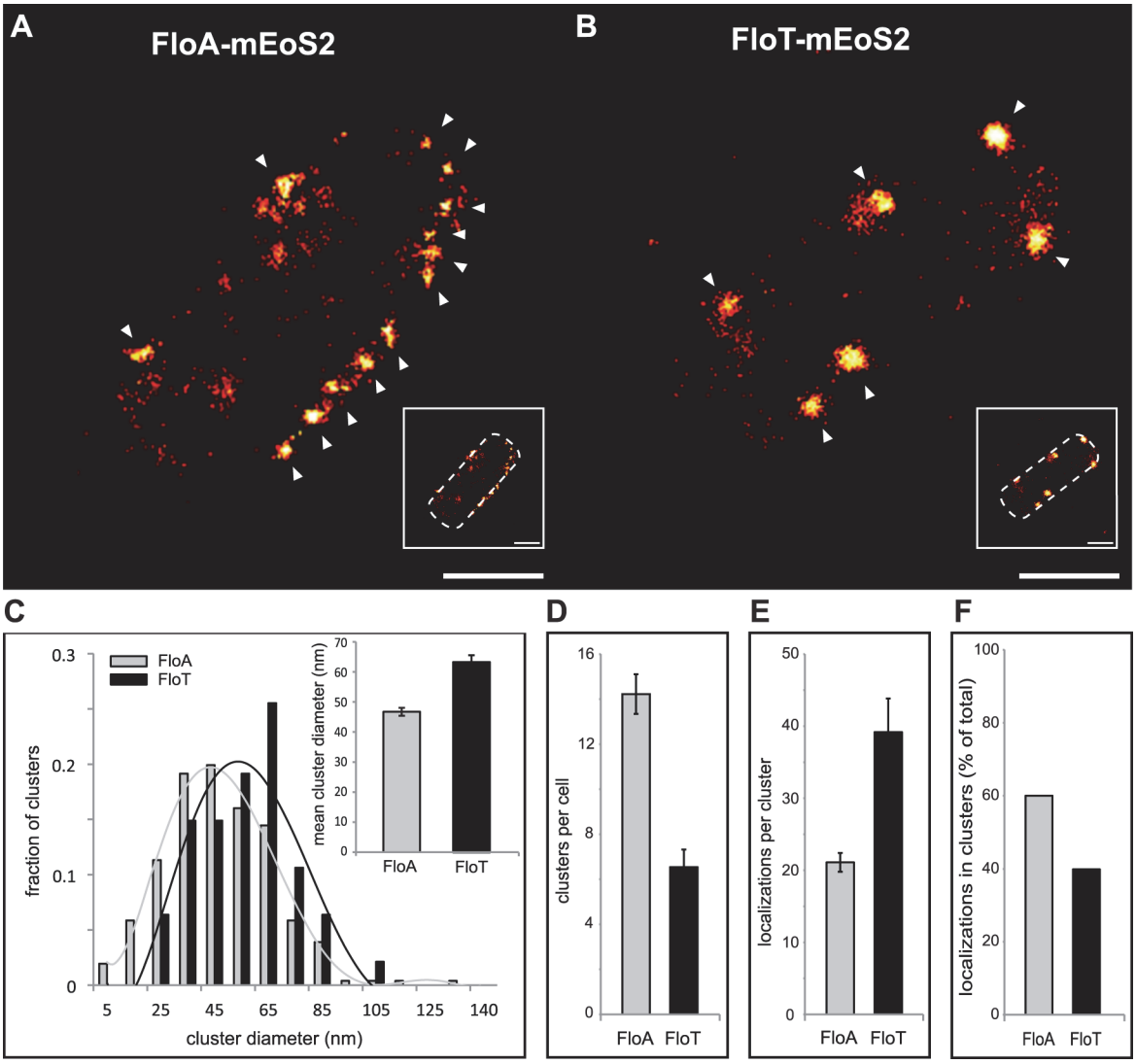

Fig 3. FloA and FloT distribute differently within the bacterial microdomains. (A and B) PALM images of cells labeled with FloA-mEoS2 (A) or FloT-mEoS2 (B) translational fusions grown to stationary phase and fixed with PFA (4%). With increasing localization density the color code changes from red to yellow. White arrows indicate the localization of a cluster. Scale bars are 500 nm. Detail of the right bottom of each panel shows a dashed-line decorated PALM picture as a general indicator of the cell outline. Scale bar is 500 nm. **(C)** Comparative graph of the diameter of the clusters that were generated by FloA-mEoS2 and FloT-mEoS2 fluorescence signal. The upper right corner shows a graph with the mean of the diameter of the FloA and FloT clusters. **(D)** Comparative graph of the number of clusters detected in FloA-mEoS2 and FloT-mEoS2 labeled cells. **(E)** Comparative graph of the number of FloA and FloT localizations per cluster. **(F)** Comparative graph of the percentage of localizations that organized in clusters.

doi:10.1371/journal.pgen.1005140.g003

signals detected by PALM and further validation by western blot analysis suggested that FloT is more abundant than FloA in cells and yet, based on our results, is concentrated in a lower number of foci (S4C and S4D Fig).

Spatial organization of flotillin distribution is driven by flotillin interaction

The molecular basis of the asymmetrical distribution of FloA and FloT was explored by monitoring the intra- and inter-specific interactions that occur between FloA and FloT flotillins. To do this, we used a bacterial two-hybrid (BTH) assay, in which FloA and FloT were tagged to T25 or T18 catalytic domains of an adenylate cyclase that reconstitute the enzyme upon

interaction of two proteins [33]. A fully active adenylate cyclase produces cAMP, which accumulates in the cytoplasm and triggers the expression of a cAMP-inducible *lacZ* reporter gene [33]. Using this assay, we detected a strong interaction signal with FloA alone (Fig 4A) (Instructions of the manufacturer define a positive signal if above the threshold of 700 Miller Units [33]). Likewise, a strong interaction signal was detected with FloT (Fig 4A). This is indicative of the capacity of FloA and FloT to form homo-oligomers. However, when we assayed the interactions between FloA and FloT, the interaction signal was less prominent in comparison to the FloA-FloA and FloT-FloT interactions, suggesting that flotillins are prone to form homo-oligomers while hetero-oligomerization occurs to a lesser extent (Fig 4A). The propensity to form homo-oligomers suggests different interaction properties between FloA and FloT, which is probably a determinant in the generation of distinct subcellular distribution patterns.

Both FloA and FloT have a N-terminal region that anchors the protein to the membrane and the SPFH domain that is characteristic of this protein family (for stomatin, prohibitin, flotillin and HflK/C) [34,35]. However, the C-terminal region, which is the most variable region between FloA and FloT, contains four glutamate-alanine repeats (EA repeats) that are responsible for the oligomerization of human FLO-1 and FLO-2 (Figs 2A and S3A) [36] and are probably important in determining the interactions between FloA and FloT. We performed site-directed mutagenesis of the C-terminal region of each flotillin, which generated several variants of FloA and FloT, in which each one of the four EA repeats was replaced (EA→GL) (S5B Fig). We assayed the interaction properties of each one of the resultant variants using a BTH approach. FloA-FloA and FloT-FloT interactions did not occur when we altered the EA2 or EA4 repeats ($\leq$ 700 Miller Units). Additionally, FloA-FloA interaction was abrogated when EA1 was mutated ($\leq$ 700 Miller Units) while EA3 seemed to minimally affect the homo-oligomerization of both FloA and FloT ($\geq$ 700 Miller Units) (Fig 4B). Moreover, the localization pattern of GFP-labeled variants was examined. Variants with EA2 and EA4 altered repeats showed poor aggregation and a severe decrease in the number of foci (Fig 4C and 4D). Alterations in EA1 affected severely the oligomerization of FloA while the variants with altered EA3 showed mild alterations in their distribution pattern (Fig 4C and 4D). None of the distribution patterns were appreciably altered in the absence of the alternative flotillin, suggesting that additional interaction motifs may exist to facilitate hetero-oligomerization (S5C Fig). Since the expression of the altered variants was still detected by western blot analysis (S5D Fig), it is possible that they become dispersed throughout the cellular membrane. Thus, we constructed a mEOS2--tagged version of FloA(EA4) and FloT(EA2) to study their subcellular distribution pattern using PALM microscopy. By using this approach, we detected a large number of single fluorescent proteins randomly dispersed across the cellular membrane (Fig 4E and 4F) rather than organized in foci.

The abovementioned results suggest that FloA and FloT display distinct subcellular distribution pattern, due in part to their different oligomerization affinities, which are determined by the specific interactions that occurred at the C-terminal region of each flotillin. We confirmed these observations by generating a chimeric version of FloA that contains the C-terminal region of FloT ($FloA_T$) and a chimeric version of FloT that contains the C-terminal region of FloA ($FloT_A$). GFP-fused versions of these proteins were generated to examine their subcellular distribution pattern (Fig 5). Using this approach, we consistently observed that the distribution pattern of $FloA_T$ resulted different from wild-type FloA and resembled the distribution pattern of wild-type FloT. Likewise, the distribution pattern of $FloT_A$ resulted very different from the wild-type FloT pattern, showing approximately 13 smaller foci per cell, which is similar to the distribution of wild-type FloA. These results are in agreement with what is shown in Fig 4 and confirmed that the c-termini regions confer specific oligomerization properties to each flotillin.

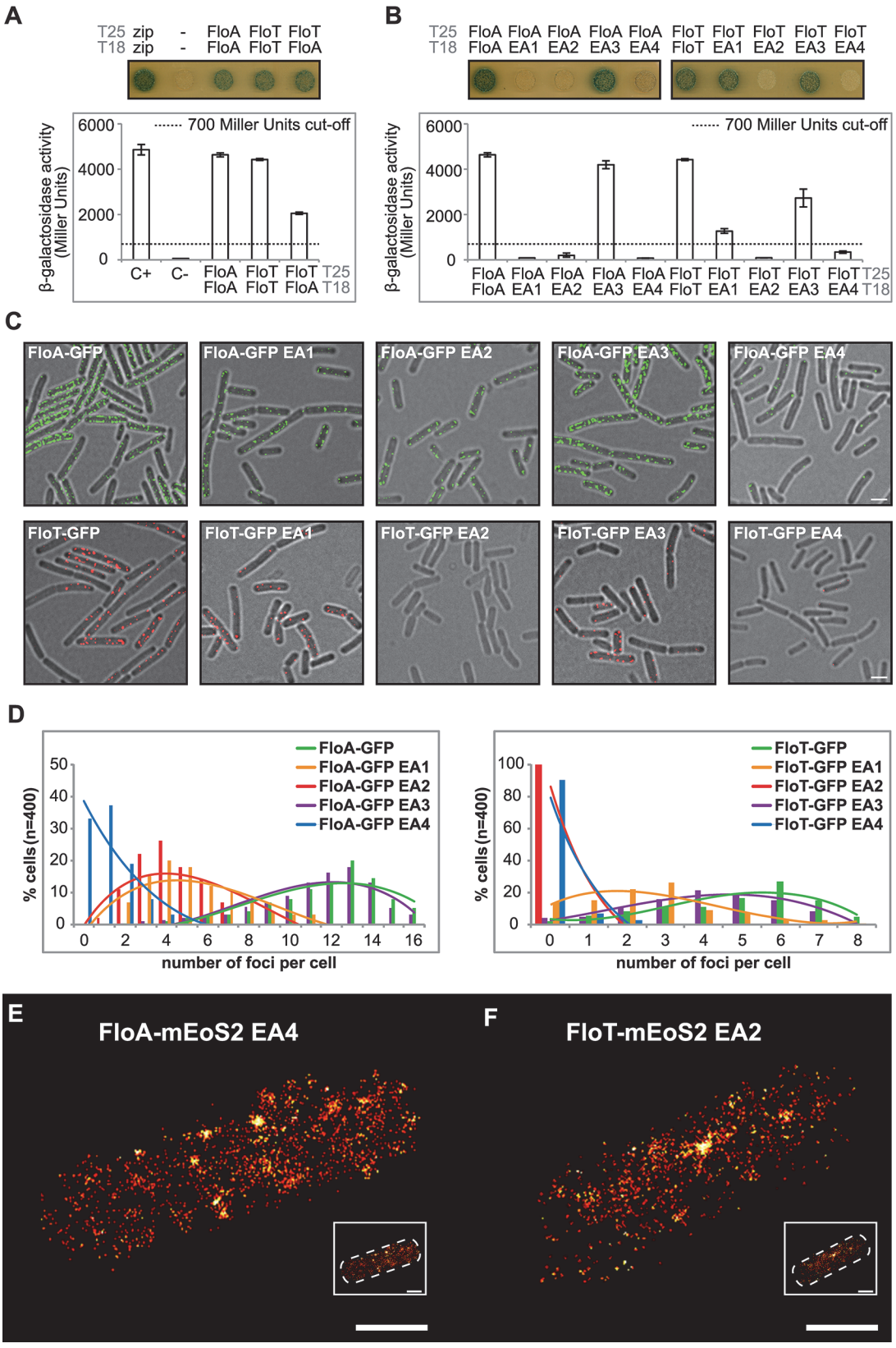
A
T25 zip - FloA FloT FloT
T18 zip - FloA FloT FloA
β-galactosidase activity (Miller Units)
700 Miller Units cut-off
C+ C- FloA FloA FloT FloT FloT FloA T25 T18
B
T25 FloA FloA EA1 FloA EA2 FloA EA3 FloA EA4 FloT FloT FloT EA1 FloT EA2 FloT EA3 FloT EA4
T18
C
FloA-GFP
FloA-GFP EA1
FloA-GFP EA2
FloA-GFP EA3
FloA-GFP EA4
FloT-GFP
FloT-GFP EA1
FloT-GFP EA2
FloT-GFP EA3
FloT-GFP EA4
D
% cells (n=400)
number of foci per cell
E
FloA-mEoS2 EA4
F
FloT-mEoS2 EA2

Fig 4. Oligomerization properties of FloA and FloT. (A) BTH analysis to study the interactions between FloA and FloT. Interaction activates *lacZ* and this degrades X-Gal (blue). The two cytoplasmic domains of a leucine-zipper represent a positive control (pKT25-zip + pUT18C-zip). The negative control is represented by the *E. coli* strains harboring empty plasmids (pKNT25 + pUT18). Plasmids containing FloA, FloT and EA variants are pKNT25 (T25) or pUT18 (T18). Dashed line indicates the threshold limit of 700 Miller Units that defines a positive ($\geq$ 700 Miller Units) and a negative interaction signal ($\leq$ 700 Miller Units) according to the instructions of the manufacturer. **(B)** BTH analysis between the EA1 to EA4 variants of FloA and FloT. Positive controls are wild type FloA and FloT. Dashed line indicates the threshold limit of 700 Miller Units that defines a positive and a negative interaction signal. **(C)** Fluorescence microscopy of cells expressing GFP-tagged versions of EA variants of FloA (Upper row). Fluorescence microscopy of cells expressing GFP-tagged versions of EA variants of FloT (Bottom row). Scale bar is 2 μm. (D) Quantification of the number of foci per cell (n = 400) of the distinct GFP-tagged versions of EA variants of FloA (left panel) and FloT (right panel). **(E and F)** PALM images of cells expressing the EA4 variant of FloA-mEoS2 (E) and EA2 variant of FloT-mEoS2 (F). Scale bars are 500 nm. Detail of the right bottom of each panel shows a dashed-line decorated PALM picture as a general indicator of the cell outline. Scale bar is 500 nm.

doi:10.1371/journal.pgen.1005140.g004

FloA and FloT tether distinct signal transduction pathways

We were interested in exploring the biological significance of cells expressing two different flotillins with distinct spatio-temporal distribution patterns. We hypothesized that this may occur because these are two functionally different flotillins and therefore, they serve as scaffold in tethering the components of distinct signal transduction pathways in *B. subtilis*. We explored this hypothesis by first identifying the proteins that distinctively bind to either FloA or FloT. To do this, His^6-tagged versions of FloA and FloT were expressed in *B. subtilis* cells. The membrane fraction was resolved by blue-native PAGE (BN-PAGE) to allow the separation of the membrane protein complexes in their natural oligomeric states [37]. Our BN-PAGE assays used a polyacrylamide gradient of 4%–20%, which allows the resolution of membrane-bound

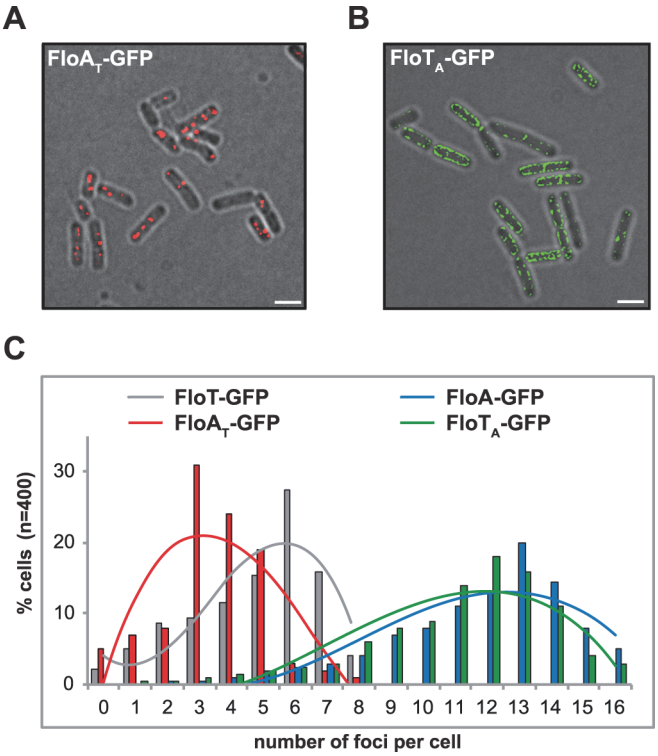

Fig 5. C-terminal region of FloA and FloT plays a role in their oligomerization properties. (A) Fluorescence microscopy image of cells expressing a GFP-tagged version of $FloA_T$. Fluorescence signal is represented in red (scale bar is 2 μm) **(B)** Fluorescence microscopy image of cells expressing a GFP-tagged version of $FloT_A$. Fluorescence signal is represented in green (scale bar is 2 μm). **(C)** Quantification of the number of foci per cell (n = 400) in different genetic backgrounds.

doi:10.1371/journal.pgen.1005140.g005

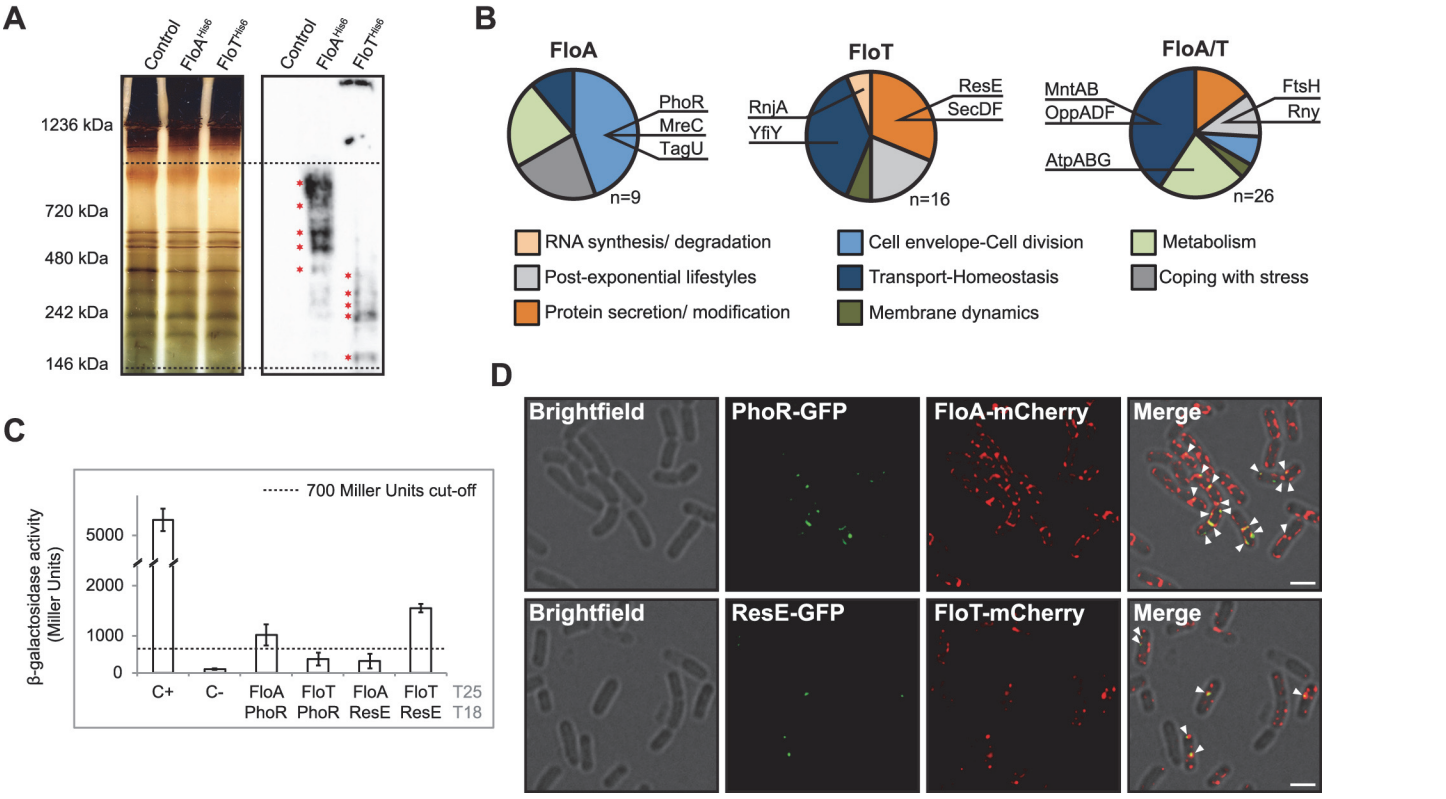

Fig 6. Physiological processes associated with FloA or FloT. (A) Silver-stained BN-PAGE that resolves the protein complexes from the membrane fraction of different strains (left panel). Western blot assay, using antibodies against His^6, to detect flotillin-interacting protein complexes on the BN-PAGE (right panel). Dashed lines define the higher (1000 KDa) and lower (100 KDa) resolution limit of protein complexes in a 4%-20% BN-PAGE. Red asterisks denote the bands that were analyzed by MS. **(B)** Functional classification of the proteins identified in association FloA (left), FloT (centre) or both FloA and FloT (right). Dashed lines define the higher (1,000 KDa) and lower (100 KDa) resolution limit of protein complexes in a 4%-20% BN-PAGE. Red asterisks denote the bands that were analyzed by MS. **(C)** BTH assay to study the interactions between FloA or FloT and the PhoR and ResE flotillin-associated kinases. Dashed line indicates the threshold limit of 700 Miller Units that defines a positive ($\geq$ 700 Miller Units) and a negative interaction signal ($\leq$ 700 Miller Units) according to the instructions of the manufacturer. **(D)** Fluorescence microscopy images of colocalization of fluorescence signals. Upper row shows a double-labeled strain expressing PhoR-GFP and FloA-mCherry translational fusions. Fluorescence signals are represented in green and red, respectively. Colocalization of both green and red fluorescence signals merges in a yellow signal (indicated with a white arrow). Scale bar is 2 μm. Bottom row shows a double-labeled strain expressing ResE-GFP and FloT-mCherry translational fusions. Fluorescence signals are represented in green and red, respectively. Colocalization of both green and red fluorescence signal merges in a yellow signal (indicated with a white arrow). Scale bar is 2 μm.

doi:10.1371/journal.pgen.1005140.g006

protein complexes with a molecular weight between 100 kDa and 1000 kDa. BN-PAGE coupled to immunoblotting, using antibodies against the His^6 tag, was used to identify a number of membrane-associated protein complexes that exclusively interacted with FloA or FloT (Fig 6A and S3 Table). The corresponding bands were identified by mass spectrometry (MS) and validated as components of the protein cargo of the FMMs previously identified in analyses of the DRM fraction [12,13,17] (S3 Table).

MS analysis identified nine membrane proteins exclusively associated with FloA (Fig 6B). Their functional classification suggested their active participation in processes related to cell envelope regulation and cell division regulation. Those include the cytoskeletal-associated proteins MreC and PBP1A/1B or proteins related to cell wall remodeling, such as TagU and PhoR [38] (Fig 6B). We were particularly interested in the PhoR-FloA interaction, as this is a signaling kinase that activates a cascade that is related to cell wall organization [39] and is probably representative of the contribution of FloA to the FMMs. Using a BTH assay, we confirmed a specific interaction between PhoR and FloA ($\geq$ 700 Miller Units) that was not observed

between PhoR and FloT ($\leq$ 700 Miller Units) (Fig 6C). In contrast, a total number of sixteen proteins were identified in exclusive association with FloT and their functional classification suggested an important role in adaptation to stationary phase (Fig 6B). This is the case for YclQ, YhfQ or YfiY proteins involved in siderophore uptake (reviewed in [40]); the protein secretion components SecA, SecDF and YacD, which have been correlated to FloT in previous studies [13] and the membrane-bound sensor kinase ResE, required for antibiotic, siderophore production and adaptation to oxygen-limiting conditions [41]. BTH analysis confirmed the interaction of ResE and FloT ($\geq$ 700 Miller Units) that was not observed between ResE and FloA ($\leq$ 700 Miller Units) (Fig 6C). We also identified a group of twenty-six proteins that interacted with both FloA and FloT (Fig 6B). The functional classification of this group is more diverse but generally related to cell differentiation processes. This includes the metalloprotease FtsH, required for the activation of Spo0A and thus, biofilm formation and sporulation [42] and known to interact with FloA and FloT from previous studies [13,16,17] and the OppABCDF oligopeptide permease, responsible for importing peptidic signals to activate biofilm formation or natural competence [43].

To investigate in more detail the interactions between FloA-PhoR and FloT-ResE that we discovered in the BN-PAGE and the bacterial two-hybrid analysis, we performed co-localization experiments using FloA-mCherry, PhoR-GFP and FloT-mCherry, ResE-GFP double-labeled strains. We confirmed by RT-PCR analyses that PhoR-GFP and ResE-GFP translational fusions complemented Δ*phoR* and Δ*resE* mutants respectively, which suggested that the translational fusions were functional (S6 Fig). Co-localization of FloA and PhoR signals was detected by fluorescence microscopy. Likewise, we also detected co-localization of the FloT and ResE signals (Fig 6D). Colocalization of PhoR and ResE with their respective flotillin was detected in all cells examined (Pearson's correlation coefficients $R^2 = 0.82$ and $R^2 = 0.85$, respectively). These results suggest that FloA-PhoR and FloT-ResE are spatially correlated and support our hypothesis that FloA-PhoR and FloT-ResE physically interact. The specific interaction detected between PhoR and ResE sensor kinases and their respective flotillins was explored in further experiments to better understand how the scaffold activity of bacterial flotillins physically influences the activity of their signaling partners. The most direct hypothesis is that scaffold proteins facilitate signal transduction through tethering of signaling partners, because they enforce proximity and increase the likelihood of their interaction [44]. Thus, we investigated the effect of increasing concentrations of the scaffold flotillins on the interaction and activity of PhoR and ResE. PhoR and ResE belong to the PhoPR and ResDE two-component systems (TCS), which comprise a receptor histidine kinase and their cognate response regulator (PhoP and ResD). Histidine kinases are activated by forming homodimers, autophosphorylate and generate a phosphotransfer reaction to their response regulators. First, we generated a BTH assay to quantitatively monitor the homo-dimerization of PhoR and ResE (Fig 7A). This assay was complemented with a pSEVA modulable vector system [45], to generate different strains that produced lower, medium and higher levels of their respective flotillins that were further validated by immunoblotting (Fig 7A). These strains were used to quantitatively monitor the homo-dimerization efficiency of PhoR and ResE kinases with different concentrations of FloA and FloT, respectively. Both PhoR and ResE kinases responded similarly to increasing concentrations of their respective flotillins. A slight improvement in their interaction efficiency was observed with lower concentration of flotillins, which improved with medium concentration of the flotillins. Importantly, the BTH assay that produced higher concentration of the flotillins showed a decrease in the interaction efficiency of both kinases. This is consistent with the typical limitation of scaffold proteins, in that higher concentrations of the scaffold titrate signaling partners into separate complexes, thus inhibiting their interaction [46] (Fig 7B), as it has been experimentally shown in the scaffold protein Ste5 in yeast [47]

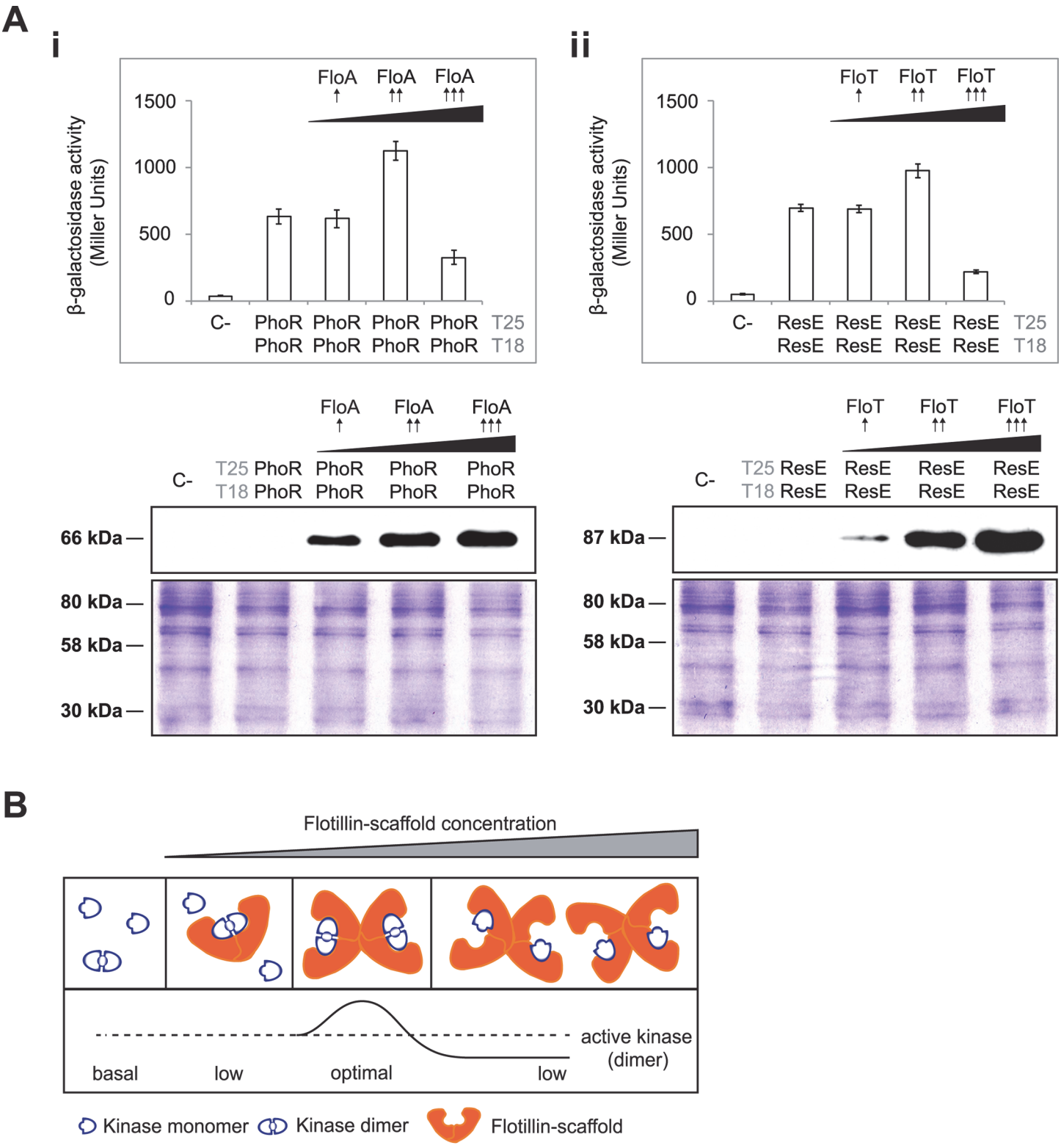

Fig 7. Tethering of signaling partners mediated by flotillins. (A) BTH assay to quantify the interaction of PhoR (i) and ResE (ii) under different concentrations of flotillins (upper panels). Dashed line indicates the threshold limit of 700 Miller Units that defines a positive (≥ 700 Miller Units) and a negative interaction signal (≤ 700 Miller Units) according to the instructions of the manufacturer. Lower- (pSEVA-621), medium- (pSEVA-631) and high-copy (pSEVA-641) plasmids expressing His^6-tagged FloA and FloT rendered lower (↑), medium (↑↑) and higher (↑↑↑) concentration of flotillin in the BTH assay,

respectively, according to immunoblot analysis (lower panels). SDS-PAGE are shown as loading control. **(B)** Inhibition of the activity of a protein complex by scaffold titration. Protein assembly by scaffold proteins has potential drawbacks. At high concentrations, scaffolds may titrate enzyme and substrate away from each other.

doi:10.1371/journal.pgen.1005140.g007

and the JIP1 scaffold human cells [48]. This suggests that bacterial flotillins act as scaffold proteins to specifically facilitate signal transduction through tethering of signaling partners.

To investigate the influence of flotillins in the activation of PhoPR and ResDE TCS, we performed qRT-PCR analysis to quantify the transcription of genes which expression is strongly controlled by PhoP and ResD regulators (Fig 8A and 8B). We detected that the expression of the PhoP-regulated genes *glpQ* and *tuaB* involved in cell envelope metabolism [49,50] were reduced in a strain lacking the kinase PhoR and a strain lacking FloA. Likewise, the expression of the ResD-regulated gene *sboX*, responsible for the production of the antibiotic subtilosin [51], and *yclJ*, a gene that encodes for a regulatory protein [52] was reduced in a strain lacking the kinase ResE and a strain lacking FloT (Fig 8A and 8B). Control strains producing tagged versions of the cognate regulators (PhoP-3xFlag and ResD-3xFlag) showed comparable level of the regulators among the different strains, suggesting that the deletion of the respective flotillin specifically affects the activity of each cognate regulator, which in turn inhibits the expression of regulated genes.

Activation of the cognate regulators promotes a conformational change that impacts gene expression. Thus, the protein-protein interaction experiments were coupled to an in-depth analysis of the transcriptional profile of *B. subtilis* cells lacking *floA* or *floT* genes. The Δ*floA* and Δ*floT* mutants were grown to stationary phase. Total RNA was purified and used to perform microarray analysis using whole-genome *B. subtilis* genechips. Experiments were performed in triplicate and genes were considered differentially expressed when $\geq$2 fold in expression was detected in all replicates. Our microarray analysis indicated 123 genes to be differentially expressed (S4–S6 Tables and GEO database accession number GSE47918). 77 of these genes belong to different signaling regulons of *B. subtilis*, which were organized in a Voronoi treemap (Fig 8C). Each sector of the Voronoi treemap represents a gene and is labeled with the name of the gene that it represents. Each section is labeled in a two-color code to denote upregulated genes (in green) and downregulated genes (in red). There is no biological significance associated with the different shapes that are assigned to each sector. The magnitude of the fold change can be examined in supplemental S4–S6 Tables. This categorization revealed a group of genes whose expression depended on *floA* expression and a second group whose expression depended on *floT* expression. For instance, cells lacking *floA* showed induction of a large number of genes related to cell envelope metabolism, represented by *sigM* and *yhdl*, *yhdK*, *yfml* and *csbB* and *ytrGABCDEF sigM*-induced genes [53]. Additional genes related to cell wall reorganization were also detected (*ytgP*, *dnaA*, *scpA* and *scpB*), including *tagAB* and *tagDEFGH* operons, which are known of being repressed by PhoPR. Cells lacking *floT* displayed a strong inhibition of the genes that constitute the ResDE regulon (*qcrABC*, *ykuNOP*, *dhbABCEF*, *hmp*, *nasDE and sboXA-albABCDEFG*) [54]. Their expression is particularly prominent at stationary phase, when the production of the antibiotic subtilosin (*sboXA-albABCDEFG*) [51] and the siderophore bacillibactin (*dhbABCEF*) [55] is necessary. To validate the results obtained by microarray analysis, we performed qRT-PCR gene expression analysis on several genes that belong to the different regulons that are represented in the Voronoi treemap. qRT-PCR analysis showed comparable results to microarray analysis (Fig 8D).

The differential regulation of gene expression that is caused by the activity of FloA and FloT was manifested at the physiological level. We detected phenotypic differences in the Δ*floA* and the Δ*floT* mutants that may be related to the different expression of the controlled genes. For

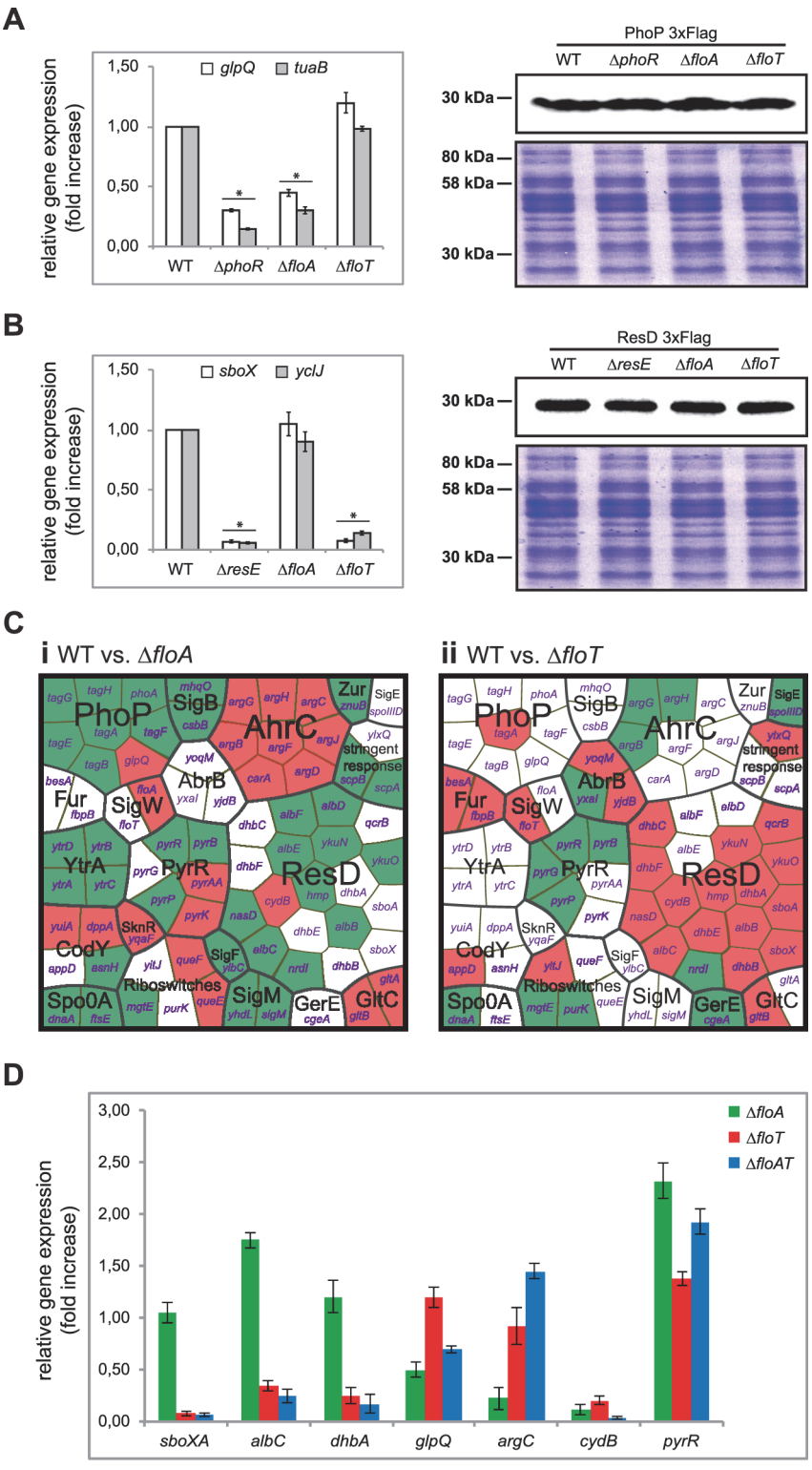

Fig 8. Flotillins influence kinase-dependent activation of PhoP and ResD regulators. (A) Left panel shows qRT-PCR of the PhoP-regulated genes *glpQ* and *tuaB* in different genetic backgrounds. Statistically significant differences are marked with an asterisk (Student's t-test $p \leq 0.05$). Right panel shows immunoblot assay to detect PhoP-3xFlag in different genetic backgrounds. **(B)** Left panel shows qRT-PCR of the ResD-regulated genes *sboX* and *yclJ* in different genetic backgrounds (Student's t-test $p \leq 0.05$). Right panel shows immunoblot assay to detect ResD-3xFlag in different genetic backgrounds (right panel). **(C)** Genome-

wide gene expression analysis of flotillin-regulated genes. Voronoi treemaps represent upregulated genes (green sectors) and downregulated genes (red sectors) in the Δ*floA* mutant (i) and Δ*floT* mutant (ii) in comparison to the wild-type strain. Genes whose expression was altered are represented and functionally classified in regulons. Each section is labeled with the name of the genes that represents. **(D)** qRT-PCR analysis of selected genes from the genome-wide gene expression analysis to validate the microarray data.

doi:10.1371/journal.pgen.1005140.g008

instance, when mutants were grown in Fe^{2+}-containing growth medium, only the Δ*floA* mutant accumulated the extracellular red pigment pulcherrimin (Fig 9A), resulting from the condensation of Fe^{2+} with the dipeptide pulcherriminic acid (Leu-Leu) (abs 420 nm) [56]. Pulcherriminic acid accumulates and is released into the medium in response to an excess of amino acid residues that decorate peptidoglycan precursors of bacterial cell wall synthesis, which is usually indicative of a defective cell wall metabolism [56–59]. This suggest that Δ*floA* mutant is defective in cell wall turnover and is consistent to our proteomic and transcriptomic analyses, suggesting that FloA plays a role in the regulation of cell wall metabolism. Moreover, the Δ*floA* mutant showed reduced sensitivity to the antibiotic vancomycin (Fig 9B), similar to other cases in which reduced sensitivity to vancomycin has been observed in cell-wall deficient strains. Vancomycin binds to the C-terminal D-Ala-D-Ala sequence of the pentapeptide peptidoglycan, thereby preventing the integration of peptidoglycan subunits into the cell wall. Cells that show a defective peptidoglycan turnover also show a reduced number of targets to the action of vancomycin and therefore, reduced sensitivity to the action of this antibiotic [60–62]. However, a defective cell wall often implies a less efficient barrier against the diffusion of other antibiotics [63–65], as is the case of the membrane pore-former sublancin [66]. Accordingly, the Δ*floA* mutant shows a higher sensitivity to the glycopeptide sublancin [67].

Likewise, we tested the capacity of the Δ*floA* and Δ*floT* mutants to adapt to stress-related conditions that are typically associated with cultures that undergo stationary phase. When we grew the Δ*floA* and Δ*floT* mutants under oxygen-limiting conditions, only the Δ*floT* mutant displayed a defective growth (Fig 9C). In contrast, the Δ*floA* mutant was able to grow at similar rate to the wild-type strain. The incapacity of the Δ*floT* mutant to adapt to oxygen-limiting conditions could be attributed to a defective activation of the ResDE regulon, as the activation of this regulon is necessary to allow nitrate respiration and thus, cell growth in oxygen-limiting conditions. Our data shows that this mechanism seemed defective only in the Δ*floT* mutant, which grew poorly in oxygen-limiting conditions (Fig 9D). This is consistent with the role that FloT plays in the regulation of stationary phase and stress-related cellular processes, including the activation of the ResDE regulon, which we have detected in our proteomic and transcriptomic data. Taken together, Fig 9E shows a tentative model that integrates our proteomic, transcriptomic and physiological data. This model shows how FloA and FloT scaffold tether distinct signal transduction pathways, which ultimately control different cellular processes in *B. subtilis*. Furthermore, this model illustrates how functionally different FMMs regulate different genetic networks in a bacterial cell, which leads to the activation of different physiological processes.

Discussion

There is growing recognition of the importance of eukaryotic lipid rafts in numerous cellular processes as diverse as protein sorting, membrane trafficking, compartmentalizing signaling cascades or pathogen entry [2,68]. This functional diversity is currently attributed to a different lipid and protein composition of lipid rafts, as it is hypothesized that a heterogeneous population of lipid rafts could exist on cellular membranes specialized on different biological processes [3–5]. Yet, the molecular mechanisms by which cells generate and regulate raft

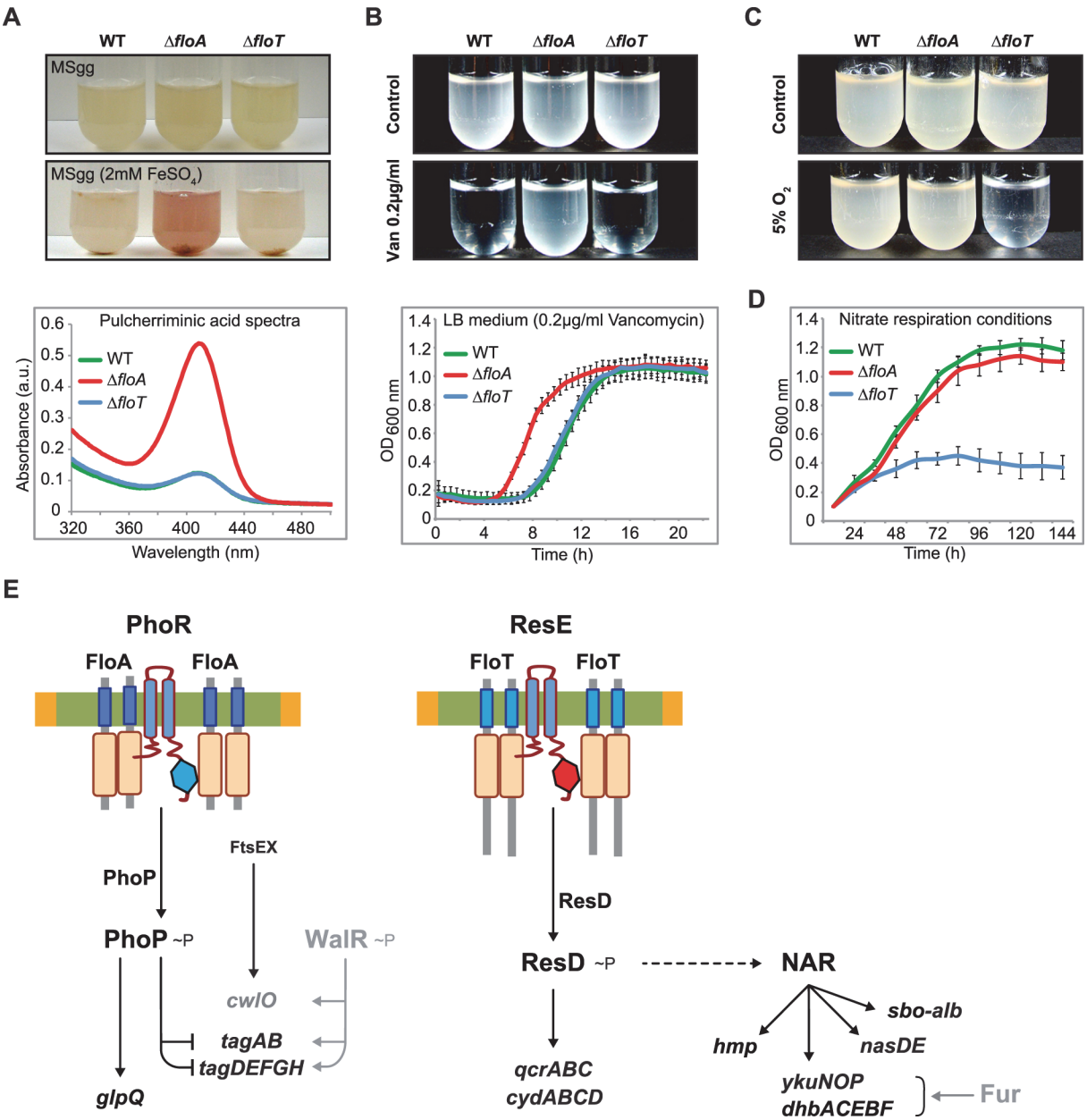

Fig 9. FloA and FloT flotillins influence different physiological processes. (A) Upper panel shows different strains grown in liquid MSgg medium and MSgg supplemented with 2mM $FeSO_4$ to stationary phase. Bottom panel shows the spectrum of pulcherriminic acid that was measured in cell extracts. **(B)** Upper panel shows the pictures of cultures of different strains that were grown with or without vancomycin (0,2 µg/ml) (MSgg liquid medium). Bottom panel shows their growth curve in the presence of vancomycin (0,2 µg/ml) (LB liquid medium). **(C)** Pictures of cultures of different strains that were grown in MSgg liquid medium in regular atmosphere or under oxygen-limiting conditions. Cells were incubated at 30°C for 72h. **(D)** Growth of the different strains in the absence of oxygen. MSgg medium was modified by replacing glutamate and glycerol with glucose 1% and $NaNO_3$ 0,2% **(E)** Schematic representation of the specific signaling pathways that are associated with FloA or FloT. Genes detected in the microarray analysis whose expression was influenced by flotillins are represented in black.

doi:10.1371/journal.pgen.1005140.g009

heterogeneity are still unclear. Nevertheless, it is assumed that cells likely regulate the process of raft diversification, to avoid the assembly of membrane signaling platforms that could simultaneously send distinct and conflicting signals to the cell. Here we use a bacterial model to show that *B. subtilis* cells are able to diversify FMMs into distinct families of signaling

platforms, which are specialized in regulating distinct cellular processes, supporting the current hypothesis that a heterogeneous population of functionally specialized microdomains could exist on cellular membranes.

The discovery of the existence of FMMs adds to other examples of compartmentalization of macromolecules in bacteria, which demonstrate that bacteria are sophisticated organisms with an intricate cellular organization [69,70]. The biological significance of bacterial FMMs could be similar to the role of lipid rafts in eukaryotic cells. One possible function of FMMs could be the generation of a specific microenvironment to protect certain biological processes from inadequate conditions and non-specific interactions. For instance, spatial separation of signal transduction pathways may benefit their interaction specificity. Another plausible role for FMMs is to serve as platforms that control the assembly of membrane-bound protein complexes. By accumulating functionally related proteins in subcellular compartments, the likelihood of interaction increases and thus protein-protein interactions can be efficiently organized in space and time [2,11]. This phenomenon is facilitated by the activity of flotillins, which are FMMs-localized scaffold proteins that coordinate the physical assembly of protein interaction partners [44].

FloA and FloT seem to behave like other scaffold proteins that were described in eukaryotic cells, by specifically tethering signaling partners at lower concentrations or titrating, and thereby inhibiting their interaction at higher concentrations [44,46–48]. We show in this report that FloA and FloT self-interact and distinctively distribute within the FMMs of *B. subtilis*. Furthermore, FloA and FloT bind to and facilitate the interaction of different protein components and thus, activate different signal transduction cascades. The main force involved in generating raft heterogeneity is the uneven spatio-temporal distribution of two distinct flotillins FloA and FloT, Similarly, there are two flotillin paralogs in metazoans, FLO-1 and FLO-2, which show differential expression in distinct tissues, suggesting that these proteins may display certain level of specialization in scaffolding distinct cellular processes [71]. Based on this, it is possible that distinct families of lipid rafts may exist in the membrane of eukaryotic cells as well, yet this hypothesis still needs to be experimentally addressed.

Why do cells need or use different rafts? Cells may use this strategy to deliberately activate diverse cellular processes in time to ultimately dictate cell fate [3,72]. Here we show an example in which FMM remodeling occurs during bacterial growth using differential regulatory programs for flotillin expression. While FloA is constitutively expressed, the expression of FloT is restricted to stationary phase. Bacteria could use this mechanism to restrict the assembly and activation of particular protein components to stationary phase. Furthermore, the expression of a different scaffolding protein at stationary phase could help to rapidly adapt the signal transduction networks to face new environmental conditions. Bacteria possibly use this strategy to deliberately activate diverse cellular processes in time to ultimately ensure an effective activation of signaling processes during the lifespan of a bacterium [3,72].

Cells control the expression of each flotillin to restrict their expression to the growth stage in which their functionality is necessary. FloA preferentially tethers protein components associated with cell wall turnover and primary metabolism. Consequently, the Δ*floA* mutant shows a defect in cell wall turnover. In contrast to FloA, FloT is responsible for tethering protein components that are related to adaptation to stationary phase, such as production of siderophores and antibiotics. In addition to this, we found several proteins associated with the FMMs that interact with both FloA and FloT and are related to biofilm formation and sporulation (see Fig 4). An example of this is the membrane-bound protease FtsH that is required for biofilm formation and sporulation [42], which has been shown to interact with FloA and FloT [13,16,17], as we confirmed in this report. Based on these results, it is likely that the Δ*floA* Δ*floT* double mutant shows additional and more pleiotropic defects in signal transduction than the Δ*floA*

and Δ*floT* single mutants [17]. Likewise, a pleiotropic defect in cell division and biofilm formation has been associated with the overproduction of both FloA and FloT, which is not observable with the overproduction of either FloA or FloT separately [16].

The differential distribution of flotillin within lipid rafts opens additional questions as to whether other structural components of the lipid rafts, like for instance the constituent lipids, show a different spatio-temporal distribution pattern and thus, may also contribute to raft heterogeneity. All these questions were hindered by the difficulty to characterize subcellular structures in the past. However, the development of recent technologies is changing our knowledge about the structure and function of subcellular structures, including lipid rafts [73,74]. The development of super-resolution microscopes and corresponding data analysis methods may well ease the study of bacteria and offer a tractable model to study the role of membrane microdomains, which is rather complicated in their eukaryotic counterparts. The finding that bacteria organize membrane microdomains functionally and structurally equivalent to lipid rafts represents a remarkable level of sophistication in the organization of bacterial signaling networks that allow prokaryotes to amplify and integrate diverse stimuli. Overall, the spatio-temporal organization of signaling networks in bacteria evidences that bacteria are more complex organisms than previously appreciated.

Materials and Methods

Strains, media and growth conditions

Bacillus subtilis undomesticated wild type NCIB 3610 was used as parental strain in this study [23]. *Escherichia coli* DH5α and *B. subtilis* 168 strains were used for standard cloning and transformation procedures. A full strain list is shown in S1 Table. Selective LB agar was supplemented with antibiotics at final concentrations of: ampicillin 100 μg/ml; spectinomycin 100 μg/ml; erythromycin 2 μg/ml and lincomycin 25 μg/ml, tetracycline 5 μg/ml; chloramphenicol 3 μg/ml; kanamycin 50 μg/ml. When required, surfactin (Sigma, USA) was added from a stock solution to a final concentration of 5 μM. To maintain *B. subtilis* cells at exponential phase, cells were grown in shaking liquid LB cultures at 37° C overnight. Liquid LB medium was inoculated with 1:100 volume of the overnight culture and grown to OD600nm = 0.3 with vigorous shaking (200 rpm). To prolong growth at exponential phase, cells were repeatedly passed to fresh LB medium. Passaging was performed when cells reached OD600nm = 0.3. We repeated this procedure as described in [24] for approximately 20 generations prior to cell examination. To search for regulatory proteins that control the expression of *floA* and *floT* genes, the collection of mutants harboring the P_{floA}-*yfp* and P_{floT}-*yfp* transcriptional reporters were grown overnight in LB medium at 37°C with continuous agitation (200 rpm). After this, 2 μl of the overnight LB culture was spotted on MSgg agar plates and colonies were allowed to grow at 30°C for 72 h. Images were taken on a Nikon SMZ 1500 Zoom Stereomicroscope equipped with an AxioCam color (Zeiss, Germany). To monitor gene expression, YFP reporter signals were detected using a 520/20 excitation and BP535/30 emission filter. The excitation time was set to 5 s. Unlabeled wild type strain was used as negative control to determine the background.

Construction of strains

Deletion mutants were generated using long flanking homology PCR [75] (using the primers listed in S3 Table). Markerless gene deletions were used to generate the Δ*floA*, Δ*floT* and Δ*floA* Δ*floT* mutants. Upstream and downstream regions of the *floA* and *floT* genes were joined by long flanking homology PCR [75] and cloned into the vector pMAD [76]. Gene deletion occurs via a sequential process of double recombination. Isolation of the mutants was achieved by counterselection, as described in [76]. The strains harboring the P_{floA}-GFP and P_{floT}-GFP

transcriptional reporters were generated by cloning the promoter region of *floA* and *floT* into the vector pKM003 containing the *gfp* gene and integrating the constructs into the bacterial genome at the *amyE* locus. The vector pKM003 was kindly provided by Dr. David Rudner (Harvard Medical School, USA).

Translational fusions were constructed by long flanking homology PCR and subsequently cloned into pDR183 or pKM003. The vector pDR183 was kindly provided by Dr. David Rudner. These plasmids allowed the integration of the constructs into the bacterial genome at the *lacA* and *amyE* locus, respectively. Unless specified in the body of the paper, the translational fusions were expressed under the control of their natural promoters. When overexpression of FloA or FloT was necessary (e. g. BN-PAGE), *floA* and *floT* genes were cloned in the pDR111 plasmid under the expression control of an IPTG-inducible promoter P_{hp} [77–79]. The constructs were integrated into the bacterial genome at the *amyE* locus. Linearized vectors were added to *B. subtilis* 168 cells grown in competence inducing conditions. Double recombination occurred at the *amyE* locus when using the plasmids pDR111 and pKM003 or the *lacA* locus when using the plasmid pDR183. Cells were plated on corresponding selective media and colonies were checked for integration of constructed fusions by colony PCR. Utilizing the same strategy, GFP translational fusions of the kinases ResE and PhoR were generated using the vector pSG1154 and placed under the expression control of a constitutive promoter. SPP1 phage transduction was used to transfer constructs from *B. subtilis* 168 to wild type NCIB 3610, according to [80].

Site-directed mutagenesis of the EA C-terminal repeats of FloA and FloT was performed by using an overlap extension PCR. We used an adaption of the protocol that is published in [81]. Complementary primers that harbored the desired mutation were generated and used to amplify *floA* and *floT* genes in combination with outer primers (S2 Table). Two DNA fragments resulted from each gene were subsequently joined to one single fragment using long flanking homology PCR. The resulting gene was further sequenced to confirm the presence of the mutation. Mutations replaced glutamic acid by leucine and alanine by glycine in each specified EA repeat. The resultant variants were fused to GFP or mEOS2 and cloned into pDR183 under the expression control of their own promoter. This allowed the integration of the constructs into the bacterial genome at *lacA* locus by a single event of double recombination.

Fluorescence microscopy and image analysis

Cells were collected from the cultures by centrifugation, resuspended in 500 μl paraformaldehyde (4%) and incubated 7 min at room temperature to effect fixation. Samples were then subjected to three washing steps and resuspended in PBS buffer. Samples were finally mounted on microscope slides with thin agarose pads (0.8% agarose in PBS). Variations of growth conditions and preparation methods are specified in figure legends. Images were taken on a Leica DMI6000B inverted microscope. The microscope is equipped with a Leica CRT6000 illumination system, a HCX PL APO oil immersion objective with 100 x 1.47 magnification, a Leica DFC630FX color camera and an environment control system. The following filters were used to detect fluorescence signals: BP480/40 excitation filter and BP527/30 emission filter to detect GFP, BP546/40 excitation filter and BP600/40 emission filter to detect mCherry. GFP and mCherry fluorescence was observed by applying excitation times between 100 and 200 ms, while transmitted light images were taken at 36 ms exposure. Leica Application Suite Advanced Fluorescence V3.7 was used to process raw data and fluorescence signals were deconvoluted using AutoQuant software (MediaCybernetics). Further processing of images and calculation of Pearson's correlation coefficient were performed using ImageJ. To calculate Pearson's correlation coefficient, we selected 200 cells that simultaneously expressed both kinase and flotillin

signals. Pearson's correlation takes into consideration PhoR/ResE clusters and estimate whether flotillins clusters colocalize with them.

Photoactivated localization microscopy (PALM)

PALM was performed as described elsewhere [32]. Briefly, we used an inverted microscope (Olympus IX-71) equipped with an oil-immersion objective (60x, NA 1.45; Olympus) [82]. A 405 nm diode laser (Cube 405–100C, Coherent, USA) was used for converting mEOS2 from the green to the red fluorescent state, and a 568 nm laser (Sapphire 568 LP; Coherent, USA) was used for excitation of the converted state. A dichroic mirror (FF580-FDi01-25x36, Semrock, USA) in the excitation path and two emission filters (ET 575 LP, Chroma and FF01-630/92, Semrock, USA) in the detection path were used to image the fluorescence light with an electronmultiplying CCD camera (EMCCD; Ixon DU897, Andor, USA). A pixel size of 106 nm was achieved by using additional lenses. About 20000 frames were recorded with a frame rate of 10 or 20Hz at an excitation intensity of 5kW/cm² (568nm) until no mEOS2 signals could be detected any further. For photoconversion, the 405nm laser was pulsed with a frequency matching the frame rate, with a pulse duration between 1 and 50ms at irradiation intensities of <1 kW/cm². The PALM image stacks were analyzed with the open source software rapidSTORM [83,84], version 2.21. Only single spot events with more than 250 photons were used for image reconstruction. mEOS2 protein fluorescent in consecutive frames was summarized with the "track emissions" filter of rapidSTORM in order to be localized only once and improve localization precision.

Cluster analyses were performed by an in house written python routine (python 2.7.3, Python Software Foundation). The position of one mEOS2 fluorophore was determined as a single localization according to our software rapidSTORM by fitting a Gaussian function to the Point Spread Function. Clusters were defined by either one connected pixel area in image-based analysis or by a cloud of scattered localizations with spatial coherence in localization. Spatial coherence implies that the increased local density of localizations follows a Gaussian distribution within the cluster, which is indicative of the nonrandom distribution of localizations. Using the untracked localization raw data set and the corresponding super-resolved image, a mask was generated to define possible cluster candidates and separate them from the localization pseudo background. A nearest neighbor based global density threshold was applied to assist the separation process, i.e. all localizations exhibiting a nearest neighbor distance above 50 nm were pre-discarded. According to the mask, the tracked localization data set was then filtered by cropping single cluster candidates and rejecting those with just two or less remaining tracked localizations. Cluster diameters where determined by calculating the standard deviation of the localization cloud from its center of mass. The stated cluster diameters represent the FWHM, which was derived from the standard deviation.

Flow cytometry

B. subtilis strains harboring translational fusions were grown overnight in LB agar. 3 ml liquid MSgg was inoculated with cells from the overnight culture and grown to stationary phase (OD600nm = 3.5). Next, cells from 1 ml MSgg culture were collected by centrifugation and re-suspended in PBS buffer. To disperse cells, sonication was applied in three series of 10 pulses (power output 0.72 / cycle 50%). Finally, cells were diluted 1:200 in PBS buffer and used for analysis. Flow cytometry experiments were conducted using a benchtop MACSQuant Analyzer (Miltenyi Biotech, Germany). Single cells were detected in two scatter channels (FSC, SSC) and one fluorescence channel (B1). Cells were excited by the blue laser (488 nm) coupled to a 488/10 nm filter and detected as size (FSC) and granularity (SSC) signals. GFP fluorescence (B1)

was detected by excitation of cells with the blue laser (488 nm) coupled to a 525/50 nm filter. The voltage intensity of channels was set as follows: forward scatter channel (FSC) 265 V, sideward scatter channel (SSC) 410 V and B1 channel 450 V. The number of events measured per sample was 50,000. We used a flow rate of 1,500 to 3,000 events per second. No gates were selected in any experiment. Flow cytometry data was processed with FlowJo 9.4.3 software.

Whole-genome microarray analysis

To compare the differential transcript levels in the Δ*floA*, Δ*floT* single and Δ*floT* Δ*floA* double mutants, cells were grown in MSgg medium until the late exponential phase and their transcriptome was compared to that of the wild type strain NCIB 3610. Up- and downregulated genes are listed in S3–S5 Tables (Bayes p value $\leq$ 1.0 x 10–3). The microarray data has been validated for various genes using quantitative RT-PCR experiments (Fig 8). The isolation of total RNA, cDNA synthesis, hybridization, scanning, data normalization has been performed as described previously using three independent biological replicates for each strain [85]. Briefly, pellets were frozen in liquid nitrogen and stored at -80°C. RNA extraction was performed with the Macaloid/Roche protocol [85,86], RNA concentration and purity was measured using NanoDrop ND-1000 Spectrophotometer. RNA samples were reverse transcribed into cDNA using the Superscript III reverse transcriptase kit (Invitrogen, USA) and labeled with Cy3 or Cy5 monoreactive dye (GE Healthcare, The Netherlands). Labeled and purified cDNA samples (Nucleospin Extract II, Biokè, The Netherlands) were hybridized in Ambion Slidehyb #1 buffer (Ambion Europe Ltd) at 48°C for 16 h. The arrays were constructed according to [87]. Briefly, specific oligonucleotides for all 4,107 open reading frames of *B*. *subtilis* 168 were spotted in triplicate onto aldehyde-coated slides (Cell Associates) and further handled using standard protocols for aldehyde slides. Due to the array design, the transcript levels of the plasmid-encoded genes of *B*. *subtilis* 3610 are not determined. Slide spotting, slide treatment after spotting and slide quality control were done as before [88]. After hybridization, slides were washed for 5 min in 2x SSC with 0.5% SDS, 2 times 5 min in 1x SSC with 0.25% SDS, 5 min in 1x SSC 0.1% SDS, dried by centrifugation (2 min, 2.000 rpm) and scanned in GenePix 4200AL (Axon Instruments, USA). Fluorescent signals were quantified using ArrayPro 4.5 (Media Cybernetics, USA) and further processed and normalized with MicroPrep [89]. CyberT [90] was used to perform statistical analysis. Genes with a Bayes P-value of $\leq$ 1.0 x 10^{-4} were considered significantly affected.

Quantitative PCR experiments were performed as described before [91]. Gene classification was adapted from [92,93]. Data processing in Voronoi treemap was performed with TreeMap software (Macrofocus GMbH, Switzerland). RNA samples obtained as described above for the microarray experiments were treated with RNase-free DNase I (Thermo Fisher Scientific, Germany) for 60 min at 37°C. Reverse transcription was performed with 50 pmol random nonamers on 2 μg of total RNA using RevertAidTM H Minus M-MuLV Reverse Transcriptase (Thermo Fisher Scientific, Germany). Quantification of cDNA was performed on an iQ5 Real-Time PCR System (BioRad, USA) using Maxima SYBR Green qPCR Master Mix (Thermo Fisher Scientific, Germany). We performed 8 replicates reactions per gene analyzed. The primers used are listed in S2 Table. The amount of target cDNA was normalized to the level of *girB* cDNA [94].

BN-PAGE and immunoblotting

To overexpress the His-tagged version of flotillins (S1 Table), cells from a freshly streaked LB agar plate were used to inoculate 100 ml liquid MSgg medium supplemented with 1 mM IPTG. Cultures were incubated overnight at 37°C with agitation (200 rpm). Cells were collected by

centrifugation, resuspended in buffer H [95] containing 1 mM PMSF and lysed in a French pressure cell at 10,000 psi. Cell debris was removed by standard centrifugation at 12,000 x g for 10 min. Membranes were isolated from the supernatant by ultracentrifugation at 100,000 x g, 4°C for 1 h. Pellets containing membranes were carefully resuspended in solubilization buffer A, supplemented with 10% glycerol and 1 mM PMSF protease inhibitor [37]. Samples were subjected to one step of shock freezing in liquid nitrogen and thawed on ice. Membranes were solubilized using 1% dodecyl maltoside (DDM—Glycon Biochemicals, Germany) and prepared for blue native PAGE as described by [37]. To separate protein complexes, samples were mounted on a 4–20% Roti-PAGE gradient gel (Carl Roth, Germany) and blue native PAGE was run for 3 h at 15 mA. Native gels were used for standard immunoblotting procedures without further processing. After blotting, PVDF membranes were destained to eliminate Coomassie staining and washed with TBS-T. His-tagged flotillins were detected using a polyclonal anti-His antibody (MicroMol, Germany). Bands of native complexes that contained the proteins of interest were cut and analyzed by mass spectrometry (LC/MS).

Peptides identified by LC/MS were aligned to the *B. subtilis* proteome by using MASCOT Peptide Mass Fingerprint software http://www.matrixscience.com. The protein libraries used for peptide alignment were Uniprot-Swissprot http://www.uniprot.org/, NCBInr http://www.ncbi.nlm.nih.gov/protein, EST-EMBL http://www.ebi.ac.uk/ena/, and Subtilist http://genolist.pasteur.fr/SubtiList/. Alignment conditions were restricted to significance threshold $p < 0.05$ and ions score cut-off = 15. Protein mass was unrestricted, peptide mass tolerance was 10 ppm and the fragment mass tolerance was 0.02 Da. We systematically discarded proteins that were identified with less than 20% of amino acid coverage or MudPIT score below 700. Even if peptides match randomly, it is possible to obtain multiple matches to a single protein. MudPIT score is a Poisson distribution that defines a threshold to discard random matches based on the ratio between the number of spectra and the number of entries in the database. For MudPIT results, the score for each protein is the amount of peptides (peptide abundance) that are above the threshold.

Bacterial two-hybrid analysis

floA and *floT* genes as well as the versions of these genes with altered EA-repeats and kinase genes *phoR* and *resE* were PCR-amplified (using primers specified in S1 Table) and cloned into the pKNT25 or pUT18 plasmids (EuroMedex, France). Each one of these plasmids contains a gene that encodes for one of the two catalytic domains of the adenylate cyclase from *Bordetella pertussis* (referred to as T25 and T18 catalytic domains). The genes of interest were cloned and C-terminally fused to the T25 and T18 encoding genes. Plasmids were propagated in the *E. coli* BTH101 strain (S2 Table). Positive control was the two oligomers of the leucine zipper GCN4, which are fused into the pKT25-zip and pUT18C-zip plasmids respectively. This was provided by EuroMedex. An *E. coli* strain harboring pKNT25 and pUT18 plasmids was used as a negative control (S2 Table). Protein-interaction assays were performed following the protocol previously described by Karimova *et al.* [33]. Experiments that required LB plates 100 μg/ml Ampicillin, 50 μg/ml Kanamycin and 40 μg/ml X-Gal were incubated 48h at 30°C. The appearance of blue product indicated protein interaction that can be monitored and quantified. Quantification of Miller units was performed to monitor the efficiency of protein interactions according to [96].

To assay the scaffold activity of FloA and FloT, the kinase genes *phoR* and *resE* were PCR-amplified and cloned into the pKNT25 and pUT18 plasmids. *phoR* and *resE* were C-terminally fused to the T15 and T18 encoding genes and propagated in *E. coli* BTH101 strain. Protein-interaction assays were performed following the protocol previously described by Karimova *et al.*

[33] to determine the interaction efficiency between PhoR-PhoR and ResE-ResE. These strains were subsequently used to clone pSEVA modulable plasmids [45] that produce different levels of FloA and FloT. We specifically used pSEVA-621, pSEVA-631 and pSEVA-641 plasmids to produce FloA and FloT at different concentrations. These plasmids contain distinct replication origins and propagate in *E. coli* at low, medium and high copy number, respectively. This generates low, medium and high concentration of FloA and FloT in the in bacterial two-hybrid *E. coli* strains in which the plasmids are propagated. Experiments that required the propagation of pSEVA vectors were performed in LB medium with 100 μg/ml Ampicillin, 50 μg/ml Kanamycin and 10 μg/ml Gentamicin. Quantification of the Miller units was performed to monitor the efficiency of protein interactions, as it is described in [96].

Physiological assays

Pulcherriminic acid was estimated by using a method adapted from [56,97]. Cell samples containing pulcherrimin were washed twice with methanol and once with distilled water before extraction with 2M NaOH. The amount of pulcherriminic acid that was converted to the sodium salt turned yellow and could be determined spectrophotometrically as a specific peak in absorbance at 410 nm. To assess the sensitivity of wild-type and flotillin mutant strains to vancomycin, MSgg was supplemented with 0.2 μg/ml Vancomycin. Similarly, strains were grown in LB medium supplemented with 0.2 μg/ml Vancomycin in a Tecan Infinite 200 Pro Microplate Reader at 37°C with agitation (200 rpm). Growth was measured at OD = 595nm. The growth curves shown are a mean of three independent experiments. To grow *B. subtilis* in anaerobic conditions (i.e. nitrate respiration), MSgg medium was modified by replacing glutamate with sodium nitrate (0,2%) and glycerol with glucose (1%). Liquid cultures were grown in 2.5 L seal chambers containing Oxoid CampyGen (5% O_2) or anaerobic atsmosphere generation bags (Oxoid, UK).

Accession numbers

Gene Expression Omnibus (GEO): Accession database number GSE47918
http://www.ncbi.nlm.nih.gov/geo/query/acc.cgi?token = fxkbdeiukswcgxs&acc=GSE47918

Supporting Information

S1 Fig. (Related to main Fig 1) Differential expression of *floA* and *floT* genes. (A) Gene expression profile of *floA* (top panel) and *floT* (bottom panel) genes under 249 different growing conditions, according to the published database [21,22]. Overall dataset can be found at *B. subtilis* expression data browser http://migale.jouy.inra.fr. and also at SubtiExpress browser at http://subtiwiki.uni-goettingen.de/apps/expression. The gene expression profiles of different cultures growing in LB medium are marked in blue. The gene expression profiles of cells growing in different MSgg growing conditions are marked in red. Expression levels are given in arbitrary units. Details of growth conditions and gene expression levels are presented on the right. **(B)** Flow cytometry analysis monitoring the expression of P_{floA}-*gfp* and P_{floT}-*gfp* transcriptional fusions at single cell level. *B. subtilis* cells harboring the transcriptional fusions were grown in LB medium to exponential phase (upper panel) and MSgg medium to stationary phase (bottom panel). X-axis represents fluorescence signal in arbitrary units and Y-axis represents cell count for each strain (50,000 cells were counted). Variations in the gene expression level were exclusively detected in the channel that monitored P_{floT}-*gfp* transcriptional fusion. **(C)** Flow cytometry analysis monitoring the expression of the FloA-GFP and FloT-GFP translational fusions at single cell level. Cells were grown in LB medium to exponential phase (upper panel) or MSgg medium to stationary phase (bottom panel). X-axis represents fluorescence signal in arbitrary

units and Y-axis represents cell count for each strain (50,000 cells were counted). Variations in the protein expression level were exclusively detected in the channel that monitored FloT-GFP translational fusion. **(D)** Variation of the *floA* and *floT* gene expression in 29 different regulatory mutants. Regulatory genes known to influence diverse signal transduction cascades were systematically deleted in in *B. subtilis* strains labeled with the P_{floA}-*yfp* and P_{floT}-*yfp* transcriptional fusions. The resulting strains were examined for their ability to regulate the expression of *floA* and *floT* genes. Cells were grown in MSgg agar plates at 30°C for 72h. Fluorescence images were taken on a Nikon SMZ 1500 Zoom Stereomicroscope equipped with an AxioCam color (Carl Zeiss). The most prominent differences in the expression of *floA* and *floT* genes were detected in the Δ*spo0A* and Δ*abrB* genetic backgrounds, which were subsequently followed up in additional experiments at the gene expression level. We also detected differences in the expression of *floT* in the Δ*dlt* mutant but this could be due to an indirect influence to the activation of Spo0A, as it has been published elsewhere [98].
(EPS)

S2 Fig. (Related to main Fig 1) The cell-cell communication signal surfactin activates the expression of FloT via Spo0A. (A) Fluorescence microscopy pictures of cells labeled with the FloA-GFP in different growing conditions. Scale bars are 2 μm. Growing conditions did not alter the number of FloA foci per cell. **(B)** Quantification of the number of foci per cell (n = 400 cells) in cells labeled with FloA-GFP at different growing conditions. Cells showed similar number of foci at different growing conditions. **(C)** Fluorescence microscopy picture of cells labeled with FloT-GFP in different growing conditions. Scale bars are 2 μm. Cells that were grown in LB medium showed lower number of foci compared to cells that were grown in MSgg medium or LB medium complemented with surfactin 5 μM. **(D)** Quantification of the number of foci per cell (n = 400 cells) in cells labeled with FloT-GFP at different growing conditions. Cells that were grown in LB medium showed lower number of foci compared to the rest of growing conditions. **(E)** Fluorescence microscopy picture of different strains labeled with FloT-GFP. Scale bars are 2 μm. Cells that lack Spo0A showed a very low number of foci that did not change in medium complemented with surfactin 5 μM. **(F)** Quantification of the number of foci per cell (n = 400 cells) in cells deficient in Spo0A and labeled with FloT-GFP. In the absence of Spo0A the number of FloT foci decreases dramatically and it does not change with the addition of surfactin to the medium.
(EPS)

S3 Fig. (Related to main Fig 2) FloA and FloT from *B. subtilis* are two different flotillin-like proteins. (A) Scheme of human FLO-1 and FLO-2 protein structures (left panel) in comparison to FloA and FloT from *B. subtilis* (right panel). The N-terminal region of the human FLO-1 attaches to the cellular membrane using a palmitate residue (represented in blue) and/or a myristate residue that is represented in red in the case of FLO-2. The prohibitin homology domain (PHB or SPFH domain) that is typically present in all flotillin proteins is represented in green. In both, human and bacterial flotillins, the C-terminal region contains four EA repeats. The amino acid sequence of this region is magnified. Each EA repeat region is highlighted in orange for better visualization. Scale bar is 100 amino acids. The N-terminal region of the FloA and FloT bacterial flotillins attaches to the cellular membrane using a membrane-anchoring domain that directly binds to the cellular membrane (represented in blue). **(B)** Fluorescence microscopy pictures of fields of cells labeled with the translational fusions FloA-GFP (left upper panel) and FloT-GFP (right upper panel) and FloA-mCherry (left bottom panel) and FloT-mCherry (right bottom panel). Both FloA and FloT flotillin proteins distribute in foci across the bacterial membrane, yet the number of foci organized by FloA is more abundant than the number of foci organized by FloT. Cells were grown in MSgg at 37°C to early

stationary phase. Scale bar is 4μm.
(EPS)

S4 Fig. (Related to main Fig 3) Subcellular organization of FloA and FloT at high-resolution level. (A and B) Fluorescence microscopy pictures at high-resolution level using super-resolution imaging by photoactivated localization microscopy (PALM). In this case, FloA and FloT were fused to the photoactivatable monomeric protein PAmCherry and expressed in *B. subtilis* cells. This is a photoactivatable monomeric red fluorescent protein derived from the classical mCherry fluorescent protein. FloA-PAmCherry (Panel A) and FloT-PAmCherry (Panel B) show distribution in foci across the membrane. Clusters are indicated with white arrows. A definition of cluster is in the body of the paper. Data obtained by using PAmCherry is consistent with the data obtained by using fluorescence microscopy and mEOS2/PALM microscopy and validates the distribution of foci presented in main Fig 3. Scale bar is 500 nm. Panel A shows a detail of a dashed-line decorated PALM picture of a FloA-PAmCherry expressing cell as a general indicator of the cell outline. Scale bar is 500 nm. Panel B shows a detail of a dashed-line decorated PALM picture of a FloT-PAmCherry expressing cell as a general indicator of the cell outline. Scale bar is 500 nm. **(C)** Western blot analysis to detect FloA-GFP and FloT-GFP proteins. FloT is more abundant than FloA. Cells expressing GFP-tagged variants were expressed in *B. subtilis* using the native promoter. Cells were grown in MSgg at 37°C to early stationary phase. Western blot analysis was performed using purified cellular membranes. Detection was performed using polyclonal antibodies against GFP epitope. Positive control is a non-labelled wild type strain. SDS-PAGE is shown as loading control. **(D)** Relative intensity of the signal detected in the western blot analysis.
(EPS)

S5 Fig. (Related to main Figs 4 and 5) Alteration of the subcellular organization of FloA and FloT. (A) (i) Fluorescence microscopy pictures of a time-lapse experiment using two different *B. subtilis* strains labeled with the translational fusions FloA-GFP (upper row) and FloT-GFP (bottom row). FloA and FloT flotillins show highly dynamic properties [15,16]. Fluorescence foci of FloA-GFP and FloT-GFP rapidly reorganize across the bacterial membrane. A white arrow in the bottom row exemplifies the dynamism of the foci. It shows two foci that are able to quickly reorganize into one single focus. For this experiment, cells were grown in MSgg at 37°C to early stationary phase. Time scale is given in seconds. Scale bars are 2μm. **(ii)** Fluorescence microscopy pictures of a time-lapse experiment using two different *Escherichia coli* strains expressing the translational fusions FloA-GFP (upper row) and FloT-GFP (bottom row). Fluorescence foci of FloA-GFP and FloT-GFP reorganize across the membrane of *E. coli* cells in a comparable organization and dynamic pattern than in *B. subtilis* cells. **(B)** Alteration of the EA repeats from the Ct region of FloA and FloT was performed by site-directed mutagenesis. We replaced glutamic acid (E) and alanine (A) amino acids with leucine (L) and glycine (G), respectively. L and G amino acids were chosen for amino acid replacement due to the subtle changes in the structure or polarity of the amino acid backbones, which guarantees a minimum level of interference with protein folding. Differences in amino acid replacement are framed in red for better visualization. **(C)** Fluorescence microscopy pictures evidencing the distribution pattern of FloT (upper row) and FloA (bottom row) in the absence of the alternative flotillin. The absence of one flotillin does not affect the distribution pattern of the other flotillin and the differences that were detected in the number of foci were not significant, according to our statistical analysis (Student's t-test $p \leq 0.05$). However, alterations of the EA repeats caused a severe alteration in the distribution pattern of the flotillins. Fluorescence microscopy of cells expressing GFP-tagged versions of FloT and its different EA variants in a *floA*-deficient genetic background (upper row). Fluorescence microscopy of cells expressing

GFP-tagged versions of FloA and its different EA variants in a *floT*-deficient background (bottom row). Scale bars are 2μm. Cells were grown in MSgg at 37°C to early stationary phase. **(D)** Western blot analysis of wild-type FloA and FloT expression levels in relation to FloA EA4 and FloT EA2 variants. GFP-tagged version of FloA and FloT variants were expressed in *B. subtilis* using their native promoter. Cells were grown in MSgg at 37°C to early stationary phase. Western blot analysis was performed using purified cellular membranes. Flotillin detection was performed using polyclonal antibodies against GFP epitope. Positive control is a non-labelled wild type strain. SDS-PAGE are shown as loading control.
(EPS)

S6 Fig. (Related to main Fig 8) The translational fusions PhoR-GFP and ResE-GFP are functional in *B. subtilis* cells. (A) qRT-PCR of the PhoP-regulated genes *tuaB* in different genetic backgrounds. Δ*phoR* mutant complemented with PhoR-GFP translational fusion recovered the expression of *tuaB* gene. Statistically significant differences are marked with an asterisk (Student's t-test $p \leq 0.05$). **(B)** qRT-PCR of the ResD-regulated gene *yclJ* in different genetic backgrounds. Δ*resD* mutant complemented with ResD-GFP translational fusion recovered the expression of *yclJ* gene. Statistically significant differences are marked with an asterisk (Student's t-test $p \leq 0.05$).
(EPS)

S1 Table. (Related to material and methods) List of strains and plasmids used in this study.
(DOCX)

S2 Table. (Related to material and methods) List of primers used in this study.
(DOCX)

S3 Table. (Related to main Fig 6) List of proteins identified in membrane-associated protein complexes that interacted exclusively with either FloA (green squares) or FloT (yellow squares), or FloA and FloT (blue squares).
(DOCX)

S4 Table. (Related to main Figs 7 and 8) List of genes that are significantly up or downregulated (Bayes.p value <10–4) in the Δ*floA* cells compared to wild-type cells. Mean indicates log 2 transformed expression ratios.
(DOCX)

S5 Table. (Related to main Figs 7 and 8) List of genes that are significantly up or downregulated (Bayes.p value <10–4) in the Δ*floT* cells compared to wild-type cells. Mean indicates log 2 transformed expression ratios.
(DOCX)

S6 Table. (Related to main Figs 7 and 8) List of genes that are significantly up or downregulated (Bayes.p value <10–4) in the Δ*floA* Δ*floT* cells compared to wild-type cells. Mean indicates log 2 transformed expression ratios.
(DOCX)

Acknowledgments

We thank Dr. Stan Gorski for his help in editing this manuscript. We thank Ned S. Windgreen (Princeton University), Daniel Kearns (Indiana University) and Richard Losick (Harvard University) for critical comments.

Author Contributions

Conceived and designed the experiments: OPK ATK MS DL. Performed the experiments: JS TK BMS GK CF ATK DL. Analyzed the data: ATK MS DL. Contributed reagents/materials/analysis tools: OPK. Wrote the paper: DL.

References

1. Simons K, Ikonen E (1997) Functional rafts in cell membranes. Nature 387: 569–572. PMID: 9177342
2. Lingwood D, Simons K (2010) Lipid rafts as a membrane-organizing principle. Science 327: 46–50. doi: 10.1126/science.1174621 PMID: 20044567
3. Neumann AK, Itano MS, Jacobson K (2010) Understanding lipid rafts and other related membrane domains. F1000 Biol Rep 2: 31. doi: 10.3410/B2-31 PMID: 20606718
4. Lingwood D, Kaiser HJ, Levental I, Simons K (2009) Lipid rafts as functional heterogeneity in cell membranes. Biochem Soc Trans 37: 955–960. doi: 10.1042/BST0370955 PMID: 19754431
5. Mishra S, Joshi PG (2007) Lipid raft heterogeneity: an enigma. J Neurochem 103 Suppl 1: 135–142. PMID: 17986148
6. Dermine JF, Duclos S, Garin J, St-Louis F, Rea S, et al. (2001) Flotillin-1-enriched lipid raft domains accumulate on maturing phagosomes. J Biol Chem 276: 18507–18512. PMID: 11279173
7. Lang DM, Lommel S, Jung M, Ankerhold R, Petrausch B, et al. (1998) Identification of reggie-1 and reggie-2 as plasmamembrane-associated proteins which cocluster with activated GPI-anchored cell adhesion molecules in non-caveolar micropatches in neurons. J Neurobiol 37: 502–523. PMID: 9858255
8. Langhorst MF, Reuter A, Stuermer CA (2005) Scaffolding microdomains and beyond: the function of reggie/flotillin proteins. Cell Mol Life Sci 62: 2228–2240. PMID: 16091845
9. Morrow IC, Parton RG (2005) Flotillins and the PHB domain protein family: rafts, worms and anaesthetics. Traffic 6: 725–740. PMID: 16101677
10. Stuermer CA (2011) Reggie/flotillin and the targeted delivery of cargo. J Neurochem 116: 708–713. doi: 10.1111/j.1471-4159.2010.07007.x PMID: 21214550
11. Michel V, Bakovic M (2007) Lipid rafts in health and disease. Biol Cell 99: 129–140. PMID: 17064251
12. Lopez D, Kolter R (2010) Functional microdomains in bacterial membranes. Genes Dev 24: 1893–1902. doi: 10.1101/gad.1945010 PMID: 20713508
13. Bach JN, Bramkamp M (2013) Flotillins functionally organize the bacterial membrane. Mol Microbiol 88: 1205–1217. doi: 10.1111/mmi.12252 PMID: 23651456
14. Dempwolff F, Moller HM, Graumann PL (2012) Synthetic motility and cell shape defects associated with deletions of flotillin/reggie paralogs in *Bacillus subtilis* and interplay of these proteins with NfeD proteins. J Bacteriol 194: 4652–4661. doi: 10.1128/JB.00910-12 PMID: 22753055
15. Donovan C, Bramkamp M (2009) Characterization and subcellular localization of a bacterial flotillin homologue. Microbiology 155: 1786–1799. doi: 10.1099/mic.0.025312-0 PMID: 19383680
16. Mielich-Suss B, Schneider J, Lopez D (2013) Overproduction of flotillin influences cell differentiation and shape in *Bacillus subtilis*. MBio 4: e00719–00713. doi: 10.1128/mBio.00719-13 PMID: 24222488
17. Yepes A, Schneider J, Mielich B, Koch G, Garcia-Betancur JC, et al. (2012) The biofilm formation defect of a *Bacillus subtilis* flotillin-defective mutant involves the protease FtsH. Mol Microbiol 86: 457–471. doi: 10.1111/j.1365-2958.2012.08205.x PMID: 22882210
18. Babuke T, Ruonala M, Meister M, Amaddii M, Genzler C, et al. (2009) Hetero-oligomerization of reggie-1/flotillin-2 and reggie-2/flotillin-1 is required for their endocytosis. Cell Signal 21: 1287–1297. doi: 10.1016/j.cellsig.2009.03.012 PMID: 19318123
19. Banning A, Tomasovic A, Tikkanen R (2011) Functional aspects of membrane association of reggie/flotillin proteins. Curr Protein Pept Sci 12: 725–735. PMID: 22329548
20. Amaddii M, Meister M, Banning A, Tomasovic A, Mooz J, et al. (2012) Flotillin-1/reggie-2 protein plays dual role in activation of receptor-tyrosine kinase/mitogen-activated protein kinase signaling. J Biol Chem 287: 7265–7278. doi: 10.1074/jbc.M111.287599 PMID: 22232557
21. Nicolas P, Mader U, Dervyn E, Rochat T, Leduc A, et al. (2012) Condition-dependent transcriptome reveals high-level regulatory architecture in *Bacillus subtilis*. Science 335: 1103–1106. doi: 10.1126/science.1206848 PMID: 22383849
22. Buescher JM, Liebermeister W, Jules M, Uhr M, Muntel J, et al. (2012) Global network reorganization during dynamic adaptations of *Bacillus subtilis* metabolism. Science 335: 1099–1103. doi: 10.1126/science.1206871 PMID: 22383848

23. Branda SS, Gonzalez-Pastor JE, Ben-Yehuda S, Losick R, Kolter R (2001) Fruiting body formation by *Bacillus subtilis*. Proc Natl Acad Sci U S A 98: 11621–11626. PMID: 11572999

24. Lopez D, Gontang EA, Kolter R (2010) Potassium sensing histidine kinase in *Bacillus subtilis*. Methods Enzymol 471: 229–251. doi: 10.1016/S0076-6879(10)71013-2 PMID: 20946851

25. Hamon MA, Lazazzera BA (2001) The sporulation transcription factor Spo0A is required for biofilm development in *Bacillus subtilis*. Mol Microbiol 42: 1199–1209. PMID: 11886552

26. Hahn J, Roggiani M, Dubnau D (1995) The major role of Spo0A in genetic competence is to downregulate abrB, an essential competence gene. J Bacteriol 177: 3601–3605. PMID: 7768874

27. Fujita M, Gonzalez-Pastor JE, Losick R (2005) High- and low-threshold genes in the Spo0A regulon of *Bacillus subtilis*. J Bacteriol 187: 1357–1368. PMID: 15687200

28. Jiang M, Shao W, Perego M, Hoch JA (2000) Multiple histidine kinases regulate entry into stationary phase and sporulation in *Bacillus subtilis*. Mol Microbiol 38: 535–542. PMID: 11069677

29. LeDeaux JR, Yu N, Grossman AD (1995) Different roles for KinA, KinB, and KinC in the initiation of sporulation in *Bacillus subtilis*. J Bacteriol 177: 861–863. PMID: 7836330

30. Landgraf D, Okumus B, Chien P, Baker TA, Paulsson J (2012) Segregation of molecules at cell division reveals native protein localization. Nat Methods 9: 480–482. doi: 10.1038/nmeth.1955 PMID: 22484850

31. Betzig E, Patterson GH, Sougrat R, Lindwasser OW, Olenych S, et al. (2006) Imaging intracellular fluorescent proteins at nanometer resolution. Science 313: 1642–1645. PMID: 16902090

32. Lando D, Endesfelder U, Berger H, Subramanian L, Dunne PD, et al. (2012) Quantitative single-molecule microscopy reveals that CENP-A(Cnp1) deposition occurs during G2 in fission yeast. Open biology 2: 120078. doi: 10.1098/rsob.120078 PMID: 22870388

33. Karimova G, Pidoux J, Ullmann A, Ladant D (1998) A bacterial two-hybrid system based on a reconstituted signal transduction pathway. Proc Natl Acad Sci U S A 95: 5752–5756. PMID: 9576956

34. Tavernarakis N, Driscoll M, Kyrpides NC (1999) The SPFH domain: implicated in regulating targeted protein turnover in stomatins and other membrane-associated proteins. Trends Biochem Sci 24: 425–427. PMID: 10542406

35. Rivera-Milla E, Stuermer CA, Malaga-Trillo E (2006) Ancient origin of reggie (flotillin), reggie-like, and other lipid-raft proteins: convergent evolution of the SPFH domain. Cell Mol Life Sci 63: 343–357. PMID: 16389450

36. Neumann-Giesen C, Falkenbach B, Beicht P, Claasen S, Luers G, et al. (2004) Membrane and raft association of reggie-1/flotillin-2: role of myristoylation, palmitoylation and oligomerization and induction of filopodia by overexpression. Biochem J 378: 509–518. PMID: 14599293

37. Wittig I, Braun HP, Schagger H (2006) Blue native PAGE. Nat Protoc 1: 418–428. PMID: 17406264

38. Scheffers DJ, Pinho MG (2005) Bacterial cell wall synthesis: new insights from localization studies. Microbiol Mol Biol Rev 69: 585–607. PMID: 16339737

39. Muller JP, An Z, Merad T, Hancock IC, Harwood CR (1997) Influence of Bacillus subtilis phoR on cell wall anionic polymers. Microbiology 143 (Pt 3): 947–956.

40. Moore CM, Helmann JD (2005) Metal ion homeostasis in Bacillus subtilis. Current Opinion in Microbiology 8: 188–195. PMID: 15802251

41. Nakano MM, Zuber P, Glaser P, Danchin A, Hulett FM (1996) Two-component regulatory proteins ResD-ResE are required for transcriptional activation of fnr upon oxygen limitation in *Bacillus subtilis*. J Bacteriol 178: 3796–3802. PMID: 8682783

42. Le AT, Schumann W (2009) The Spo0E phosphatase of Bacillus subtilis is a substrate of the FtsH metalloprotease. Microbiology 155: 1122–1132. doi: 10.1099/mic.0.024182-0 PMID: 19332814

43. Perego M, Higgins CF, Pearce SR, Gallagher MP, Hoch JA (1991) The oligopeptide transport system of *Bacillus subtilis* plays a role in the initiation of sporulation. Mol Microbiol 5: 173–185. PMID: 1901616

44. Good MC, Zalatan JG, Lim WA (2011) Scaffold proteins: hubs for controlling the flow of cellular information. Science 332: 680–686. doi: 10.1126/science.1198701 PMID: 21551057

45. Silva-Rocha R, Martinez-Garcia E, Calles B, Chavarria M, Arce-Rodriguez A, et al. (2013) The Standard European Vector Architecture (SEVA): a coherent platform for the analysis and deployment of complex prokaryotic phenotypes. Nucleic Acids Res 41: D666–675. doi: 10.1093/nar/gks1119 PMID: 23180763

46. Levchenko A, Bruck J, Sternberg PW (2000) Scaffold proteins may biphasically affect the levels of mitogen-activated protein kinase signaling and reduce its threshold properties. Proc Natl Acad Sci U S A 97: 5818–5823. PMID: 10823939

47. Chapman SA, Asthagiri AR (2009) Quantitative effect of scaffold abundance on signal propagation. Mol Syst Biol 5: 313. doi: 10.1038/msb.2009.73 PMID: 19888208

48. Dickens M, Rogers JS, Cavanagh J, Raitano A, Xia Z, et al. (1997) A cytoplasmic inhibitor of the JNK signal transduction pathway. Science 277: 693–696. PMID: 9235893

49. Botella E, Hubner S, Hokamp K, Hansen A, Bisicchia P, et al. (2011) Cell envelope gene expression in phosphate-limited *Bacillus subtilis* cells. Microbiology 157: 2470–2484. doi: 10.1099/mic.0.049205-0 PMID: 21636651

50. Lahooti M, Harwood CR (1999) Transcriptional analysis of the *Bacillus subtilis* teichuronic acid operon. Microbiology 145 (Pt 12): 3409–3417. PMID: 10627039

51. Nakano MM, Zheng G, Zuber P (2000) Dual control of sbo-alb operon expression by the Spo0 and ResDE systems of signal transduction under anaerobic conditions in *Bacillus subtilis*. J Bacteriol 182: 3274–3277. PMID: 10809710

52. Hartig E, Geng H, Hartmann A, Hubacek A, Munch R, et al. (2004) *Bacillus subtilis* ResD induces expression of the potential regulatory genes yclJK upon oxygen limitation. J Bacteriol 186: 6477–6484. PMID: 15375128

53. Eiamphungporn W, Helmann JD (2008) The *Bacillus subtilis* sigma(M) regulon and its contribution to cell envelope stress responses. Mol Microbiol 67: 830–848. doi: 10.1111/j.1365-2958.2007.06090.x PMID: 18179421

54. Reents H, Munch R, Dammeyer T, Jahn D, Hartig E (2006) The Fnr regulon of *Bacillus subtilis*. J Bacteriol 188: 1103–1112. PMID: 16428414

55. May JJ, Wendrich TM, Marahiel MA (2001) The dhb operon of *Bacillus subtilis* encodes the biosynthetic template for the catecholic siderophore 2,3-dihydroxybenzoate-glycine-threonine trimeric ester bacillibactin. J Biol Chem 276: 7209–7217. PMID: 11112781

56. Uffen RL, Canale-Parola E (1972) Synthesis of pulcherriminic acid by *Bacillus subtilis*. J Bacteriol 111: 86–93. PMID: 4204912

57. von Dohren H (2009) Charged tRNAs charge into secondary metabolism. Nat Chem Biol 5: 374–375. doi: 10.1038/nchembio0609-374 PMID: 19448602

58. Cryle MJ, Bell SG, Schlichting I (2010) Structural and biochemical characterization of the cytochrome P450 CypX (CYP134A1) from *Bacillus subtilis*: a cyclo-L-leucyl-L-leucyl dipeptide oxidase. Biochemistry 49: 7282–7296. doi: 10.1021/bi100910y PMID: 20690619

59. Gondry M, Sauguet L, Belin P, Thai R, Amouroux R, et al. (2009) Cyclodipeptide synthases are a family of tRNA-dependent peptide bond-forming enzymes. Nat Chem Biol 5: 414–420. doi: 10.1038/nchembio.175 PMID: 19430487

60. Daum RS, Gupta S, Sabbagh R, Milewski WM (1992) Characterization of *Staphylococcus aureus* isolates with decreased susceptibility to vancomycin and teicoplanin: isolation and purification of a constitutively produced protein associated with decreased susceptibility. J Infect Dis 166: 1066–1072. PMID: 1402017

61. Reipert A, Ehlert K, Kast T, Bierbaum G (2003) Morphological and genetic differences in two isogenic *Staphylococcus aureus* strains with decreased susceptibilities to vancomycin. Antimicrob Agents Chemother 47: 568–576. PMID: 12543661

62. Sieradzki K, Tomasz A (2003) Alterations of cell wall structure and metabolism accompany reduced susceptibility to vancomycin in an isogenic series of clinical isolates of *Staphylococcus aureus*. J Bacteriol 185: 7103–7110. PMID: 14645269

63. Lambert PA (2002) Cellular impermeability and uptake of biocides and antibiotics in Gram-positive bacteria and mycobacteria. J Appl Microbiol 92 Suppl: 46S–54S. PMID: 12000612

64. Sakoulas G, Bayer AS, Pogliano J, Tsuji BT, Yang SJ, et al. (2012) Ampicillin enhances daptomycin- and cationic host defense peptide-mediated killing of ampicillin- and vancomycin-resistant *Enterococcus faecium*. Antimicrob Agents Chemother 56: 838–844. doi: 10.1128/AAC.05551-11 PMID: 22123698

65. Wolf D, Dominguez-Cuevas P, Daniel RA, Mascher T (2012) Cell envelope stress response in cell wall-deficient L-forms of *Bacillus subtilis*. Antimicrob Agents Chemother 56: 5907–5915. doi: 10.1128/AAC.00770-12 PMID: 22964256

66. Kouwen TR, Trip EN, Denham EL, Sibbald MJ, Dubois JY, et al. (2009) The large mechanosensitive channel MscL determines bacterial susceptibility to the bacteriocin sublancin 168. Antimicrob Agents Chemother 53: 4702–4711. doi: 10.1128/AAC.00439-09 PMID: 19738010

67. Butcher BG, Helmann JD (2006) Identification of *Bacillus subtilis* sigma-dependent genes that provide intrinsic resistance to antimicrobial compounds produced by Bacilli. Mol Microbiol 60: 765–782. PMID: 16629676

68. Simons K, Gerl MJ (2010) Revitalizing membrane rafts: new tools and insights. Nat Rev Mol Cell Biol 11: 688–699. doi: 10.1038/nrm2977 PMID: 20861879

69. Govindarajan S, Nevo-Dinur K, Amster-Choder O (2012) Compartmentalization and spatiotemporal organization of macromolecules in bacteria. FEMS Microbiol Rev 36: 1005–1022. doi: 10.1111/j.1574-6976.2012.00348.x PMID: 22775310

70. Rudner DZ, Losick R (2010) Protein subcellular localization in bacteria. Cold Spring Harb Perspect Biol 2: a000307. doi: 10.1101/cshperspect.a000307 PMID: 20452938

71. Zhao F, Zhang J, Liu YS, Li L, He YL (2011) Research advances on flotillins. Virol J 8: 479. doi: 10.1186/1743-422X-8-479 PMID: 22023811

72. Mishra S, Joshi PG (2007) Lipid raft heterogeneity: an enigma. Journal of neurochemistry 103 Suppl 1: 135–142. PMID: 17986148

73. Munro S (2003) Lipid rafts: elusive or illusive? Cell 115: 377–388. PMID: 14622593

74. Shaw AS (2006) Lipid rafts: now you see them, now you don't. Nat Immunol 7: 1139–1142. PMID: 17053798

75. Wach A (1996) PCR-synthesis of marker cassettes with long flanking homology regions for gene disruptions in *S. cerevisiae*. Yeast 12: 259–265. PMID: 8904338

76. Arnaud M, Chastanet A, Debarbouille M (2004) New vector for efficient allelic replacement in naturally nontransformable, low-GC-content, gram-positive bacteria. Appl Environ Microbiol 70: 6887–6891. PMID: 15528558

77. Britton RA, Eichenberger P, Gonzalez-Pastor JE, Fawcett P, Monson R, et al. (2002) Genome-wide analysis of the stationary-phase sigma factor (sigma-H) regulon of *Bacillus subtilis*. J Bacteriol 184: 4881–4890. PMID: 12169614

78. Erwin KN, Nakano S, Zuber P (2005) Sulfate-dependent repression of genes that function in organosulfur metabolism in *Bacillus subtilis* requires Spx. J Bacteriol 187: 4042–4049. PMID: 15937167

79. Nakano S, Kuster-Schock E, Grossman AD, Zuber P (2003) Spx-dependent global transcriptional control is induced by thiol-specific oxidative stress in *Bacillus subtilis*. Proc Natl Acad Sci U S A 100: 13603–13608. PMID: 14597697

80. Yasbin RE, Young FE (1974) Transduction in *Bacillus subtilis* by bacteriophage SPP1. J Virol 14: 1343–1348. PMID: 4214946

81. Weickert MJ, Chambliss GH (1990) Site-directed mutagenesis of a catabolite repression operator sequence in *Bacillus subtilis*. Proc Natl Acad Sci U S A 87: 6238–6242. PMID: 2117276

82. van de Linde S, Loschberger A, Klein T, Heidbreder M, Wolter S, et al. (2011) Direct stochastic optical reconstruction microscopy with standard fluorescent probes. Nat Protoc 6: 991–1009. doi: 10.1038/nprot.2011.336 PMID: 21720313

83. Wolter S, Endesfelder U, van de Linde S, Heilemann M, Sauer M (2011) Measuring localization performance of super-resolution algorithms on very active samples. Opt Express 19: 7020–7033. doi: 10.1364/OE.19.007020 PMID: 21503016

84. Wolter S, Loschberger A, Holm T, Aufmkolk S, Dabauvalle MC, et al. (2012) rapidSTORM: accurate, fast open-source software for localization microscopy. Nat Methods 9: 1040–1041. doi: 10.1038/nmeth.2224 PMID: 23132113

85. Kovacs AT, Kuipers OP (2011) Rok regulates yuaB expression during architecturally complex colony development of *Bacillus subtilis* 168. J Bacteriol 193: 998–1002. doi: 10.1128/JB.01170-10 PMID: 21097620

86. van Hijum SA, de Jong A, Baerends RJ, Karsens HA, Kramer NE, et al. (2005) A generally applicable validation scheme for the assessment of factors involved in reproducibility and quality of DNA-microarray data. BMC Genomics 6: 77. PMID: 15907200

87. van Hijum SA, de Jong A, Buist G, Kok J, Kuipers OP (2003) UniFrag and GenomePrimer: selection of primers for genome-wide production of unique amplicons. Bioinformatics 19: 1580–1582. PMID: 12912842

88. Kuipers OP, de Jong A, Baerends RJ, van Hijum SA, Zomer AL, et al. (2002) Transcriptome analysis and related databases of *Lactococcus lactis*. Antonie Van Leeuwenhoek 82: 113–122. PMID: 12369183

89. van Hijum SA, Garcia de la Nava J, Trelles O, Kok J, Kuipers OP (2003) MicroPreP: a cDNA microarray data pre-processing framework. Appl Bioinformatics 2: 241–244. PMID: 15130795

90. Baldi P, Long AD (2001) A Bayesian framework for the analysis of microarray expression data: regularized t-test and statistical inferences of gene changes. Bioinformatics 17: 509–519. PMID: 11395427

91. Mironczuk AM, Manu A, Kuipers OP, Kovacs AT (2011) Distinct roles of ComK1 and ComK2 in gene regulation in *Bacillus cereus*. PLoS One 6: e21859. doi: 10.1371/journal.pone.0021859 PMID: 21747963

92. Mader U, Schmeisky AG, Florez LA, Stulke J (2012) SubtiWiki—a comprehensive community resource for the model organism *Bacillus subtilis*. Nucleic Acids Res 40: D1278–1287. doi: 10.1093/nar/gkr923 PMID: 22096228

93. Moszer I, Glaser P, Danchin A (1995) SubtiList: a relational database for the *Bacillus subtilis* genome. Microbiology 141 (Pt 2): 261–268.

94. Livak KJ, Schmittgen TD (2001) Analysis of relative gene expression data using real-time quantitative PCR and the 2(-Delta Delta C(T)) Method. Methods 25: 402–408. PMID: 11846609

95. Campo N, Marquis KA, Rudner DZ (2008) SpoIIQ anchors membrane proteins on both sides of the sporulation septum in *Bacillus subtilis*. J Biol Chem 283: 4975–4982. PMID: 18077456

96. Miller JH (1972) Experiments in Molecular Genetics. Cold Spring Harbor: Cold Spring Harbor Laboratories.

97. Uffen RL, Canale-Parola E (1969) Isolation of pulcherriminic acid from cultures of *Bacillus cereus* var. alesti. Z Allg Mikrobiol 9: 231–233. PMID: 4985560

98. Lopez D, Vlamakis H, Losick R, Kolter R (2009) Cannibalism enhances biofilm development in *Bacillus subtilis*. Mol Microbiol 74: 609–618. doi: 10.1111/j.1365-2958.2009.06882.x PMID: 19775247

Schneider_FigS1

A

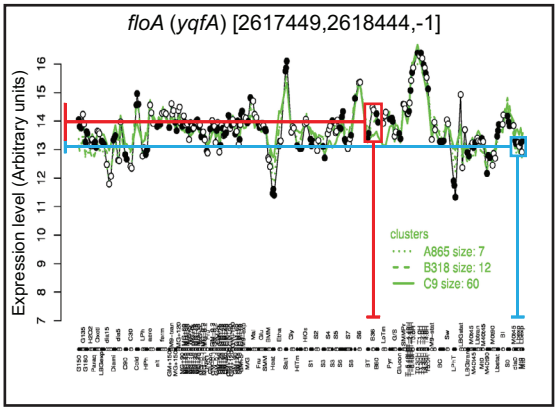

floA (*yqfA*)

LB exp	Expression level
O.D.$_{600}$ approx. 0.5	13.2516^{a1}
	13.3741^{a2}
	13.2756^{a3}
MSgg stat	**Expression level**
(BT) 24h of growth with shaking	13.6939^{b1}
	12.912^{b2}
(B36) 36h of growth without shaking	14.8771^{c1}
	14.6758^{c2}
(B60) 60h of growth without shaking	14.5319^{d1}
	14.268^{d2}

a1,a2,a3; b1,b2; c1,c2; d1,d2: different replicates of this growth condition

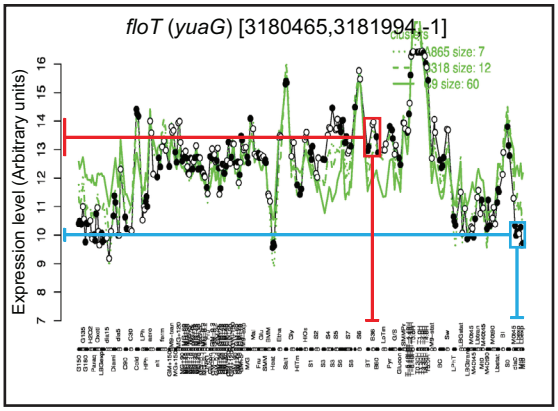

floT (*yuaG*)

LB exp	Expression level
O.D.$_{600}$ approx. 0.5	9.4645^{a1}
	10.0373^{a2}
	9.7324^{a3}
MSgg stat	**Expression level**
(BT) 24h of growth with shaking	13.1491^{b1}
	12.3817^{b2}
(B36) 36h of growth without shaking	14.4045^{c1}
	14.0512^{c2}
(B60) 60h of growth without shaking	13.6942^{d1}
	13.176^{d2}

a1,a2,a3; b1,b2; c1,c2; d1,d2: different replicates of this growth condition

B

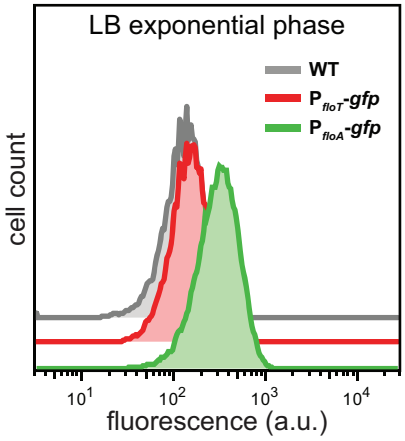

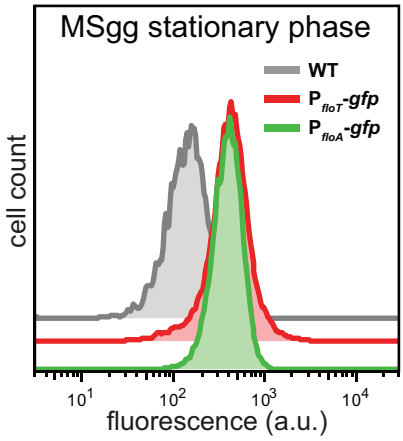

C

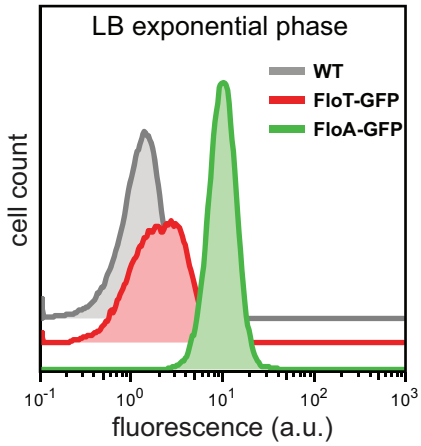

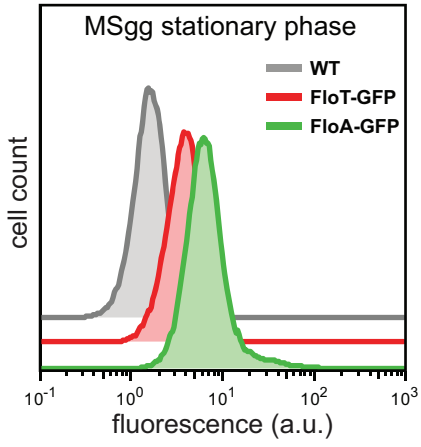

D

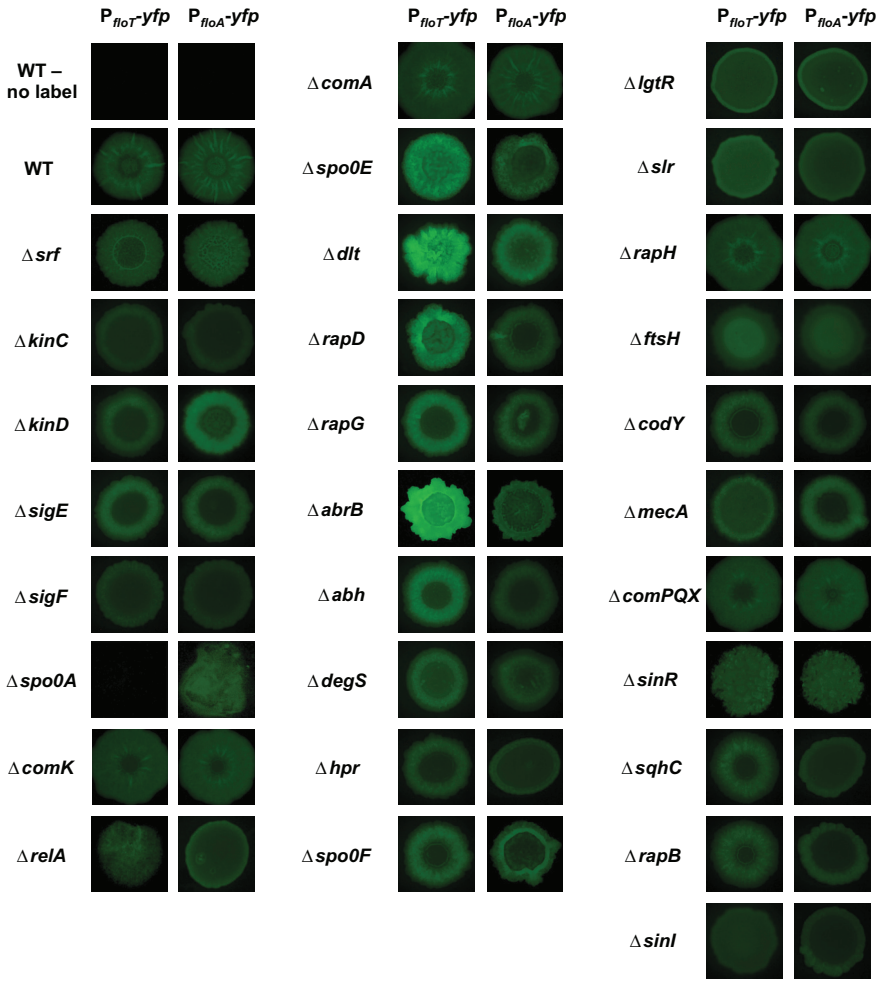

Schneider_FigS2

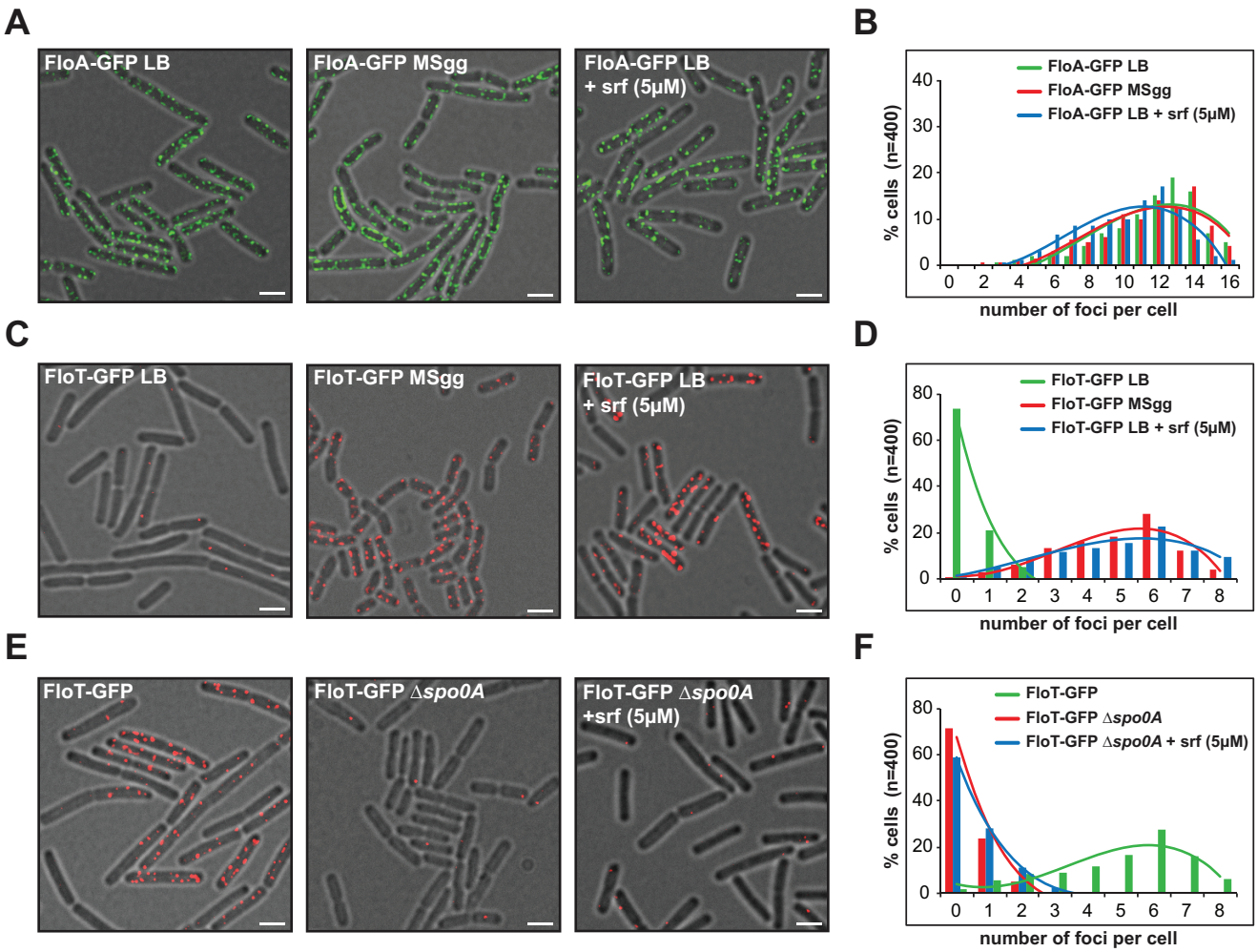

Schneider_FigS3

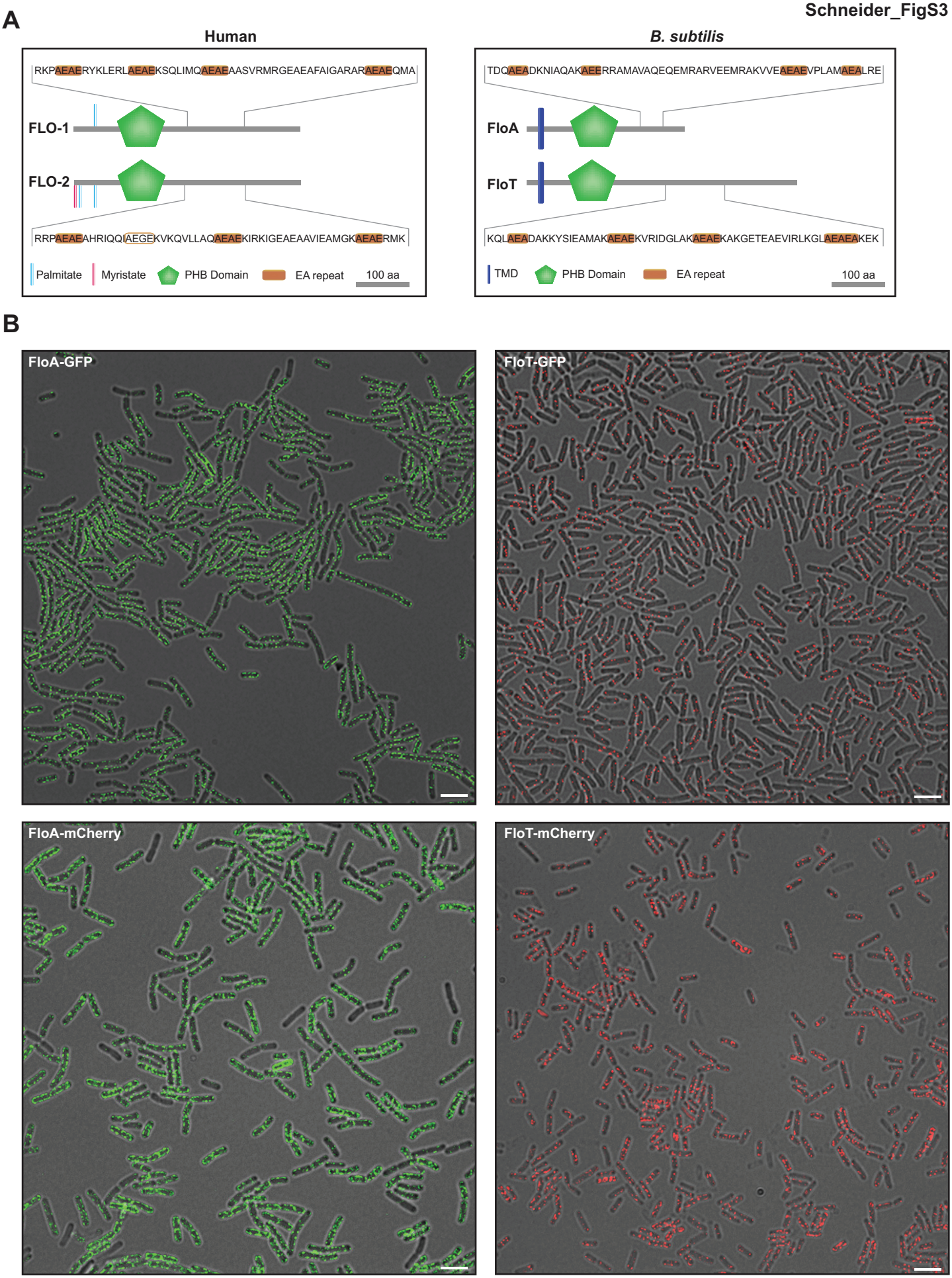

Schneider_FigS4

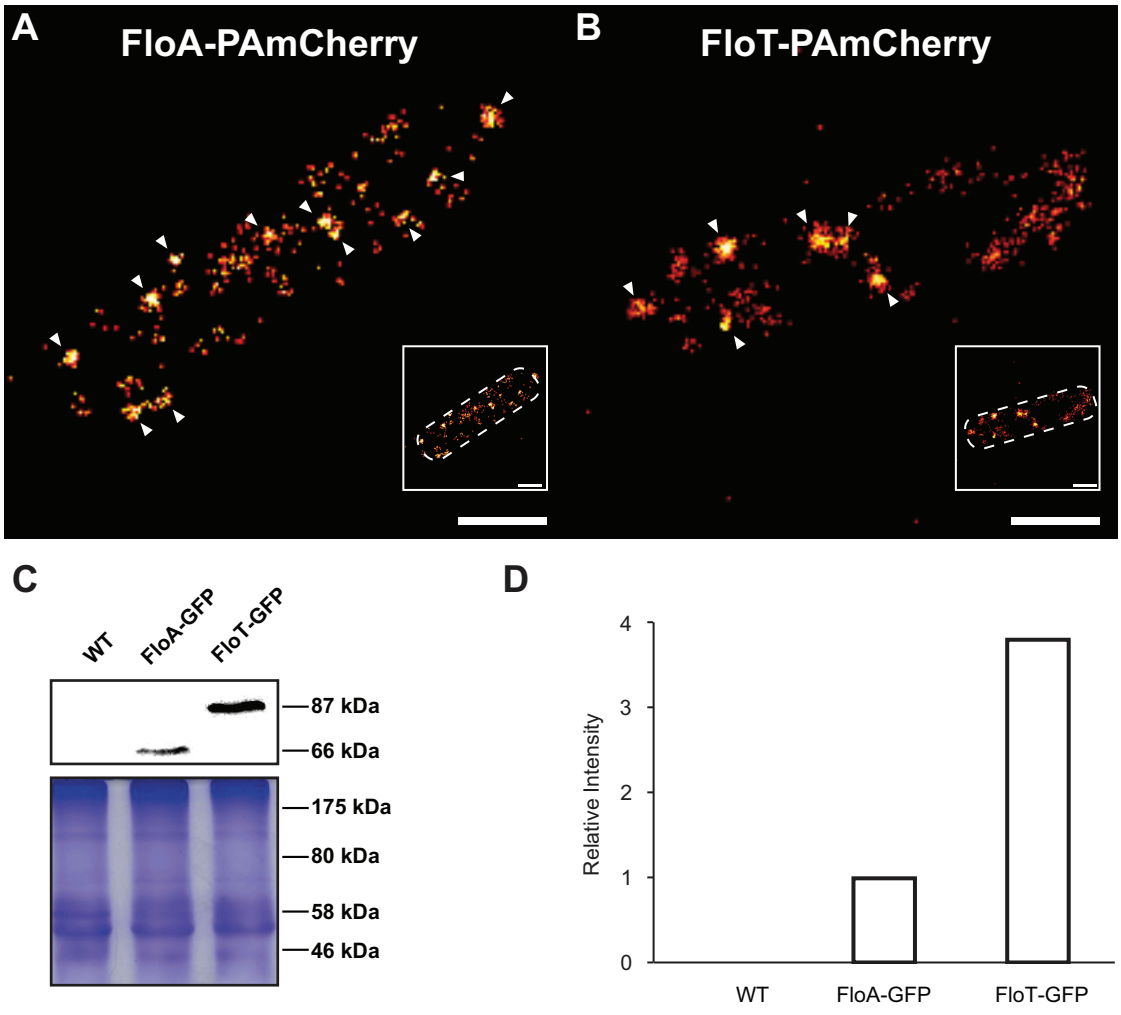

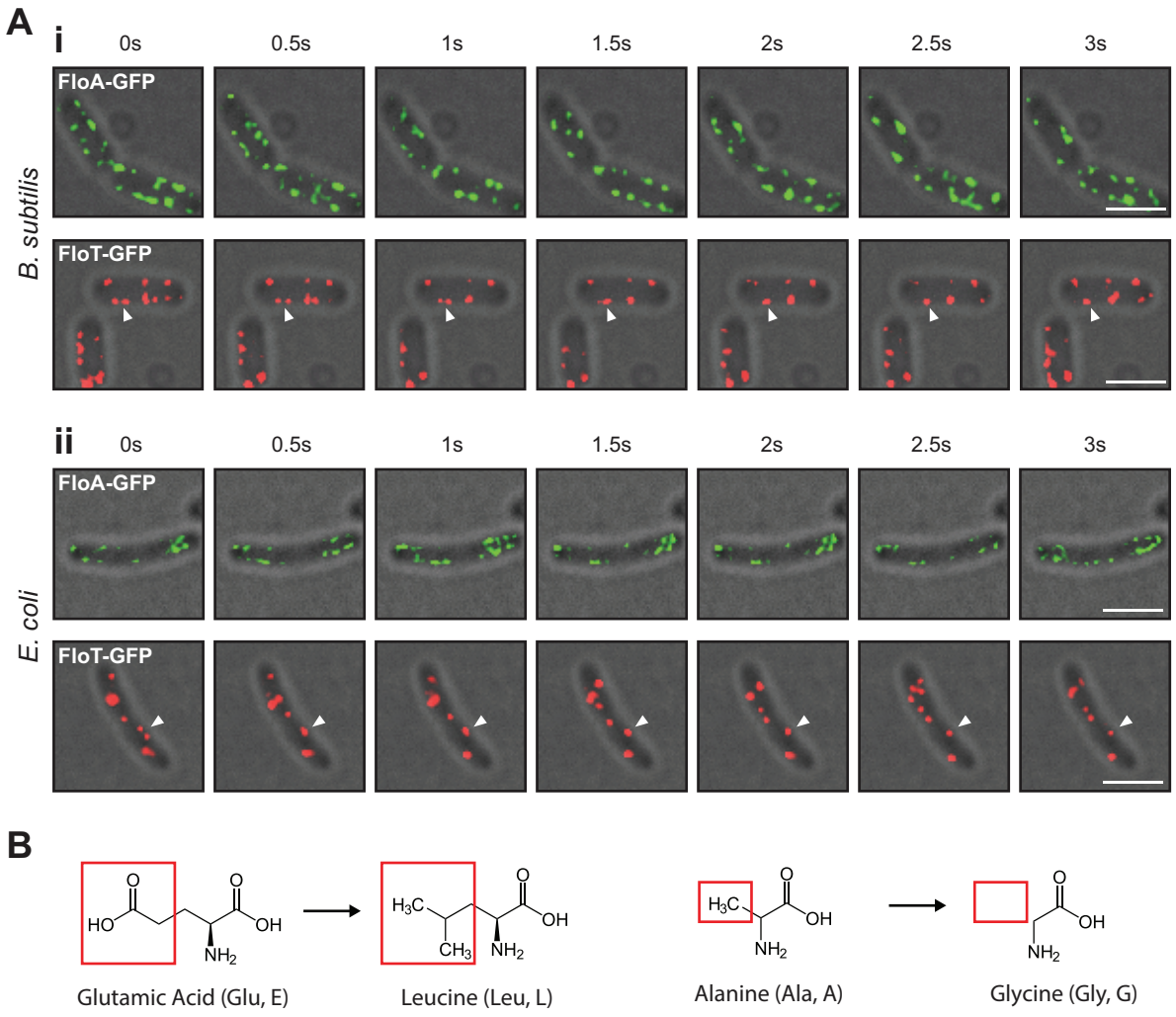
A
i
0s
0.5s
1s
1.5s
2s
2.5s
3s
FloA-GFP
FloT-GFP
B. subtilis
ii
E. coli

B
Glutamic Acid (Glu, E)
Leucine (Leu, L)
Alanine (Ala, A)
Glycine (Gly, G)

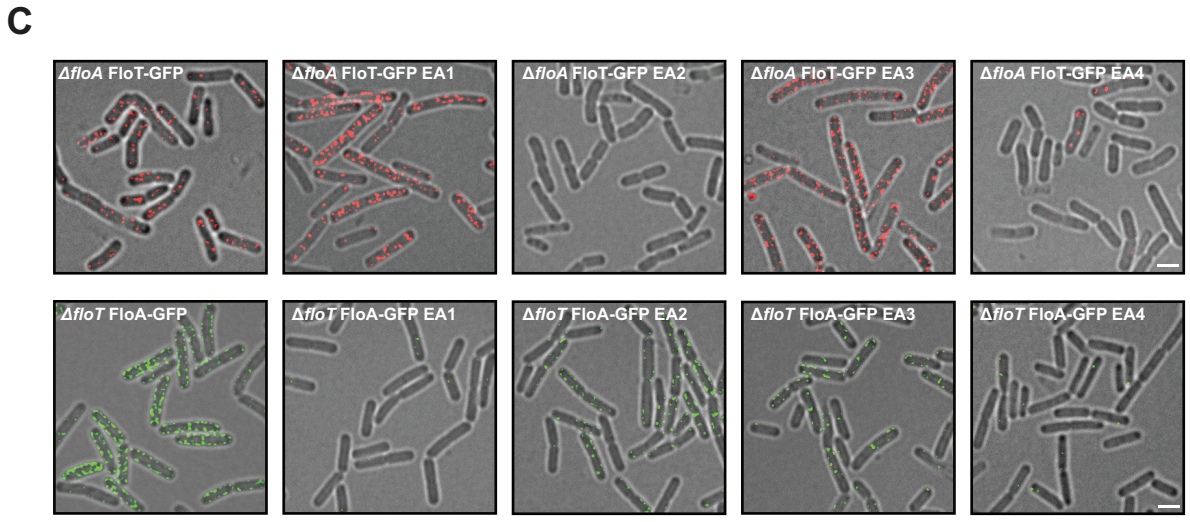
C
ΔfloA FloT-GFP
ΔfloA FloT-GFP EA1
ΔfloA FloT-GFP EA2
ΔfloA FloT-GFP EA3
ΔfloA FloT-GFP EA4
ΔfloT FloA-GFP
ΔfloT FloA-GFP EA1
ΔfloT FloA-GFP EA2
ΔfloT FloA-GFP EA3
ΔfloT FloA-GFP EA4

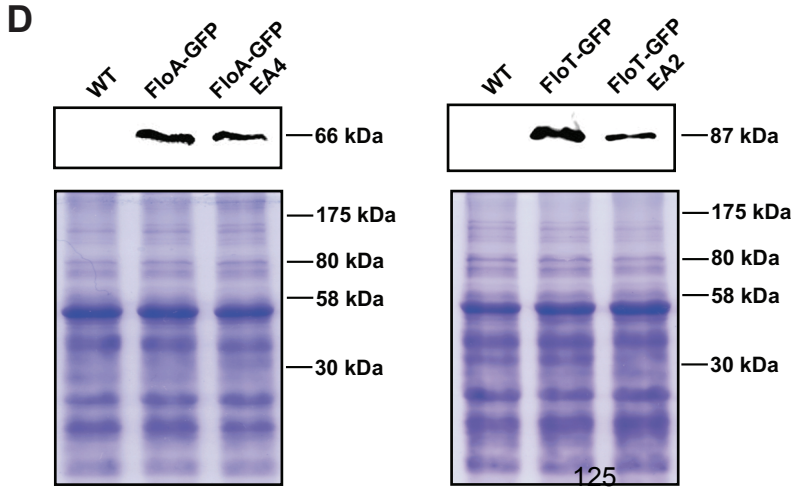
D
WT
FloA-GFP
FloA-GFP EA4
66 kDa
175 kDa
80 kDa
58 kDa
30 kDa
WT
FloT-GFP
FloT-GFP EA2
87 kDa
175 kDa
80 kDa
58 kDa
30 kDa

Schneider_FigS6

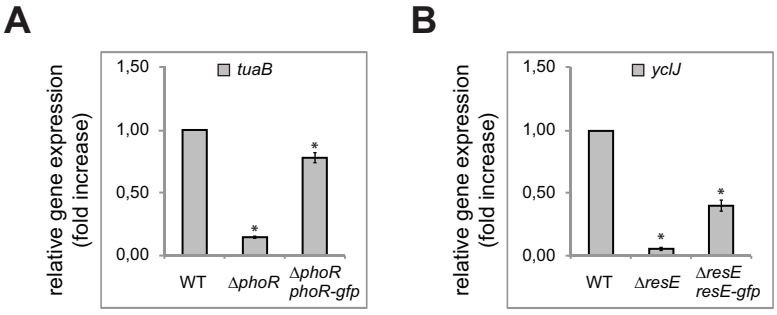

1 **Supplemental Information**

2 **Supplemental Tables**

3

4 **Supplemental Table S1 (Related to material and methods):** List of strains and plasmids

5 used in this study

Strain	Genotype	Reference
DL1	Wild type (NCIB 3610)	[1]
DL2	Wild type 168	[2]
GK129	3610 *lacA*::P_{floT}-*yfp* (*mls*)	This study
GK38	168 *amyE*::P_{floT}-*yfp* (*spc*)	This study
GK43	3610 Δ*srf*::*mls amyE*::P_{floT}-*yfp* (*spc*)	This study
GK45	3610 Δ*kinC*::*cm amyE*::P_{floT}-*yfp* (*spc*)	This study
GK47	3610 Δ*kinD*::*tet amyE*::P_{floT}-*yfp* (*spc*)	This study
GK49	3610 Δ*sigE*::*mls amyE*::P_{floT}-*yfp* (*spc*)	This study
GK51	3610 Δ*sigF*::*km amyE*::P_{floT}-*yfp* (*spc*)	This study
GK53	3610 Δ*spo0A*::*mls amyE*::P_{floT}-*yfp* (*spc*)	This study
GK55	3610 Δ*comA*::*cm amyE*::P_{floT}-*yfp* (*spc)*	This study
GK57	3610 Δ*spo0E*::*km amyE*::P_{floT}-*yfp* (*spc*)	This study
GK59	3610 Δ*dlt*::*tet amyE*::P_{floT}-*yfp* (*spc*)	This study
GK61	3610 Δ*rapD*::*km amyE*::P_{floT}-*yfp* (*spc*)	This study
GK63	3610 Δ*rapG*::*cm amyE*::P_{floT}-*yfp* (*spc*)	This study
GK65	3610 Δ*abrB*::*tet amyE*::P_{floT}-*yfp* (*spc*)	This study
GK67	3610 Δ*abh*::*km amyE*::P_{floT}-*yfp* (*spc*)	This study
GK69	3610 Δ*degS*::*tet amyE*::P_{floT}-*yfp* (*spc*)	This study
GK71	3610 Δ*lgtR*::*cm amyE*::P_{floT}-*yfp* (*spc*)	This study
GK73	3610 Δ*slr*::*tet amyE*::P_{floT}-*yfp* (*spc*)	This study
GK75	3610 Δ*rapH*::*km amyE*::P_{floT}-*yfp* (*spc*)	This study
GK77	3610 Δ*ftsH*::*km amyE*::P_{floT}-*yfp* (*spc*)	This study
GK109	3610 Δ*codY*::*spc lacA*::P_{floT}-*yfp* (*mls*)	This study
GK110	3610 Δ*mecA*::*spc lacA*::P_{floT}-*yfp* (*mls*)	This study
GK111	3610 Δ*compqx*::*spc lacA*::P_{floT}-*yfp* (*mls*)	This study
GK112	3610 Δ*sinR*::*spc lacA*::P_{floT}-*yfp* (*mls*)	This study
GK113	3610 Δ*comK*::*spc lacA*::P_{floT}-*yfp* (*mls*)	This study
GK119	3610 Δ*relA*::*km amyE*::P_{floT}-*yfp* (*spc*)	This study
GK126	3610 Δ*hpr*::*cm* l*acA*::P_{floT}-*yfp* (*mls*)	This study
GK127	3610 Δ*spo0F*::*km lacA*::P_{floT}-*yfp* (*mls*)	This study
GK128	3610 Δ*rapD*::*cm lacA*::P_{floT}-*yfp* (*mls*)	This study
GK131	3610 Δ*sqhC*::*km lacA*::P_{floT}-*yfp* (*mls*)	This study
GK132	3610 Δ*rapB*::*spc* l*acA*::P_{floT}-*yfp* (*mls*)	This study
GK133	3610 Δ*sinI*::*spc lacA*::P_{floT}-*yfp* (*mls*)	This study
GK82	168 *amyE*::P_{floA}-*yfp* (*spc*)	This study
GK83	3610 *amyE*::P_{floA}-*yfp* (*spc*)	This study
GK116	168 *lacA*::P_{floA}-*yfp* (*mls*)	This study
GK84	3610 Δ*srf*::*mls amyE*::P_{floA}-*yfp* (*spc*)	This study
GK85	3610 Δ*kinC*::*cm amyE*::P_{floA}-*yfp* (*spc*)	This study
GK86	3610 Δ*kinD*::*tet amyE*::P_{floA}-*yfp* (*spc*)	This study
GK87	3610 Δ*sigE*::*mls amyE*::P_{floA}-*yfp* (*spc*)	This study
GK88	3610 Δ*sigF*::*km amyE*::P_{floA}-*yfp* (*spc*)	This study
GK96	3610 Δ*spo0A*::*mls amyE*::P_{floA}-*yfp* (*spc*)	This study
GK99	3610 Δ*comA*::*cm amyE*::P_{floA}-*yfp* (*spc*)	This study
GK100	3610 Δ*spo0E*::*km amyE*::P_{floA}-*yfp* (*spc*)	This study
GK92	3610 Δ*dlt*::*tet amyE*::P_{floA}-*yfp* (*spc*)	This study

GK93	3610 Δ*rapD*::*km amyE*::P_{floA}-*yfp* (*spc*)	This study
GK95	3610 Δ*rapG*::*cm amyE*::P_{floA}-*yfp* (*spc*)	This study
GK89	3610 Δ*abrB*::*tet amyE*::P_{floA}-*yfp* (*spc*)	This study
GK90	3610 Δ*abh*::*km amyE*::P_{floA}-*yfp* (*spc*)	This study
GK91	3610 Δ*degS*::*tet amyE*::P_{floA}-*yfp* (*spc*)	This study
GK97	3610 Δ*lgtR*::*cm amyE*::P_{floA}-*yfp* (*spc*)	This study
GK98	3610 Δ*slr*::*tet amyE*::P_{floA}-*yfp* (*spc*)	This study
GK94	3610 Δ*rapH*::*km amyE*::P_{floA}-*yfp* (*spc*)	This study
GK124	3610 Δ*ftsH*::*km lacA*::P_{floA}-*yfp* (*mls*)	This study
GK125	3610 Δ*codY*::*spc lacA*::P_{floA}-*yfp* (*mls*)	This study
GK123	3610 Δ*mecA*::*spc lacA*::P_{floA}-*yfp* (*mls*)	This study
GK122	3610 Δ*compqx*::*spc lacA*::P_{floA}-*yfp* (*mls*)	This study
GK121	3610 Δ*sinR*::*spc lacA*::P_{floA}-*yfp* (*mls*)	This study
GK120	3610 Δ*comK*::*spc lacA*::P_{floA}-*yfp* (*mls*)	This study
GK102	3610 Δ*relA*::*km amyE*::P_{floA}-*yfp* (*spc*)	This study
GK134	3610 Δ*hpr*::*cm lacA*::P_{floA}-*yfp* (*mls*)	This study
GK135	3610 Δ*spo0F*::*km lacA*::P_{floA}-*yfp* (*mls*)	This study
GK139	3610 Δ*rapD*::*cm lacA*::P_{floA}-*yfp* (*mls*)	This study
GK137	3610 Δ*sqhC*::*km lacA*::P_{floA}-*yfp* (*mls*)	This study
GK138	3610 Δ*rapB*::*spc lacA*::P_{floA}-*yfp* (*mls*)	This study
GK136	3610 Δ*sinI*::*spc lacA*::P_{floA}-*yfp* (*mls*)	This study
DL573	3610 Δ*spo0A*::*mls*	[1]
DL383	3610 Δ*abrB*::*tet*	[3]
JS136	3610 *amyE*::*floA-gfp* (*spc*)	This study
JS280	3610 *amyE*::*floT-gfp* (*spc*)	This study
JS170	3610 Δ*spo0A*::*mls amyE*::*floA-gfp* (*spc*)	This study
JS169	3610 Δ*spo0A*::*mls amyE*::*floT-gfp* (*spc*)	This study
JS177	3610 Δ*spo0A*::*mls* Δ*abrB*::*tet amyE*::*floA-gfp* (*spc*)	This study
JS181	3610 Δ*spo0A*::*mls* Δ*abrB*::*tet amyE*::*floT-gfp* (*spc*)	This study
JS183	168 *lacA*::*floT-rfp* (*mls*)	This study
JS320	168 *lacA*::*floA-rfp* (*mls*)	This study
JS186	3610 *lacA*::*floT-rfp* (*mls*) *amyE*::*floA-gfp* (*spc*)	This study
JS321	3610 *lacA*::*floA-rfp* (*mls*) *amyE*::*floT-gfp* (*spc*)	This study
JS134	3610 *lacA*::*floA-mEos2* (*mls*)	This study
JS153	3610 *lacA*::*floT-mEos2* (*mls*)	This study
JS119	3610 Δ*floT* (markerless)	[4]
JS152	3610 Δ*floA* (markerless)	[4]
JS201	3610 Δ*floT* (markerless) *amyE*::P_{hp}-*floT*-His^6 (*spc*)	[5]
JS202	3610 Δ*floA* (markerless) *amyE*::P_{hp}-*floA*-His^6 (*spc*)	[5]
JS303	168 *amyE*::*floT-gfp* [A342G,E343L,A344G] (*spc*)	This study
JS304	168 *amyE*::*floT-gfp* [A357G,E358L,A359G,E360L] (*spc*)	This study
JS305	168 *amyE*::*floT-gfp* [A370G,E371L,A372G,E373L] (*spc*)	This study
JS306	168 *amyE*::*floT-gfp* [A390G,E391L,A392G,E393L,A394G] (*spc*)	This study
JS310	168 *amyE*::*floA-gfp* [A240G,E241L,A242G] (*spc*)	This study
JS311	168 *amyE*::*floA-gfp* [A251G,E252L,E252L] (*spc*)	This study
JS317	168 *amyE*::*floA-gfp* [E278L,A279G,E280L,A281G,E282L] (*spc*)	This study
JS312	168 *amyE*::*floA-gfp* [A288G,E289L,A290G] (*spc*)	This study
JS334	3610 Δ*floT* (markerless) *lacA*::*floT-mEos2* [A357G,E358L,A359G,E360L] (mls)	This study
JS335	3610 Δ*floA* (markerless) *lacA*::*floA-mEos2* [A288G,E289L,A290G] (mls)	This study
JS461	168 *lacA*::$floA_T$-*gfp* (*mls*)	This study
JS470	168 *lacA*::$floT_A$-*gfp* (*mls*)	This study
JS166	3610 *lacA*::*floT-PAmCherry* (*mls*)	This study
JS167	3610 *lacA*::*floA-PAmCherry* (*mls*)	This study
BM155	168 Δ*floT* (markerless)	This study
DL1401	168 Δ*floA*::*mls*	[6]
JS338	168 Δ*floA*::*mls amyE*::*floT-gfp* [A342G,E343L,A344G] (*spc*)	This study
JS341	168 Δ*floA*::*mls amyE*::*floT-gfp* [A357G,E358L,A359G,E360L] (*spc*)	This study

JS339	168 Δ*floA::mls amyE::floT-gfp* [A370G,E371L,A372G,E373L] (*spc*)	This study
JS342	168 Δ*floA::mls amyE::floT-gfp* [A390G,E391L,A392G,E393L,A394G] (*spc*)	This study
JS343	168 Δ*floA::mls amyE::floT-gfp* (*spc*)	This study
JS345	168 Δ*floT* (markerless) *amyE::floA-gfp* [A240G,E241L,A242G] (*spc*)	This study
JS346	168 Δ*floT* (markerless) *amyE::floA-gfp* [A251G,E252L,E252L] (*spc*)	This study
JS347	168 Δ*floT* (markerless) *amyE::floA-gfp* [E278L,A279G,E280L,A281G,E282L] (*spc*)	This study
JS348	168 Δ*floT* (markerless) *amyE::floA-gfp* [A288G,E289L,A290G] (*spc*)	This study
JS357	168 Δ*floT* (markerless) *amyE::floA-gfp* (*spc*)	This study
DL1662	168 *amyE::P_{hp}-phoP-3xFlag* (*spc*)	This study
DL1664	168 *amyE::P_{hp}-resD-3xFlag* (*spc*)	This study
DL1666	168 Δ*floA::mls amyE::P_{hp}-phoP-3xFlag* (*spc*)	This study
DL1668	168 Δ*floA::mls amyE::P_{hp}-resD-3xFlag* (*spc*)	This study
DL1670	168 Δ*floT* (markerless) *amyE::P_{hp}-phoP-3xFlag* (*spc*)	This study
DL1672	168 Δ*floT* (markerless) *amyE::P_{hp}-resD-3xFlag* (*spc*)	This study
DL1681	168 Δ*phoR::km amyE::P_{hp}-phoP-3xFlag* (*spc*)	This study
DL1679	168 Δ*resE::km amyE::P_{hp}-resD-3xFlag* (*spc*)	This study
JS506	168 *lacA::floT-rfp* (*mls*) *amyE::resE-gfp* (*spc*)	This study
JS508	168 *lacA::floA-rfp* (*mls*) *amyE::phoR-gfp* (*spc*)	This study
JS517	168 Δ*resE::km amyE::resE-gfp* (*spc*)	This study
JS518	168 Δ*phoR::km amyE::phoR-gfp* (*spc*)	This study
DL95	*E. coli* DH5α	[7]
JS263	*E. coli* DH5α pDR183 *P_{floT}-floT-gfp*	This study
JS314	*E. coli* DH5α pDR111 *P_{floA}-floA-gfp*	This study
BM263	*E. coli* BTH101	[8]
BM261	*E. coli* DH5α pKT25-*zip*	This study
BM262	*E. coli* DH5α pUT18C-*zip*	This study
BM258	*E. coli* DH5α pKNT25	This study
BM259	*E. coli* DH5α pUT18	This study
JS369	*E. coli* BTH101 pKT25-*zip* pUT18C-*zip*	This study
JS368	*E. coli* BTH101 pKNT25 pUT18	This study
JS360	*E. coli* BTH101 pKNT25-*floT* pUT18-*resE*	This study
JS378	*E. coli* BTH101 pKNT25-*floT* pUT18-*phoR*	This study
JS379	*E. coli* BTH101 pKNT25-*floA* pUT18-*resE*	This study
JS362	*E. coli* BTH101 pKNT25-*floA* pUT18-*phoR*	This study
JS370	*E. coli* BTH101 pKNT25-*floT* pUT18-*floT*	This study
JS371	*E. coli* BTH101 pKNT25-*floT* pUT18-*floA*	This study
JS372	*E. coli* BTH101 pKNT25-*floA* pUT18-*floT*	This study
JS373	*E. coli* BTH101 pKNT25-*floA* pUT18-*floA*	This study
JS394	*E. coli* BTH101 pKNT25-*floT* pUT18-*floT* [A342G,E343L,A344G]	This study
JS395	*E. coli* BTH101 pKNT25-*floT* pUT18-*floT* [A357G,E358L,A359G,E360L]	This study
JS380	*E. coli* BTH101 pKNT25-*floT* pUT18-*floT* [A370G,E371L,A372G,E373L]	This study
JS381	*E. coli* BTH101 pKNT25-*floT* pUT18-*floT* [A390G,E391L,A392G,E393L,A394G]	This study
JS396	*E. coli* BTH101 pKNT25-*floA* pUT18-*floA* [A240G,E241L,A242G]	This study
JS397	*E. coli* BTH101 pKNT25-*floA* pUT18-*floA* [A251G,E252L,E252L]	This study
JS382	*E. coli* BTH101 pKNT25-*floA* pUT18-*floA* [E278L,A279G,E280L,A281G,E282L]	This study
JS383	*E. coli* BTH101 pKNT25-*floA* pUT18-*floA* [A288G,E289L,A290G]	This study
JS442	*E. coli* DH5α pSEVA641	[9]
JS445	*E. coli* DH5α pSEVA631	[9]
JS446	*E. coli* DH5α pSEVA621	[9]
JS441	*E. coli* BTH101 pKNT25-*phoR* pUT18-*phoR*	This study
JS443	*E. coli* BTH101 pKNT25-*resE* pUT18-*resE*	This study
JS444	*E. coli* DH5α pSEVA641 *P_{floA}-floA-His*[b]	This study
JS447	*E. coli* DH5α pSEVA631 *P_{floA}-floA-His*[b]	This study

JS448	*E. coli* DH5α pSEVA621 P_{floA}-*floA-His*^{6}	This study
JS450	*E. coli* DH5α pSEVA641 P_{floT}-*floT-His*^{6}	This study
JS451	*E. coli* DH5α pSEVA631 P_{floT}-*floT-His*^{6}	This study
JS452	*E. coli* DH5α pSEVA621 P_{floT}-*floT-His*^{6}	This study

1. Branda SS, Gonzalez-Pastor JE, Ben-Yehuda S, Losick R, Kolter R (2001) Fruiting body formation by *Bacillus subtilis*. Proc Natl Acad Sci U S A 98: 11621-11626.

2. Moszer I, Glaser P, Danchin A (1995) SubtiList: a relational database for the *Bacillus subtilis* genome. Microbiology 141 (Pt 2): 261-268.

3. Hamon MA, Stanley NR, Britton RA, Grossman AD, Lazazzera BA (2004) Identification of AbrB-regulated genes involved in biofilm formation by *Bacillus subtilis*. Mol Microbiol 52: 847-860.

4. Yepes A, Schneider J, Mielich B, Koch G, Garcia-Betancur JC, et al. (2012) The biofilm formation defect of a *Bacillus subtilis* flotillin-defective mutant involves the protease FtsH. Mol Microbiol 86: 457-471.

5. Mielich-Suss B, Schneider J, Lopez D (2013) Overproduction of flotillin influences cell differentiation and shape in *Bacillus subtilis*. MBio 4: e00719-00713.

6. Lopez D, Kolter R (2010) Functional microdomains in bacterial membranes. Genes Dev 24: 1893-1902.

7. Reusch RN, Hiske TW, Sadoff HL (1986) Poly-beta-hydroxybutyrate membrane structure and its relationship to genetic transformability in *Escherichia coli*. J Bacteriol 168: 553-562.

8. Karimova G, Pidoux J, Ullmann A, Ladant D (1998) A bacterial two-hybrid system based on a reconstituted signal transduction pathway. Proc Natl Acad Sci U S A 95: 5752-5756.

9. Silva-Rocha R, Martinez-Garcia E, Calles B, Chavarria M, Arce-Rodriguez A, et al. (2013) The Standard European Vector Architecture (SEVA): a coherent platform for the analysis and deployment of complex prokaryotic phenotypes. Nucleic Acids Res 41: D666-675.

Supplemental Table S2 (Related to material and methods): List of primers used in this study.

Name	Sequence (5'-3')	Description
JS23	ATGAGTGCGATTAAGCCAGAC	*mEos2* fw
JS24	TTTTGGATCCTTATCGTCTGGCATTGTCAGG	*mEos2* rv (BamHI)
JS37	TTTTCTCGAGTTATCGTCTGGCATTGTCAGG	*mEos2* rv (XhoI)
JS13	TAATGAATTCGTGAGCAGTCAACTGTC	P_{floA} fw (EcoRI)
JS40	CGGATCCATATAACTTCTCCTCCTTAGCAGATTTGACCAATCCC	P_{floA} rv (PCR *floA*)
JS41	AAAAGTCGACCGCAGCAGTCAGCTGC	P_{floT} fw (SalI)
JS38	CATTGTCATATCAAATTCCTCCTTAATCAATGCATTGATGAACGG	P_{floT} rv (PCR *floT*)
JS4	TTTTGTCGACTAAGGAGGAGATATGACAATGCCGATTAT	*floT* fw (SalI)
JS1	TTTTGCATGCTTACTCTGATTTTTGGATCG	*floT* rv (SphI)
JS26	GTCTGGCTTAATCGCACTCATCTCTGATTTTTGGATCGTTTTGG	*floT* rv (PCR *mEos2*)
JS2	TTTTGTCGACTAAGGAGGATATATGGATCCGTCAACAC	*floA* fw (SalI)
JS3	TTTTGCATGCTTATGATTTGCGGTCTTCA	*floA* rv (SphI)
JS29	GTCTGGCTTAATCGCACTCATTGATTTGCGGTCTTCATCCGAAG	*floA* rv (PCR *mEos2*)
JS72	CCAAAACGATCCAAAAATCAGAGATGAGTAAAGGAGAAGAACTTTTC	*gfp* fw (PCR *floT*)
JS73	GAAAAGTTCTTCTCCTTTACTCATCTCTGATTTTTGGATCGTTTTGG	*floT* rv (PCR *gfp*)
BM9	AAAAGCATGCTTATTTGTATAGTTCATCCATGC	*gfp* rv (SphI)
JS52	CCTCGCCCTTGCTCACCATCTCTGATTTTTGGATCGTTTTGG	*floT* rv (PCR *rfp*)
JS101	CATCTTCTGATGATGCCATTGATTTGCGGTCTTCATCCGAAG	*floA* rv (PCR *rfp*)
BM84	AAAAGCATGCTTACTTGTACAGCTCGTCCAT	*rfp* rv (SphI)
JS46	ATGGTGAGCAAGGGCGAGG	*PAmCherry* fw
JS47	TTTTCTCGAGTTACTTGTACAGCTCGTCCATG	*PAmCherry* rv (XhoI)
JS49	CCTCGCCCTTGCTCACCATAGCAGCTGATTTGCGGTCTTCATCCGAAG	*floA* rv (PCR *PAmCherry*)
JS51	CCTCGCCCTTGCTCACCATAGCAGCCTCTGATTTTTGGATCGTTTTGG	*floT* rv (PCR *PAmCherry*)
BM30	CAAACAGCTCGGGCTAGGCGATGCCAAGAA	*floT* rv EA-Repeat 1
BM31	TTCTTGGCATCGCCTAGCCCGAGCTGTTTG	*floT* fw EA-Repeat 1
BM32	AATGGCAAAGGGTCTGGGGCTAAAAGTAAGAA	*floT* rv EA-Repeat 2
BM33	TTCTTACTTTTAGCCCCAGACCCTTTGCCATT	*floT* fw EA-Repeat 2
BM34	GCTAGCAAAAGGACTAGGGCTAAAAGCGAAAG	*floT* rv EA-Repeat 3
BM35	CTTTCGCTTTTAGCCCTAGTCCTTTTGCTAGC	*floT* fw EA-Repeat 3
BM36	CCTGAAAGGTCTTGGACTAGGGCTAGGAAAAGAGAAAATT	*floT* rv EA-Repeat 4
BM37	AATTTTCTCTTTTCCTAGCCCTAGTCCAAGACCTTTCAGG	*floT* fw EA-Repeat 4
BM41	AACCGATCAGGGCCTGGGTGATAAAAACAT	*floA* rv EA-Repeat 1
BM42	ATGTTTTTATCACCCAGGCCCTGATCGGTT	*floA* fw EA-Repeat 1
BM43	GCAGGCAAAAGGGCTACTACGACGTGCGAT	*floA* rv EA-Repeat 2
BM44	ATCGCACGTCGTAGTAGCCCTTTTGCCTGC	*floA* fw EA-Repeat 2
BM45	GAAAGTAGTACTAGGCCTGGGGCTAGTGCCGCTTG	*floA* rv EA-Repeat 3
BM46	CAAGCGGCACTAGCCCCAGGCCTAGTACTACTTTC	*floA* fw EA-Repeat 3
BM47	GCTTGCGATGGGACTAGGTTTGCGTGAAGG	*floA* rv EA-Repeat 4
BM48	CCTTCACGCAAACCTAGTCCCATCGCAAGC	*floA* fw EA-Repeat 4
JS103	TTTTGCATGCATGACAATGCCGATTATAATGATC	*floT* fw (ShI)
JS104	TTTTGGTACCCGCTCTGATTTTTGGATCGTTTTGG	*floT* rv (KpnI)
JS105	TTTTGCATGCATGGATCCGTCAACACTTATG	*floA* fw (SphI)
JS106	TTTTGGTACCCGTGATTTGCGGTCTTCATCCG	*floA* rv (KpnI)
JS107	TTTTGCATGCATGAAATTTTGGAAAAGCGTAG	*resE* fw (SphI)
JS108	TTTTGGTACCCGCCGTTTTGTCGGAATATAAAAAG	*resE* rv (KpnI)
JS109	TTTTGCATGCATGAATAAATACCGTGTGCGCC	*phoR* fw (SphI)
JS110	TTTTGGTACCCGGGCGGACTTTTCAGCGGCC	*phoR* rv (KpnI)
JS130	TTTTGCATGCTTACTATTTATCGTCGTCATCTTTG	*flag* rv (SphI)
JS126	GGAGGAGCCAAAAATGAATGAAGACTACAAAGACCATGACGGT	*flag* fw (PCR *phoP*)

	G	
JS127	CACCGTCATGGTCTTTGTAGTCTTCATTCATTTTTGGCTCCTCC	*phoP* rv (PCR *flag*)
JS128	TTATAAATTTGAGGTCGGCGCTGAAGACTACAAAGACCATGACG GTG	*flag* fw (PCR *resD*)
JS129	CACCGTCATGGTCTTTGTAGTCTTCAGCGCCGACCTCAAATTTA TAA	*resD* rv (PCR *flag*)
JS131	AAAAGTCGACTAAGGAGGAACTACTATGAACAAGAAAATTTTAG TTGTGG	*phoP* fw (SalI)
JS132	AAAAGTCGACTAAGGAGGAACTACTATGGACCAAACGAACGAAA CAAA	*resD* fw (SalI)
JS133	GCGAAGAATTTCTTTTTCTTCTAGAATATCAATTGAGAGAATTTC AAAC	*floA* N-terminus rv (PCR $floA_T$)
JS134	GTTTGAAATTCTCTCAATTGATATTCTAGAAGAAAAAGAAATTCTT CGC	*floT* C-terminus fw (PCR $floA_T$)
JS135	TTTTTGCCGATATCTACATCTGCTTCTATTTGTTTTTGGCGTTCG AT	*floT* N-terminus rv (PCR $floT_A$)
JS136	ATCGAACGCCAAAAACAAATAGAAGCAGATGTAGATATCGGCAA AAA	*floA* C-terminus fw (PCR $floT_A$)
JS137	GTCGGCGCTGAATGAAATTTTGCAGCGAACCATTTGAGGTGATA	*km* fw (PCR *resE* up)
JS138	TATCACCTCAAATGGTTCGCTGCAAAATTTCATTCAGCGCCGAC	*resE* up rv (PCR *km*)
JS139	GCCTACGAGGAATTTGTATCGCGGTAAAATCGAGTCTGAATTTG	*resE* down fw (PCR *km*)
JS140	CAAATTCAGACTCGATTTTACCGCGATACAAATTCCTCGTAGGC	*km* rv (PCR *resE* down)
JS141	TTTTGTCGACCGACACCCATTATTATGCTGAC	*resE* up fw (SalI)
JS142	TTTTGCATGCCGGCAGCAATTGCTGATCCC	*resE* down rv (SphI)
JS143	CTGGAGGAGCCAAAAATGAATGCAGCGAACCATTTGAGGTGAT A	*km* fw (PCR *phoR* up)
JS144	TATCACCTCAAATGGTTCGCTGCATTCATTTTTGGCTCCTCCAG	*phoR* up rv (PCR *km*)
JS145	GCCTACGAGGAATTTGTATCGGTCCGCCTAATGTTTACAAAGG	*phoR* down fw (PCR *km*)
JS146	CCTTTGTAAACATTAGGCGGACCGATACAAATTCCTCGTAGGC	*km* rv (PCR *phoR* down)
JS147	TTTTGTCGACCCCATTTTAATGCTGACAGCG	*phoR* up fw (SalI)
JS148	TTTTGCATGCCAGGCGGGGTTTTCTGTCTG	*phoR* down rv (SphI)
oTB42	AGGATTGGAAGCTGTTCGT	*girB* fw
oTB43	TGACTTCTACCGCAGGAC	*girB* rv
oTB44	CAAAGGTTGTGCAACATGC	*sboAX*
oTB45	CCCATAGACCGAATAGACCT	*sboAX* rv
oTB46	TGTCTTTCGTCCATTCGCT	*albC* fw
oTB47	GATTCCACATCCAAACCGAC	*albC* rv
oTB48	TAGCGATGAGGAATGGGAGG	*dhbA* fw
oTB49	CGTAAACATCACAGCCGCA	*dhbA* rv
oTB50	ATATCGCCGTGACCCTC	*argC* fw
oTB51	CCAGTTTCTTCATTCCAGCC	*argC* rv
oTB52	GGCAGTCTAATTCCTCCGT	*cydB* fw
oTB53	CAAAGAAGCGTTACCGTCAC	*cydB* rv
oTB54	GCATTGAACAGATTGAGGGA	*pyrR* fw
oTB55	CATCCATTCCTGCTCTGAC	*pyrR* rv
oTB94	GATTCTGTCTTACGAAACCGCT	*glpQ* fw
oTB95	GTCTTTCACCCAACCCATTCC	*glpQ* rv

4

Supplemental Table S3 (Related to main figure 6): List of proteins identified in membrane-associated protein complexes that interacted exclusively with either FloA (■) or FloT (■), or FloA and FloT (■).

	Protein	Description	Functional category	sequence coverage FloA / FloT	
■	Eno	enolase, glycolytic/ gluconeogenic enzyme	Post-exponential lifestyles	60%	55%
■	FtsH*†	cell-division protein / general stress protein (class III heat-shock)		28%	30%
■	McpA†	methyl-accepting chemotaxis protein		-	25%
■	McpB†	methyl-accepting chemotaxis protein		-	21%
■	Rny	RNase Y, 5' end sensitive endoribonuclease, involved in the degradation/processing of mRNA		40%	31%
■	YcdA*	lipoprotein, required for swarming motility		-	60%
■	MreC*	cell-shape determining protein	Cell envelope/ Cell divison	41%	-
■	PhoR	two-component sensor histidine kinase involved in phosphate regulation		22%	-
■	PonA	penicillin-binding proteins 1A/1B		23%	-
■	RasP	control of cell division and SigW activity		26%	29%
■	RodZ	required for cell shape determination		31%	40%
■	TagU†	protein involved in cell wall teichoic acid biosynthesis		33%	-
■	YceH	unknown; similar to toxic anion resistance protein	Coping with stress	41%	-
■	YtxH	unknown; similar to general stress protein		60%	-
■	FloA†	flottilin-like protein (in addition to FloT), resistence protein (against sublancin)	Membrane dynamics	48%	51%
■	FloT*	similar to flotillin 1, orchestration of physiological processes in lipid microdomains		-	81%
■	AtpA*	ATP synthase (subunit alpha)	Metabolism	56%	55%
■	AtpB*	ATP synthase (subunit a)		86%	75%
■	AtpG†	ATP synthase (subunit gamma)		59%	40%
■	DhaS	aldehyde dehydrogenase		40%	-
■	MsmE	multiple sugar-binding protein		61%	-
■	QoxA*	cytochrome aa3 quinol oxidase (subunit II)		52%	62%
■	RocG	arginine utilization, controls the activity of GltC		51%	54%
■	SdhA†	succinate dehydrogenase (flavoprotein subunit)		39%	44%
■	BdbD*	thiol-disulfide oxidoreductase	Protein secretion/ modification	71%	73%
■	PrkC	protein kinase C, induce germination of spores in response to DAP-type, and not to Lys-type cell wall muropeptides		-	49%
■	PrsA*	protein secretion (post-translocation molecular chaperone)		84%	83%
■	ResE	two-component sensor kinase, regulation of aerobic and anaerobic respiration		-	30%
■	SecA	preprotein translocase subunit (ATPase)		-	62%
■	SecDF	protein-export membrane protein		-	38%
■	SpoIIIA	component of the SpoIIIA-SpoIIQ type III		46%	37%

	H	secretion system residing in the forespore membrane			
	SpoIIQ	component of the SpoIIIAH-SpoIIQ type III secretion system residing in the forespore membrane		82%	66%
	YacD	similar to secretion protein PrsA		-	52%
	AapA	amino acid permease	Transport-Homeostasis	51%	-
	AppA	oligopeptide ABC transporter (oligopeptide-binding protein)		60%	69%
	FeuA*	ABC transporter for the siderophores Fe-enterobactin and Fe-bacillibactin		81%	68%
	FhuD*†	ferrichrome ABC transporter (ferrichrome-binding protein)		32%	48%
	MntA†	manganese ABC transporter (membrane protein)		62%	76%
	MntB	manganese ABC transporter (ATP-binding protein)		64%	52%
	NupO	ABC transporter for guanosine (ATP-binding protein)		-	39%
	OppA*†	oligopeptide ABC transporter (binding protein) (initiation of sporulation, competence development)		53%	78%
	OppD	oligopeptide ABC transporter (ATP-binding protein) (initiation of sporulation, competence development)		58%	69%
	OppF	oligopeptide ABC transporter (ATP-binding protein) (initiation of sporulation, competence development)		37%	63%
	OpuAA	glycine betaine ABC transporter (ATP-binding protein)		52%	40%
	YclQ†	petrobactin (3.4-catecholate siderophore) ABC transporter (binding protein)		-	77%
	YfiY†	ABC transporter for the siderophore schizokinen and arthrobactin		-	75%
	YfmC	iron/ citrate ABC transporter (binding protein)		62%	56%
	YhfQ†	iron/ citrate ABC transporter (solute-binding protein)		-	37%
	YknX	ABC-type antimicrobial peptide transporter (permease) for the export of the SdpC toxin		-	60%
	YxeB*	hydroxamate siderophore ABC transporter (only ferrioxamine)		60%	53%
	yxeM*	putative cysteine ABC transporter (binding protein)		-	78%
	RnjA	RNase J1	RNA synthesis /degradation	-	43%

5

Supplemental Table S4 (Related to main figures 7 and 8): List of genes that are significantly up or downregulated (Bayes.p value <10-4) in the Δ*floA* cells compared to wild-type cells. Mean indicates log 2 transformed expression ratios.

locus tag	gene	Mean	Bayes.p	annotation
BSU25380	*floA*	-1,62	10^{-9}	flotillin-like protein
BSU15510	*pyrAA*	-1,21	10^{-7}	carbamoyl phosphate synthase small subunit
BSU40660	*yybF*	-1,11	10^{-6}	permease
BSU11220	*argD*	-1,07	10^{-7}	acetylornithine aminotransferase
BSU11230	*carA*	-1,02	10^{-6}	carbamoyl phosphate synthase small subunit
BSU15520	*pyrAB*	-0,96	10^{-7}	carbamoyl phosphate synthase large subunit
BSU11210	*argB*	-0,93	10^{-6}	acetylglutamate kinase
BSU29440	*argH*	-0,91	10^{-6}	argininosuccinate lyase
BSU11190	*argC*	-0,85	10^{-6}	N-acetyl-gamma-glutamyl-phosphate reductase
BSU11250	*argF*	-0,84	10^{-6}	ornithine carbamoyltransferase
BSU29450	*argG*	-0,83	10^{-5}	argininosuccinate synthase
BSU10410	*yhzC*	-0,78	10^{-6}	hypothetical protein
BSU11200	*argJ*	-0,78	10^{-4}	ornithine acetyltransferase
BSU38750	*cydB*	-0,77	10^{-4}	cytochrome bd ubiquinol oxidase subunit II
BSU27330	*udk*	-0,76	10^{-4}	uridine kinase
BSU15530	*pyrK*	-0,74	10^{-5}	dihydroorotate dehydrogenase electron transfer subunit
BSU23980	*yqiX*	-0,71	10^{-5}	high affinity arginine ABC transporter binding lipoprotein
BSU13750	*ykvM*	-0,70	10^{-5}	7-cyano-7-deazaguanine reductase
BSU03060	*lctP*	-0,68	10^{-4}	L-lactate permease
BSU19550	*yodC*	-0,64	10^{-4}	oxidoreductase
BSU23960	*yqiZ*	-0,62	10^{-5}	high affinity arginine ABC transporter ATP-binding protein
BSU00140	*dck*	-0,59	10^{-4}	deoxyadenosine/deoxycytidine kinase
BSU38570	*licA*	-0,57	10^{-4}	PTS system lichenan-specific transporter subunit IIA
BSU13740	*ykvL*	-0,53	10^{-4}	queuosine biosynthesis enzyme
BSU16580	*polC*	-0,53	10^{-4}	DNA polymerase III
BSU02130	*glpQ*	-0,53	10^{-4}	glycerophosphoryl diester phosphodiesterase
BSU06170	*ydjE*	-0,52	10^{-4}	sugar kinase
BSU09460	*yhdG*	-0,52	10^{-4}	branched-chain amino acid transporter
BSU17400	*ymaB*	-0,51	10^{-4}	hypothetical protein
BSU11760	*cotX*	-0,51	10^{-4}	spore coat protein
BSU14590	*pdhB*	-0,51	10^{-4}	pyruvate dehydrogenase E1 component subunit beta
BSU11700	*thiF*	-0,49	10^{-4}	thiamine/molybdopterin biosynthesis
BSU04200	*ydaE*	-0,48	10^{-4}	hypothetical protein
BSU18450	*gltA*	-0,47	10^{-4}	glutamate synthase large subunit
BSU15210	*spoVE*	-0,45	10^{-4}	factor for spore cortex peptidoglycan synthesis
BSU35730	*tagE*	0,37	10^{-4}	alpha-glucosyltransferase
BSU35700	*tagH*	0,40	10^{-4}	teichoic acid transport system ATP-binding protein
BSU35710	*tagG*	0,42	10^{-4}	teichoic acid translocation permease protein
BSU28040	*radC*	0,42	10^{-4}	DNA repair protein
BSU08690	*ygaD*	0,43	10^{-4}	ABC transporter ATP-binding protein
BSU35750	*tagA*	0,43	10^{-4}	N-acetylmannosaminyltransferase
BSU20880	*yopI*	0,45	10^{-4}	hypothetical protein
BSU02860	*ycdI*	0,46	10^{-4}	Zn(II) transporter ATP-binding protein
BSU13270	*ykoI*	0,46	10^{-4}	hypothetical protein
BSU37160	*rpoE*	0,46	10^{-4}	DNA-directed RNA polymerase subunit delta
BSU19390	*yojN*	0,47	10^{-4}	nitric-oxide reductase

BSU17350	*ymzC*	0,47	10^{-4}	hypothetical protein
BSU22910	*ypfA*	0,48	10^{-4}	cyclic diGMP binding protein
BSU32870	*yusO*	0,48	10^{-4}	MarR family transcriptional regulator
BSU20950	*yopB*	0,49	10^{-4}	transcriptional regulator
BSU05050	*lrpA*	0,50	10^{-4}	Lrp/AsnC family transcriptional regulator
BSU35760	*tagB*	0,50	10^{-4}	CDP-glycerol:glycerophosphate glycerophosphotransferase
BSU00270	*yaaO*	0,51	10^{-4}	lysine decarboxylase
BSU31890	*yukC*	0,51	10^{-5}	bacteriocin production protein
BSU06400	*yebE*	0,52	10^{-4}	hypothetical protein
BSU39910	*yxnB*	0,52	10^{-4}	hypothetical protein
BSU37210	*ywjC*	0,52	10^{-4}	hypothetical protein
BSU20840	*yopM*	0,53	10^{-4}	hypothetical protein
BSU01780	*glmS*	0,53	10^{-4}	glucosamine--fructose-6-phosphate aminotransferase
BSU00010	*dnaA*	0,53	10^{-4}	chromosome replication initiator
BSU40180	*yydF*	0,54	10^{-4}	peptide controlling LiaRS
BSU35720	*tagF*	0,54	10^{-4}	CDP-glycerol glycerophosphotransferase
BSU00710	*yacC*	0,55	10^{-4}	heat shock protein
BSU25680	*yqeG*	0,56	10^{-5}	hydrolase
BSU14960	*ylbC*	0,56	10^{-4}	hypothetical protein
BSU09410	*phoA*	0,56	10^{-4}	alkaline phosphatase
BSU25720	*yqeD*	0,56	10^{-4}	hypothetical protein
BSU01750	*ybbP*	0,57	10^{-4}	hypothetical protein
BSU00750	*pabA*	0,57	10^{-4}	anthranilate synthase glutamine amidotransferase
BSU16120	*topA*	0,57	10^{-4}	DNA topoisomerase I
BSU11640	*yjbQ*	0,57	10^{-4}	Na+/H+ antiporter
BSU15120	*yllA*	0,57	10^{-4}	nucleoid associated protein
BSU20790	*yopR*	0,57	10^{-4}	integrase
BSU20800	*yopQ*	0,57	10^{-4}	hypothetical protein
BSU27520	*yrzC*	0,57	10^{-4}	cysteine biosynthesis transcriptional regulator
BSU16950	*pbpX*	0,57	10^{-4}	penicillin-binding endopeptidase X
BSU15300	*bpr*	0,58	10^{-4}	bacillopeptidase F
BSU00100	*dacA*	0,58	10^{-4}	D-alanyl-D-alanine carboxypeptidase
BSU41020	*thdF*	0,58	10^{-4}	tRNA modification GTPase
BSU03300	*nasD*	0,59	10^{-5}	assimilatory nitrite reductase subunit
BSU20910	*yopF*	0,59	10^{-4}	hypothetical protein
BSU14170	*ykuP*	0,59	10^{-4}	short-chain flavodoxin
BSU21730	*ypmS*	0,60	10^{-4}	hypothetical protein
BSU37430	*albG*	0,60	10^{-4}	hypothetical protein
BSU10980	*yitG*	0,61	10^{-4}	efflux transporter
BSU40440	*dnaC*	0,61	10^{-4}	replicative DNA helicase
BSU40610	*yybK*	0,62	10^{-4}	hypothetical protein
BSU37380	*albB*	0,62	10^{-4}	hypothetical protein
BSU28600	*yshB*	0,62	10^{-5}	hypothetical protein
BSU09330	*yhcZ*	0,63	10^{-4}	two-component response regulator
BSU05470	*ydfM*	0,65	10^{-4}	divalent cation efflux transporter
BSU25140	*yqfR*	0,65	10^{-5}	ATP-dependent RNA helicase
BSU01960	*ybdB*	0,65	10^{-5}	sporulation killing factor biosynthesis and export
BSU23210	*ypuH*	0,67	10^{-5}	chromosome condensation and segregation factor
BSU13040	*hmp*	0,67	10^{-4}	nitric oxide dioxygenase
BSU02870	*yceA*	0,69	10^{-5}	high affinity Zn(II) ABC transporter permease
BSU14630	*speA*	0,70	10^{-5}	arginine decarboxylase
BSU30430	*ytrD*	0,70	10^{-4}	ABC transporter permease
BSU30050	*ytgP*	0,70	10^{-4}	hypothetical protein
BSU35260	*ftsE*	0,71	10^{-5}	cell-division ABC transporter ATP-binding protein
BSU09510	*yhdL*	0,72	10^{-5}	negative regulator of the activity of sigmaM

BSU08600	*csbB*	0,75	10^{-6}	glycosyl transferase family protein
BSU21130	*yonD*	0,75	10^{-5}	hypothetical protein
BSU13060	*ykjA*	0,76	10^{-5}	hypothetical protein
BSU39920	*asnH*	0,76	10^{-6}	asparagine synthetase
BSU17370	*ymaA*	0,76	10^{-5}	ribonucleotide reductase stimulatory protein
BSU21050	*yonN*	0,76	10^{-5}	HU-related DNA-binding protein
BSU15490	*pyrB*	0,77	10^{-4}	aspartate carbamoyltransferase
BSU00800	*yazB*	0,79	10^{-6}	transcriptional regulator
BSU09520	*sigM*	0,81	10^{-6}	RNA polymerase sigma factor
BSU00780	*folB*	0,83	10^{-5}	dihydroneopterin aldolase
BSU19160	*yocC*	0,84	10^{-6}	hypothetical protein
BSU30450	*ytrB*	0,86	10^{-5}	ABC transporter ATP-binding protein
BSU00770	*sul*	0,90	10^{-6}	dihydropteroate synthase
BSU23220	*ypuG*	0,90	10^{-7}	segregation and condensation protein A
BSU13300	*ykoK*	0,90	10^{-6}	magnesium transporter
BSU21090	*yonH*	0,95	10^{-6}	capsid protein
BSU37400	*albD*	0,96	10^{-8}	hypothetical protein
BSU00790	*folK*	0,98	10^{-6}	7, 8-dihydro-6-hydroxymethylpterin-pyrophosphokinase
BSU37410	*albE*	1,00	10^{-8}	hydrolase
BSU37420	*albF*	1,00	10^{-7}	subtilosin production peptidase
BSU05490	*ydfO*	1,01	10^{-5}	dioxygenase
BSU37390	*albC*	1,02	10^{-6}	subtilosin production transporter
BSU00760	*pabC*	1,05	10^{-7}	4-amino-4-deoxychorismate lyase
BSU15480	*pyrP*	1,10	10^{-6}	uracil permease
BSU30440	*ytrC*	1,11	10^{-7}	ABC transporter permease
BSU30460	*ytrA*	1,12	10^{-7}	GntR family transcriptional regulator
BSU15470	*pyrR*	1,52	10^{-8}	bifunctional pyrimidine regulatory protein

Supplemental Table S5 (Related to main figures 7 and 8): List of genes that are significantly up or downregulated (Bayes.p value <10-4) in the Δ*floT* cells compared to wild-type cells. Mean indicates log 2 transformed expression ratios.

locus tag	gene	Mean	Bayes.p	annotation
BSU31010	*floT*	-1,89	10^{-9}	flotillin-like protein
BSU03300	*nasD*	-1,04	10^{-8}	assimilatory nitrite reductase subunit
BSU13040	*hmp*	-1,00	10^{-7}	nitric oxide dioxygenase
BSU31990	*dhbC*	-0,93	10^{-6}	isochorismate synthase
BSU14150	*ykuN*	-0,93	10^{-9}	flavodoxin
BSU31980	*dhbE*	-0,92	10^{-7}	2,3-dihydroxybenzoate-AMP ligase
BSU37360	*sboX*	-0,92	10^{-7}	bacteriocin-like product
BSU17660	*yncF*	-0,92	10^{-4}	deoxyuridine 5'-triphosphate pyrophosphatase
BSU14160	*ykuO*	-0,88	10^{-9}	hypothetical protein
BSU37350	*sboA*	-0,84	10^{-7}	subtilosin A
BSU22550	*qcrB*	-0,83	10^{-5}	cytochrome b
BSU31970	*dhbB*	-0,83	10^{-6}	isochorismatase
BSU32000	*dhbA*	-0,83	10^{-6}	2,3-dihydroxybenzoate-2,3-dehydrogenase
BSU11990	*yjdB*	-0,81	10^{-4}	hypothetical protein
BSU31960	*dhbF*	-0,79	10^{-7}	siderophore bacillibactin synthetase
BSU04530	*ydbN*	-0,77	10^{-6}	hypothetical protein
BSU38750	*cydB*	-0,72	10^{-4}	cytochrome bd ubiquinol oxidase subunit II
BSU19680	*yozE*	-0,70	10^{-4}	hypothetical protein
BSU20580	*yoqM*	-0,69	10^{-6}	membrane bound protein
BSU37390	*albC*	-0,69	10^{-4}	subtilosin production transporter
BSU16620	*ylxQ*	-0,69	10^{-4}	hypothetical protein
BSU30020	*ytzE*	-0,67	10^{-4}	DeoR family transcriptional regulator
BSU37310	*fnr*	-0,65	10^{-6}	FNR/CAP family transcriptional regulator
BSU32010	*besA*	-0,61	10^{-4}	bacillibactin trilactone hydrolase
BSU04810	*immA*	-0,51	10^{-4}	immunity anti-repressor
BSU11010	*yitJ*	-0,51	10^{-4}	homocysteine S-methyltransferase
BSU18380	*iseA*	-0,51	10^{-6}	inhibitor of cell-separation enzymes
BSU11360	*appD*	-0,47	10^{-5}	oligopeptide ABC transporter ATP-binding protein
BSU37370	*albA*	-0,47	10^{-5}	antilisterial bacteriocin (subtilosin) production protein
BSU00370	*abrB*	-0,47	10^{-4}	transcriptional regulator
BSU40180	*yydF*	-0,46	10^{-5}	peptide controlling LiaRS
BSU03230	*ycgP*	-0,46	10^{-4}	transcriptional regulator
BSU24620	*tasA*	-0,46	10^{-4}	major biofilm matrix component
BSU17710	*tatAC*	-0,46	10^{-4}	twin-arginine pre-protein translocation pathway protein
BSU19300	*yozC*	-0,43	10^{-4}	hypothetical protein
BSU02040	*ybdN*	-0,43	10^{-4}	hypothetical protein
BSU33770	*spbC*	-0,43	10^{-4}	sporulation killing factor
BSU20420	*yorD*	-0,42	10^{-4}	hypothetical protein
BSU05030	*yddM*	-0,41	10^{-5}	helicase
BSU04820	*immR*	-0,41	10^{-4}	XRE family transcriptional regulator
BSU01620	*feuB*	-0,38	10^{-4}	iron-uptake protein
BSU31030	*yuaE*	-0,38	10^{-4}	hypothetical protein
BSU33750	*sdpA*	-0,38	10^{-4}	export of killing factor
BSU05020	*phrI*	-0,38	10^{-4}	secreted regulator of the activity of phosphatase RapI
BSU03780	*phrC*	-0,35	10^{-4}	secreted regulator of the activity of phosphatase RapC
BSU23150	*resA*	-0,34	10^{-4}	thiol-disulfide oxidoreductase
BSU33600	*smpB*	-0,34	10^{-4}	SsrA-binding protein
BSU00490	*spoVG*	-0,33	10^{-4}	regulatory protein

BSU18310	*ppsD*	-0,32	10^{-4}	plipastatin synthetase
BSU35750	*tagA*	-0,24	10^{-4}	N-acetylmannosaminyltransferase
BSU31580	*maeN*	0,31	10^{-4}	Na+/malate symporter
BSU01780	*glmS*	0,35	10^{-4}	glucosamine--fructose-6-phosphate aminotransferase
BSU21810	*dfrA*	0,36	10^{-4}	dihydrofolate reductase
BSU29600	*braB*	0,37	10^{-4}	branched-chain amino acid/Na+ symporter
BSU14030	*ykuC*	0,37	10^{-4}	efflux transporter
BSU09280	*glpF*	0,39	10^{-4}	glycerol permease
BSU37150	*pyrG*	0,39	10^{-4}	CTP synthetase
BSU06430	*purK*	0,41	10^{-4}	phosphoribosylaminoimidazole carboxylase ATPase subunit
BSU16950	*pbpX*	0,41	10^{-4}	penicillin-binding endopeptidase
BSU07340	*yfnA*	0,41	10^{-4}	metabolite permease
BSU03580	*yczE*	0,45	10^{-4}	integral inner membrane protein
BSU03050	*ldh*	0,48	10^{-4}	L-lactate dehydrogenase
BSU15490	*pyrB*	0,48	10^{-4}	aspartate carbamoyltransferase
BSU23980	*artP*	0,50	10^{-4}	high affinity arginine ABC transporter binding lipoprotein
BSU23970	*artQ*	0,58	10^{-6}	high affinity arginine ABC transporter permease
BSU29450	*argG*	0,60	10^{-5}	argininosuccinate synthase
BSU15470	*pyrR*	0,64	10^{-4}	bifunctional pyrimidine regulatory protein PyrR/uracil phosphoribosyltransferase
BSU33330	*lysP*	0,66	10^{-5}	lysine permease

Supplemental Table S6 (Related to main figures 7 and 8): List of genes that are significantly up or downregulated (Bayes.p value <10-4) in the Δ*floA* Δ*floT* cells compared to wild-type cells. Mean indicates log 2 transformed expression ratios.

locus tag	gene	Mean	Bayes.p	annotation
BSU31010	*floT*	-1,77	10^{-7}	flotillin-like protein
BSU36750	*spoIID*	-1,49	10^{-7}	stage II sporulation autolysin
BSU14150	*ykuN*	-1,30	10^{-6}	flavodoxin
BSU13750	*ykvM*	-1,28	10^{-5}	7-cyano-7-deazaguanine reductase
BSU14160	*ykuO*	-1,21	10^{-6}	hypothetical protein
BSU13740	*ykvL*	-1,18	10^{-6}	queuosine biosynthesis enzyme
BSU31970	*dhbB*	-1,10	10^{-5}	isochorismatase
BSU37360	*sboX*	-1,09	10^{-6}	bacteriocin-like product
BSU25380	*floA*	-1,08	10^{-5}	flotillin-like protein
BSU31980	*dhbE*	-1,07	10^{-5}	2,3-dihydroxybenzoate-AMP ligase
BSU31960	*dhbF*	-1,07	10^{-4}	bacillibactin synthetase
BSU18450	*gltA*	-1,05	10^{-6}	glutamate synthase large subunit
BSU13730	*ykvK*	-1,04	10^{-5}	6-pyruvoyl tetrahydrobiopterin synthase
BSU03300	*nasD*	-1,03	10^{-5}	assimilatory nitrite reductase subunit
BSU13920	*splA*	-1,00	10^{-4}	TRAP-like transcriptional regulator
BSU37350	*sboA*	-0,96	10^{-5}	subtilosin A
BSU31990	*dhbC*	-0,95	10^{-4}	isochorismate synthase
BSU04530	*ydbN*	-0,93	10^{-5}	hypothetical protein
BSU17900	*yneE*	-0,92	10^{-4}	hypothetical protein
BSU13720	*ykvJ*	-0,91	10^{-4}	pre-queuosine 0 synthase
BSU40660	*yybF*	-0,91	10^{-4}	permease
BSU38750	*cydB*	-0,88	10^{-4}	cytochrome bd ubiquinol oxidase subunit II
BSU18560	*yoaD*	-0,86	10^{-4}	2-hydroxyacid dehydrogenase
BSU11010	*yitJ*	-0,82	10^{-4}	homocysteine S-methyltransferase
BSU18440	*gltB*	-0,81	10^{-4}	glutamate synthase subunit beta
BSU32720	*yurZ*	-0,81	10^{-5}	hypothetical protein
BSU10410	*yhzC*	-0,78	10^{-4}	hypothetical protein
BSU11000	*yitI*	-0,78	10^{-4}	N-acetyltransferase
BSU11360	*appD*	-0,77	10^{-5}	oligopeptide ABC transporter ATP-binding protein
BSU01140	*ybaC*	-0,76	10^{-4}	proline iminopeptidase
BSU37380	*albB*	-0,74	10^{-4}	hypothetical protein
BSU19370	*odhA*	-0,74	10^{-4}	2-oxoglutarate dehydrogenase
BSU06850	*yeeK*	-0,62	10^{-4}	spore associated protein
BSU03010	*amhX*	-0,54	10^{-4}	amidohydrolase
BSU01120	*fusA*	-0,52	10^{-4}	elongation factor G
BSU08860	*ssuD*	-0,50	10^{-4}	alkanesulfonate monooxygenase
BSU35700	*tagH*	0,58	10^{-4}	teichoic acid transport system ATP-binding protein
BSU06420	*purE*	0,58	10^{-4}	phosphoribosylaminoimidazole carboxylase I
BSU24940	*yqzC*	0,60	10^{-4}	hypothetical protein
BSU29440	*argH*	0,60	10^{-4}	argininosuccinate lyase

BSU15500	*pyrC*	0,61	10^{-4}	dihydroorotase
BSU03850	*ycnC*	0,62	10^{-4}	TetR family transcriptional regulator
BSU19210	*yocH*	0,64	10^{-4}	cell wall-binding protein
BSU31890	*yukC*	0,65	10^{-4}	bacteriocin production protein
BSU25140	*yqfR*	0,66	10^{-4}	ATP-dependent RNA helicase; cold shock
BSU29600	*braB*	0,67	10^{-4}	branched-chain amino acid/Na^{+} symporter
BSU23960	*yqiZ*	0,67	10^{-4}	high affinity arginine ABC transporter ATP-binding protein
BSU40100	*ahpF*	0,68	10^{-4}	alkyl hydroperoxide reductase
BSU18120	*alsT*	0,68	10^{-4}	amino acid carrier protein
BSU29570	*sspA*	0,69	10^{-4}	small acid-soluble spore protein
BSU06430	*purK*	0,69	10^{-4}	phosphoribosylaminoimidazole carboxylase ATPase subunit
BSU09710	*yheI*	0,70	10^{-4}	ABC transporter ATP-binding protein
BSU23210	*ypuH*	0,70	10^{-4}	chromosome condensation and segregation factor
BSU37150	*pyrG*	0,70	10^{-4}	CTP synthetase
BSU03580	*yczE*	0,71	10^{-4}	integral inner membrane protein
BSU11210	*argB*	0,72	10^{-4}	acetylglutamate kinase
BSU00010	*dnaA*	0,72	10^{-4}	chromosome replication initiator
BSU07340	*yfnA*	0,72	10^{-4}	metabolite permease
BSU30350	*yttB*	0,73	10^{-4}	efflux transporter
BSU14630	*speA*	0,73	10^{-4}	arginine decarboxylase
BSU39960	*yxaI*	0,74	10^{-4}	hypothetical protein
BSU19160	*yocC*	0,78	10^{-4}	hypothetical protein
BSU23220	*ypuG*	0,79	10^{-4}	segregation and condensation protein A
BSU07430	*yfmL*	0,79	10^{-4}	ATP-dependent RNA helicase
BSU29660	*rpsD*	0,79	10^{-4}	30S ribosomal protein S4
BSU10160	*yhgE*	0,79	10^{-4}	methyl-accepting protein
BSU02870	*yceA*	0,80	10^{-4}	high affinity Zn(II) ABC transporter permease
BSU13130	*proA*	0,81	10^{-4}	gamma-glutamyl phosphate reductase
BSU11200	*argJ*	0,82	10^{-5}	ornithine acetyltransferase
BSU12100	*yjeA*	0,82	10^{-4}	secreted deoxyriboendonuclease
BSU23970	*yqiY*	0,84	10^{-5}	high affinity arginine ABC transporter permease
BSU29450	*argG*	0,84	10^{-5}	argininosuccinate synthase
BSU05470	*ydfM*	0,89	10^{-4}	divalent cation efflux transporter
BSU35250	*ftsX*	0,92	10^{-4}	cell-division ABC transporter
BSU23980	*yqiX*	0,95	10^{-6}	high affinity arginine ABC transporter binding lipoprotein
BSU11190	*argC*	0,97	10^{-6}	N-acetyl-gamma-glutamyl-phosphate reductase
BSU15490	*pyrB*	1,10	10^{-7}	aspartate carbamoyltransferase
BSU15480	*pyrP*	1,13	10^{-6}	uracil permease
BSU33330	*yvsH*	1,13	10^{-6}	lysine permease
BSU15470	*pyrR*	1,47	10^{-7}	bifunctional pyrimidine regulatory protein PyrR/uracil phosphoribosyltransferase

Microbiology (2015), **00**, 1–18 DOI 10.1099/mic.0.000137

In vivo characterization of the scaffold activity of flotillin on the membrane kinase KinC of *Bacillus subtilis*

Johannes Schneider,[1,2] Benjamin Mielich-Süss,[1,2] Richard Böhme[1,2] and Daniel Lopez[1,2,3]

Correspondence
Daniel Lopez
daniel.Lopez@uni-wuerzburg.de
or dlopez@cnb.csic.es

[1]Research Centre for Infectious Diseases (ZINF), University of Würzburg, Würzburg 97080, Germany

[2]Institute for Molecular Infection Biology (IMIB), University of Würzburg, Würzburg 97080, Germany

[3]National Center for Biotecnology (CNB), Spanish Research Council (CSIC), Madrid 28050, Spain

Received 8 April 2015
Revised 6 July 2015
Accepted 7 July 2015

Scaffold proteins are ubiquitous chaperones that bind to proteins and facilitate the physical interaction of the components of signal transduction pathways or multi-enzymic complexes. In this study, we used a biochemical approach to dissect the molecular mechanism of a membrane-associated scaffold protein, FloT, a flotillin-homologue protein that is localized in functional membrane microdomains of the bacterium *Bacillus subtilis*. This study provides unambiguous evidence that FloT physically binds to and interacts with the membrane-bound sensor kinase KinC. This sensor kinase activates biofilm formation in *B. subtilis* in response to the presence of the self-produced signal surfactin. Furthermore, we have characterized the mechanism by which the interaction of FloT with KinC benefits the activity of KinC. Two separate and synergistic effects constitute this mechanism: first, the scaffold activity of FloT promotes more efficient self-interaction of KinC and facilitates dimerization into its active form. Second, the selective binding of FloT to KinC prevents the occurrence of unspecific aggregation between KinC and other proteins that may generate dead-end intermediates that could titrate the activity of KinC. Flotillin proteins appear to play an important role in prokaryotes in promoting effective binding of signalling proteins with their correct protein partners.

INTRODUCTION

Spatio-temporal organization of proteins in membranes and organelles promotes interaction specificity and optimizes the efficiency of biological reactions (DeLoache & Dueber, 2013; Diekmann & Pereira-Leal, 2013). An interesting question is how scaffold proteins assemble interacting components (Good *et al.*, 2011). Scaffold proteins are chaperones that bind to proteins and facilitate the physical interaction of the components of signal transduction pathways or multi-enzymic cascades (Bauer & Pelkmans, 2006; Chapman & Asthagiri, 2009; Good *et al.*, 2011). This type of protein is present in all kingdoms of life but has traditionally been studied in eukaryotes (Good *et al.*, 2011). For instance, the scaffold protein Ste5 mediates essential steps in the three-tiered mating MAPK signalling cascade in yeast (Chapman & Asthagiri, 2009). Likewise, the scaffold protein JIP1 tethers c-Jun N-terminal kinase (JNK) in the MAPK signalling pathway in human cells (Dickens *et al.*, 1997).

Membrane-bound flotillins are part of the family of scaffold proteins. Flotillins preferentially localize in the lipid rafts of eukaryotic cells (Babuke & Tikkanen, 2007; Morrow & Parton, 2005; Otto & Nichols, 2011; Stuermer, 2011; Zhao *et al.*, 2011), in which a large number of proteins related to signal transduction and membrane trafficking concentrate (Simons & Ikonen, 1997). Thus, it is believed that the scaffold activity of flotillin may recruit proteins that must be localized in lipid rafts to be active and may facilitate their interaction and oligomerization (Babuke & Tikkanen, 2007; Morrow & Parton, 2005; Otto & Nichols, 2011; Stuermer, 2011; Zhao *et al.*, 2011). Consequently, flotillins play a central role in the organization of the multi-component protein reactions that are harboured in the lipid rafts (Babuke & Tikkanen, 2007; Stuermer, 2011; Zhao *et al.*, 2011) and their perturbation affects the functionality of numerous raft-associated signal transduction pathways (Bodrikov *et al.*, 2011; Chen

Abbreviations: β-gal, β-galactosidase; B3H, bacterial three-hybrid; BN, blue native; BTH, bacterial two-hybrid; CFP, cyan fluorescence protein; DDM, *n*-dodecyl-β-D-maltoside; FMM, functional membrane microdomain; MW, molecular mass

Three supplementary tables and five supplementary figures are available with the online Supplementary Material.

et al., 2006; Hattori *et al.*, 2006; Marin *et al.*, 2013; Schneider *et al.*, 2008).

We recently showed that bacteria organize many signal transduction cascades and multi-protein reactions in functional membrane microdomains (FMMs) (López & Kolter, 2010b) that are functionally and structurally similar to the lipid rafts of eukaryotic cells (Simons & Ikonen, 1997). FMMs are discrete membrane regions enriched in polyisoprenoid lipids and bacterial flotillin proteins (Tavernarakis *et al.*, 1999). Bacterial flotillins seem to play a similar role to eukaryotic flotillins, acting as scaffold proteins and favouring the recruitment of FMM-associated proteins to promote interactions and oligomerization (Good *et al.*, 2011; Langhorst *et al.*, 2005). The bacterial model *Bacillus subtilis* is currently the best-established cellular system to explore the biological significance of FMMs in prokaryotic membranes (Bach & Bramkamp, 2013; Dempwolff *et al.*, 2012a; Donovan & Bramkamp, 2009; López & Kolter, 2010b; Mielich-Süss *et al.*, 2013; Yepes *et al.*, 2012). The FMMs of *B. subtilis* contain two different flotillin-like proteins, FloT and FloA, similar to the eukaryotic flotillins FLO-1 and FLO-2 (Bramkamp & Lopez, 2015; Stuermer & Plattner, 2005; Zhao *et al.*, 2011). Flotillins, including those found in *B. subtilis*, present a membrane-anchoring N-terminal region (Bach & Bramkamp, 2015) and the so-called PHB domain (*p*ro*hib*itin domain), which appears important for the functionality of flotillins although its precise role is still unknown (Bach & Bramkamp, 2015; Tavernarakis *et al.*, 1999). FloT was the first flotillin-like protein discovered in bacteria (Tavernarakis *et al.*, 1999) and further experimental studies have demonstrated its association with FMMs in *Bacillus halodurans* (Zhang *et al.*, 2005). Moreover, FloT has a heterogeneous distribution in discrete puncta across the bacterial membrane and was found to influence sporulation in *B. subtilis*, as cells lacking FloT showed reduced sporulation efficiency (Donovan & Bramkamp, 2009). FloT is co-localized with FloA in FMMs, which also cluster other proteins related to signal transduction and cell–cell communication (López & Kolter, 2010b). Consequently, a flotillin-defective *B. subtilis* strain showed severe impairments in biofilm formation, sporulation, activation of natural competence and motility, suggesting that the scaffold activity of flotillin is important for the correct functionality of many signalling transduction pathways that are associated with FMMs (Bach & Bramkamp, 2013; Dempwolff *et al.*, 2012a; Donovan & Bramkamp, 2009; López & Kolter, 2010b; Mielich-Süss *et al.*, 2013; Yepes *et al.*, 2012).

One of the first signalling transduction pathways found in association with the FMMs of *B. subtilis* was the route to biofilm formation that is triggered by the membrane-bound sensor kinase KinC. KinC is one of the five sensor kinases (KinA–E) that phosphorylate the master regulator Spo0A responsible for biofilm formation in *B. subtilis*, by transferring a phosphoryl-group to Spo0A via a Spo0F/Spo0B phosphorelay system (Jiang *et al.*, 2000; LeDeaux *et al.*, 1995). The activation of the KinA–E kinases is driven by the action of specific signals of unknown nature (López & Kolter, 2010a; McLoon *et al.*, 2011; Shemesh & Chai, 2013). However, it was recently discovered that KinC responds to a particular type of membrane damage that is caused by a battery of small molecules, including the self-produced molecule surfactin (López *et al.*, 2009, 2010). The presence of surfactin activates KinC, and phosphorylates Spo0A with subsequent activation of the signalling pathway for biofilm formation (López *et al.*, 2009, 2010). In order to sense surfactin, KinC must be localized in the FMMs of *B. subtilis* where it co-localizes with FloT and FloA (López & Kolter, 2010b). Moreover, deletion of *floT* and *floA* genes results in mis-localization of KinC and also abrogates KinC activity, which prevents the flotillin-defective strain from expressing matrix genes and forming a biofilm in response to the signal surfactin (López & Kolter, 2010b).

The study of scaffold proteins, and more precisely bacterial flotillins, is relatively new and there are numerous questions that need to be answered to fully understand their biological significance. One of the most interesting questions in relation to prokaryotic flotillins is how these proteins benefit the interaction of specific protein components. It is currently believed that scaffold proteins coordinate the physical assembly of protein interaction partners (Good *et al.*, 2011) thereby increasing local concentrations of these proteins and, thus, the likelihood of interaction of components (Lingwood & Simons, 2010; Michel & Bakovic, 2007). However, the role of bacterial flotillins over their interacting partners, such as KinC, has yet to be elucidated.

In this study, we used a biochemical approach to provide unambiguous evidence for the influence of the scaffold activity of FloT on the interaction of KinC and other membrane-bound sensor kinases of *B. subtilis*. First, we used protein–protein interaction experiments to demonstrate that FloT strongly binds to KinC and to KinD to a lesser extent. Second, we showed that the interaction of FloT with KinC promotes more efficient oligomerization of KinC and, therefore, the assembly of the active dimeric form of this kinase. At the same time, FloT inhibited non-specific aggregation of KinC with other kinases and prevented the titration of the activity of this kinase via formation of dead-end intermediates. In summary, flotillins facilitated specific interaction of signalling proteins and prevented the formation of non-active intermediates.

METHODS

Strains, media and culture conditions. All bacterial strains used in this study are listed in Table S1 available in the online Supplementary Material. *B. subtilis* NCIB 3610 was used in all experiments unless otherwise stated (Branda *et al.*, 2001). *Escherichia coli* strain BTH101 was used in all experiments unless otherwise stated (Karimova *et al.*, 1998). *E. coli* strain DH5α (Reusch *et al.*, 1986) was used for cloning purposes. Cells were usually propagated in Luria–Bertani (LB)

medium containing ampicillin (100 μg ml^{-1}), kanamycin (50 μg ml^{-1}) or gentamicin (2 and 10 μg ml^{-1}) when required.

Generation of labelled strains of *B. subtilis*. Translational fusions P_{hp}FloT–His6 and P_{hp}KinC–CFP (*c*yan fluorescence protein) were constructed by long flanking homology PCR and subsequently cloned into the plasmids pKM003 and pDR183, respectively. P_{hp} is an IPTG-inducible promoter. Primers are listed in Table S2; plasmids are listed in Table S3. These plasmids allowed the integration of the constructs into the bacterial genome at the *lacA* and *amyE* loci, respectively. The translational fusions were expressed under the control of an IPTG-inducible promoter (Britton *et al.*, 2002; Erwin *et al.*, 2005; Nakano *et al.*, 2003). Linearized vectors were added to *B. subtilis* 168 cells grown in competence-inducing conditions. The constructs were integrated into the bacterial genome at the *amyE* and *lacA* loci. Double recombination occurred at the *amyE* locus when using the plasmid pKM003 or the *lacA* locus when using the plasmid pDR183. Cells were plated on corresponding selective media and colonies were checked for integration of constructed fusions by colony PCR. SPP1 phage transduction was used to transfer constructs from *B. subtilis* 168 to WT NCIB 3610, according to Yasbin & Young (1974).

Cell fractionation. Cell fractionation was performed as described by Yepes *et al.* (2014). Samples of 100 ml of cultures were harvested and cells were lysed in 25 ml SMM buffer (1 M sucrose, 0.04 M maleic acid, 0.04 M $MgCl_2$, pH 6.5) and supplemented with lysozyme (10 μg ml^{-1}) prior to sonication (four series of 12 pulses, power output 0.7 and cycle 50 %). After cell disruption, a centrifugation step (11 000 ***g*** for 10 min at 4 °C) separated the cell debris (pellet) from the total cell extract fraction. We collected the total cell extract fraction and purified the membrane fraction using ultracentrifugation (100 000 ***g*** for 1 h at 4 °C). The membrane fraction was then precipitated and solubilized in 3 ml Tris buffer [20 mM Tris/HCl (pH 7.5), 150 mM NaCl, 1 % DDM (*n*-dodecyl β-maltoside), 1 mM PMSF].

Pull-down analysis. Pull-down assays were performed using Ni-NTA resin (Qiagen) and samples were kept at 4 °C throughout the assays. The membrane fractions of the different mutants were resuspended in 7 ml binding buffer (50 mM Tris/HCl, 500 mM NaCl, 10 % glycerol, v/v, 20 mM imidazole, 1 % Tween, pH 8). Proteins (100 mg membrane per strain) were bound to 200 μl of the resin at 4 °C overnight. In order to remove unspecific binding, the resin was washed twice with wash buffer A (50 mM Tris/HCl, 500 mM NaCl, 10 % glycerol, v/v, 20 mM imidazole, pH 8) and twice with wash buffer B (same as wash buffer A but with 50 mM imidazole). His-tagged proteins were eluted using elution buffer that contained a high concentration of imidazole (50 mM Tris/HCl, 500 mM NaCl, 10 % glycerol, v/v, 500 mM imidazole). Proteins from the eluted fractions were precipitated by adding 10 % trichloroacetic acid to the sample. The protein sample was resuspended in Tris buffer (50 mM Tris/HCl).

Western blot analysis and immunodetection. Immunoblotting was carried out as previously described (Koch *et al.*, 2014). Total protein (80 μg) was separated using 12 % SDS-polyacrylamide gel. Proteins were transferred from the gel to a PVDF membrane using semi-dry blotting for 1.5 h. After blotting, the membrane was blocked with 10 % skimmed milk for 1 h and probed with 1 : 4000 diluted anti-CFP tag antibody (Living Colours) to detect the presence of KinC–CFP. Proteins were detected after incubation with the secondary antibody anti-rabbit IgG-HRP (Bio-Rad) diluted 1 : 20 000, using a chemiluminescent substrate kit (Thermo Scientific). Chemiluminescence was recorded with the Illumination System ImageQuant LAS4000 (General Electric).

Bacterial two-hybrid analysis. To perform bacterial two-hybrid (BTH) analysis, the coding sequences of *floT* and the sensor kinases were amplified from the *B. subtilis* NCIB 3610 genome and cloned in-frame into the BTH expression vectors. Sanger sequencing was used to verify that resultant colonies contained the plasmids (primers are listed in Table S2). *floT* was cloned into the pKNT25 plasmid whereas the sensor kinases were cloned into the pUT18 plasmid (EuroMedex) (Karimova *et al.*, 1998). Pairwise combinations of plasmids that expressed FloT and a sensor kinase were cotransformed in *E. coli* BTH101 strain, which harbours a *lacZ* gene under the control of a cAMP-inducible promoter. Upon interaction, the T25 and T18 catalytic domains of the adenylate cyclase form an active enzyme leading to the production of cAMP and hence to the expression of the reporter (Karimova *et al.*, 1998). Positive cells turn blue in the presence of X-Gal. Protein interaction assays were performed following the protocol previously described by Karimova *et al.* (1998). Plates were incubated for 48 h at 30 °C. pKT25-zip and pUT18C-zip served as positive controls, and the empty vectors pKNT25 and pUT18C were negative controls. For quantitative measurements, β-galactosidase (β-gal) activity was determined. The transformants were grown for 48 h at 30 °C in LB medium supplemented with ampicillin (100 μg ml^{-1}) and kanamycin (50 μg ml^{-1}). Optical density at 600 nm was determined before cells were permeabilized using chloroform and 0.01 % SDS. β-Gal activity was measured according to Miller (1972) and results are represented in Miller units.

Bacterial three-hybrid (B3H) analysis. To assay the scaffold activity of FloT, the kinase genes *kinB*, *kinC* and *kinD* were PCR-amplified and cloned into the plasmids pKNT25 and pUT18 (Karimova *et al.*, 1998). Cells were plated in LB medium with 100 μg ampicillin ml^{-1} and 50 μg kanamycin ml^{-1}, and Sanger sequencing was used to verify that resultant colonies contained the plasmids. These strains were used to perform protein–protein interaction assays following the protocol of Karimova *et al.* (1998) to determine the interaction efficiency among sensor kinases. Moreover, the strains were subsequently used to propagate pSEVA modulable plasmids (Silva-Rocha *et al.*, 2013) that produced different levels of FloT. We specifically used pSEVA-621 (2 μg gentamicin ml^{-1}), pSEVA-631 (10 μg gentamicin ml^{-1}) and pSEVA-641 (10 μg gentamicin ml^{-1}) plasmids to produce FloT at different concentrations. These plasmids contain distinct replication origins (RK2, pBR101 and pRO1600, respectively) and propagate in *E. coli* at low, medium and high copy numbers, respectively (Silva-Rocha *et al.*, 2013). This generates low, medium and high concentrations of FloA and FloT in the in BTH *E. coli* strains in which the plasmids were propagated. Experiments that required the propagation of pSEVA vectors were performed in LB medium with 100 μg ampicillin ml^{-1}, 50 μg kanamycin ml^{-1} and 2–10 μg gentamicin ml^{-1}. Miller units were quantified to monitor the efficiency of protein interactions, as described by Miller (1972).

Native PAGE. Native PAGE was performed under non-denaturing conditions adapted from standard protocols (Life Technologies). DDM (1 %)-solubilized membrane samples were equilibrated in Tris/glycine native sample buffer and run on an 8 % polyacrylamide gel. Electrophoresis was performed under non-denaturing conditions using a Tris/glycine-buffered system and run for 1 h at 150 V, followed by 1 h at 250 V.

Blue native (BN)-PAGE. Strains were streaked on LB agar and used to inoculate 100 ml liquid MSgg medium supplemented with 1 mM IPTG. Cultures were incubated overnight at 37 °C with agitation (200 r.p.m.). Cells were collected by centrifugation and membrane fractions were isolated as described above. Membranes were dissolved in 1 % DDM and prepared for BN-PAGE according to the manufacturer's protocol (Life Technologies). Briefly, membranes were dissolved in supplied BN-PAGE buffer containing 1 % DDM for 30 min on ice. Undissolved material was removed by centrifugation at 20 000 ***g*** at 4 °C for 30 min. Dissolved membrane proteins were

supplemented with Coomassie G-250 and mounted on a 4–20 % BN-PAGE gradient gel and run for 1 h at 150 V, followed by 1 h at 250 V.

Immunoblotting. Native gels were used for standard immunoblotting procedures without further processing. To unfold native proteins and expose hydrophobic sites after blotting, PVDF membranes were fixed with 8 % acetic acid, air-dried and rewetted with methanol. CFP-tagged KinC was detected using a polyclonal antibody against CFP diluted 1 : 5000 (Living colours).

Biofilm formation and sporulation assays. A detailed scheme for the procedure to biofilm formation is shown in Fig. S1. Briefly, the strains were grown overnight on LB agar. The next day, serial passaging of cells was performed in LB medium. Bacteria were grown in exponential phase for many generations to reduce the levels Spo0A, which remained activated from stationary phase cells that grew overnight. Cells with lowly activated Spo0A background were used to inculate MSgg medium. LB cultures were washed and cells dispersed in fresh MSgg medium to an OD_{600}=1.0. The cell dispersion (20 µl) was used to inoculate 1 ml MSgg medium that was placed in 24-well plates and incubated at 30 °C overnight. To perform the sporulation assay, MSgg cultures were normalized in OD_{600}. Vegetative cells were killed by incubating samples at 80 °C for 30 min. Serial dilutions were plated and c.f.u. were examined.

Fluorescence microscopy. MSgg culture (1 ml) was pelleted, cells were resuspended in 500 µl paraformaldehyde (4 %) and incubated for 7 min at room temperature to effect fixation. Samples were washed in PBS buffer and were finally mounted on microscope slides with thin agarose pads (0.8 % agarose in PBS). Images were taken on a Leica DMI6000B inverted microscope equipped with a Leica CRT6000 illumination system, a HCX PL APO oil immersion objective with × 100 1.47 magnification, a Leica DFC630FX colour camera and an environment control system. A BP480/40 excitation filter and a BP527/30 emission filter were used to detect GFP by applying excitation times between 100 and 200 ms, while transmitted light images were taken at 36 ms exposure. Leica Application Suite Advanced Fluorescence v3.7 was used to process raw data, and fluorescence signals were deconvoluted using AutoQuant software (MediaCybernetics). Further processing of images and calculation of Pearson's correlation coefficient were performed using ImageJ.

RESULTS

FloT physically interacts with KinC in *B. subtilis*

To explore the interaction affinity that exists between FloT and the membrane-bound sensor kinase KinC of *B. subtilis*, we attempted to co-purify FloT with KinC directly from the cell extracts of *B. subtilis* using a pull-down assay. To do this, we constructed a double-labelled strain of *B. subtilis* that expressed an IPTG-inducible His^6-tagged variant of FloT and a CFP-tagged variant of KinC (FloT–His^6 KinC–CFP double-labelled strain). Single-labelled strains harbouring FloT–His^6 and KinC–CFP constructs were used as control strains. We first tested whether the expression levels of FloT and KinC in the constructed strains were within a physiological range. To do this, we used Western blot analysis to compare the relative expression levels of FloT–His^6 and KinC–CFP under the control of their natural promoters and IPTG-inducible promoters. Using a Δ*kinC* mutant as genetic background, our results showed that the IPTG-inducible promoter expressed KinC–CFP approximately 10-fold higher than WT expression levels (Fig. 1a). Similarly, the Western blot analyses performed in the Δ*floT* mutant showed approximately 10-fold higher expression FloT–His^6 when expressed under the control of an IPTG-inducible promoter in comparison with the WT promoter (Fig. 1a). It is known that higher expression levels of FloT do not affect

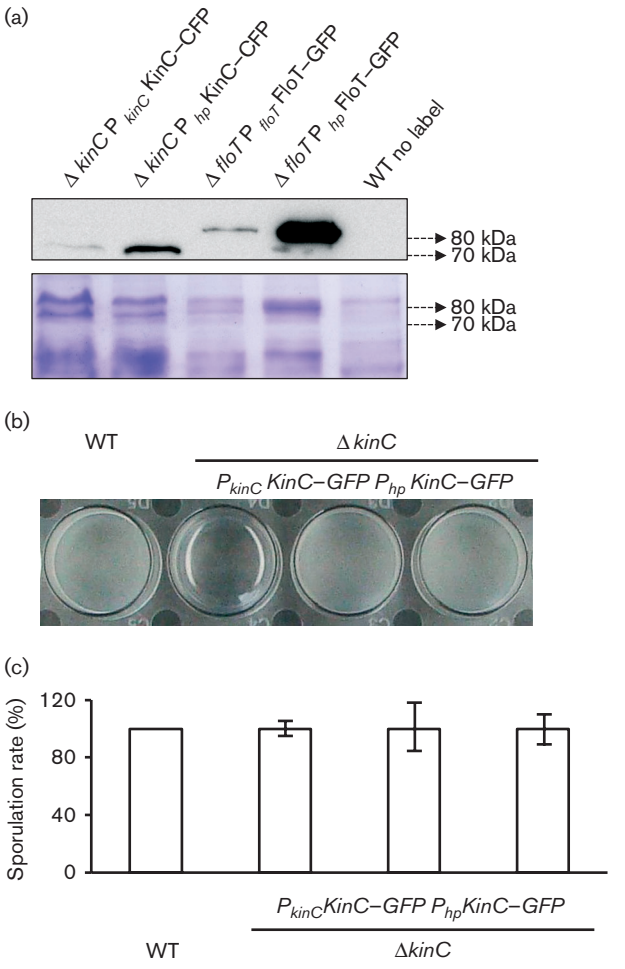

Fig. 1. Overexpression of physiologically relevant levels of KinC. (a) Immunoblot detection of native and induced levels of KinC–CFP (left lanes) and FloT–GFP (right lanes) in *B. subtilis*. Native promoters are represented by P_{kinC} and P_{floT}, respectively. IPTG-inducible promoter is represented by P_{hp}. Right lane is unlabelled WT strain that served as negative control. SDS-PAGE is shown as the loading control. (b) Pellicle formation assay in different genetic backgrounds. The KinC-deficient strain is unable to form pellicles. Complementation of the Δ*kinC* mutant with a KinC–GFP translational fusion recovered the ability to form pellicles to WT levels. Expression of KinC–GFP under the native or IPTG-induced promoter did not affect pellicle formation. Pellicle formation assay was performed in MSgg medium. Cultures were allowed to grow at 30 °C overnight. A more detailed protocol for the pellicle formation assay is described in Fig. S1.(c) Sporulation rate in Δ*kinC* mutant and complemented strains is similar to WT levels. Cultures were grown in MSgg medium at 30 °C overnight.

the physiology of *B. subtilis* (Mielich-Süss *et al.*, 2013). Yet, we ran additional experiments to determine whether the higher expression levels of KinC affect the physiology of this bacterium. We performed biofilm formation and sporulation assays of the strains that expressed WT levels of KinC–CFP and higher levels of KinC–CFP. After overnight incubation in MSgg medium, the WT strain was able to form a pellicle on the top of the culture that was not detected in the KinC mutant (Branda *et al.*, 2001; López *et al.*, 2009) (Fig. 1b). When the Δ*kinC* mutant was complemented with a copy of KinC expressed under the control of its own promoter, we observed recovery of pellicle formation to levels comparable to the WT strain (Fig. 1b). Furthermore, the Δ*kinC* mutant complemented with a copy of KinC expressed via the IPTG-inducible promoter showed recovery of pellicle formation to levels similar to those of the WT strain and the Δ*kinC* mutant complemented with the WT promoter of KinC–CFP (Fig. 1b). In addition to these results, we did not detect any alteration in the sporulation rate in all the strains tested (Fig. 1c). Altogether, these results suggest that the higher expression level of KinC and FloT in our system does not alter the physiology of *B. subtilis*.

The FloT–His^6 KinC–CFP double-labelled strain and FloT–His^6 and KinC–CFP single-labelled strains were grown to stationary phase in LB medium and their membrane fraction was purified and solubilized using 0.2 % DDM. This detergent treatment allows disaggregation of the membrane without affecting the oligomerization of protein complexes (Casey & Reithmeier, 1993). The samples were loaded onto a column of nickel-charged resin (Qiagen) that selectivity binds His^6-tagged proteins and the proteins that are directly or indirectly bound to them. The pool of proteins bound to the resin was eluted from the column using an imidazole-containing buffer and run in a SDS-PAGE (Fig. 2a). The Coomassie-stained gel showed a protein band attributable to FloT–His^6 in the lane that corresponded to the FloT–His^6 KinC–CFP double-labelled strain. The protein band migrated to approximately 57 kDa molecular mass (MW), which is the MW expected for FloT–His^6. Moreover, the protein band was detected in the lane of the FloT–His^6 single-labelled control strain. This indicates that the purification of FloT was performed successfully. Additionally, the lane of the FloT–His^6 KinC–CFP double-labelled strain showed extra protein bands that were concentrated enough to be detected in the Coomassie-stained gel. These extra bands located at approximately 80 kDa, which is the putative MW of KinC–CFP (Fig. 1a, red asterisk). Given that these protein bands were not detected in the lanes of the FloT–His^6 and KinC–CFP single-labelled strains, it is likely that these proteins were coeluted with FloT–His^6.

We performed immunoblotting to semiquantitatively detect the presence of KinC–CFP in the samples, using polyclonal antibodies against the CFP epitope. We detected a signal attributable to KinC–CFP in the positive control sample that contained the purified membrane fraction of KinC–CFP labelled cells (Fig. 2b). In contrast, the elution fraction of the KinC–CFP single-labelled strain showed no detectable signal, suggesting that KinC–CFP did not bind to the resin column in a non-specific manner (Fig. 2b). Moreover, the elution fraction of the FloT–His^6 single-labelled strain showed no detectable

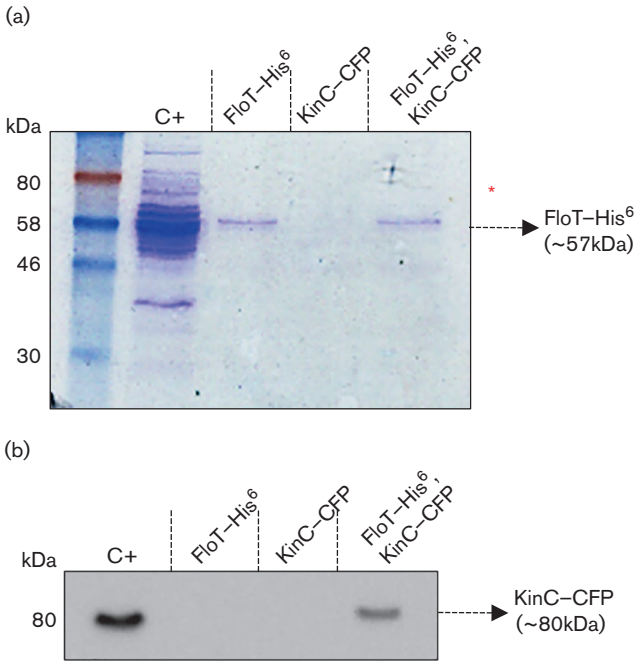

Fig. 2. KinC physically interacts with FloT in *B. subtilis* membranes. (a) Coomassie-stained SDS-PAGE of the distinct pulled-down protein samples. Positive control (C+) is the WT membrane fraction. The elution fraction from the FloT–His^6 single-labelled strain was loaded into the FloT–His^6 lane. The elution fraction from the KinC–CFP single-labelled strain was loaded into the KinC–CFP lane. Lane FloT–His^6, KinC–CFP is the elution fraction from the FloT–His^6 KinC–CFP double-labelled strain. The arrow indicates the presence of a band with the size predicted for FloT–His^6.The red asterisk indicates the presence of extra protein bands in C+ and FloT–His^6, KinC–CFP lanes with the size predicted for KinC–CFP. (b) Western blot assay using polyclonal antibodies against CFP to detect the presence of the KinC–CFP translational fusion in protein samples pulled down with the FloT–His^6 translational fusion. The arrow indicates the presence of a band with the size predicted for KinC–CFP. Positive control (C+) is the WT membrane fraction. Lane KinC–CFP is the elution fraction from a nickel-charged column loaded with a sample of the membrane fraction from the KinC–CFP single-labelled strain. In the absence of FloT–His^6, KinC–CFP does not bind to the column. Lane FloT–His^6 is the elution fraction from the membrane fraction of a FloT–His^6 single-labelled strain. No signal is detected in the absence of KinC–CFP. Lane FloT–His^6, KinC–CFP is the elution fraction from the membrane fraction of a FloT–His^6 KinC–CFP double-labelled strain. This lane shows a band with a MW attributable to KinC–CFP, according to the C+ lane.

signal, which is indicative that the signal we detected by immunoblotting was attributable to KinC–CFP (Fig. 2b). Importantly, a fluorescence band attributable to KinC–CFP was detected in the eluted fraction of the column of the FloT–His^6 KinC–CFP double-labelled strain (Fig. 2b), suggesting that KinC–CFP co-eluted with FloT–His^6. This result indicates the existence of a physical interaction between FloT and KinC in *B. subtilis* cells.

FloT interacts with KinC in a selective fashion

Having determined that FloT interacted with KinC, we investigated whether the interaction was specific or whether, in contrast, FloT was able to interact with other different membrane-bound sensor kinases. We used a BTH assay, in which FloT was tagged to the T25 catalytic domain of an adenylate cyclase and a pool of different membrane-associated sensor kinases of *B. subtilis* were tagged to the T18 catalytic domain of the adenylate cyclase. We selected a pool of structurally different membrane-bound sensor kinases that represent the structural diversity of sensor kinases that exists in *B. subtilis* membranes (Fig. S2). Upon interaction of FloT with a sensor kinase, the two catalytic domains of the adenylate cyclase reconstitute the entire enzyme (Karimova *et al.*, 1998). A fully active adenylate cyclase produces cAMP, which accumulates in the cytoplasm of the cell and triggers the expression of a cAMP-inducible *lacZ* reporter gene that is integrated in the chromosome of the cells (Karimova *et al.*, 1998).

The BTH assay revealed a strong positive interaction signal between FloT and KinC and to a lesser extent with the sensor kinases ResE and KinD (Fig. 3a). The BTH assay did not show an interaction signal between FloT and the rest of the selected membrane-bound sensor kinases (Fig. 3a), which indicates the existence of a specific interaction signal between flotillin and some sensor kinases. FloT–KinC, FloT–KinD and FloT–ResE interaction signals were detected in solid agar medium supplemented with X-Gal (50 μM) (Fig. 3a). These results are consistent with previously published experiments that demonstrate that KinC and ResE are part of the protein cargo of the FMMs of *B. subtilis* (López & Kolter, 2010a; Schneider *et al.*, 2015). ResE is part of the ResD–ResE two-component regulatory system that activates the *res* regulon under oxygen-limiting conditions and triggers the expression of genes responsible for nitrate respiration (Baruah *et al.*, 2004; Geng *et al.*, 2007; Nakano *et al.*, 1996, 1999; Nakano & Zhu, 2001). KinC and KinD are two of the five sensor kinases (KinA–E) that phosphorylate Spo0A in *B. subtilis* (Jiang *et al.*, 2000; LeDeaux *et al.*, 1995). Because KinB did not show any interaction signal with FloT under the conditions tested, it seems that the interaction of FloT with the pool of membrane-bound kinases that activate the Spo0A is predominantly with KinC and to a lesser extent with KinD.

To quantitatively determine the level of interaction between FloT and the pool of sensor kinases, cultures of these strains were grown in LB medium and the cell extracts were used to determine β-gal activity. Instructions of the manufacturer define a signal as positive if the β-gal activity is above the threshold of 700 Miller units (Karimova *et al.*, 1998). Consistently, the interactions that had negative results in solid agar plus X-Gal were also negative according to the β-gal assay (<400 Miller units) (Fig. 3b). Likewise, the interaction of FloT with KinC exhibited a strong interaction signal in the β-gal assay (>3500 Miller units) (Fig. 3b), greater than the interaction signal of FloT with ResE and KinD (~1600 and 1100 Miller units, respectively) (Fig. 3b). Based on these results, the interaction between FloT and KinC is the strongest interaction we detected using a heterologous system.

To validate the abovementioned results, we used a BTH assay to quantitatively determine several already-reported interactions of proteins with FloT in *B. subtilis* (Fig. 3c). Specifically, the membrane-bound AAA protease FtsH is known to physically interact with FloT (Bach & Bramkamp, 2013; Schneider *et al.*, 2015; Yepes *et al.*, 2012). Likewise, Bach & Bramkamp (2013) recently reported that the second flotillin of *B. subtilis*, FloA, strongly interacts with FloT. In contrast, the same report identified a pool of proteins that do not interact with FloT. Among those proteins are the RNA polymerase RpoA and the citrate synthase CitZ proteins. Both proteins are indeed cytoplasmic proteins and, therefore, it is not surprising that they did not show an interaction with FloT. Accordingly, we performed BTH assays to test the interaction between FloT and the interacting proteins FtsH and FloA. We used a similar approach to test whether FloT interacts with non-interacting proteins such as RpoA and CitZ in our BTH assay. The BTH assay showed interaction signals between FloT and FtsH, and between FloT and FloA, which were confirmed using a β-gal quantification assay (Fig. 3c, d). Moreover, we did not detect any interaction signal between FloT and the non-interacting proteins RpoA or CitZ (Fig. 3c, d). Thus, the interaction pattern of FloT in our BTH assay is in agreement with the data that has already been reported.

Having validated our BTH results to those published in the literature, we performed a number of experiments to determine the topology and relative expression levels of FloT and KinC in the BTH assay in comparison with the endogenous expression of the protein in *B. subtilis* cells. While it has already been published that the subcellular distribution pattern of FloT in *E. coli* is similar to the original pattern in *B. subtilis* cells (Schneider *et al.*, 2015), we performed additional experiments to test whether there exists any alternation in the subcellular distribution pattern of KinC when expressed in *E. coli*. *E. coli* cells labelled with the translational fusion KinC–CFP were analysed under a fluorescence microscope. The distribution of the fluorescence signal was detected in several discrete puncta across the cellular membrane, similar to the subcellular distribution pattern reported for KinC in *B. subtilis* (Fig. S3). Moreover, we performed immunoblot assays to determine if the relative protein expression levels of KinC and FloT in *B. subtilis* cells were comparable to those in the

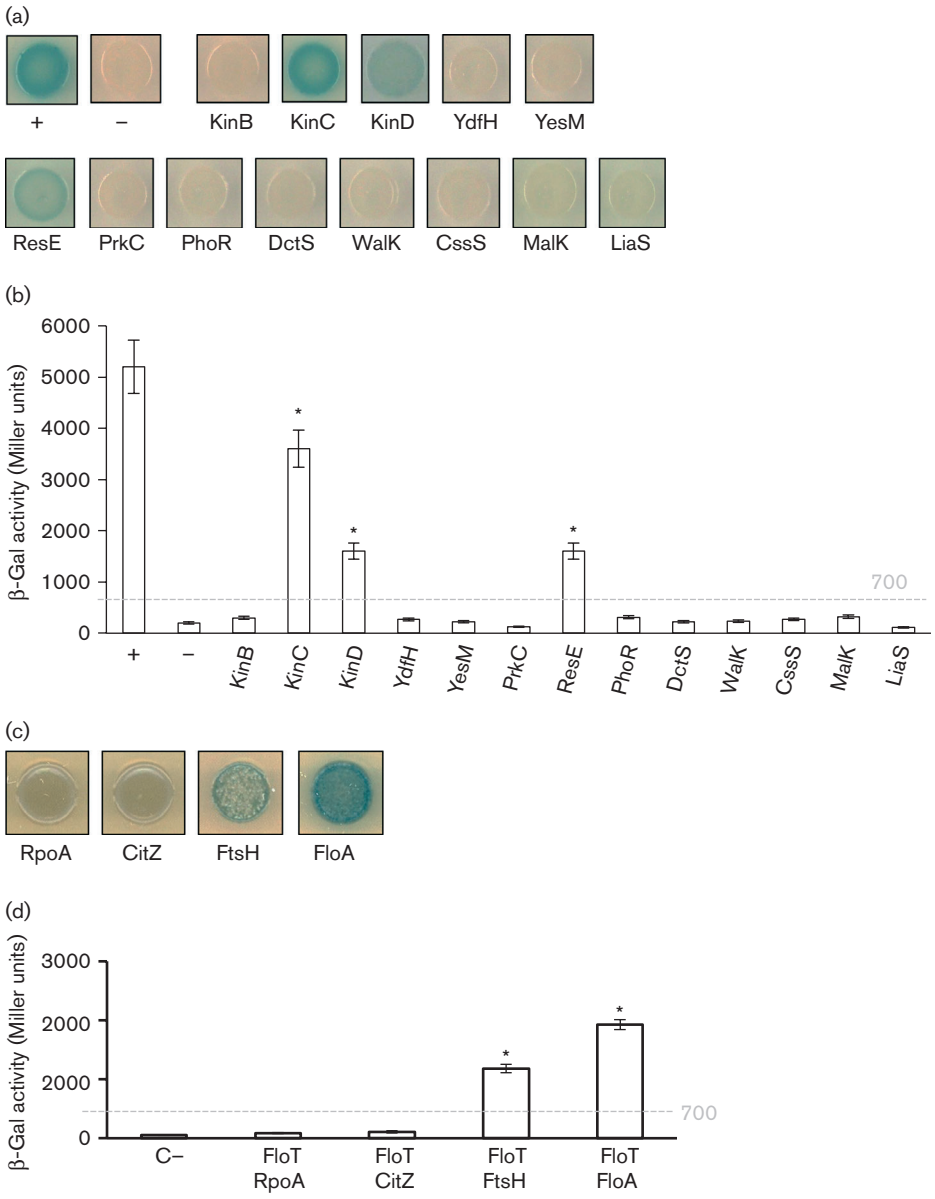

Fig. 3. Interaction affinity of FloT to several membrane-bound sensor kinases of *B. subtilis*. (a) BTH analysis to study the interactions between FloT and a pool of selected membrane-bound sensor kinases of *B. subtilis*. Interaction activates *lacZ* and this degrades X-Gal; the product of the degradation is blue. The two cytoplasmic domains of a leucine-zipper represent a positive control (pKT25-zip + pUT18C-zip). The negative control is represented by the strains harbouring empty plasmids (pKNT25 + pUT18). (b) Quantitative β-gal activity assay of the BTH system. Degradation of the substrate ONPG by β-gal generates a reaction product that can be monitored using a colorimetric assay. The activity of the enzyme is represented in Miller units. Dashed line indicates the threshold limit that defines a positive ($\geqslant$700 Miller units) or a negative interaction signal ($\leq$700 Miller units) according to the instructions of the manufacturer (EuroMedex). Results represent a mean of three independent experiments. Statistical analysis was performed using Student's *t*-test. An asterisk denotes $P \leq 0.05$. The positive control is represented by a strain harbouring two cytoplasmic domains of a leucine-zipper protein that are known to interact (pKT25-zip and pUT18C-zip). The negative control strain harbours empty plasmids (pKNT25 and pUT18). (c) BTH qualitative analysis to study the interactions between FloT and selected proteins known to interact with FloT (FtsH and FloA) and known to not interact with FloT (RpoA and CitZ). (d) BTH quantitative analysis of the interactions between FloT and proteins known to interact with FloT (FtsH and FloA) and known to not interact with FloT (RpoA and CitZ). The β-gal activity of the enzyme is represented in Miller units. Dashed line indicates the threshold limit that defines a positive ($\geqslant$700 Miller units) according to the instructions of the manufacturer (EuroMedex). C−, negative control.

4

heterologous system. WT, Δ*kinC* P_{kinC}KinC–CFP and Δ*floT* P_{floT}FloT–GFP strains were grown in MSgg medium, the proteins from the membrane fraction were purified and equal concentrations of the protein samples were resolved in SDS-PAGE. Immunoblot detection of the fluorescence protein was performed using commercially available polyclonal antibodies. We detected a signal attributable to KinC–CFP in the Δ*kinC* P_{kinC}KinC–CFP lane and a signal attributable to FloT–GFP in the Δ*floT* P_{floT}FloT–GFP lane. No signal was detected in the WT lane that was used as negative control. We detected a higher concentration of FloT than KinC in *B. subtilis* cells in a relation of approximately 10 : 1 (Fig. 4a). Next, we expressed KinC–CFP and FloT–His^6 using the same heterologous system that we used to perform the BTH assay. *E. coli* strains expressing KinC and FloT were grown in LB medium, the proteins from the membrane fraction were purified and equal concentrations of the protein samples were resolved in SDS-PAGE. Immunoblot detection of the proteins expressed revealed that FloT is expressed at a higher concentration than KinC and that the relative expression level of these two proteins in *E. coli* is approximately 6 : 1 (Fig. 4b). In summary, both expression systems produced significantly more FloT than KinC and showed close relative expression levels.

FloT facilitates the oligomerization of KinC

How does the scaffold activity of FloT influence the activity of KinC? The most direct hypothesis is that scaffold proteins promote the stability of protein complexes through tethering of interacting partners and increasing the likelihood of interaction (Good *et al.*, 2011). To investigate the effect of FloT on the oligomerization of KinC, we used a BTH assay that quantitatively monitored the homo-dimerization of KinC under increasing concentrations of FloT (henceforth referred to as B3H assay). First, we semiquantitatively determined the homo-oligomerization capacity of KinC using a BTH assay. We detected a positive interaction signal between KinC proteins (~1500 Miller units; Fig. 3c), which points to the hypothesis that KinC is prone to self-interact and oligomerize in our heterologous system. Next, the BTH assay that tested the interaction efficiency of KinC–KinC was supplemented with a pSEVA modulable vector system (Silva-Rocha *et al.*, 2013) (Fig. 5a). In pSEVA vectors, a FloT–His^6 tagged variant was cloned under the expression of its own promoter in a suite of vectors that contained distinct replication origins and, therefore, replicated at different copy numbers (Fig. 5a). This generated several B3H strains that produced lower, medium and higher levels of FloT as a direct function of the copy number of *floT* gene (Fig. 5a). We performed Western blot analyses to semiquantitatively confirm the concentration of FloT in the B3H strains generated, using antibodies against the His^6 epitope. The KinC–KinC strain carrying a lower-copy plasmid showed lower concentration of FloT (Fig. 5b). The KinC–KinC strain that carried a medium-copy plasmid showed medium concentration of FloT (Fig. 5b), and the strain that carried a high-copy plasmid showed higher concentration of FloT (Fig. 5b).

When we assayed the interaction affinity of KinC–KinC in the presence of distinct concentrations of FloT, the B3H assay showed no improvement in the interaction efficiency of KinC with lower concentration of FloT. Self-interaction of KinC improved significantly with medium concentration of FloT and showed some decrease with higher concentration of FloT (Fig. 5c). These results are consistent with the typical

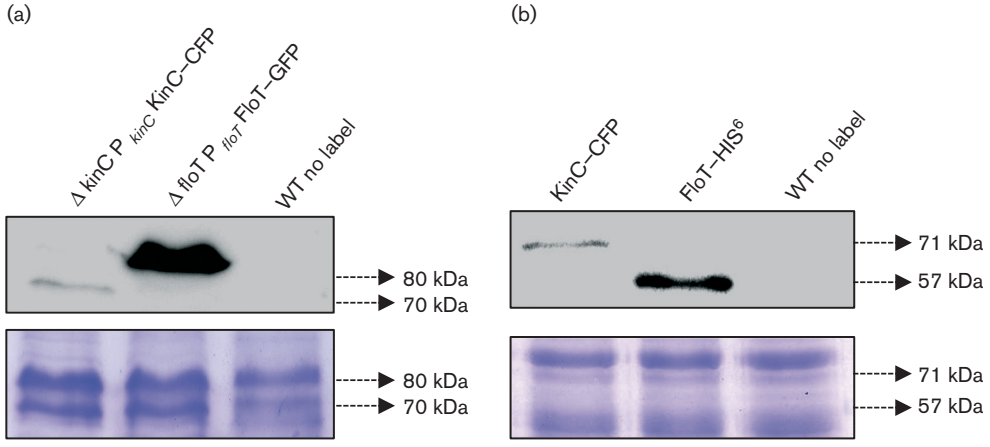

Fig. 4. KinC/FloT relative expression is comparable in *B. subtilis* and in the BTH assay. (a) Immunoblot detection of relative levels of KinC–CFP (left lane) and FloT–GFP (centre lane) in *B. subtilis* under the expression of their native promoters. Right lane is unlabelled WT strain that served as negative control. SDS-PAGE is shown as the loading control. (b) Immunoblot detection of relative levels of KinC–CFP (left lane) and FloT–His^6 (centre lane) in *E. coli* BTH strains under the expression of inducible promoters. Right lane is unlabelled WT strain that served as negative control. SDS-PAGE is shown as the loading control.

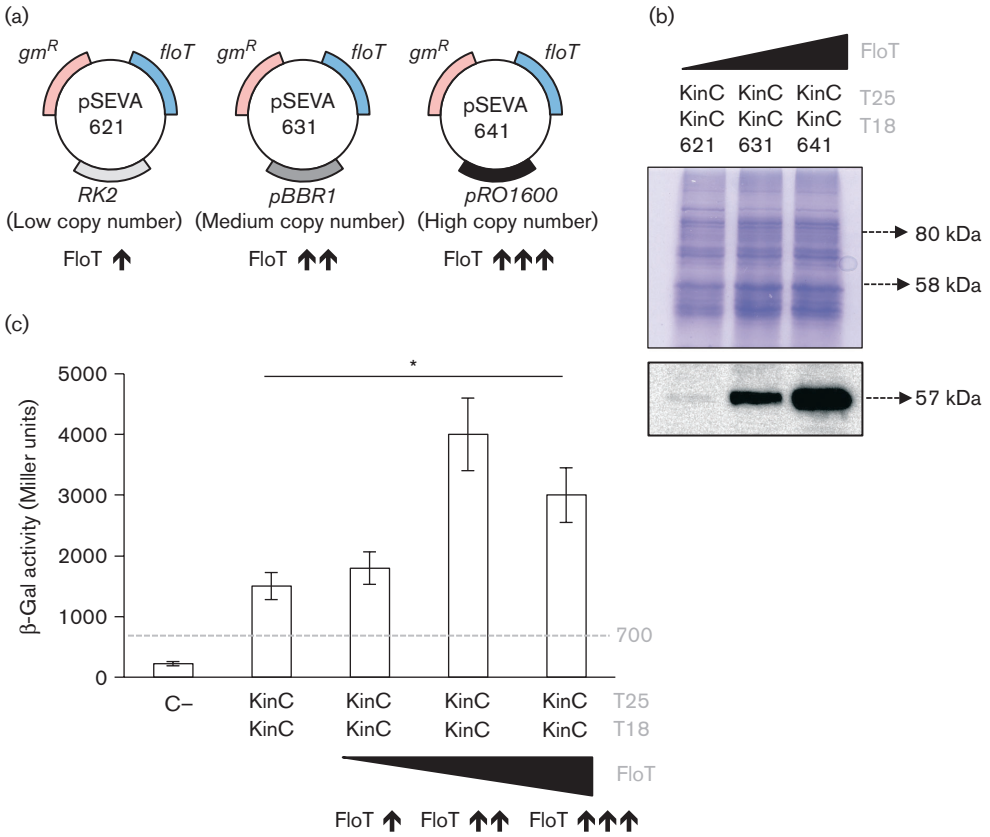

Fig. 5. The presence of FloT favours the self-interaction of KinC. (a) Schematic representation of the three different pSEVA plasmids that were used to express FloT at different concentration levels. pSEVA 621, 631 and 641 maintain similar backbones and contain a gene that provides resistance to gentamicin (gm^R) and the construct FloT–His^6.The plasmids carry a different replication origin. pSEVA 621 carries the low-copy-number replication origin RK2.pSEVA 631 carries the medium-copy-number replication origin pBR1.pSEVA 641 carries the high-copy-number replication origin pRO1600.The strains that carry each of these plasmids produce FloT at different concentration levels, in direct function of the number of *floT* genes that are expressed in the strain. (b) Immunoblot analysis showing the distinct concentrations of FloT that were produced in B3H cells when carrying lower- (pSEVA-621), medium- (pSEVA-631) and high-copy (pSEVA-641) plasmids expressing His^6-tagged FloT. Strains produced lower (↑), medium (↑ ↑) and higher (↑ ↑ ↑) concentrations of FloT in the B3H assay, respectively. SDS-PAGE is shown as the loading control. (c) B3H assay to quantify the interaction of KinC under different concentrations of FloT. Dashed line indicates the threshold limit that defines a positive (⩾700 Miller units) or a negative interaction signal (⩽700 Miller units) according to the instructions of the manufacturer. Results represent a mean of three independent experiments (*Student's *t*-test, $P \leq 0.05$). C−, negative control.

limitation of the activity of scaffold proteins that has been described in other systems (Good *et al.*, 2011; Levchenko *et al.*, 2000). It is known that optimal concentration of the scaffold protein is necessary to efficiently tether interaction partners while higher concentrations of scaffolds titrate interacting partners into separate complexes, thus inhibiting their interaction (Good *et al.*, 2011; Levchenko *et al.*, 2000). This effect has been demonstrated experimentally in the scaffold protein Ste5 in yeast (Chapman & Asthagiri, 2009) and the JIP1 scaffold of human cells (Dickens *et al.*, 1997). Our results support the hypothesis that FloT acts as typical scaffold protein to tether KinC interaction partners and promote its homo-oligomerization, similar to results reported for other scaffold proteins.

FloT does not facilitate oligomerization of non-interacting kinases

Our heterologous systems showed that FloT interacted slightly with KinD and did not interact with KinB (Fig. 3). To better understand the mechanism of action of FloT, we semiquantitatively determined the homo-oligomerization capacity of these two kinases using a B3H assay. We hypothesized that KinB–KinB interaction efficiency should not be affected by

the presence of FloT. In contrast, the interaction efficiency of KinD–KinD should show a similar pattern to the one observed with KinC–KinC. Indeed, our BTH assay showed interaction signals between KinB–KinB (~ 5500 Miller units) and KinD–KinD (~ 1500 Miller units) (Fig. 6a–d), suggesting that KinB and KinD are able to self-interact in our heterologous system.

To investigate whether FloT affects the homo-oligomerization of KinB and KinD, we generated a B3H assay to test the interaction efficiency of these kinases in the presence of increasing concentrations of FloT. We generated a number of B3H strains that, according to our immunoblot detection assay, produced lower, medium and higher levels

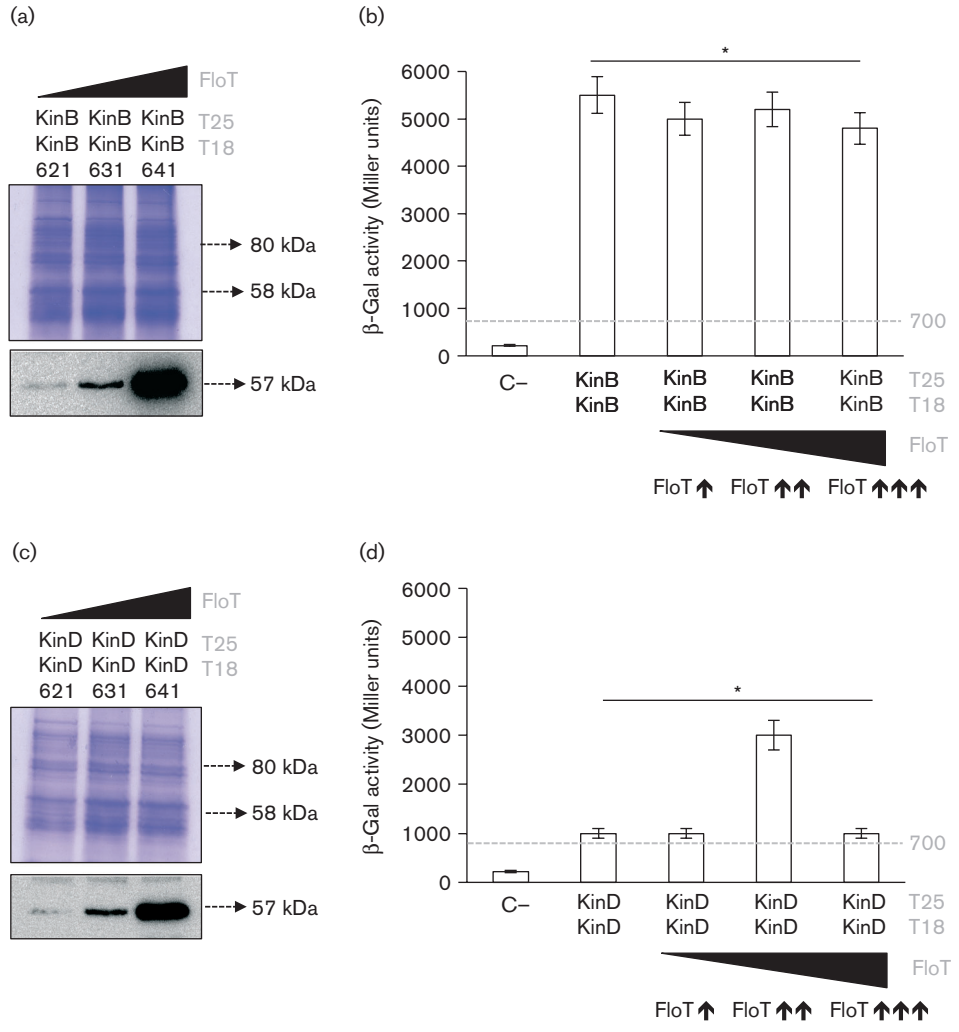

Fig. 6. FloT disfavours self-interaction of KinB but favours self-interaction of KinD. (a) B3H assay showing interaction of KinB under different concentrations of FloT. Immunoblot analysis showing the distinct concentrations of FloT that were produced in B3H cells carrying lower- (pSEVA-621), medium- (pSEVA-631) and high-copy (pSEVA-641) plasmids expressing His^6-tagged FloT. Strains produced lower (↑), medium (↑ ↑) and higher (↑ ↑ ↑) concentrations of FloT in the BTH assay, respectively. SDS-PAGE is shown as the loading control. (b) B3H assay to quantify the interaction of KinB under different concentrations of FloT. Dashed line indicates the threshold limit that defines a positive (⩾700 Miller units) or a negative interaction signal (⩽700 Miller units) according to the instructions of the manufacturer. Results represent a mean of three independent experiments (*Student's *t*-test, $P \leq 0.05$). (c) B3H assay showing interaction of KinD under different concentrations of FloT. Immunoblot analysis showing the distinct concentrations of FloT that were produced in B3H cells carrying lower- (pSEVA-621), medium- (pSEVA-631) and high-copy (pSEVA-641) plasmids expressing His^6-tagged FloT. Strains produced lower (↑), medium (↑ ↑) and higher (↑ ↑ ↑) concentrations of FloT in the B3H assay, respectively. SDS-PAGE is shown as the loading control. (d) B3H assay to quantify the interaction of KinD under different concentrations of FloT. Dashed line indicates the threshold limit that defines a positive (⩾700 Miller units) or a negative interaction signal (⩽700 Miller units) according to the instructions of the manufacturer. Results represent a mean of three independent experiments (*Student's *t*-test, $P \leq 0.05$). C−, negative control.

of FloT (Fig. 6a, c). There was no improvement in the interaction efficiency of the KinB–KinB interaction in B3H strains at any concentration of FloT tested. This suggests that oligomerization of KinB occurs in a very efficient manner in the absence of FloT and the presence of FloT does not improve the interaction efficiency of this kinase. In contrast, when we tested the KinD–KinD interaction in the B3H strains, we observed no improvement in interaction efficiency at the lower concentration of FloT but significant improvements at the medium concentration of FloT. Similar to the results for KinC, a higher concentration of FloT resulted in a significant decrease in the interaction efficiency of the KinD–KinD interaction (Fig. 6c, d), according to the typical limitation of the activity of scaffold proteins and their capacity to titrate reaction components at higher concentrations (Good *et al.*, 2011; Levchenko *et al.*, 2000).

FloT prevents unspecific interactions of KinC

One of the most important roles of scaffold proteins is to physically interact with specific proteins by guiding the assembly of proteins into productive complexes to prevent unproductive interactions, such as non-specific aggregation and the formation of dead-end intermediates (Daley, 2008). Our B3H assay provided us with an interesting approach to explore whether FloT favoured interaction specificity and prevented non-specific aggregation with other proteins. We tested interaction efficiency of KinC with KinB and KinD in the presence and absence of FloT. If interactions were detected, we assumed they were the consequence of non-specific aggregation. Given that, with a few exceptions in which hetero-associations between histidine kinases have been reported (Goodman *et al.*, 2009), sensor kinases generally show a preference for homo-oligomerization (Laub & Goulian, 2007).

Using a BTH assay, we detected a significant interaction signal between KinC and KinB and also between KinD and KinB (Fig. 7a, b). We did not detect any interaction signal between KinC and KinD. The interactions were assayed in both solid agar medium supplemented with X-Gal (50 μM) [Fig. 7a(i), b(i), c(i)] and β-gal activity from LB liquid cultures ($\sim$1100 and 900 Miller units for KinC–KinB and KinD–KinB interactions, respectively) [Fig. 7a(ii), b(ii), c(ii)]. The KinC–KinD interaction showed a negative detection signal of approximately 400 Miller units, similar to the value observed in the negative control (Fig. 7c). Therefore, it is possible that KinB has a non-specific preference for aggregation with KinC and KinD in this heterologous system.

We next investigated whether FloT played any role in preventing the formation of non-specific aggregates between KinB and KinC. We hypothesized that the selective binding of FloT to KinC may protect KinC from non-specific aggregation and unproductive titration. To explore this hypothesis, we generated a B3H assay to test the interaction efficiency of KinC–KinB under increasing concentrations of FloT. Our immunoblot detection assays showed that the strains produced increasing levels of FloT, using antibodies against the His^6 epitope (Fig. 8a). When we assayed the interaction affinity of KinC and KinB in the B3H assay, we observed a significant decrease in the interaction signal in the presence of medium and higher concentrations of FloT (Fig. 8b), suggesting that the presence of increasing concentrations of FloT inhibited non-specific aggregation of KinC. Likewise, we used a B3H assay to test the role of FloT in preventing non-specific aggregation of KinB and KinD (Fig. 8c, d). The interaction signal was also significantly decreased in presence of low concentration of FloT, similar to that observed with the KinB–KinC interaction. Furthermore, we semiquantitatively determined the efficiency of oligomerization between KinC and KinD using a B3H assay. As these proteins showed no interaction affinity, the B3H assay demonstrated that the presence of increasing concentrations of FloT did not affect this negative interaction (Fig. S4). Overall, our biochemical approach showed that FloT prevented the formation of non-productive intermediates of its interaction partners and also prevented the titration of these proteins in the formation of non-specific aggregates.

The interaction pattern of KinC is altered in a flotillin-deficient *B. subtilis*

We were interested in exploring the influence of flotillins on the oligomerization of KinC in *B. subtilis* cells. The B3H assay showed that the presence of FloT favours more efficient homo-oligomerization of KinC. Thus, we hypothesized that *B. subtilis* cells lacking flotillins would show a different pattern of oligomerization of KinC compared with WT cells. We explored this hypothesis by comparing the different oligomeric states of KinC in WT cells and flotillin-deficient *B. subtilis* cells. To perform this experiment, we used a *B. subtilis* strain lacking the two flotillins, FloA and FloT, since it is known that flotillins play redundant roles and *B. subtilis* could compensate for the absence of one flotillin with the overproduction of the other flotillin (López & Kolter, 2010b). Using this approach, a CFP-tagged version of KinC was expressed in *B. subtilis* WT and flotillin-deficient mutants. The membrane fraction was collected and solubilized using 1 % DDM. The samples were resolved using native PAGE (Wittig & Schägger, 2005, 2008). This technique of protein separation is capable of resolving proteins of a broad range of MW, from individual proteins to protein complexes and supercomplexes. Proteins are resolved based on their charge to mass ratios and maintain the protein conformation and biological activity while achieving higher sensitivity of protein detection in later steps using immunoblot analysis. We used native PAGE to resolve membrane extracts of WT cells. Immunoblot detection showed two important detection signals that were attributable to the different oligomeric states of KinC (Fig. 9a,b). Importantly, membrane extracts from the Δ*floAT* mutant were resolved in native PAGE and immunoblot detection performed to

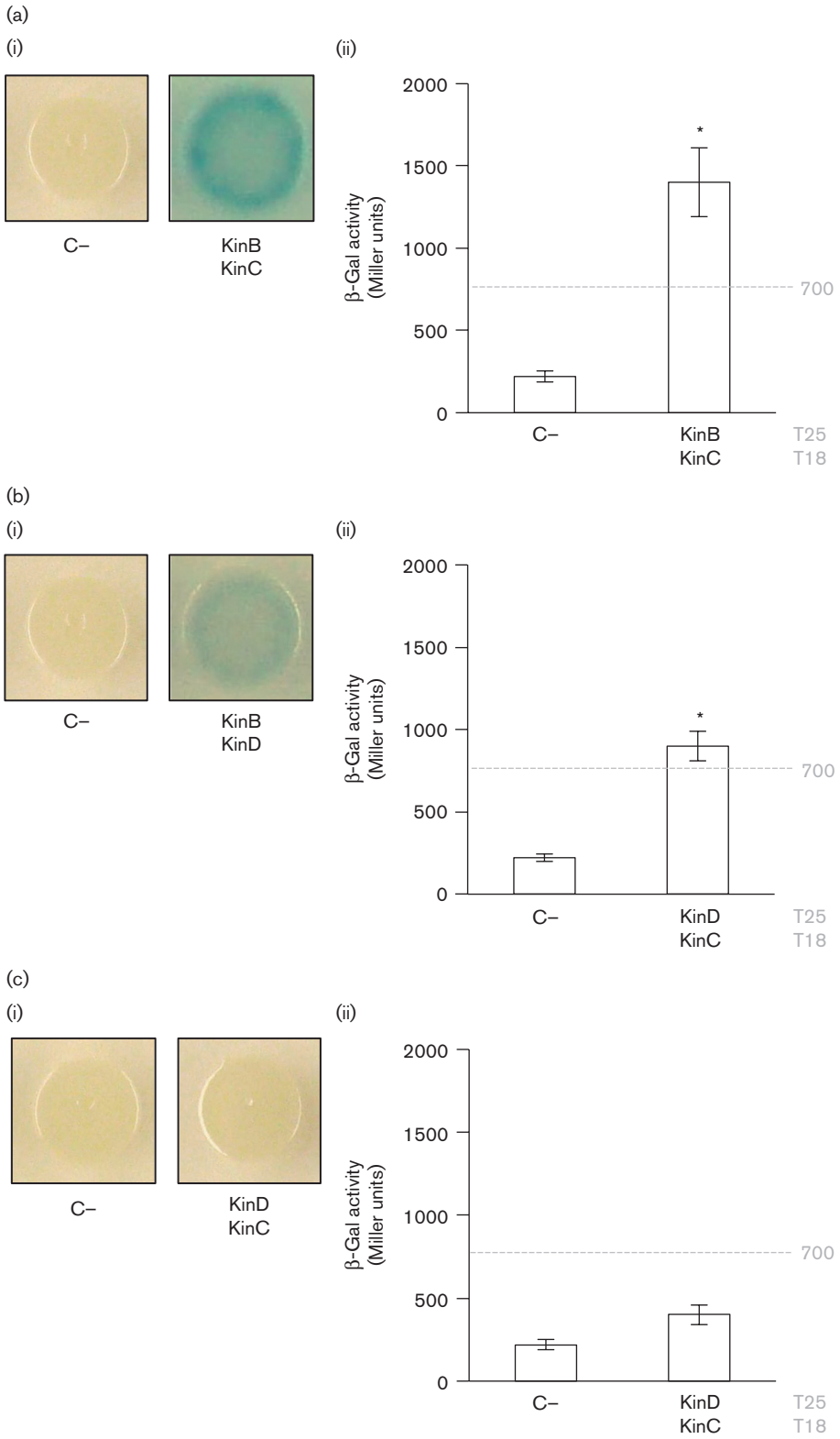

Fig. 7. KinB aggregates with KinC and KinD in a non-specific manner. [a(i)] BTH analysis to study the interactions between KinC and KinB. Interaction activates *lacZ*, which degrades the substrate X-Gal; the degradation product is blue. (ii) Quantitative β-gal activity assay of the BTH system. The activity of the enzyme is represented in Miller units. Dashed line indicates the threshold limit that defines a positive (⩾700 Miller units) or a negative interaction signal (⩽700 Miller units) according to the instructions of the manufacturer. Results represent a mean of three independent experiments (*Student's *t*-test, $P \leq 0.05$). 7

[b(i)] BTH analysis to study the interactions between KinB and KinD. (ii) Quantitative β-gal activity assay of the BTH system. The activity of the enzyme is represented in Miller units. Results represent a mean of three independent experiments (*Student's *t*-test, $P \leq 0.05$). [c(i)] BTH analysis to study the interactions between KinC and KinD. (ii) Quantitative β-gal activity assay of the BTH system. The activity of the enzyme is represented in Miller units. Results represent a mean of three independent experiments (*Student's *t*-test, $P \leq 0.05$).

detect KinC. The extracts from the Δ*floAT* mutant showed one single detection signal of KinC attributable to the lower MW signal that occurred in WT samples, suggesting that the higher MW oligomeric state of KinC is compromised in the absence of flotillin in *B. subtilis* cells.

While protein resolution in native PAGE allows a more sensitive detection of the proteins of interest, the resolution of proteins depends on the intrinsic charge of the protein, which prevents a precise estimation of the MW of the resolved protein complexes. Because of this, the samples were also resolved using BN-PAGE. BN-PAGE allows the separation of the membrane-bound protein complexes in their native state (Wittig *et al.*, 2006). This approach for protein resolution is less sensitive than native PAGE but it confers the advantage that proteins are resolved based on a charge shift, which allows an estimation of the MW of the resolved oligomeric proteins. Our BN-PAGE assays used a polyacrylamide gradient of 4–20 % to allow the resolution of membrane-bound protein complexes with a MW up to 1000 kDa (Fig. S5). BN-PAGE coupled with immunoblotting, using antibodies against the CFP tag, was used to identify a number of membrane-associated protein complexes that contained KinC. Using this approach, we also detected two important detection signals in the membrane extracts of WT cells that were attributable to the different oligomeric states of KinC (Fig. S5a). These two detection signals had MW of approximately 80 kDa and 160 kDa (Fig. S5b). Given that the MW of KinC–CFP is approximately 80 kDa, we hypothesized that the two detection bands represented the monomeric and the dimeric state of KinC in *B. subtilis*. This is consistent with mounting evidence demonstrating that sensor kinases require dimerization to become active (Capra & Laub, 2012; Krell *et al.*, 2010). We did not detect any additional detection signal beyond a tentative dimeric state of KinC, which suggests that the dimeric form of KinC was the most abundant oligomeric state of KinC in the membrane of *B. subtilis* under the conditions tested. In contrast, membrane extracts of the flotillin-deficient mutants showed one single signal attributable to the monomeric state of KinC–CFP (Fig. S5b). Furthermore, this approach does not allow detection of the KinC : KinC–CFP heterodimer due to the lower concentration of KinC in *B. subtilis*, which prevents the detection of KinC–CFP that is bound to KinC using this approach. The abrogation of detection signal for KinC oligomerization in flotillin-deficient cells is consistent with our hypothesis that flotillin plays an important role in facilitating the dimerization and thus, the activation of KinC in *B. subtilis*.

DISCUSSION

Scaffold proteins play an important role in controlling and regulating the assembly of interacting protein components in both eukaryotic and prokaryotic life (Bashor *et al.*, 2008; Bhattacharyya *et al.*, 2006; Chapman & Asthagiri, 2009; Dueber *et al.*, 2009; Good *et al.*, 2011; Levchenko *et al.*, 2000; Milano *et al.*, 2002; Park *et al.*, 2003). However, a question that remains to be answered is how scaffold proteins tether specific protein components and how this benefits the interaction of these components. In this study, we investigated the scaffold activity of the membrane-bound flotillin protein FloT of the bacterium *B. subtilis*. The genetic tractability of bacterial systems allowed us to dissect precisely the molecular mechanism underlying the interaction of scaffold proteins with their interaction partners. Flotillin is a scaffold protein typically found in the lipid rafts of eukaryotic cells (Bickel *et al.*, 1997; Dermine *et al.*, 2001; Lang *et al.*, 1998) but also in the FMMs of bacteria, which are structurally and functionally similar to eukaryotic lipid rafts (Bramkamp & Lopez, 2015). Our relatively simple biochemical approaches demonstrated that the flotillin protein FloT of *B. subtilis* behaves in a similar way to other scaffold proteins described in eukaryotic cells, by specifically increasing the interaction efficiency of interaction partners at lower concentrations, or titrating and preventing the interaction of the same interaction partners at higher concentrations (Chapman & Asthagiri, 2009; Dickens *et al.*, 1997; Good *et al.*, 2011; Levchenko *et al.*, 2000). This raises the possibility that flotillin proteins of eukaryotic lipid rafts behave like typical scaffold proteins, similar to the bacterial flotillins that we describe in this study.

One of the interaction partners of FloT in *B. subtilis* is the membrane-bound sensor kinase KinC. In this study, we used a pull-down assay coupled to a BTH assay to show that FloT physically binds to and interacts with KinC. This interaction is consistent with previous publications showing that KinC is one of the proteins harboured in the FMMs of *B. subtilis* along with FloT (López & Kolter, 2010b). KinC could be an interaction partner of the second flotillin, FloA, that is harboured in the FMMs of *B. subtilis*. However, we performed BTH analyses to test this particular interaction and results were inconclusive, suggesting that the study of FloA–KinC interaction may require a different biochemical approach. Interestingly, our BTH assay showed a newly discovered interaction between FloT and the sensor kinase KinD (Banse *et al.*, 2011). It is not surprising that FloT interacts with and mediates the activity of other sensor kinases in *B. subtilis* membranes, given that the activity of many different cellular processes, such as biofilm formation,

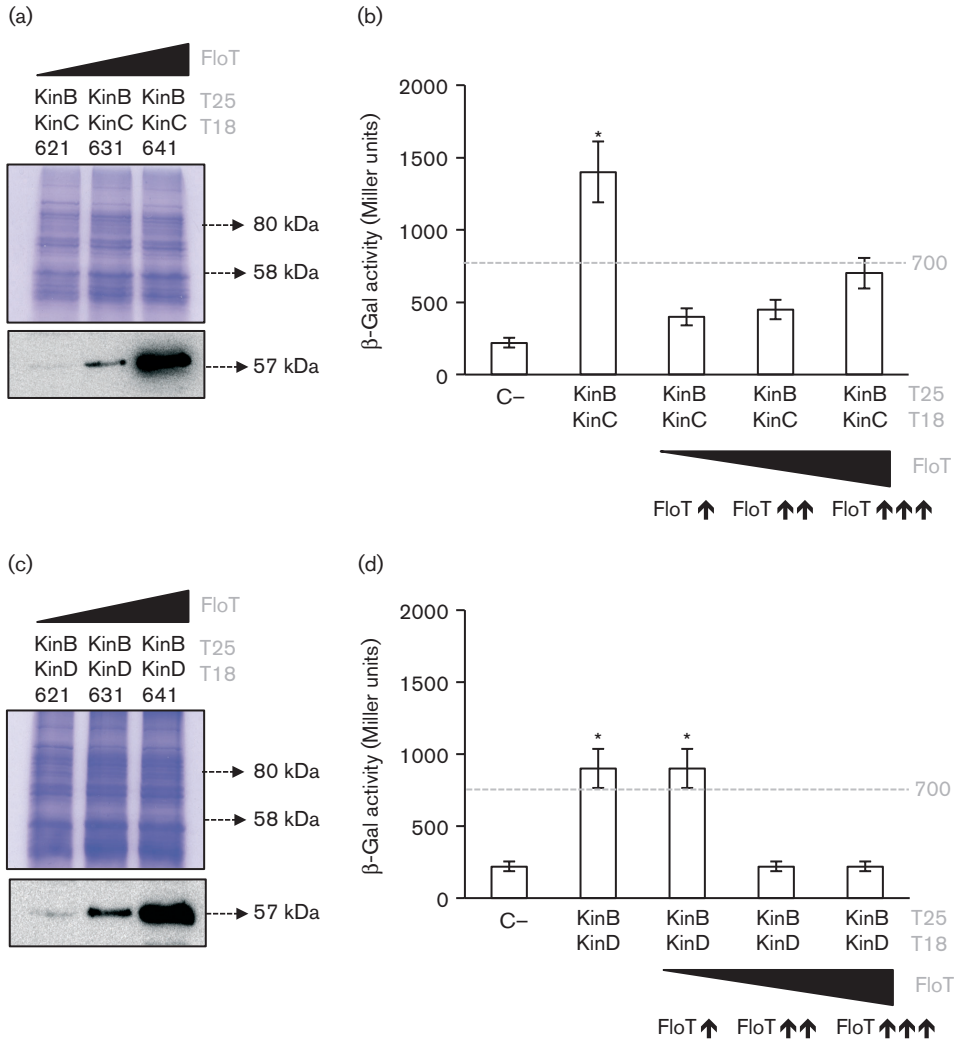

Fig. 8. The presence of FloT prevents unspecific aggregation of KinB with KinC and KinD. (a) B3H assay showing aggregation of KinB with KinC under different concentrations of FloT. Immunoblot analysis showing the distinct concentrations of FloT that were produced in B3H cells carrying lower- (pSEVA-621), medium- (pSEVA-631) and high-copy (pSEVA-641) plasmids expressing His^6-tagged FloT. Strains produced lower (↑), medium (↑ ↑) and higher (↑ ↑ ↑) concentrations of FloT in the B3H assay, respectively. SDS-PAGE is shown as the loading control. (b) B3H assay to quantify KinB–KinC aggregation under different concentrations of FloT. Dashed line indicates the threshold limit that defines a positive (⩾700 Miller units) or a negative interaction signal (≤700 Miller units) according to the instructions of the manufacturer. Results represent a mean of three independent experiments (*Student's *t*-test, $P \leq 0.05$). (c) B3H assay showing aggregation of KinB with KinD under different concentrations of FloT. Immunoblot analysis showing the distinct concentrations of FloT that were produced in B3H cells when carrying lower, medium and high-copy plasmids expressing His^6-tagged FloT. Strains produced lower (↑), medium (↑ ↑) and higher (↑ ↑ ↑) concentrations of FloT in the BTH assay, respectively. SDS-PAGE is shown as the loading control. (d) B3H assay to quantify KinB–KinD aggregation under different concentrations of FloT. Results represent a mean of three independent experiments (*Student's *t*-test, $P \leq 0.05$).

motility, competence, protease secretion, antibiotic resistance and sporulation is affected in *B. subtilis* cells lacking flotillin (Bach & Bramkamp, 2013, 2015; Dempwolff *et al.*, 2012a, b; Donovan & Bramkamp, 2009; Huang *et al.*, 1997, 1998, 1999; Lee *et al.*, 2012; López & Kolter, 2010b; Mann *et al.*, 2013; Mielich-Süss *et al.*, 2013; Yepes *et al.*, 2012) (Fig. S4).

Furthermore, the B3H assay that we designed to test the scaffold activity of FloT shows an increase in the efficiency of KinC–KinC and KinD–KinD interactions in the presence of lower and medium concentrations of FloT. Dimerization is commonly required for bacterial sensor kinases to become active (Capra & Laub, 2012; Krell *et al.*, 2010). Thus, it is possible that the scaffold activity of FloT

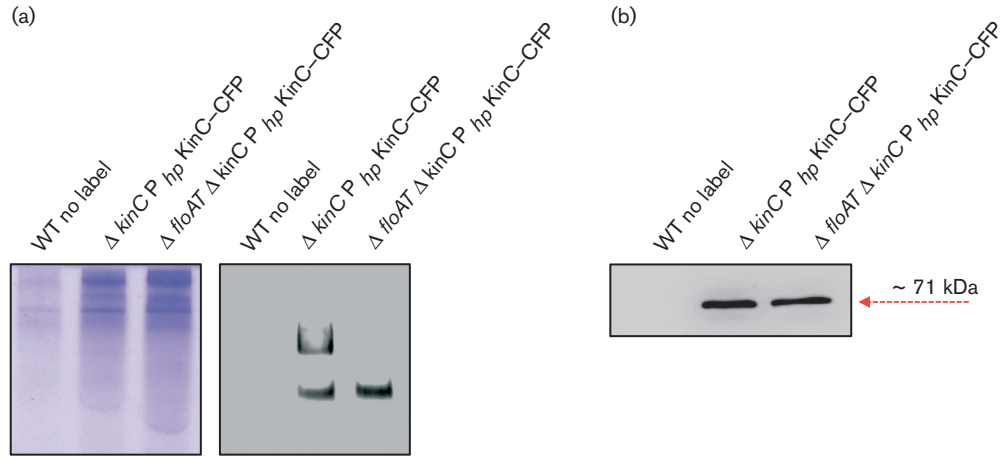

Fig. 9. The oligomerization pattern of KinC is different in *B. subtilis* cells lacking flotillin. (a) Native PAGE to resolve the membrane fraction of *B. subtilis* cells. Left lane is unlabelled WT strain that served as negative control. The coomassie-stained gel is shown as loading control (left panel). DDM-solubilized membrane samples from different genetic backgrounds were run on an 8 % polyacrylamide gel in a Tris/glycine buffered system. Higher-state KinC oligomers do not form in the absence of flotillins. The Δ*kinC* P_{hp}KinC–CFP lane resolves the membrane fraction of a complemented strain labelled with the KinC–CFP translational fusion. The Δ*floAT* Δ*kinC* P_{hp}KinC–CFP lane resolves the membrane fraction of a clean-off flotillin double mutant complemented strain that is labelled with the KinC–CFP translational fusion. Right panel shows an immunoblot detection assay of KinC–CFP using antibodies against CFP, to detect the oligomeric states of KinC in the different genetic backgrounds. (b) Immunoblot detection of KinC–CFP of different genetic backgrounds after SDS-PAGE.

facilitates the dimerization of KinC and KinD. However, while the activity of scaffold proteins assists in the interaction of protein partners, scaffold proteins are not absolutely required for the activity of proteins. Thus, the oligomerization efficiency of protein partners may vary with different experimental conditions (Devi *et al.*, 2015). We have shown that FloT benefited the interaction of KinC under two experimental conditions: in a heterologous system and also directly in *B. subtilis* membranes. BN-PAGE coupled to immunoblotting suggested that KinC preferentially formed dimers similar to the majority of sensor kinases (Capra & Laub, 2012; Krell *et al.*, 2010) and dimerization was abrogated in flotillin-defective cells. It has recently been suggested that KinC is capable of forming tetramers using a soluble variant of KinC that lacks the N-terminal membrane-anchoring region (Devi *et al.*, 2015). However, using a membrane-associated KinC we found that KinC preferred dimerization under our test conditions. We cannot rule out the possibility that tetramerization occurs in a discrete fraction of KinC that we were not able to detect in our assay, but the majority of the membrane-associated KinC oligomerized in a dimeric form under the conditions we tested.

The co-localization of KinC with FloT on the FMMs may increase dimerization of KinC. Additionally, localization of KinC within the FMMs may protect KinC from non-specific aggregation with other membrane proteins. In this study, we used a BTH assay to show that the KinC and KinD were able to interact with KinB, a membrane sensor kinase that is not associated with FMMs. These types of interactions are unlikely to occur in a specific fashion but rather as consequence of unspecific aggregation, given that sensor kinases show a strong preference for homo-oligomerization (Laub & Goulian, 2007), with a few exceptions in which hetero-oligomerization has been reported (Goodman *et al.*, 2009). Interestingly, the presence of FloT prevented non-specific aggregation of KinC and KinD, probably by interfering with non-specific binding. However, these results should be interpreted cautiously, as this protein–protein interaction approach used a heterologous system with limitations that prevent us from predicting whether this type of interaction occurs in *B. subtilis* cells. Our results raise the intriguing possibility that flotillins may play a dual role in bacterial cells, not only promoting the interaction of specific interacting protein partners but also preventing non-specific interactions that may titrate protein partners and reduce their efficiency in the activation of their respective signal transduction cascades (Fig. 8).

The scaffold activity of FloT over the physical assembly of KinC adds to other recent examples in which scaffold proteins participate in coordinating the assembly of two-component signal transduction pathways in bacteria. For instance, the universal stress protein UspC acts as a scaffold protein of the KdpDE two-component signal cascade in *E. coli*, which responds to potassium uptake under potassium-limiting growth conditions (Heermann *et al.*, 2009). Likewise, the scaffold activity of ApsX in *Staphylococcus aureus* facilitates the assembly of the ApsSR (*a*ntimicrobial *p*eptide *s*ensor) two-component signal transduction cascade that responds to cell

wall stress (Li *et al.*, 2007). Additionally, the protein CheW scaffolds the assembly of the basic structural unit for bacterial chemotaxis along with the chemotaxis kinase CheA and chemoreceptors (Li & Hazelbauer, 2011; Underbakke *et al.*, 2011). Overall, scaffold proteins seem to play an important role in bacterial signal transduction.

Acknowledgements

This work was funded by the European Research Council ERC-StG 335568-BacRafts and BFU2014-55601-P (MINECO, Spain). B. M.-S. was supported by a grant of the German Excellence Initiative to the Graduate School of Life Sciences, University of Würzburg.

References

Babuke, T. & Tikkanen, R. (2007). Dissecting the molecular function of reggie/flotillin proteins. *Eur J Cell Biol* **86**, 525–532.

Bach, J. N. & Bramkamp, M. (2013). Flotillins functionally organize the bacterial membrane. *Mol Microbiol* **88**, 1205–1217.

Bach, J. N. & Bramkamp, M. (2015). Dissecting the molecular properties of prokaryotic flotillins. *PLoS One* **10**, e0116750.

Banse, A. V., Hobbs, E. C. & Losick, R. (2011). Phosphorylation of Spo0A by the histidine kinase KinD requires the lipoprotein med in *Bacillus subtilis*. *J Bacteriol* **193**, 3949–3955.

Baruah, A., Lindsey, B., Zhu, Y. & Nakano, M. M. (2004). Mutational analysis of the signal-sensing domain of ResE histidine kinase from *Bacillus subtilis*. *J Bacteriol* **186**, 1694–1704.

Bashor, C. J., Helman, N. C., Yan, S. & Lim, W. A. (2008). Using engineered scaffold interactions to reshape MAP kinase pathway signaling dynamics. *Science* **319**, 1539–1543.

Bauer, M. & Pelkmans, L. (2006). A new paradigm for membrane-organizing and shaping scaffolds. *FEBS Lett* **580**, 5559–5564.

Bhattacharyya, R. P., Reményi, A., Good, M. C., Bashor, C. J., Falick, A. M. & Lim, W. A. (2006). The Ste5 scaffold allosterically modulates signaling output of the yeast mating pathway. *Science* **311**, 822–826.

Bickel, P. E., Scherer, P. E., Schnitzer, J. E., Oh, P., Lisanti, M. P. & Lodish, H. F. (1997). Flotillin and epidermal surface antigen define a new family of caveolae-associated integral membrane proteins. *J Biol Chem* **272**, 13793–13802.

Bodrikov, V., Solis, G. P. & Stuermer, C. A. (2011). Prion protein promotes growth cone development through reggie/flotillin-dependent N-cadherin trafficking. *J Neurosci* **31**, 18013–18025.

Bramkamp, M. & Lopez, D. (2015). Exploring the existence of lipid rafts in bacteria. *Microbiol Mol Biol Rev* **79**, 81–100.

Branda, S. S., González-Pastor, J. E., Ben-Yehuda, S., Losick, R. & Kolter, R. (2001). Fruiting body formation by *Bacillus subtilis*. *Proc Natl Acad Sci U S A* **98**, 11621–11626.

Britton, R. A., Eichenberger, P., Gonzalez-Pastor, J. E., Fawcett, P., Monson, R., Losick, R. & Grossman, A. D. (2002). Genome-wide analysis of the stationary-phase sigma factor (sigma-H) regulon of *Bacillus subtilis*. *J Bacteriol* **184**, 4881–4890.

Capra, E. J. & Laub, M. T. (2012). Evolution of two-component signal transduction systems. *Annu Rev Microbiol* **66**, 325–347.

Casey, J. R. & Reithmeier, R. A. (1993). Detergent interaction with band 3, a model polytopic membrane protein. *Biochemistry* **32**, 1172–1179.

Chapman, S. A. & Asthagiri, A. R. (2009). Quantitative effect of scaffold abundance on signal propagation. *Mol Syst Biol* **5**, 313.

Chen, T. Y., Liu, P. H., Ruan, C. T., Chiu, L. & Kung, F. L. (2006). The intracellular domain of amyloid precursor protein interacts with flotillin-1, a lipid raft protein. *Biochem Biophys Res Commun* **342**, 266–272.

Daley, D. O. (2008). The assembly of membrane proteins into complexes. *Curr Opin Struct Biol* **18**, 420–424.

DeLoache, W. C. & Dueber, J. E. (2013). Compartmentalizing metabolic pathways in organelles. *Nat Biotechnol* **31**, 320–321.

Dempwolff, F., Möller, H. M. & Graumann, P. L. (2012a). Synthetic motility and cell shape defects associated with deletions of flotillin/reggie paralogs in *Bacillus subtilis* and interplay of these proteins with NfeD proteins. *J Bacteriol* **194**, 4652–4661.

Dempwolff, F., Wischhusen, H. M., Specht, M. & Graumann, P. L. (2012b). The deletion of bacterial dynamin and flotillin genes results in pleiotrophic effects on cell division, cell growth and in cell shape maintenance. *BMC Microbiol* **12**, 298.

Dermine, J. F., Duclos, S., Garin, J., St-Louis, F., Rea, S., Parton, R. G. & Desjardins, M. (2001). Flotillin-1-enriched lipid raft domains accumulate on maturing phagosomes. *J Biol Chem* **276**, 18507–18512.

Devi, S. N., Vishnoi, M., Kiehler, B., Haggett, L. & Fujita, M. (2015). *In vivo* functional characterization of the transmembrane histidine kinase KinC in *Bacillus subtilis*. *Microbiology* **161**, 1092–1104.

Dickens, M., Rogers, J. S., Cavanagh, J., Raitano, A., Xia, Z., Halpern, J. R., Greenberg, M. E., Sawyers, C. L. & Davis, R. J. (1997). A cytoplasmic inhibitor of the JNK signal transduction pathway. *Science* **277**, 693–696.

Diekmann, Y. & Pereira-Leal, J. B. (2013). Evolution of intracellular compartmentalization. *Biochem J* **449**, 319–331.

Donovan, C. & Bramkamp, M. (2009). Characterization and subcellular localization of a bacterial flotillin homologue. *Microbiology* **155**, 1786–1799.

Dueber, J. E., Wu, G. C., Malmirchegini, G. R., Moon, T. S., Petzold, C. J., Ullal, A. V., Prather, K. L. & Keasling, J. D. (2009). Synthetic protein scaffolds provide modular control over metabolic flux. *Nat Biotechnol* **27**, 753–759.

Erwin, K. N., Nakano, S. & Zuber, P. (2005). Sulfate-dependent repression of genes that function in organosulfur metabolism in *Bacillus subtilis* requires Spx. *J Bacteriol* **187**, 4042–4049.

Geng, H., Zuber, P. & Nakano, M. M. (2007). Regulation of respiratory genes by ResD-ResE signal transduction system in *Bacillus subtilis*. *Methods Enzymol* **422**, 448–464.

Good, M. C., Zalatan, J. G. & Lim, W. A. (2011). Scaffold proteins: hubs for controlling the flow of cellular information. *Science* **332**, 680–686.

Goodman, A. L., Merighi, M., Hyodo, M., Ventre, I., Filloux, A. & Lory, S. (2009). Direct interaction between sensor kinase proteins mediates acute and chronic disease phenotypes in a bacterial pathogen. *Genes Dev* **23**, 249–259.

Hattori, C., Asai, M., Onishi, H., Sasagawa, N., Hashimoto, Y., Saido, T. C., Maruyama, K., Mizutani, S. & Ishiura, S. (2006). BACE1 interacts with lipid raft proteins. *J Neurosci Res* **84**, 912–917.

Heermann, R., Weber, A., Mayer, B., Ott, M., Hauser, E., Gabriel, G., Pirch, T. & Jung, K. (2009). The universal stress protein UspC scaffolds the KdpD/KdpE signaling cascade of *Escherichia coli* under salt stress. *J Mol Biol* **386**, 134–148.

Huang, X., Decatur, A., Sorokin, A. & Helmann, J. D. (1997). The *Bacillus subtilis* sigma(X) protein is an extracytoplasmic function sigma factor contributing to survival at high temperature. *J Bacteriol* **179**, 2915–2921.

Huang, X., Fredrick, K. L. & Helmann, J. D. (1998). Promoter recognition by *Bacillus subtilis* sigmaW: autoregulation and partial overlap with the sigmaX regulon. *J Bacteriol* **180**, 3765–3770.

Huang, X., Gaballa, A., Cao, M. & Helmann, J. D. (1999). Identification of target promoters for the *Bacillus subtilis* extracytoplasmic function sigma factor, sigma W. *Mol Microbiol* **31**, 361–371.

Jiang, M., Shao, W., Perego, M. & Hoch, J. A. (2000). Multiple histidine kinases regulate entry into stationary phase and sporulation in *Bacillus subtilis*. *Mol Microbiol* **38**, 535–542.

Karimova, G., Pidoux, J., Ullmann, A. & Ladant, D. (1998). A bacterial two-hybrid system based on a reconstituted signal transduction pathway. *Proc Natl Acad Sci U S A* **95**, 5752–5756.

Koch, G., Yepes, A., Förstner, K. U., Wermser, C., Stengel, S. T., Modamio, J., Ohlsen, K., Foster, K. R. & Lopez, D. (2014). Evolution of resistance to a last-resort antibiotic in *Staphylococcus aureus* via bacterial competition. *Cell* **158**, 1060–1071.

Krell, T., Lacal, J., Busch, A., Silva-Jiménez, H., Guazzaroni, M. E. & Ramos, J. L. (2010). Bacterial sensor kinases: diversity in the recognition of environmental signals. *Annu Rev Microbiol* **64**, 539–559.

Lang, D. M., Lommel, S., Jung, M., Ankerhold, R., Petrausch, B., Laessing, U., Wiechers, M. F., Plattner, H. & Stuermer, C. A. (1998). Identification of reggie-1 and reggie-2 as plasmamembrane-associated proteins which cocluster with activated GPI-anchored cell adhesion molecules in non-caveolar micropatches in neurons. *J Neurobiol* **37**, 502–523.

Langhorst, M. F., Reuter, A. & Stuermer, C. A. (2005). Scaffolding microdomains and beyond: the function of reggie/flotillin proteins. *Cell Mol Life Sci* **62**, 2228–2240.

Laub, M. T. & Goulian, M. (2007). Specificity in two-component signal transduction pathways. *Annu Rev Genet* **41**, 121–145.

LeDeaux, J. R., Yu, N. & Grossman, A. D. (1995). Different roles for KinA, KinB, and KinC in the initiation of sporulation in *Bacillus subtilis*. *J Bacteriol* **177**, 861–863.

Lee, Y. H., Kingston, A. W. & Helmann, J. D. (2012). Glutamate dehydrogenase affects resistance to cell wall antibiotics in *Bacillus subtilis*. *J Bacteriol* **194**, 993–1001.

Levchenko, A., Bruck, J. & Sternberg, P. W. (2000). Scaffold proteins may biphasically affect the levels of mitogen-activated protein kinase signaling and reduce its threshold properties. *Proc Natl Acad Sci U S A* **97**, 5818–5823.

Li, M. & Hazelbauer, G. L. (2011). Core unit of chemotaxis signaling complexes. *Proc Natl Acad Sci U S A* **108**, 9390–9395.

Li, M., Cha, D. J., Lai, Y., Villaruz, A. E., Sturdevant, D. E. & Otto, M. (2007). The antimicrobial peptide-sensing system aps of *Staphylococcus aureus*. *Mol Microbiol* **66**, 1136–1147.

Lingwood, D. & Simons, K. (2010). Lipid rafts as a membrane-organizing principle. *Science* **327**, 46–50.

López, D. & Kolter, R. (2010a). Extracellular signals that define distinct and coexisting cell fates in *Bacillus subtilis*. *FEMS Microbiol Rev* **34**, 134–149.

López, D. & Kolter, R. (2010b). Functional microdomains in bacterial membranes. *Genes Dev* **24**, 1893–1902.

López, D., Fischbach, M. A., Chu, F., Losick, R. & Kolter, R. (2009). Structurally diverse natural products that cause potassium leakage trigger multicellularity in *Bacillus subtilis*. *Proc Natl Acad Sci U S A* **106**, 280–285.

López, D., Gontang, E. A. & Kolter, R. (2010). Potassium sensing histidine kinase in *Bacillus subtilis*. *Methods Enzymol* **471**, 229–251.

Mann, J. M., Carabetta, V. J., Cristea, I. M. & Dubnau, D. (2013). Complex formation and processing of the minor transformation pilins of *Bacillus subtilis*. *Mol Microbiol* **90**, 1201–1215.

Marin, R., Rojo, J. A., Fabelo, N., Fernandez, C. E. & Diaz, M. (2013). Lipid raft disarrangement as a result of neuropathological progresses: a novel strategy for early diagnosis? *Neuroscience* **245**, 26–39.

McLoon, A. L., Kolodkin-Gal, I., Rubinstein, S. M., Kolter, R. & Losick, R. (2011). Spatial regulation of histidine kinases governing biofilm formation in *Bacillus subtilis*. *J Bacteriol* **193**, 679–685.

Michel, V. & Bakovic, M. (2007). Lipid rafts in health and disease. *Biol Cell* **99**, 129–140.

Mielich-Süss, B., Schneider, J. & Lopez, D. (2013). Overproduction of flotillin influences cell differentiation and shape in *Bacillus subtilis*. *MBio* **4**, e00719–e00713.

Milano, S. K., Pace, H. C., Kim, Y. M., Brenner, C. & Benovic, J. L. (2002). Scaffolding functions of arrestin-2 revealed by crystal structure and mutagenesis. *Biochemistry* **41**, 3321–3328.

Miller, J. H. (1972). *Experiments in Molecular Genetics*., Cold Spring Harbor, NY: Cold Spring Harbor Laboratories.

Morrow, I. C. & Parton, R. G. (2005). Flotillins and the PHB domain protein family: rafts, worms and anaesthetics. *Traffic* **6**, 725–740.

Nakano, M. M. & Zhu, Y. (2001). Involvement of ResE phosphatase activity in down-regulation of ResD-controlled genes in *Bacillus subtilis* during aerobic growth. *J Bacteriol* **183**, 1938–1944.

Nakano, M. M., Zuber, P., Glaser, P., Danchin, A. & Hulett, F. M. (1996). Two-component regulatory proteins ResD-ResE are required for transcriptional activation of *fnr* upon oxygen limitation in *Bacillus subtilis*. *J Bacteriol* **178**, 3796–3802.

Nakano, M. M., Zhu, Y., Haga, K., Yoshikawa, H., Sonenshein, A. L. & Zuber, P. (1999). A mutation in the 3-phosphoglycerate kinase gene allows anaerobic growth of *Bacillus subtilis* in the absence of ResE kinase. *J Bacteriol* **181**, 7087–7097.

Nakano, S., Küster-Schöck, E., Grossman, A. D. & Zuber, P. (2003). Spx-dependent global transcriptional control is induced by thiol-specific oxidative stress in *Bacillus subtilis*. *Proc Natl Acad Sci U S A* **100**, 13603–13608.

Otto, G. P. & Nichols, B. J. (2011). The roles of flotillin microdomains—endocytosis and beyond. *J Cell Sci* **124**, 3933–3940.

Park, S. H., Zarrinpar, A., Lim, W. A. & Rewiring, M. A. P. (2003). kinase pathways using alternative scaffold assembly mechanisms. *Science* **299**, 1061–1064.

Reusch, R. N., Hiske, T. W. & Sadoff, H. L. (1986). Poly-beta-hydroxybutyrate membrane structure and its relationship to genetic transformability in *Escherichia coli*. *J Bacterio* **168**, 553–562.

Schneider, A., Rajendran, L., Honsho, M., Gralle, M., Donnert, G., Wouters, F., Hell, S. W. & Simons, M. (2008). Flotillin-dependent clustering of the amyloid precursor protein regulates its endocytosis and amyloidogenic processing in neurons. *J Neurosci* **28**, 2874–2882.

Schneider, J., Klein, T., Mielich-Süss, B., Koch, G., Franke, C., Kuipers, O. P., Kovács, A. T., Sauer, M. & Lopez, D. (2015). Spatio-temporal remodeling of functional membrane microdomains organizes the signaling networks of a bacterium. *PLoS Genet* **11**, e100 5140.

Shemesh, M. & Chai, Y. (2013). A combination of glycerol and manganese promotes biofilm formation in *Bacillus subtilis* via histidine kinase KinD signaling. *J Bacteriol* **195**, 2747–2754.

Silva-Rocha, R., Martínez-García, E., Calles, B., Chavarría, M., Arce-Rodríguez, A., de Las Heras, A., Páez-Espino, A. D., Durante-Rodríguez, G., Kim, J. & other authors (2013). The Standard European Vector Architecture (SEVA): a coherent platform for the analysis and deployment of complex prokaryotic phenotypes. *Nucleic Acids Res* **41** (D1), D666–D675.

Simons, K. & Ikonen, E. (1997). Functional rafts in cell membranes. *Nature* **387**, 569–572.

Stuermer, C. A. (2011). Reggie/flotillin and the targeted delivery of cargo. *J Neurochem* **116**, 708–713.

Stuermer, C. A. & Plattner, H. (2005). The 'lipid raft' microdomain proteins reggie-1 and reggie-2 (flotillins) are scaffolds for protein interaction and signalling. *Biochem Soc Symp* **72**, 109–118.

Tavernarakis, N., Driscoll, M., Kyrpides, N. C. (1999). The SPFH domain: implicated in regulating targeted protein turnover in stomatins and other membrane-associated proteins. *Trends Biochem Sci* **24**, 425–427.

Underbakke, E. S., Zhu, Y. & Kiessling, L. L. (2011). Protein footprinting in a complex milieu: identifying the interaction surfaces of the chemotaxis adaptor protein CheW. *J Mol Biol* **409**, 483–495.

Wittig, I. & Schägger, H. (2005). Advantages and limitations of clear-\native PAGE. *Proteomics* **5**, 4338–4346.

Wittig, I. & Schägger, H. (2008). Features and applications of blue-native and clear-native electrophoresis. *Proteomics* **8**, 3974–3990.

Wittig, I., Braun, H. P. & Schägger, H. (2006). Blue native PAGE. *Nat Protoc* **1**, 418–428.

Yasbin, R. E. & Young, F. E. (1974). Transduction in *Bacillus subtilis* by bacteriophage SPP1. *J Virol* **14**, 1343–1348.

Yepes, A., Schneider, J., Mielich, B., Koch, G., García-Betancur, J. C., Ramamurthi, K. S., Vlamakis, H. & López, D. (2012). The biofilm formation defect of a *Bacillus subtilis* flotillin-defective mutant involves the protease FtsH. *Mol Microbiol* **86**, 457–471.

Yepes, A., Koch, G., Waldvogel, A., Garcia-Betancur, J. C. & Lopez, D. (2014). Reconstruction of mreB expression in *Staphylococcus aureus* via a collection of new integrative plasmids. *Appl Environ Microbiol* **80**, 3868–3878.

Zhang, H. M., Li, Z., Tsudome, M., Ito, S., Takami, H. & Horikoshi, K. (2005). *An alkali-inducible flotillin-like protein from Bacillus halodurans C-125.Protein J* **24**, 125–131.

Zhao, F., Zhang, J., Liu, Y. S., Li, L. & He, Y. L (2011). Research advances on flotillins. *Virol J* **8**, 479.

Edited by: J. Stülke

Supplementary Information

In vivo characterization of the scaffold activity of flotillin on the membrane kinase KinC of *Bacillus subtilis*

Johannes Schneider, Benjamin Mielich-Süss, Richard Bohme, Daniel Lopez*

Research Centre for Infectious Diseases. Institute for Molecular Infection Biology (ZINF-IMIB), University of Würzburg. Würzburg, 97080 Germany

*Corresponding author: Daniel Lopez (Daniel.Lopez@uni-wuerzburg.de)

Research Centre for Infectious Diseases. Institute for Molecular Infection Biology (ZINF-IMIB)

Josef-Schneider Strasse 2/ Bau D15

97080 Würzburg, Germany

Running title: FloT affects the activity and interaction specificity of KinC

22 **Supplemental Table S1:** List of strains used in this study

Number	Strain	Background	References
DL1	*B. subtilis* (NCIB 3610)	Wild type genetic background	(Branda *et al.*, 2001)
JS111	*B. subtilis* (NCIB 3610)	*amyE*::P_{hp}-*floT-his*^{6}	This study
DL1721	*B. subtilis* (NCIB 3610)	*amyE*::P_{hp}-*floT-his*^{6}, *lacA*::P_{hp}-*kinC-cfp*	This study
DL1563	*B. subtilis* (NCIB 3610)	*ΔfloA, ΔfloT*	This study
DL1448	*B. subtilis* (NCIB 3610)	*ΔfloA::mls ΔfloT::spc*	(Yepes *et al.*, 2012)
DL227	*B. subtilis* (NCIB 3610)	*ΔkinC::mls*	(Lopez *et al.*, 2009)
DL147	*B. subtilis* (NCIB 3610)	*ΔkinC::cm*	(Lopez *et al.*, 2009)
DL2	*B. subtilis* 168	Wild type genetic background	(Moszer *et al.*, 1995)
DL95	*E. coli* DH5α	Wild type genetic background	(Reusch *et al.*, 1986)
BM263	*E. coli* BTH101	Wild type genetic background	(Karimova *et al.*, 1998)
JS525	*B. subtilis* (NCIB 3610)	*ΔkinC::cm, lacA*::P_{kinC}-*kinC-cfp*	This study
DL1724	*B. subtilis* (NCIB 3610)	*ΔfloT, lacA*::P_{floT}-*floT-gfp*	This study
JS533	*B. subtilis* (NCIB 3610)	*ΔfloT, lacA*::P_{hp}-*floT-gfp*	This study
DL1722	*B. subtilis* (NCIB 3610)	*ΔkinC::cm, lacA*::P_{hp}-*kinC-cfp*	This study
DL1723	*B. subtilis* (NCIB 3610)	*ΔkinC::cm, ΔfloA, ΔfloT, lacA*::P_{hp}-*kinC-cfp*	This study
BM261	*E. coli* DH5α	pKT25-*zip*	(Karimova *et al.*, 1998)
BM262	*E. coli* DH5α	pUT18C-*zip*	(Karimova *et al.*, 1998)
BM258	*E. coli* DH5α	pKNT25	(Karimova *et al.*, 1998)
BM259	*E. coli* DH5α	pUT18	(Karimova *et al.*, 1998)
JS369	*E. coli* BTH101	pKT25-*zip* pUT18C-*zip*	(Karimova *et al.*, 1998)
JS368	*E. coli* BTH101	pKNT25 pUT18	(Karimova *et al.*, 1998)
RB-7	*E.coli* DH5α	pUT18::*liaS*	This study
RB-8	*E.coli* DH5α	pUT18::*dctS*	This study
RB-9	*E.coli* DH5α	pUT18::*walK*	This study
RB-10	*E.coli* DH5α	pUT18::*cssS*	This study
RB-11	*E.coli* DH5α	pUT18::*kinC*	This study
RB-12	*E.coli* DH5α	pUT18::*yesM*	This study
RB-13	*E.coli* DH5α	pUT18::*ydfH*	This study
RB-14	*E.coli* DH5α	pUT18::*kinB*	This study
RB-15	*E.coli* DH5α	pUT18::*malK*	This study
DL1686	*E.coli* DH5α	pUT18::*kinD*	This study
JS349	*E.coli* DH5α	pUT18::*resE*	This study
JS353	*E.coli* DH5α	pUT18::*phoR*	This study
DL1693	*E.coli* DH5α	pUT18::*kinB*	This study
DL1694	*E.coli* DH5α	pKNT25::*floT*	This study
DL1688	*E.coli* DH5α	pKNT25::*kinD*	This study
DL1690	*E.coli* DH5α	pKNT25::*kinB*	This study

DL1690	*E.coli* DH5α	pKNT25::*kinC*	This study
JS526	*E.coli* DH5α	pUT18::*citZ*	This study
JS529	*E.coli* DH5α	pUT18::*rpoA*	This study
JS350	*E.coli* DH5α	pUT18::*ftsH*	This study
JS359	*E.coli* DH5α	pUT18::*floA*	(Schneider *et al.*, 2015)
JS524	*E.coli* DH5α	pKNT25::P_{kinC}-*kinC-cfp*	This study
JS452	*E.coli* DH5α	pSEVA 621-*floT-his*^{6}	(Schneider *et al.*, 2015)
JS451	*E.coli* DH5α	pSEVA 631-*floT-his*^{6}	(Schneider *et al.*, 2015)
JS450	*E.coli* DH5α	pSEVA 641-*floT-his*^{6}	(Schneider *et al.*, 2015)
RB-17	*E.coli* BTH101	pUT18::*liaS* pKNT25::*floT*	This study
RB-19	*E.coli* BTH101	pUT18::*walK* pKNT25::*floT*	This study
RB-21	*E.coli* BTH101	pUT18::*cssS* pKNT25::*floT*	This study
RB-23	*E.coli* BTH101	pUT18::*dctS* pKNT25::*floT*	This study
RB-25	*E.coli* BTH101	pUT18::*kinC* pKNT25::*floT*	This study
RB-27	*E.coli* BTH101	pUT18::*yesM* pKNT25::*floT*	This study
RB-29	*E.coli* BTH101	pUT18::*ydfH* pKNT25::*floT*	This study
RB-31	*E.coli* BTH101	pUT18::*kinB* pKNT25::*floT*	This study
RB-33	*E.coli* BTH101	pUT18::*malK* pKNT25::*floT*	This study
RB-35	*E.coli* BTH101	pUT18::*prkC* pKNT25::*floT*	This study
JS530	*E.coli* BTH101	pUT18::*rpoA* pKNT25::*floT*	This study
JS531	*E.coli* BTH101	pUT18::*citZ* pKNT25::*floT*	This study
JS361	*E.coli* BTH101	pUT18::*ftsH* pKNT25::*floT*	This study
JS371	*E.coli* BTH101	pUT18::*floA* pKNT25::*floT*	(Schneider *et al.*, 2015)
DL1695	*E.coli* BTH101	pUT18::*kinD* pKNT25::*floT*	This study
DL1696	*E.coli* BTH101	pUT18::*kinB* pKNT25::*kinB*	This study
DL1697	*E.coli* BTH101	pUT18::*kinC* pKNT25::*kinC*	This study
DL1698	*E.coli* BTH101	pUT18::*kinD* pKNT25::*kinD*	This study
DL1699	*E.coli* BTH101	pUT18::*kinB* pKNT25::*kinB* pSEVA 621-*floT-his*^{6}	This study
DL1700	*E.coli* BTH101	pUT18::*kinB* pKNT25::*kinB* pSEVA 631-*floT-his*^{6}	This study
DL1701	*E.coli* BTH101	pUT18::*kinB* pKNT25::*kinB* pSEVA 641-*floT-his*^{6}	This study
DL1702	*E.coli* BTH101	pUT18::*kinC* pKNT25::*kinC* pSEVA 621-*floT-his*^{6}	This study
DL1703	*E.coli* BTH101	pUT18::*kinC* pKNT25::*kinC* pSEVA 631-*floT-his*^{6}	This study
DL1704	*E.coli* BTH101	pUT18::*kinC* pKNT25::*kinC* pSEVA 641-*floT-his*^{6}	This study
DL1705	*E.coli* BTH101	pUT18::*kinD* pKNT25::*kinD* pSEVA 621-*floT-his*^{6}	This study
DL1706	*E.coli* BTH101	pUT18::*kinD* pKNT25::*kinD* pSEVA 631-*floT-his*^{6}	This study
DL1707	*E.coli* BTH101	pUT18::*kinD* pKNT25::*kinD* pSEVA 641-*floT-his*^{6}	This study
DL1708	*E.coli* BTH101	pUT18::*kinC* pKNT25::*kinB*	This study
DL1709	*E.coli* BTH101	pUT18::*kinC* pKNT25::*kinD*	This study
DL1710	*E.coli* BTH101	pUT18::*kinB* pKNT25::*kinD*	This study
DL1711	*E.coli* BTH101	pUT18::*kinC* pKNT25::*kinB* pSEVA 621-*floT-his*^{6}	This study

DL1712	*E.coli* BTH101	pUT18::*kinC* pKNT25::*kinB* pSEVA 631-*floT-his*^{6}	This study
DL1713	*E.coli* BTH101	pUT18::*kinC* pKNT25::*kinB* pSEVA 641-*floT-his*^{6}	This study
DL1714	*E.coli* BTH101	pUT18::*kinC* pKNT25::*kinD* pSEVA 621-*floT-his*^{6}	This study
DL1715	*E.coli* BTH101	pUT18::*kinC* pKNT25::*kinD* pSEVA 631-*floT-his*^{6}	This study
DL1716	*E.coli* BTH101	pUT18::*kinC* pKNT25::*kinD* pSEVA 641-*floT-his*^{6}	This study
DL1717	*E.coli* BTH101	pUT18::*kinB* pKNT25::*kinD* pSEVA 621-*floT-his*^{6}	This study
DL1718	*E.coli* BTH101	pUT18::*kinB* pKNT25::*kinD* pSEVA 631-*floT-his*^{6}	This study
DL1719	*E.coli* BTH101	pUT18::*kinB* pKNT25::*kinD* pSEVA 641-*floT-his*^{6}	This study

Supplemental Table S2: List of primers used in this study

Number	*Restriction sites*	Sequence 5'-3'	bp
1	*kinC* fw (BamHI)	TTTTGGATCCATGAGAAAATATCAAGCTCGTATC	34
2	*kinC* rv (KpnI)	TTTTGGTACCCGGCTGTCTGATTTTAAAGGCAAAAC	36
3	*yesM* fw (BamHI)	TTTTGGATCCATGAAGAAAAGAGTTGCTGGCTG	33
4	*yesM* rv (KpnI)	TTTTGGTACCCGCACCACCTCATTTCGGCAC	31
5	*ydfH* fw (BamHI)	TTTTGGATCCTTGCTTATAAGGAATCCTTTTAAAG	35
6	*ydfH* rv (KpnI)	TTTTGGTACCCGTTCATCTTGCATCTCTCCCTG	33
7	*kinD* fw (SphI)	TTTTGCATGCATGTTGGAGCGATGCAAATTG	31
8	*kinD* rv (KpnI)	TTTTGGTACCCGTGATGCGGATACGGGGAG	30
9	*kinB* fw (SphI)	TTTTGCATGCATGGAAATTCTAAAAGACTATCTTC	35
10	*kinB* rv (KpnI)	TTTTGGTACCCGGTGAGGAAGATCAGCGGG	30
11	*dctS* fw (SphI)	TTTTGCATGCATGAACAAAAAGAAGCTCTCAATC	34
12	*dctS* rv (KpnI)	TTTTGGTACCCGCGAGCCATGCTGTGCTTCC	31
13	*cssS* fw (SphI)	TTTTGCATGCATGAAAAACAAGCCGCTCGCG	31
14	*cssS* rv (KpnI)	TTTTGGTACCTTTTGGCACTGCTATGCGGTATG	33
15	*walK* fw (SphI)	TTTTGCATGCATGAATAAGGTTGGTTTTTTTCGG	34
16	*walK* rv (KpnI)	TTTTGGTACCCGCGCTTCATCCCAATCATCCTC	33
17	*prkC* fw (SphI)	TTTTGCATGCGTGCTAATCGGCAAGCGGATC	31
18	*prkC* rv (KpnI)	TTTTGGTACCCGTTCATCTTTCGGATACTCAATGG	35
19	*malK* fw (SphI)	TTTTGCATGCATGAAAAAAACATTAAAACTGCAAAC	36
20	*malK* rv (KpnI)	TTTTGGTACCCGATCATGATTTTCCTCCTTCGG	33
21	*liaS* fw (SphI)	TTTTGCATGCATGAGAAAAAAAATGCTTGCCAG	33
22	*liaS* rv (KpnI)	TTTTGGTACCCGATCAATAATACTCGAATCACGTTCG	37
JS107	*resE* fw (SphI)	TTTTGCATGCATGAAATTTTGGAAAAGCGTAG	32
JS108	*resE* rv (KpnI)	TTTTGGTACCCGCCGTTTTGTCGGAATATAAAAAG	35
JS109	*phoR* fw (SphI)	TTTTGCATGCATGAATAAATACCGTGTGCGCC	32
JS110	*phoR* rv (KpnI)	TTTTGGTACCCGGGCGGACTTTTCAGCGGCC	31
DL147	P_{kinC} fw (SalI)	TTTTGTCGACGGGATACTTTACATAT	26
JS111	*ftsH* fw (SphI)	TTTTGCATGCATGAATCGGGTCTTCCGTAATAC	33

Js112	*ftsH* rv (BamHI)	TTTTGGATCCTCCTCTTTCGTATCGTCTTTCTTTTC	36
JS194	*citZ* fw (BamHI)	AAAAGGATCCCATGACAGCGACACGCG	28
JS195	*citZ* rv (KpnI)	AAAAGGTACCCGGGCTCTTTCTTCAATCGG	31
JS196	*rpoA* fw (BamHI)	AAAAGGATCCCATGATCGAGATTGAAAAAC	31
JS197	*rpoA* rv (KpnI)	AAAAGGTACCCGATCGTCTTTGCGAAGTC	30

Supplemental Table S3: List of plasmids used in this study

Name	Background	Reference
pKM003	Ectopic integration into *amyE* locus of *B. subtilis* (spc^R)	Prof. Rudner (HMS, USA)
pDR183	Ectopic integration into *lacA* locus of *B. subtilis* (mls^R)	Prof. Rudner (HMS, USA)
pDR111	Ectopic integration into *amyE* locus of *B. subtilis* (spc^R)	(Britton *et al.*, 2002)
pSEVA 621	Replication in *E. coli* (gm^R) (RK2 replication origin)	(Silva-Rocha *et al.*, 2013)
pSEVA631	Replication in *E. coli* (gm^R) (pBR101 replication origin)	(Silva-Rocha *et al.*, 2013)
pSEVA641	Replication in *E. coli* (gm^R) (pRO1600 replication origin)	(Silva-Rocha *et al.*, 2013)
pMAD	Replication in Gram + (mls^R) (pE194 replication origin)	(Arnaud *et al.*, 2004)
pKNT25	Replication in *E. coli* (Km^R) (low copy number)	(Karimova *et al.*, 1998)
pUT18	Replication in *E. coli* (Amp^R) (high copy number)	(Karimova *et al.*, 1998)

References

Arnaud, M., Chastanet, A. & Debarbouille, M. (2004). New vector for efficient allelic replacement in naturally nontransformable, low-GC-content, gram-positive bacteria. *Appl Environ Microbiol* **70**, 6887-6891.

Branda, S. S., Gonzalez-Pastor, J. E., Ben-Yehuda, S., Losick, R. & Kolter, R. (2001). Fruiting body formation by *Bacillus subtilis*. *Proc Natl Acad Sci U S A* **98**, 11621-11626.

Britton, R. A., Eichenberger, P., Gonzalez-Pastor, J. E., Fawcett, P., Monson, R., Losick, R. & Grossman, A. D. (2002). Genome-wide analysis of the stationary-phase sigma factor (sigma-H) regulon of *Bacillus subtilis*. *J Bacteriol* **184**, 4881-4890.

Karimova, G., Pidoux, J., Ullmann, A. & Ladant, D. (1998). A bacterial two-hybrid system based on a reconstituted signal transduction pathway. *Proc Natl Acad Sci U S A* **95**, 5752-5756.

Lopez, D., Fischbach, M. A., Chu, F., Losick, R. & Kolter, R. (2009). Structurally diverse natural products that cause potassium leakage trigger multicellularity in *Bacillus subtilis*. *Proc Natl Acad Sci U S A* **106**, 280-285.

Moszer, I., Glaser, P. & Danchin, A. (1995). SubtiList: a relational database for the *Bacillus subtilis* genome. *Microbiology* **141 (Pt 2)**, 261-268.

Reusch, R. N., Hiske, T. W. & Sadoff, H. L. (1986). Poly-beta-hydroxybutyrate membrane structure and its relationship to genetic transformability in *Escherichia coli*. *J Bacteriol* **168**, 553-562.

Schneider, J., Klein, T., Mielich-Suss, B., Koch, G., Franke, C., Kuipers, O. P., Kovacs, A. T., Sauer, M. & Lopez, D. (2015). Spatio-temporal Remodeling of Functional Membrane Microdomains Organizes the Signaling Networks of a Bacterium. *PLoS Genet* **11**, e1005140.

Silva-Rocha, R., Martinez-Garcia, E., Calles, B. & other authors (2013). The Standard European Vector Architecture (SEVA): a coherent platform for the analysis and deployment of complex prokaryotic phenotypes. *Nucleic Acids Res* **41**, D666-675.

Yepes, A., Schneider, J., Mielich, B., Koch, G., Garcia-Betancur, J. C., Ramamurthi, K. S., Vlamakis, H. & Lopez, D. (2012). The biofilm formation defect of a *Bacillus subtilis* flotillin-defective mutant involves the protease FtsH. *Mol Microbiol* **86**, 457-471.

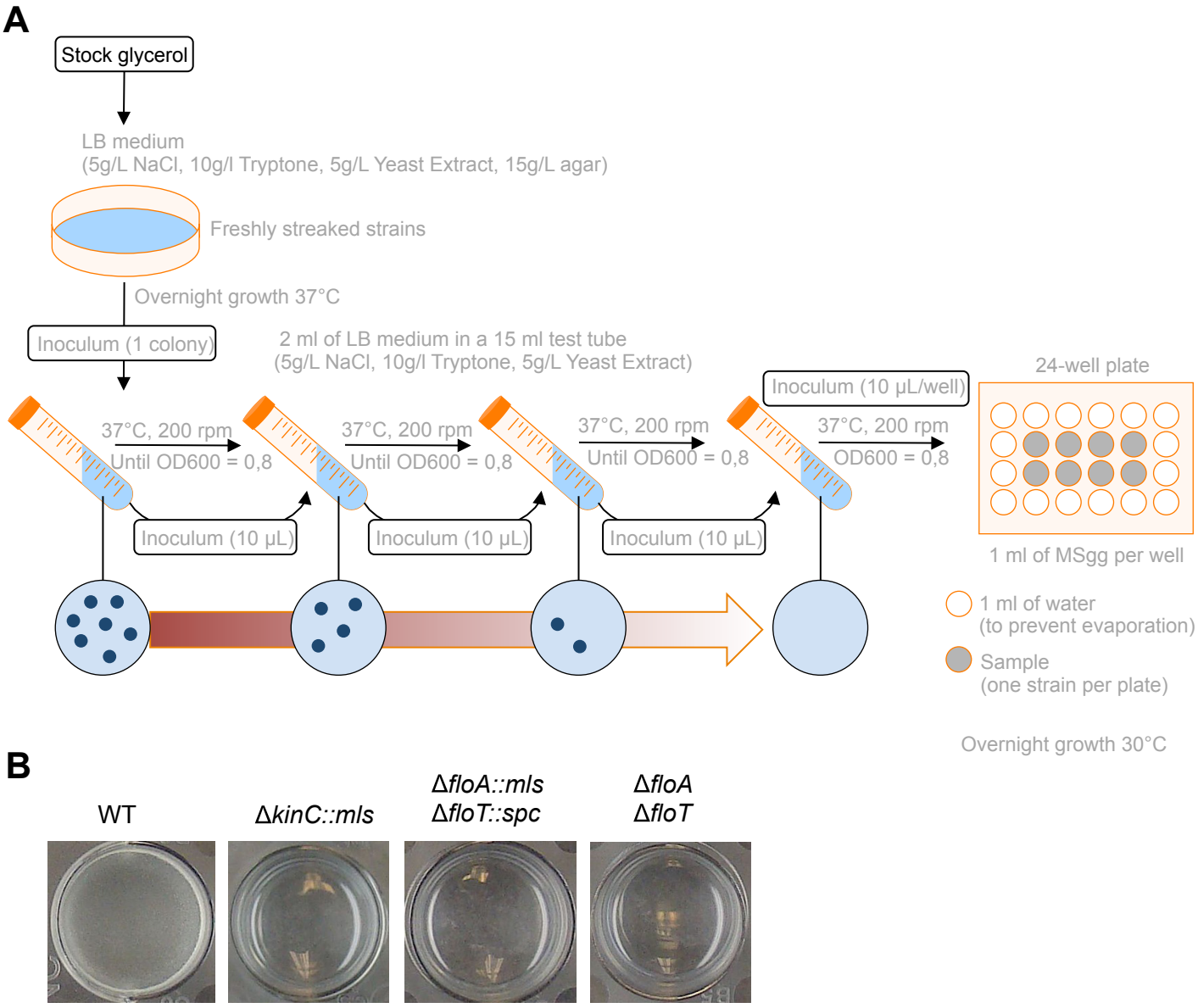

Supplemental figure S1: A flotillin-deficient strain of *Bacillus subtilis* is deficient in pellicle formation. **(A)** Schematic protocol to assay pellicle formation in *B. subtilis* NCIB3610 strain in liquid MSgg medium. By performing serial passaging of cells in LB medium, bacteria grow in exponential phase for many generations and minimize any Spo0A that remains activated from stationary phase cells. Cells with lowly activated Spo0A background can be used to compare the ability of different strains to activate Spo0A and therefore to form biofilm. The reduction of activated Spo0A in cultures during serial passaging can be visualized because cultures reduce the formation of clumps during growth (represented in blue). At the end of the passaging, cultures should be completely homogeneous. This is used to inoculate MSgg medium in 24-well plates and incubated at 30°C overnight. **(B)** pellicle formation assay in different genetic backgrounds. Strains that are deficient in flotillin are unable to form pellicles in the conditions tested.

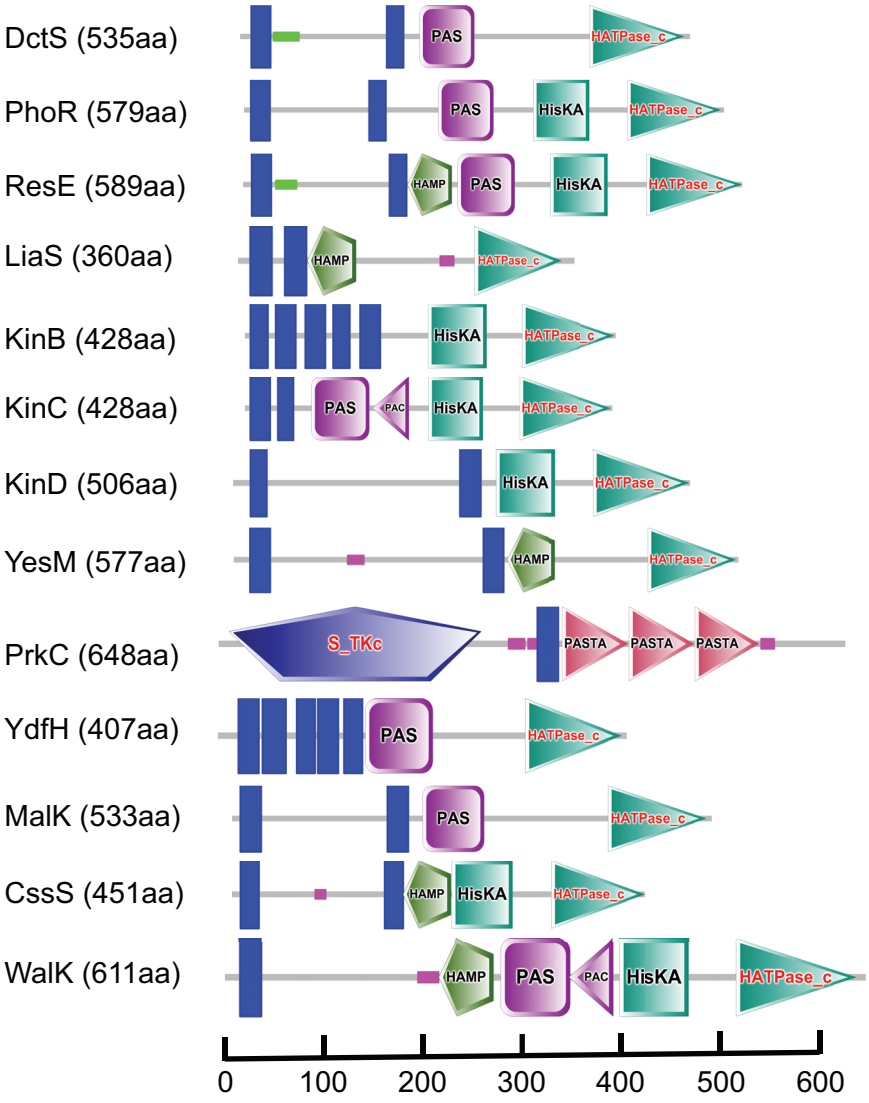

Supplemental figure S2: Comparative diagram of the distinct membrane-bound sensor kinases that were tested in the BTH to assay their interaction with the flotillin protein FloT. The membrane-anchored regions are represented in blue. PAS domains are represented in purple, the PASTA domains are represented in red, the kinase and ATPase domain is presented in pale green. HAMP domain are presented in dark green. The serine-threonine kinase domain of PkrC is represented in dark blue. Left column shows the name of each sensor kinase and the protein length of each one of the kinases is shown in brackets. An amino acid scale bar is shown in the bottom. The molecular structures of the sensor kinases have been adapted from:

http://smart.embl-heidelberg.de

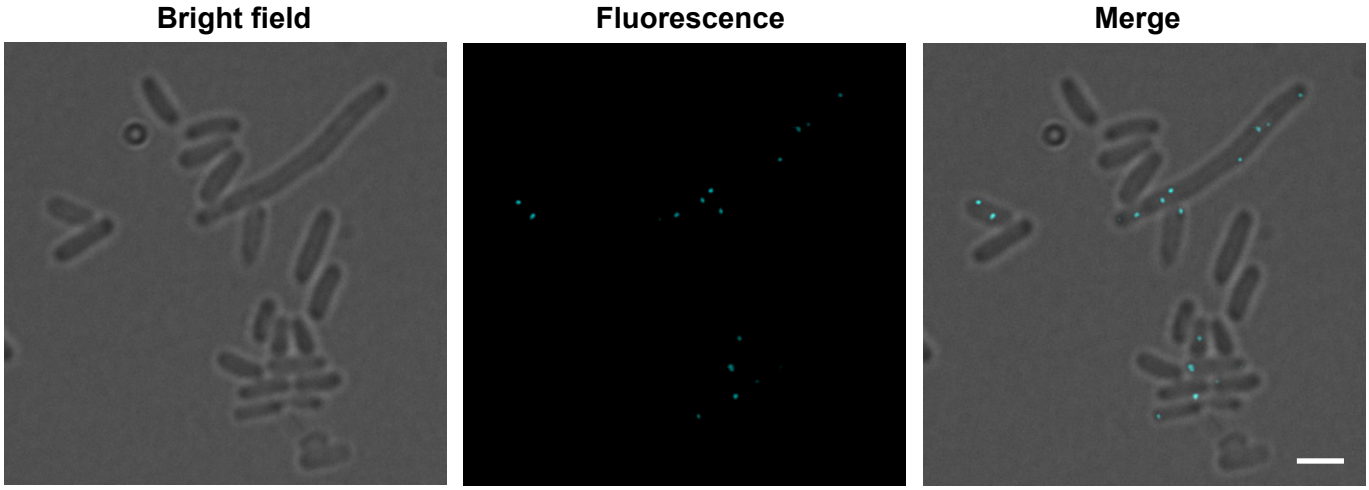

Supplemental figure S3: Subcellular localization of KinC in *E. coli* cells shows distribution in discrete puncta. Fluorescence microscopy pictures of *E. coli* cells labeled with KinC-CFP translational fusion expressed under the control of an IPTG-inducible promoter. Cells were grown in LB medium until stationary phase. Induction of the expression of the translational fusion was performed by adding IPTG to the mid-exponential growing medium to a final concentration of 1 mM. Fluorescence signal associated with FloT is represented in cyan. Scale bar is 2 µm.

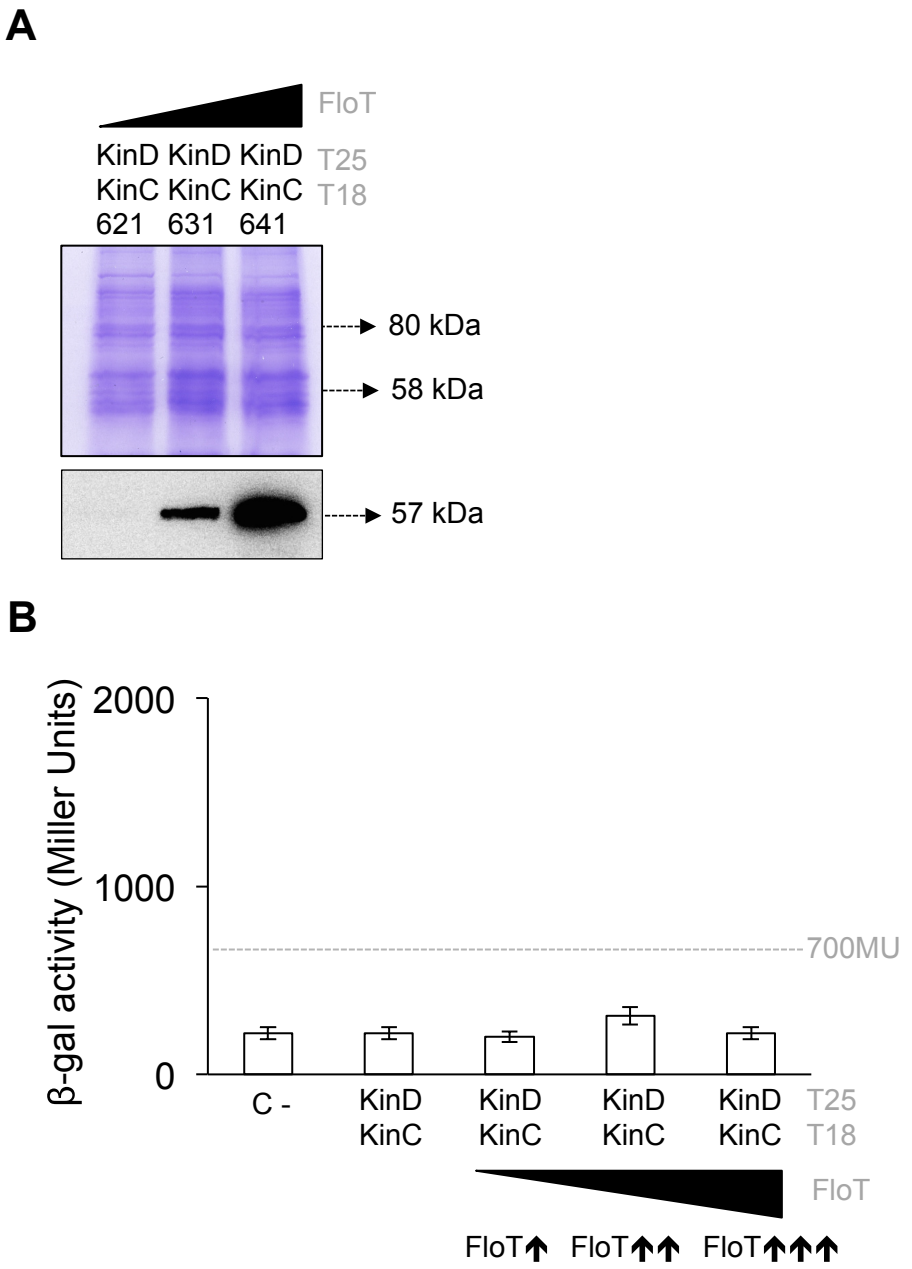

Supplemental figure S4: FloT does not favor aggregation of KinC with KinD. (A) Immunoblot analysis showing the distinct concentrations of FloT that are produced in B3H cells when carrying lower- (pSEVA-621), medium- (pSEVA-631) and high-copy (pSEVA-641) plasmids expressing His6-tagged FloT. Strains produced lower (↑), medium (↑↑) and higher (↑↑↑) concentration of FloT in the BTH assay, respectively. SDS-PAGE is shown as loading control. **(B)** B3H assay to quantify the interaction of KinC with KinD under different concentrations of FloT. Dashed line indicates the threshold limit of 700 Miller Units that defines a positive interaction signal. Results represent a mean of three independent experiments. We detected no interaction between KinC with KinD and the presence of FloT did not favor any aggregation between these two kinases.

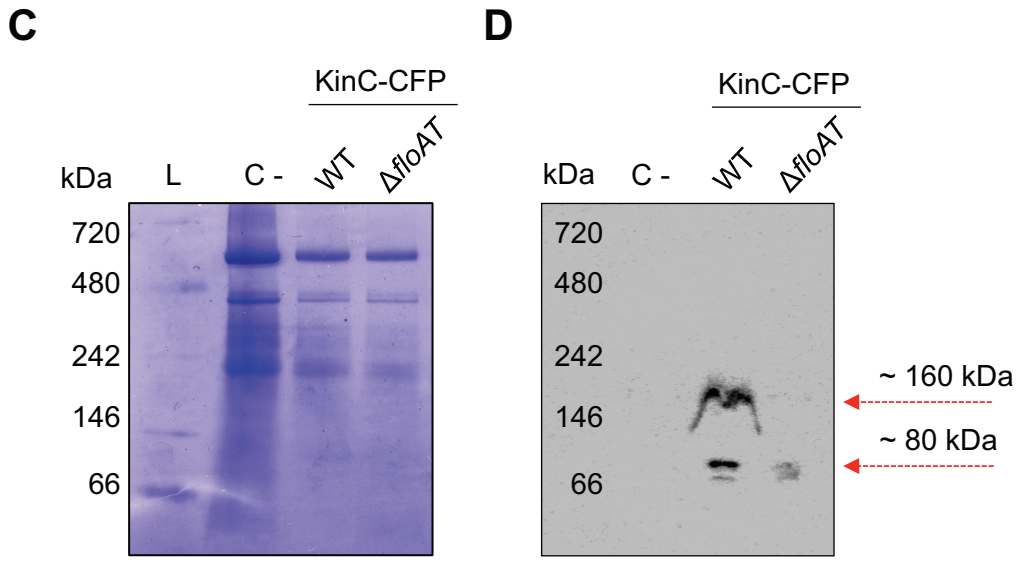

Supplemental figure S5: The oligomerization pattern of KinC is different in *B. subtilis* cells lacking flotillin. Coomassie-stained BN-PAGE that resolves the protein complexes from the membrane fraction of *B. subtilis.* The C- lane serves as a negative control and resolves the membrane fraction of an unlabeled wild-type strain. The WT lane resolves the membrane fraction of a wild-type strain labeled with the KinC-CFP translational fusion. The Δ*floAT* lane resolves the membrane fraction of a clean-off flotillin-double mutant labeled with the KinC-CFP translational fusion. **(d)** Western blot assay, using antibodies against CFP, to detect the oligomeric states of KinC in the different genetic backgrounds resolved in the BN-PAGE. Signals detected are labeled with a dashed red arrow and their estimated MW is represented above.

5. Materials and Methods

This section indexes materials and methods used in this dissertation. Detailed descriptions are available on corresponding pages of published manuscripts in the results section (**4.**) and supplemental material and methods used in these manuscripts.

5.1 Strains, media and growth conditions

See pages 40, 76, 107 and 143.

5.2 Construction of strains

See pages 41, 77, 107 and 144.

5.3 Fluorescence microscopy and image analysis

See pages 42, 77, 108 and 145.

5.4 Photoactivated localization microscopy (PALM)

See a detailed description on page 109.

5.5 Flow cytometry

See pages 42, 77 and 109.

5.6 Whole-genome microarray analysis

See the description on page 110.

5.8 Native PAGE

Description can be found on page 144.

5.7 BN-PAGE and immunoblotting

Detailed descriptions can be found on pages 78, 110, 144 and 145.

5.8 Bacterial two-hybrid analysis

Detailed description available on pages 111 and 144.

5.9 Bacterial three-hybrid analysis (B3H assay)

See pages 111 and 144.

5.10 Physiological assays

See pages 112, 145 and 166.

5.11 Cell fractionation

See detailed description on pages 42 and 144.

5.12 Pull-down analysis

See descriptions on pages 42 and 144.

5.13 Spore counting

See detailed description on page 42.

6. Discussion

6.1 Lipid raft controversy

Simons and Ikonen proposed the model of lipid rafts in 1997 (*10*). Twenty-five years later and after more than 6.000 papers published in the field, the concept of lipid rafts is still challenged with debatable hypotheses (*186-188*). The source of this controversy mainly comes from three different technical limitations in the study of lipid rafts. First, the lack of standardized biochemical approaches to purify lipid rafts. Detergent solubilization with non-ioninc detergents, such as Triton X-100, followed by gradient centrifugation is generally used to obtain the detergent-resistant membrane fraction (DRM) that is enriched in lipid rafts (*189*). DRMs can be further used to analyze protein content and study the pool of proteins that are associated with lipid rafts. Although it is known that the DRM fraction is highly enriched in proteins associated with lipid rafts, the solubilization of membranes using detergent treatment is a rather aggressive approach that can generate artifacts and false-positive results depending on the concentration and type of detergents used or the temperature in which the membrane disaggregation takes place. These now obvious technical considerations were overlooked at the beginning of the exploration of lipid rafts and generated results that were difficult to reconcile. Furthermore, this led to question the existence of lipid rafts and whether they were artifacts generated during the preparation of samples. As a consequence, it is now known that raft separation by detergent disaggregation should not be the main criterion to classify a protein as part of the protein cargo of lipid rafts (12, 20, 60) and that alternative methodology is required to validate any raft-associated protein of interest.

Secondly, visualization of membrane domains has been a challenging task in the research of lipid rafts due to the nanoscale range of these membrane signaling platforms, which are below the resolution limit of conventional light microscopy. The problem resided in

the variability of the colocalization and sizes of the lipid rafts, which led to the collection of conceptually different results by different research groups and this in turn caused skepticism about the raft concept. However, new microscopy techniques that allow a resolution below the diffraction limit of visible light (200-300 nm) have been developed. In order to address the visualization of lipid rafts at higher resolution, stimulated emission depletion (STED), structured illumination microscopy (SIM), as well as techniques that can provide resolution down to single molecules by using stochastic fluorescence detection such as photoactivated localization microscopy (PALM) and direct stochastic optical reconstruction (dSTORM), are used.

The third area of difficulty in the study of lipid rafts is the complexity that entails the manipulation of eukaryotic cells. Those challenges were assumed to be inevitable, because the existence of lipid rafts has traditionally been associated with eukaryotic cells and their assembly depends on the presence of cholesterol, which is absent in the membranes of most bacteria and archaea. Questions related to the architecture and functionality of lipid rafts are generally difficult to address in eukaryotic models due to the complicated methodology used for genetic manipulation. However, it has recently been shown that bacteria are also able to organize many signal transduction cascades and protein transport processes in functional membrane microdomains (FMMs) constituted by specific lipids (*19*), *i.e.* bacterial membranes contain lipid rafts similar to those found in eukaryotic cells (*10*). The assembly of FMMs (2010) involves the biosynthesis of polyisoprenoid lipids in the membrane and their co-localization with bacterial flotillin-like proteins (*20*). Bacterial flotillins seem to play a similar role as eukaryotic flotillins, acting as protein scaffolds in recruiting proteins that need to be localized in lipid rafts to promote interactions and oligomerization (*21, 22*). Similar to eukaryotic flotillin proteins, flotillins in bacteria play an essential role in organizing and maintaining the correct architecture of the FMMs.

6.2 Functional microdomain heterogeneity

Despite the large number of technical and methodological challenges in the field of lipid rafts, the situation gradually clarified due in part to an increasing number of efforts that have been performed to overcome the abovementioned limitations. The field now continuously expands to address new findings in the architecture and functionality of lipid rafts. One of the most important challenges consists in exploring the possibility that distinct types of raft species exist within the same cell. These rafts are presumably composed of different protein and lipid constituents, allowing the cell to control diverse biological processes (*190, 191*).

The hypothesis for the coexistence of distinct families of lipid rafts comes from the large number of roles that are associated with lipid rafts in the literature, which are as diverse as intracellular sorting of proteins, membrane trafficking, signal transduction and pathogen entry. This diversity of functions could be related to the diversity in both the lipid and protein composition of lipid rafts. Thus, it is plausible that the DRM fraction contains a heterogeneous population of lipid rafts. For instance, raft-associated caveolae are generally found in a membrane fraction that is different from the DMRs generated by Triton X-100 treatment. Moreover, DRMs can be isolated using a wide variety of detergents like Brij 58, Brij 96, Brij 98, CHAPS, Lubrol WX, octylglucoside, Nonidet P40. Quantitative analysis of the lipid content of the DRMs yields a differential enrichment of cholesterol and sphingolipids depending on the use of different detergent purification protocols.

In this work I show that FMMs in the membrane of bacteria, which are equivalent platforms to lipid rafts, are able to organize in at least two different types of membrane microdomains showing distinct protein composition and biological function. The co-occurrence of distinct types of FMMs is temporally regulated. While one particular type of FMM is constitutively present in bacterial membranes, the second type of FMM occurs at

stationary phase because its assembly is triggered by the presence of a self-produced signaling molecule to ensure the activation of specific signal transduction cascades at the right place and time during cell growth.

It is very likely that the constituent lipids play an important role in the organization of different types of FMMs in bacterial cells but this is still an unexplored field in which much work needs to be performed. However, bacterial flotillins have already been shown to influence membrane fluidity and thus organization of lipids in the cellular membrane (*100*), although the molecular structure of these constituent lipids is still unresolved. Moreover, we have developed a new set of improved biochemical methods and super-resolution microscopy techniques to address these questions in the years to come (*165, 192*). Unlike their complex eukaryotic counterparts, bacteria provide a genetically tractable model system that facilitates the investigation of functional membrane microdomains, which together with the newly developed approaches will allow us to perform a deeper investigation of the biological significance of FMMs in bacterial membranes.

6.3 Scaffold activity of bacterial flotillins

Scaffold proteins are considered as very important modulators of signaling pathways that selectively regulate the assembly of protein complexes (*193*). It has been proposed that by adjusting the scaffold concentration, cells are able to influence signaling amplitude and timing, resulting in an alteration of physiological responses of preexisting signaling pathways (*21, 193, 194*). Due to their ability to modulate important signaling networks, scaffold proteins have been a major target of evolutionary variations and pathogens, but also biochemical engineering (*21*). Besides tethering and stabilizing proteins in complexes, scaffold proteins can additionally play a very active and catalytic role (*195*). Although they are not essential to initiate signaling processes, they are very important tools for the cell to specifically adapt and control signal outcome in space and time (*184, 196, 197*). Thus, activities such as facilitating

receptor or kinase oligomerization also depend on timely expression and assembly of the corresponding scaffold. Nevertheless, the mechanism by which scaffold proteins effectively tether interaction partners and facilitate the assembly of functional protein complexes is not entirely understood. However, the most direct hypothesis is that scaffold proteins promote the stability of protein complexes through tethering of interacting partners and thereby increasing the likelihood of interaction (*21*).

I have developed a combination of biochemical approaches, including a BTH and B3H approach as well as resolution of protein complexes using BN-PAGE to investigate whether FloA and FloT of *B. subtilis* act as scaffold proteins. Based on the results I have obtained by these approaches, I could verify that the prokaryotic flotillins FloA and FloT exhibit scaffolding activity and behave like other described scaffolding proteins. While lower flotillin scaffold concentration improved the interaction efficiency of kinases, a higher concentration of the flotillins resulted in decreased kinase interaction (*184, 185*). This is consistent with the limitation that other scaffold proteins exhibit, in that higher concentrations of the scaffold titrate signaling partners into separate complexes and inhibit their interaction (*198*), which has been shown for the scaffold protein Ste5 in yeast (*199*) and the JIP1 scaffold in human cells (*200*). This suggests that bacterial flotillins act as scaffold proteins to specifically facilitate signal transduction through tethering of signaling partners (*100, 183-185*).

There are several examples of scaffold proteins in bacteria, which participate in coordinating the assembly of two-component signal transduction pathways, preceding FloA and FloT. For instance, the universal stress protein UspC acts as a scaffold protein of the KdpDE two-component system in *Escherichia coli*, which responds to potassium uptake under potassium limiting growth conditions (*201*). Likewise, the scaffold activity of ApsX in *Staphylococcus aureus* facilitates the assembly of the ApsSR (antimicrobial peptide sensor)

two-component signal transduction cascade that responds to cell wall stress (*202*). Additionally, the protein CheW of *Escherichia coli* scaffolds the assembly of the basic structural unit for bacterial chemotaxis along with the chemotaxis kinase CheA and chemoreceptors (*203, 204*). Overall, scaffold proteins seem to play an important role in bacterial signal transduction and may have ultimately evolved high substrate specificity (*195*). The intricate interplay between the *B. subtilis* flotillin FloT and the signaling kinase KinC provides clues for this hypothesis (*185*). Surely, it will be necessary to analyze other scaffold proteins on their abilities to facilitate interaction of specific protein components and also, to see if they are able to prevent unspecific binding of proteins to their interaction partners. This mechanism could be a fundamental trait of scaffold proteins that has previously been underestimated.

6.4 General organization of proteins and lipids in cellular microdomains

In order to manage the organization of a multitude of cellular processes, cells might intentionally generate different types of microdomains. Besides varying lipid species, different proteins present in the rafts likely also confer specific properties and contribute to the integrity and the functionality of these microdomains. Consequently, several questions arise concerning protein constituents. Are there proteins functioning as structural components of lipid rafts? Do these proteins help in the organization of specific lipid species? Answering questions of this sort will be crucial to describe the characteristics of these membrane microdomains and their biological significance more precisely. For instance, the study of the functionality of flotillins has contributed tremendously to clarify important aspects of the functionality of lipid rafts. In this dissertation I describe that bacterial flotillins do not only recruit proteins to the FMMs, but also act as scaffold proteins to facilitate the interaction/oligomerization of these proteins. Moreover, it is possible that the FMMs act as a protective environment for specific proteins to prevent protease degradation and unspecific binding to other proteins that do not localize in the FMMs.

6. Discussion

It has been proposed that several proteins are able to directly bind to specific lipid species, like cholesterol or sphingolipids, and thereby associate with raft domains (*205*). Studying different mechanisms of raft localization and how this could affect protein functionality will be of major interest in future investigations that aim to unravel the mechanisms whereby proteins associate with bacterial FMMs, in addition to flotillin-mediated recruitment. For example, it has recently been shown that the human EGF receptor can change into its active conformation simply by binding to a specific raft lipid (*206*). Thus, controlling lipid composition of membrane rafts is a fine-tuned cellular process that not only ensures membrane integrity, but also guarantees the presence and activity of distinct protein components. The overall lipid composition of bacterial FMMs however has yet to be elucidated and resulting constituents will very likely hint to proteins or mechanisms involved in generating functional heterogeneity and diversity.

7. Bibliography

1. H. E. Grecco, M. Schmick, P. I. Bastiaens, Signaling from the living plasma membrane. *Cell* **144**, 897 (Mar 18, 2011).
2. R. Lindner, H. Y. Naim, Domains in biological membranes. *Experimental cell research* **315**, 2871 (Oct 15, 2009).
3. F. Schroeder, J. K. Woodford, J. Kavecansky, W. G. Wood, C. Joiner, Cholesterol domains in biological membranes. *Mol Membr Biol* **12**, 113 (Jan-Mar, 1995).
4. S. J. Singer, G. L. Nicolson, The fluid mosaic model of the structure of cell membranes. *Science* **175**, 720 (Feb 18, 1972).
5. G. van Meer, D. R. Voelker, G. W. Feigenson, Membrane lipids: where they are and how they behave. *Nat Rev Mol Cell Biol* **9**, 112 (Feb, 2008).
6. D. Lingwood, K. Simons, Lipid rafts as a membrane-organizing principle. *Science* **327**, 46 (Jan 1, 2010).
7. K. Simons, J. L. Sampaio, Membrane organization and lipid rafts. *Cold Spring Harb Perspect Biol* **3**, a004697 (Oct, 2011).
8. G. van Meer, K. Simons, Lipid polarity and sorting in epithelial cells. *Journal of cellular biochemistry* **36**, 51 (Jan, 1988).
9. B. A. Tsui-Pierchala, M. Encinas, J. Milbrandt, E. M. Johnson, Jr., Lipid rafts in neuronal signaling and function. *Trends Neurosci* **25**, 412 (Aug, 2002).
10. K. Simons, E. Ikonen, Functional rafts in cell membranes. *Nature* **387**, 569 (Jun 5, 1997).
11. I. C. Morrow, R. G. Parton, Flotillins and the PHB domain protein family: rafts, worms and anaesthetics. *Traffic* **6**, 725 (Sep, 2005).
12. T. Babuke, R. Tikkanen, Dissecting the molecular function of reggie/flotillin proteins. *Eur J Cell Biol* **86**, 525 (Sep, 2007).
13. G. P. Otto, B. J. Nichols, The roles of flotillin microdomains--endocytosis and beyond. *J Cell Sci* **124**, 3933 (Dec 1, 2011).
14. C. A. Stuermer, Reggie/flotillin and the targeted delivery of cargo. *J Neurochem* **116**, 708 (Mar, 2011).
15. F. Zhao, J. Zhang, Y. S. Liu, L. Li, Y. L. He, Research advances on flotillins. *Virol J* **8**, 479 (2011).
16. V. Michel, M. Bakovic, Lipid rafts in health and disease. *Biol Cell* **99**, 129 (Mar, 2007).
17. C. A. Stuermer, Reggie/flotillin and the targeted delivery of cargo. *Journal of neurochemistry* **116**, 708 (Mar, 2011).
18. F. Zhao, J. Zhang, Y. S. Liu, L. Li, Y. L. He, Research advances on flotillins. *Virol J* **8**, 479 (2011).
19. D. Lopez, R. Kolter, Functional microdomains in bacterial membranes. *Genes Dev* **24**, 1893 (Sep 1, 2010).
20. N. Tavernarakis, M. Driscoll, N. C. Kyrpides, The SPFH domain: implicated in regulating targeted protein turnover in stomatins and other membrane-associated proteins. *Trends Biochem Sci* **24**, 425 (Nov, 1999).
21. M. C. Good, J. G. Zalatan, W. A. Lim, Scaffold proteins: hubs for controlling the flow of cellular information. *Science* **332**, 680 (May 6, 2011).
22. M. F. Langhorst, A. Reuter, C. A. Stuermer, Scaffolding microdomains and beyond: the function of reggie/flotillin proteins. *Cell Mol Life Sci* **62**, 2228 (Oct, 2005).
23. K. Simons, M. J. Gerl, Revitalizing membrane rafts: new tools and insights. *Nat Rev Mol Cell Biol* **11**, 688 (Oct, 2010).

24. D. T. Browman, M. B. Hoegg, S. M. Robbins, The SPFH domain-containing proteins: more than lipid raft markers. *Trends in cell biology* **17**, 394 (Aug, 2007).
25. J. B. Parsons, C. O. Rock, Bacterial lipids: metabolism and membrane homeostasis. *Prog Lipid Res* **52**, 249 (Jul, 2013).
26. H. J. Kaiser *et al.*, Order of lipid phases in model and plasma membranes. *Proc Natl Acad Sci U S A* **106**, 16645 (Sep 29, 2009).
27. K. Simons, J. L. Sampaio, Membrane organization and lipid rafts. *Cold Spring Harb Perspect Biol* **3**, a004697 (Oct, 2011).
28. J. Dahl, The role of cholesterol in mycoplasma membranes. *Subcell Biochem* **20**, 167 (1993).
29. M. Lin, Y. Rikihisa, Ehrlichia chaffeensis and Anaplasma phagocytophilum lack genes for lipid A biosynthesis and incorporate cholesterol for their survival. *Infection and immunity* **71**, 5324 (Sep, 2003).
30. C. J. Jackson *et al.*, A novel sterol 14alpha-demethylase/ferredoxin fusion protein (MCCYP51FX) from Methylococcus capsulatus represents a new class of the cytochrome P450 superfamily. *The Journal of biological chemistry* **277**, 46959 (Dec 6, 2002).
31. H. B. Bode *et al.*, Steroid biosynthesis in prokaryotes: identification of myxobacterial steroids and cloning of the first bacterial 2,3(S)-oxidosqualene cyclase from the myxobacterium Stigmatella aurantiaca. *Molecular microbiology* **47**, 471 (Jan, 2003).
32. D. Lopez, R. Kolter, Functional microdomains in bacterial membranes. *Genes & development* **24**, 1893 (Sep 1, 2010).
33. T. Bosak, R. M. Losick, A. Pearson, A polycyclic terpenoid that alleviates oxidative stress. *Proc Natl Acad Sci U S A* **105**, 6725 (May 6, 2008).
34. G. Ourisson, M. Rohmer, K. Poralla, Prokaryotic hopanoids and other polyterpenoid sterol surrogates. *Annu Rev Microbiol* **41**, 301 (1987).
35. J. H. Cvejic *et al.*, Bacterial triterpenoids of the hopane series as biomarkers for the chemotaxonomy of Burkholderia, Pseudomonas and Ralstonia spp. *FEMS Microbiol Lett* **183**, 295 (Feb 15, 2000).
36. S. V. Dobritsa, D. Potter, T. E. Gookin, A. M. Berry, Hopanoid lipids in Frankia: identification of squalene-hopene cyclase gene sequences. *Can J Microbiol* **47**, 535 (Jun, 2001).
37. D. M. Doughty, R. C. Hunter, R. E. Summons, D. K. Newman, 2-Methylhopanoids are maximally produced in akinetes of Nostoc punctiforme: geobiological implications. *Geobiology* **7**, 524 (Dec, 2009).
38. T. Hartner, K. L. Straub, E. Kannenberg, Occurrence of hopanoid lipids in anaerobic Geobacter species. *FEMS Microbiol Lett* **243**, 59 (Feb 1, 2005).
39. A. Pearson *et al.*, Diversity of hopanoids and squalene-hopene cyclases across a tropical land-sea gradient. *Environ Microbiol* **11**, 1208 (May, 2009).
40. A. Pearson, D. B. Rusch, Distribution of microbial terpenoid lipid cyclases in the global ocean metagenome. *ISME J* **3**, 352 (Mar, 2009).
41. C. L. Schmerk, M. A. Bernards, M. A. Valvano, Hopanoid production is required for low-pH tolerance, antimicrobial resistance, and motility in Burkholderia cenocepacia. *J Bacteriol* **193**, 6712 (Dec, 2011).
42. A. Pearson *et al.*, Diversity of hopanoids and squalene-hopene cyclases across a tropical land-sea gradient. *Environmental microbiology* **11**, 1208 (May, 2009).
43. A. Pearson, S. R. Flood Page, T. L. Jorgenson, W. W. Fischer, M. B. Higgins, Novel hopanoid cyclases from the environment. *Environ Microbiol* **9**, 2175 (Sep, 2007).

44. G. Siedenburg, D. Jendrossek, Squalene-hopene cyclases. *Appl Environ Microbiol* **77**, 3905 (Jun, 2011).
45. J. P. Saenz, E. Sezgin, P. Schwille, K. Simons, Functional convergence of hopanoids and sterols in membrane ordering. *Proc Natl Acad Sci U S A* **109**, 14236 (Aug 28, 2012).
46. E. Kannenberg, K. Poralla, The influence of hopanoids on growth of Mycoplasma mycoides. *Arch Microbiol* **133**, 100 (Dec, 1982).
47. R. A. Moreau, J. Agnew, K. B. Hicks, M. J. Powell, Modulation of lipoxygenase activity by bacterial hopanoids. *J Nat Prod* **60**, 397 (Apr, 1997).
48. K. Poralla, G. Muth, T. Hartner, Hopanoids are formed during transition from substrate to aerial hyphae in Streptomyces coelicolor A3(2). *FEMS Microbiol Lett* **189**, 93 (Aug 1, 2000).
49. R. F. Seipke, R. Loria, Hopanoids are not essential for growth of Streptomyces scabies 87-22. *J Bacteriol* **191**, 5216 (Aug, 2009).
50. R. F. Taylor, Bacterial triterpenoids. *Microbiol Rev* **48**, 181 (Sep, 1984).
51. A. Vershinin, Biological functions of carotenoids--diversity and evolution. *Biofactors* **10**, 99 (1999).
52. G. Y. Liu *et al.*, Staphylococcus aureus golden pigment impairs neutrophil killing and promotes virulence through its antioxidant activity. *The Journal of experimental medicine* **202**, 209 (Jul 18, 2005).
53. R. Khaneja *et al.*, Carotenoids found in Bacillus. *Journal of applied microbiology* **108**, 1889 (Jun, 2010).
54. H. Duc le, P. D. Fraser, N. K. Tam, S. M. Cutting, Carotenoids present in halotolerant Bacillus spore formers. *FEMS microbiology letters* **255**, 215 (Feb, 2006).
55. F. Kawai *et al.*, Cardiolipin domains in Bacillus subtilis marburg membranes. *Journal of bacteriology* **186**, 1475 (Mar, 2004).
56. M. Schlame, Cardiolipin synthesis for the assembly of bacterial and mitochondrial membranes. *J Lipid Res* **49**, 1607 (Aug, 2008).
57. H. Palsdottir, C. Hunte, Lipids in membrane protein structures. *Biochimica et biophysica acta* **1666**, 2 (Nov 3, 2004).
58. E. Mileykovskaya, W. Dowhan, Cardiolipin membrane domains in prokaryotes and eukaryotes. *Biochimica et biophysica acta* **1788**, 2084 (Oct, 2009).
59. E. Mileykovskaya, M. Zhang, W. Dowhan, Cardiolipin in energy transducing membranes. *Biochemistry (Mosc)* **70**, 154 (Feb, 2005).
60. T. Romantsov *et al.*, Cardiolipin promotes polar localization of osmosensory transporter ProP in Escherichia coli. *Molecular microbiology* **64**, 1455 (Jun, 2007).
61. J. L. Camberg *et al.*, Synergistic stimulation of EpsE ATP hydrolysis by EpsL and acidic phospholipids. *The EMBO journal* **26**, 19 (Jan 10, 2007).
62. E. Mileykovskaya, W. Dowhan, Role of membrane lipids in bacterial division-site selection. *Curr Opin Microbiol* **8**, 135 (Apr, 2005).
63. C. S. Lopez, A. F. Alice, H. Heras, E. A. Rivas, C. Sanchez-Rivas, Role of anionic phospholipids in the adaptation of Bacillus subtilis to high salinity. *Microbiology* **152**, 605 (Mar, 2006).
64. M. Tsai *et al.*, Staphylococcus aureus requires cardiolipin for survival under conditions of high salinity. *BMC microbiology* **11**, 13 (2011).
65. J. D. Unsay, K. Cosentino, Y. Subburaj, A. J. Garcia-Saez, Cardiolipin effects on membrane structure and dynamics. *Langmuir* **29**, 15878 (Dec 23, 2013).

66. C. Donovan, M. Bramkamp, Characterization and subcellular localization of a bacterial flotillin homologue. *Microbiology* **155**, 1786 (Jun, 2009).
67. P. E. Bickel *et al.*, Flotillin and epidermal surface antigen define a new family of caveolae-associated integral membrane proteins. *The Journal of biological chemistry* **272**, 13793 (May 23, 1997).
68. T. Schulte, K. A. Paschke, U. Laessing, F. Lottspeich, C. A. Stuermer, Reggie-1 and reggie-2, two cell surface proteins expressed by retinal ganglion cells during axon regeneration. *Development* **124**, 577 (Jan, 1997).
69. C. A. Stuermer, The reggie/flotillin connection to growth. *Trends Cell Biol* **20**, 6 (Jan, 2010).
70. T. Babuke *et al.*, Hetero-oligomerization of reggie-1/flotillin-2 and reggie-2/flotillin-1 is required for their endocytosis. *Cell Signal* **21**, 1287 (Aug, 2009).
71. A. Banning, A. Tomasovic, R. Tikkanen, Functional aspects of membrane association of reggie/flotillin proteins. *Curr Protein Pept Sci* **12**, 725 (Dec, 2011).
72. M. Amaddii *et al.*, Flotillin-1/reggie-2 protein plays dual role in activation of receptor-tyrosine kinase/mitogen-activated protein kinase signaling. *J Biol Chem* **287**, 7265 (Mar 2, 2012).
73. N. Tavernarakis, M. Driscoll, N. C. Kyrpides, The SPFH domain: implicated in regulating targeted protein turnover in stomatins and other membrane-associated proteins. *Trends Biochem Sci* **24**, 425 (Nov, 1999).
74. G. P. Solis *et al.*, Reggie/flotillin proteins are organized into stable tetramers in membrane microdomains. *The Biochemical journal* **403**, 313 (Apr 15, 2007).
75. C. H. Haney, S. R. Long, Plant flotillins are required for infection by nitrogen-fixing bacteria. *Proceedings of the National Academy of Sciences of the United States of America* **107**, 478 (Jan 5, 2010).
76. A. J. Edgar, J. M. Polak, Flotillin-1: gene structure: cDNA cloning from human lung and the identification of alternative polyadenylation signals. *The international journal of biochemistry & cell biology* **33**, 53 (Jan, 2001).
77. I. Levental, D. Lingwood, M. Grzybek, U. Coskun, K. Simons, Palmitoylation regulates raft affinity for the majority of integral raft proteins. *Proc Natl Acad Sci U S A* **107**, 22050 (Dec 21, 2010).
78. C. Neumann-Giesen *et al.*, Membrane and raft association of reggie-1/flotillin-2: role of myristoylation, palmitoylation and oligomerization and induction of filopodia by overexpression. *Biochem J* **378**, 509 (Mar 1, 2004).
79. C. A. Stuermer *et al.*, Glycosylphosphatidyl inositol-anchored proteins and fyn kinase assemble in noncaveolar plasma membrane microdomains defined by reggie-1 and -2. *Molecular biology of the cell* **12**, 3031 (Oct, 2001).
80. O. O. Glebov, N. A. Bright, B. J. Nichols, Flotillin-1 defines a clathrin-independent endocytic pathway in mammalian cells. *Nature cell biology* **8**, 46 (Jan, 2006).
81. J. F. Dermine *et al.*, Flotillin-1-enriched lipid raft domains accumulate on maturing phagosomes. *The Journal of biological chemistry* **276**, 18507 (May 25, 2001).
82. M. F. Langhorst *et al.*, Reggies/flotillins regulate cytoskeletal remodeling during neuronal differentiation via CAP/ponsin and Rho GTPases. *European journal of cell biology* **87**, 921 (Dec, 2008).
83. B. A. John, M. Meister, A. Banning, R. Tikkanen, Flotillins bind to the dileucine sorting motif of beta-site amyloid precursor protein-cleaving enzyme 1 and influence its endosomal sorting. *The FEBS journal* **281**, 2074 (Apr, 2014).

84. N. Kato, M. Nakanishi, N. Hirashima, Flotillin-1 regulates IgE receptor-mediated signaling in rat basophilic leukemia (RBL-2H3) cells. *Journal of immunology* **177**, 147 (Jul 1, 2006).
85. C. A. Baumann *et al.*, CAP defines a second signalling pathway required for insulin-stimulated glucose transport. *Nature* **407**, 202 (Sep 14, 2000).
86. M. Amaddii *et al.*, Flotillin-1/reggie-2 protein plays dual role in activation of receptor-tyrosine kinase/mitogen-activated protein kinase signaling. *The Journal of biological chemistry* **287**, 7265 (Mar 2, 2012).
87. D. M. Jacobowitz, A. T. Kallarakal, Flotillin-1 in the substantia nigra of the Parkinson brain and a predominant localization in catecholaminergic nerves in the rat brain. *Neurotoxicity research* **6**, 245 (2004).
88. S. C. Kao, A. M. Krichevsky, K. S. Kosik, L. H. Tsai, BACE1 suppression by RNA interference in primary cortical neurons. *The Journal of biological chemistry* **279**, 1942 (Jan 16, 2004).
89. A. Schneider *et al.*, Flotillin-dependent clustering of the amyloid precursor protein regulates its endocytosis and amyloidogenic processing in neurons. *The Journal of neuroscience : the official journal of the Society for Neuroscience* **28**, 2874 (Mar 12, 2008).
90. P. Hazarika *et al.*, Up-regulation of Flotillin-2 is associated with melanoma progression and modulates expression of the thrombin receptor protease activated receptor 1. *Cancer research* **64**, 7361 (Oct 15, 2004).
91. C. Lin *et al.*, Knockdown of FLOT1 impairs cell proliferation and tumorigenicity in breast cancer through upregulation of FOXO3a. *Clinical cancer research : an official journal of the American Association for Cancer Research* **17**, 3089 (May 15, 2011).
92. X. Wang *et al.*, Flotillin-2 is associated with breast cancer progression and poor survival outcomes. *J Transl Med* **11**, 190 (2013).
93. W. Gao *et al.*, Plasma membrane proteomic analysis of human Gastric Cancer tissues: revealing flotillin 1 as a marker for Gastric Cancer. *BMC Cancer* **15**, 367 (May 7, 2015).
94. S. Pust *et al.*, Flotillins as regulators of ErbB2 levels in breast cancer. *Oncogene* **32**, 3443 (Jul 18, 2013).
95. S. Chiba, K. Ito, Y. Akiyama, The Escherichia coli plasma membrane contains two PHB (prohibitin homology) domain protein complexes of opposite orientations. *Molecular microbiology* **60**, 448 (Apr, 2006).
96. H. M. Zhang *et al.*, An alkali-inducible flotillin-like protein from Bacillus halodurans C-125. *The protein journal* **24**, 125 (Feb, 2005).
97. M. Cao, T. Wang, R. Ye, J. D. Helmann, Antibiotics that inhibit cell wall biosynthesis induce expression of the Bacillus subtilis sigma(W) and sigma(M) regulons. *Molecular microbiology* **45**, 1267 (Sep, 2002).
98. E. Rivera-Milla, C. A. Stuermer, E. Malaga-Trillo, Ancient origin of reggie (flotillin), reggie-like, and other lipid-raft proteins: convergent evolution of the SPFH domain. *Cellular and molecular life sciences : CMLS* **63**, 343 (Feb, 2006).
99. F. Dempwolff, H. M. Moller, P. L. Graumann, Synthetic motility and cell shape defects associated with deletions of flotillin/reggie paralogs in Bacillus subtilis and interplay of these proteins with NfeD proteins. *Journal of bacteriology* **194**, 4652 (Sep, 2012).
100. J. N. Bach, M. Bramkamp, Flotillins functionally organize the bacterial membrane. *Molecular microbiology* **88**, 1205 (Jun, 2013).

101. B. Mielich-Suss, J. Schneider, D. Lopez, Overproduction of flotillin influences cell differentiation and shape in Bacillus subtilis. *MBio* **4**, e00719 (2013).
102. A. Yepes *et al.*, The biofilm formation defect of a Bacillus subtilis flotillin-defective mutant involves the protease FtsH. *Molecular microbiology* **86**, 457 (Oct, 2012).
103. A. Banning, A. Tomasovic, R. Tikkanen, Functional aspects of membrane association of reggie/flotillin proteins. *Curr Protein Pept Sci* **12**, 725 (Dec, 2011).
104. T. Babuke *et al.*, Hetero-oligomerization of reggie-1/flotillin-2 and reggie-2/flotillin-1 is required for their endocytosis. *Cellular signalling* **21**, 1287 (Aug, 2009).
105. A. M. Tareen *et al.*, The Campylobacter jejuni Cj0268c protein is required for adhesion and invasion in vitro. *PLoS One* **8**, e81069 (2013).
106. D. A. Brown, Isolation and use of rafts. *Curr Protoc Immunol* **Chapter 11**, Unit 11 10 (Nov, 2002).
107. S. S. Branda, F. Chu, D. B. Kearns, R. Losick, R. Kolter, A major protein component of the Bacillus subtilis biofilm matrix. *Molecular microbiology* **59**, 1229 (Feb, 2006).
108. D. B. Kearns, F. Chu, S. S. Branda, R. Kolter, R. Losick, A master regulator for biofilm formation by Bacillus subtilis. *Molecular microbiology* **55**, 739 (Feb, 2005).
109. M. Fujita, R. Losick, Evidence that entry into sporulation in Bacillus subtilis is governed by a gradual increase in the level and activity of the master regulator Spo0A. *Genes & development* **19**, 2236 (Sep 15, 2005).
110. M. A. Hamon, B. A. Lazazzera, The sporulation transcription factor Spo0A is required for biofilm development in Bacillus subtilis. *Molecular microbiology* **42**, 1199 (Dec, 2001).
111. P. J. Piggot, D. W. Hilbert, Sporulation of Bacillus subtilis. *Curr Opin Microbiol* **7**, 579 (Dec, 2004).
112. A. D. Grossman, Genetic networks controlling the initiation of sporulation and the development of genetic competence in Bacillus subtilis. *Annu Rev Genet* **29**, 477 (1995).
113. J. R. LeDeaux, N. Yu, A. D. Grossman, Different roles for KinA, KinB, and KinC in the initiation of sporulation in Bacillus subtilis. *Journal of bacteriology* **177**, 861 (Feb, 1995).
114. M. Jiang, W. Shao, M. Perego, J. A. Hoch, Multiple histidine kinases regulate entry into stationary phase and sporulation in Bacillus subtilis. *Molecular microbiology* **38**, 535 (Nov, 2000).
115. D. Lopez, E. A. Gontang, R. Kolter, Potassium sensing histidine kinase in Bacillus subtilis. *Methods in enzymology* **471**, 229 (2010).
116. D. Lopez, M. A. Fischbach, F. Chu, R. Losick, R. Kolter, Structurally diverse natural products that cause potassium leakage trigger multicellularity in Bacillus subtilis. *Proceedings of the National Academy of Sciences of the United States of America* **106**, 280 (Jan 6, 2009).
117. S. N. Devi, M. Vishnoi, B. Kiehler, L. Haggett, M. Fujita, In vivo functional characterization of the transmembrane histidine kinase KinC in Bacillus subtilis. *Microbiology*, (Feb 20, 2015).
118. A. T. Le, W. Schumann, The Spo0E phosphatase of Bacillus subtilis is a substrate of the FtsH metalloprotease. *Microbiology* **155**, 1122 (Apr, 2009).
119. S. Zellmeier, U. Zuber, W. Schumann, T. Wiegert, The absence of FtsH metalloprotease activity causes overexpression of the sigmaW-controlled pbpE

gene, resulting in filamentous growth of Bacillus subtilis. *Journal of bacteriology* **185**, 973 (Feb, 2003).
120. K. Ito, Y. Akiyama, Cellular functions, mechanism of action, and regulation of FtsH protease. *Annual review of microbiology* **59**, 211 (2005).
121. G. Steglich, W. Neupert, T. Langer, Prohibitins regulate membrane protein degradation by the m-AAA protease in mitochondria. *Molecular and cellular biology* **19**, 3435 (May, 1999).
122. J. P. Hendrick, W. Wickner, SecA protein needs both acidic phospholipids and SecY/E protein for functional high-affinity binding to the Escherichia coli plasma membrane. *The Journal of biological chemistry* **266**, 24596 (Dec 25, 1991).
123. K. Dalal, C. S. Chan, S. G. Sligar, F. Duong, Two copies of the SecY channel and acidic lipids are necessary to activate the SecA translocation ATPase. *Proceedings of the National Academy of Sciences of the United States of America* **109**, 4104 (Mar 13, 2012).
124. B. A. Lazazzera, The intracellular function of extracellular signaling peptides. *Peptides* **22**, 1519 (Oct, 2001).
125. M. Perego, C. F. Higgins, S. R. Pearce, M. P. Gallagher, J. A. Hoch, The oligopeptide transport system of Bacillus subtilis plays a role in the initiation of sporulation. *Molecular microbiology* **5**, 173 (Jan, 1991).
126. J. Meisner *et al.*, FtsEX is required for CwlO peptidoglycan hydrolase activity during cell wall elongation in Bacillus subtilis. *Molecular microbiology* **89**, 1069 (Sep, 2013).
127. A. Atrih, G. Bacher, G. Allmaier, M. P. Williamson, S. J. Foster, Analysis of peptidoglycan structure from vegetative cells of Bacillus subtilis 168 and role of PBP 5 in peptidoglycan maturation. *Journal of bacteriology* **181**, 3956 (Jul, 1999).
128. Y. Kawai *et al.*, A widespread family of bacterial cell wall assembly proteins. *The EMBO journal* **30**, 4931 (Dec 14, 2011).
129. D. Varon, S. A. Boylan, K. Okamoto, C. W. Price, Bacillus subtilis gtaB encodes UDP-glucose pyrophosphorylase and is controlled by stationary-phase transcription factor sigma B. *Journal of bacteriology* **175**, 3964 (Jul, 1993).
130. J. Dresler, J. Klimentova, J. Stulik, Bacterial protein complexes investigation using blue native PAGE. *Microbiological research* **166**, 47 (Jan 20, 2011).
131. H. Schagger, G. von Jagow, Blue native electrophoresis for isolation of membrane protein complexes in enzymatically active form. *Anal Biochem* **199**, 223 (Dec, 1991).
132. H. Schagger, K. Pfeiffer, Supercomplexes in the respiratory chains of yeast and mammalian mitochondria. *The EMBO journal* **19**, 1777 (Apr 17, 2000).
133. I. Arnold, K. Pfeiffer, W. Neupert, R. A. Stuart, H. Schagger, Yeast mitochondrial F1F0-ATP synthase exists as a dimer: identification of three dimer-specific subunits. *The EMBO journal* **17**, 7170 (Dec 15, 1998).
134. S. Sunderhaus *et al.*, Carbonic anhydrase subunits form a matrix-exposed domain attached to the membrane arm of mitochondrial complex I in plants. *The Journal of biological chemistry* **281**, 6482 (Mar 10, 2006).
135. N. V. Dudkina, J. Heinemeyer, W. Keegstra, E. J. Boekema, H. P. Braun, Structure of dimeric ATP synthase from mitochondria: an angular association of monomers induces the strong curvature of the inner membrane. *FEBS letters* **579**, 5769 (Oct 24, 2005).
136. A. Poetsch, D. Neff, H. Seelert, H. Schagger, N. A. Dencher, Dye removal, catalytic activity and 2D crystallization of chloroplast H(+)-ATP synthase purified by blue native electrophoresis. *Biochimica et biophysica acta* **1466**, 339 (Jun 1, 2000).

137. V. Reisinger, L. A. Eichacker, Analysis of membrane protein complexes by blue native PAGE. *Proteomics* **6 Suppl 2**, 6 (Sep, 2006).
138. H. Eubel, L. Jansch, H. P. Braun, New insights into the respiratory chain of plant mitochondria. Supercomplexes and a unique composition of complex II. *Plant physiology* **133**, 274 (Sep, 2003).
139. F. Krause, Detection and analysis of protein-protein interactions in organellar and prokaryotic proteomes by native gel electrophoresis: (Membrane) protein complexes and supercomplexes. *Electrophoresis* **27**, 2759 (Jul, 2006).
140. J. P. Lasserre *et al.*, A complexomic study of Escherichia coli using two-dimensional blue native/SDS polyacrylamide gel electrophoresis. *Electrophoresis* **27**, 3306 (Aug, 2006).
141. P. Bessonneau, V. Besson, I. Collinson, F. Duong, The SecYEG preprotein translocation channel is a conformationally dynamic and dimeric structure. *The EMBO journal* **21**, 995 (Mar 1, 2002).
142. J. Behrendt, U. Lindenstrauss, T. Bruser, The TatBC complex formation suppresses a modular TatB-multimerization in Escherichia coli. *FEBS letters* **581**, 4085 (Aug 21, 2007).
143. F. Stenberg *et al.*, Protein complexes of the Escherichia coli cell envelope. *The Journal of biological chemistry* **280**, 34409 (Oct 14, 2005).
144. D. Schneider *et al.*, Assembly of the Escherichia coli NADH:ubiquinone oxidoreductase (complex I). *Biochimica et biophysica acta* **1777**, 735 (Jul-Aug, 2008).
145. J. N. Bach, M. Bramkamp, Dissecting the molecular properties of prokaryotic flotillins. *PLoS One* **10**, e0116750 (2015).
146. I. C. Morrow *et al.*, Flotillin-1/reggie-2 traffics to surface raft domains via a novel golgi-independent pathway. Identification of a novel membrane targeting domain and a role for palmitoylation. *The Journal of biological chemistry* **277**, 48834 (Dec 13, 2002).
147. C. Neumann-Giesen *et al.*, Membrane and raft association of reggie-1/flotillin-2: role of myristoylation, palmitoylation and oligomerization and induction of filopodia by overexpression. *The Biochemical journal* **378**, 509 (Mar 1, 2004).
148. T. Parasassi, G. De Stasio, A. d'Ubaldo, E. Gratton, Phase fluctuation in phospholipid membranes revealed by Laurdan fluorescence. *Biophys J* **57**, 1179 (Jun, 1990).
149. S. A. Sanchez, M. A. Tricerri, E. Gratton, Laurdan generalized polarization fluctuations measures membrane packing micro-heterogeneity in vivo. *Proceedings of the National Academy of Sciences of the United States of America* **109**, 7314 (May 8, 2012).
150. R. Mercier, P. Dominguez-Cuevas, J. Errington, Crucial role for membrane fluidity in proliferation of primitive cells. *Cell Rep* **1**, 417 (May 31, 2012).
151. J. Dinic, H. Biverstahl, L. Maler, I. Parmryd, Laurdan and di-4-ANEPPDHQ do not respond to membrane-inserted peptides and are good probes for lipid packing. *Biochim Biophys Acta* **1808**, 298 (Jan, 2011).
152. K. Gaus, T. Zech, T. Harder, Visualizing membrane microdomains by Laurdan 2-photon microscopy. *Mol Membr Biol* **23**, 41 (Jan-Feb, 2006).
153. G. Wheeler, K. M. Tyler, Widefield microscopy for live imaging of lipid domains and membrane dynamics. *Biochimica et biophysica acta* **1808**, 634 (Mar, 2011).
154. H. Strahl, F. Burmann, L. W. Hamoen, The actin homologue MreB organizes the bacterial cell membrane. *Nat Commun* **5**, 3442 (2014).

155. R. F. de Almeida, A. Fedorov, M. Prieto, Sphingomyelin/phosphatidylcholine/cholesterol phase diagram: boundaries and composition of lipid rafts. *Biophys J* **85**, 2406 (Oct, 2003).
156. E. Betzig, A. Lewis, A. Harootunian, M. Isaacson, E. Kratschmer, Near Field Scanning Optical Microscopy (NSOM): Development and Biophysical Applications. *Biophys J* **49**, 269 (Jan, 1986).
157. S. Hell, E. H. K. Stelzer, Fundamental improvement of resolution with a 4Pi-confocal fluorescence microscope using two-photon excitation. *Optics Communications* **93**, 277 (1992).
158. M. G. Gustafsson, D. A. Agard, J. W. Sedat, I5M: 3D widefield light microscopy with better than 100 nm axial resolution. *J Microsc* **195**, 10 (Jul, 1999).
159. M. G. Gustafsson, Nonlinear structured-illumination microscopy: wide-field fluorescence imaging with theoretically unlimited resolution. *Proceedings of the National Academy of Sciences of the United States of America* **102**, 13081 (Sep 13, 2005).
160. M. J. Rust, M. Bates, X. Zhuang, Sub-diffraction-limit imaging by stochastic optical reconstruction microscopy (STORM). *Nat Methods* **3**, 793 (Oct, 2006).
161. M. Heilemann *et al.*, Subdiffraction-resolution fluorescence imaging with conventional fluorescent probes. *Angewandte Chemie* **47**, 6172 (2008).
162. E. Betzig *et al.*, Imaging intracellular fluorescent proteins at nanometer resolution. *Science* **313**, 1642 (Sep 15, 2006).
163. K. I. Willig, B. Harke, R. Medda, S. W. Hell, STED microscopy with continuous wave beams. *Nat Methods* **4**, 915 (Nov, 2007).
164. M. Heilemann, S. van de Linde, A. Mukherjee, M. Sauer, Super-resolution imaging with small organic fluorophores. *Angewandte Chemie* **48**, 6903 (2009).
165. H. Mizuno *et al.*, Fluorescent probes for superresolution imaging of lipid domains on the plasma membrane. *Chemical Science* **2**, 1548 (2011).
166. D. M. Owen *et al.*, PALM imaging and cluster analysis of protein heterogeneity at the cell surface. *J Biophotonics* **3**, 446 (Jul, 2010).
167. N. Morone *et al.*, Three-dimensional reconstruction of the membrane skeleton at the plasma membrane interface by electron tomography. *The Journal of cell biology* **174**, 851 (Sep 11, 2006).
168. E. I. Tocheva, Z. Li, G. J. Jensen, Electron cryotomography. *Cold Spring Harb Perspect Biol* **2**, a003442 (Jun, 2010).
169. T. J. LaRocca *et al.*, Cholesterol lipids of Borrelia burgdorferi form lipid rafts and are required for the bactericidal activity of a complement-independent antibody. *Cell host & microbe* **8**, 331 (Oct 21, 2010).
170. R. Erni, M. D. Rossell, C. Kisielowski, U. Dahmen, Atomic-resolution imaging with a sub-50-pm electron probe. *Physical review letters* **102**, 096101 (Mar 6, 2009).
171. J. E. Schnitzer, D. P. McIntosh, A. M. Dvorak, J. Liu, P. Oh, Separation of caveolae from associated microdomains of GPI-anchored proteins. *Science* **269**, 1435 (Sep 8, 1995).
172. L. Rajendran *et al.*, Asymmetric localization of flotillins/reggies in preassembled platforms confers inherent polarity to hematopoietic cells. *Proceedings of the National Academy of Sciences of the United States of America* **100**, 8241 (Jul 8, 2003).
173. M. Simons *et al.*, Exogenous administration of gangliosides displaces GPI-anchored proteins from lipid microdomains in living cells. *Molecular biology of the cell* **10**, 3187 (Oct, 1999).

174. K. Kasahara *et al.*, Involvement of gangliosides in glycosylphosphatidylinositol-anchored neuronal cell adhesion molecule TAG-1 signaling in lipid rafts. *The Journal of biological chemistry* **275**, 34701 (Nov 3, 2000).
175. T. Mitsuda, K. Furukawa, S. Fukumoto, H. Miyazaki, T. Urano, Overexpression of ganglioside GM1 results in the dispersion of platelet-derived growth factor receptor from glycolipid-enriched microdomains and in the suppression of cell growth signals. *The Journal of biological chemistry* **277**, 11239 (Mar 29, 2002).
176. H. Sprong, P. van der Sluijs, G. van Meer, How proteins move lipids and lipids move proteins. *Nat Rev Mol Cell Biol* **2**, 504 (Jul, 2001).
177. D. A. Brown, J. K. Rose, Sorting of GPI-anchored proteins to glycolipid-enriched membrane subdomains during transport to the apical cell surface. *Cell* **68**, 533 (Feb 7, 1992).
178. D. M. Lang *et al.*, Identification of reggie-1 and reggie-2 as plasmamembrane-associated proteins which cocluster with activated GPI-anchored cell adhesion molecules in non-caveolar micropatches in neurons. *J Neurobiol* **37**, 502 (Dec, 1998).
179. C. Zurzolo, W. van't Hof, G. van Meer, E. Rodriguez-Boulan, Glycosphingolipid clusters and the sorting of GPI-anchored proteins in epithelial cells. *Braz J Med Biol Res* **27**, 317 (Feb, 1994).
180. S. Moffett, D. A. Brown, M. E. Linder, Lipid-dependent targeting of G proteins into rafts. *The Journal of biological chemistry* **275**, 2191 (Jan 21, 2000).
181. P. Scheiffele, M. G. Roth, K. Simons, Interaction of influenza virus haemagglutinin with sphingolipid-cholesterol membrane domains via its transmembrane domain. *The EMBO journal* **16**, 5501 (Sep 15, 1997).
182. A. Kimura, C. A. Baumann, S. H. Chiang, A. R. Saltiel, The sorbin homology domain: a motif for the targeting of proteins to lipid rafts. *Proceedings of the National Academy of Sciences of the United States of America* **98**, 9098 (Jul 31, 2001).
183. M. Bramkamp, D. Lopez, Exploring the existence of lipid rafts in bacteria. *Microbiol Mol Biol Rev* **79**, 81 (Mar, 2015).
184. J. Schneider *et al.*, Spatio-temporal Remodeling of Functional Membrane Microdomains Organizes the Signaling Networks of a Bacterium. *PLoS genetics* **11**, e1005140 (Apr, 2015).
185. J. Schneider, B. Mielich-Suss, R. Bohme, D. Lopez, In vivo characterization of the scaffold activity of flotillin on the membrane kinase KinC of Bacillus subtilis. doi:10.1099/mic.0.000137, *Microbiology*, *in press* (2015).
186. S. Munro, Lipid rafts: elusive or illusive? *Cell* **115**, 377 (Nov 14, 2003).
187. A. S. Shaw, Lipid rafts: now you see them, now you don't. *Nat Immunol* **7**, 1139 (Nov, 2006).
188. K. Cottingham, Do you believe in lipid rafts? Biologists are turning to several analytical techniques to find out whether lipid rafts really exist? *Analytical chemistry* **76**, 403A (Nov 1, 2004).
189. D. A. Brown, E. London, Structure of detergent-resistant membrane domains: does phase separation occur in biological membranes? *Biochemical and biophysical research communications* **240**, 1 (Nov 7, 1997).
190. D. Lingwood, H. J. Kaiser, I. Levental, K. Simons, Lipid rafts as functional heterogeneity in cell membranes. *Biochemical Society transactions* **37**, 955 (Oct, 2009).
191. A. K. Neumann, M. S. Itano, K. Jacobson, Understanding lipid rafts and other related membrane domains. *F1000 Biol Rep* **2**, 31 (2010).

192. R. J. Morris, A. Jen, A. Warley, Isolation of nano-meso scale detergent resistant membrane that has properties expected of lipid 'rafts'. *Journal of neurochemistry* **116**, 671 (Mar, 2011).
193. C. J. Bashor, N. C. Helman, S. Yan, W. A. Lim, Using engineered scaffold interactions to reshape MAP kinase pathway signaling dynamics. *Science* **319**, 1539 (Mar 14, 2008).
194. S. A. Chapman, A. R. Asthagiri, Quantitative effect of scaffold abundance on signal propagation. *Molecular systems biology* **5**, 313 (2009).
195. M. Good, G. Tang, J. Singleton, A. Remenyi, W. A. Lim, The Ste5 scaffold directs mating signaling by catalytically unlocking the Fus3 MAP kinase for activation. *Cell* **136**, 1085 (Mar 20, 2009).
196. A. Zanin-Zhorov *et al.*, Scaffold protein Disc large homolog 1 is required for T-cell receptor-induced activation of regulatory T-cell function. *Proceedings of the National Academy of Sciences of the United States of America* **109**, 1625 (Jan 31, 2012).
197. J. Muller, S. Ory, T. Copeland, H. Piwnica-Worms, D. K. Morrison, C-TAK1 regulates Ras signaling by phosphorylating the MAPK scaffold, KSR1. *Molecular cell* **8**, 983 (Nov, 2001).
198. A. Levchenko, J. Bruck, P. W. Sternberg, Scaffold proteins may biphasically affect the levels of mitogen-activated protein kinase signaling and reduce its threshold properties. *Proc Natl Acad Sci U S A* **97**, 5818 (May 23, 2000).
199. S. A. Chapman, A. R. Asthagiri, Quantitative effect of scaffold abundance on signal propagation. *Mol Syst Biol* **5**, 313 (2009).
200. M. Dickens *et al.*, A cytoplasmic inhibitor of the JNK signal transduction pathway. *Science* **277**, 693 (Aug 1, 1997).
201. R. Heermann *et al.*, The universal stress protein UspC scaffolds the KdpD/KdpE signaling cascade of Escherichia coli under salt stress. *J Mol Biol* **386**, 134 (Feb 13, 2009).
202. M. Li *et al.*, The antimicrobial peptide-sensing system aps of Staphylococcus aureus. *Mol Microbiol* **66**, 1136 (Dec, 2007).
203. M. Li, G. L. Hazelbauer, Core unit of chemotaxis signaling complexes. *Proc Natl Acad Sci U S A* **108**, 9390 (Jun 7, 2011).
204. E. S. Underbakke, Y. Zhu, L. L. Kiessling, Protein footprinting in a complex milieu: identifying the interaction surfaces of the chemotaxis adaptor protein CheW. *J Mol Biol* **409**, 483 (Jun 17, 2011).
205. F. X. Contreras, A. M. Ernst, F. Wieland, B. Brugger, Specificity of intramembrane protein-lipid interactions. *Cold Spring Harb Perspect Biol* **3**, (Jun, 2011).
206. U. Coskun, M. Grzybek, D. Drechsel, K. Simons, Regulation of human EGF receptor by lipids. *Proceedings of the National Academy of Sciences of the United States of America* **108**, 9044 (May 31, 2011).

Appendix

"Dissertation Based on Several Published Manuscripts"

Statement of individual author contributions and of legal second publication rights

Publication (complete reference):

Yepes, A., **Schneider, J.**, Mielich, B., Koch, G., Garcia-Betancur, J.C., Ramamurthi, K.S., Vlamakis, H., López, D., The biofilm formation defect of a Bacillus subtilis flotillin-defective mutant involves the protease FtsH. *Molecular microbiology* **86**, 457 (Oct, 2012).

Participated in	**Author Initials,** Responsibility decreasing from left to right				
Study Design	DL	AY	JS	BM	GK
Data Collection	AY	JS	DL	BM	GK
Data Analysis and Interpretation	AY	JS	DL	BM	GK
Manuscript Writing	DL	AY	JS	BM	GK

Publication (complete reference):

B. Mielich-Suss, **J. Schneider**, D. Lopez, Overproduction of flotillin influences cell differentiation and shape in Bacillus subtilis. *MBio* **4**, e00719 (2013).

Participated in	**Author Initials,** Responsibility decreasing from left to right				
Study Design	DL	BM	JS		
Data Collection	BM	JS	DL		
Data Analysis and Interpretation	BM	JS	DL		
Manuscript Writing	DL	BM	JS		

Publication (complete reference):

J. Schneider, T. Klein, B. Mielich-Süss, G. Koch, C. Franke, O.P. Kuipers, A.T. Kovács, M. Sauer, D. Lopez, Spatio-temporal Remodeling of Functional Membrane Microdomains Organizes the Signaling Networks of a Bacterium. *PLoS genetics* **11**, e1005140 (Apr, 2015).

Participated in	**Author Initials,** Responsibility decreasing from left to right				
Study Design	DL	MS	ATK	OPK	
Data Collection	JS	TK	BM	GK	CF
Data Analysis and Interpretation	JS	DL	ATK	MS	
Manuscript Writing	DL	JS			

Appendix

"Dissertation Based on Several Published Manuscripts"

Statement of individual author contributions and of legal second publication rights

Publication (complete reference): Manuscript published ahead of print.

J. Schneider, B. Mielich-Suss, R. Bohme, D. Lopez, In vivo characterization of the scaffold activity of flotillin on the membrane kinase KinC of Bacillus subtilis. *Microbiology*, *in press* (2015).

Participated in	**Author Initials,** Responsibility decreasing from left to right				
Study Design	DL	JS	BM		
Data Collection	JS	DL	BM	RB	
Data Analysis and Interpretation	JS	DL	BM	RB	
Manuscript Writing	DL	JS	BM		

I confirm that I have obtained permission from both the publishers and the co-authors for legal second publication.

I also confirm my primary supervisor's acceptance.

Doctoral Researcher's Name Date Place Signature

Appendix

CURRICULUM VITAE

PUBLICATIONS

Publications in peer-reviewed journals

- **J. Schneider**, B. Mielich-Suss, R. Bohme, D. Lopez, In vivo characterization of the scaffold activity of flotillin on the membrane kinase KinC of Bacillus subtilis. *Microbiology*, *in press* (2015).
- **J. Schneider**, T. Klein, B. Mielich-Süss, G. Koch, C. Franke, O.P. Kuipers, A.T. Kovács, M. Sauer, D. Lopez (2015), **Spatio-temporal Remodeling of Functional Membrane Microdomains Organizes the Signaling Networks of a Bacterium.** *PLoS genetics* **11**, e1005140 (Apr, 2015).
- B. Mielich-Süss, **J. Schneider**, D. Lopez, **Overproduction of flotillin influences cell differentiation and shape in Bacillus subtilis.** *MBio* **4**, e00719 (2013).
- Yepes, A., **Schneider, J.**, Mielich, B., Koch, G., Garcia-Betancur, J.C., Ramamurthis, K.S., Vlamakis, H., López, D. (2012), **The biofilm formation defect of a *Bacillus subtilis* flotillin-defective mutant involves the protease FtsH.** *Molecular Microbiology* doi: 10.1111/j.1365-2958.2012.08205.x.
- Garcia-Betancur, J. C., Yepes, A., **Schneider, J**., Lopez, D. **Single-cell Analysis of *Bacillus subtilis* Biofilms Using Fluorescence Microscopy and Flow Cytometry.** *J. Vis. Exp.* (60), e3796, doi:10.3791/3796 (2012).
- **Schneider, J.**, Yepes, A., Garcia-Betancur, J.C., Westedt, I., Mielich, B., Lopez, D. (2012), **Streptomycin-induced expression in *Bacillus subtilis* of YtnP, a lactonase-homologous protein that inhibits development and streptomycin production in *Streptomyces griseus*.** *Applied and Environmental Microbiology 78, 599-603*

Oral presentations in international meetings

- **J. Schneider,** B. Mielich-Süß, G. Koch, D. Lopez, **Organizing lipid rafts in bacteria** – 7th International Conference on Gram-Positive Microorganisms 2013, Montecatini Terme, Italy

Poster presentations in international meetings

- **J. Schneider,** T. Klein, B. Mielich-Süss, G. Koch, C. Franke, O.P. Kuipers, A.T. Kovács, M. Sauer, D. Lopez - **Organizing lipid rafts in bacteria.** MolMicroMeeting 2014, Würzburg
- **J. Schneider,** B. Mielich, D. Lopez **Differential expression of two flotillin-like proteins in *Bacillus subtilis*** - MolMicroMeeting 2012, Würzburg
- **J. Schneider**, B. Mielich, D. Lopez **Differential expression of two flotillin-like proteins in *Bacillus subtilis*** - VAAM 2012, Tübingen
- B. Mielich, **J. Schneider**, D. Lopez **Overexpression of Flotillins affects septum formation in *Bacillus subtilis*** - MolMicroMeeting 2012, Würzburg
- B. Mielich, **J. Schneider**, D. Lopez **Overexpression of Flotillins affects septum formation in *Bacillus subtilis*** - VAAM 2012, Tübingen
- **J. Schneider**, Participation at the FEMS Leopoldina Meeting 2011, Würzburg